Synthesis, characterisation and application of low molecular weight and polymeric 1,3-di-2-thienylbenzo[c]thiophenes

Dissertation

for the award of the academic degree of

Doctor of Natural Science (Dr. rer. nat.)

from the faculty of Biology, Chemistry and Geosciences

University of Bayreuth, Germany

submitted by

Roman Kisselev

born in Ivanovo, Russia

Bayreuth, 2004

Synthese, Charakterisierung und Anwendung von niedermolekularen und polymeren 1,3-di-2-thienylbenzo[c]thiophene

Dissertation

Zur Erlangung des akademischen Grades eines

Doktors der Naturwissenschaften

der Fakultät für Biologie, Chemie und Geowissenschaften

der Universität Bayreuth

vorgelegt von

Diplom Chemiker

Roman Kisselev

aus Ivanovo, Russland

Bayreuth, 2004

Die vorliegende Arbeit wurde in der Zeit von Oktober 2000 bis Mai 2004 am Lehrstuhl für Makromolekulare Chemie I der Universität Bayreuth angefertigt.

Vollständiger Abdruck der von Fakultät Biologie, Chemie und Geowissenschaften der Universität Bayreuth genehmigten Dissertation zur Erlangung des akademischen Grades Doktor der Naturwissenschaften (Dr. rer. nat.)

Datum der Einreichung der Arbeit:	27.05.2004
Datum des wissenschaftlichen Kolloquiums:	28.07.2004

Prüfungsausschuß:

Professor Dr.	*Carlo Unverzagt*	*(Vorsitzender)*
Privatdozent Dr.	*Mukundan Thelakkat*	*(Erstgutachter)*
Professor Dr.	*Karlheinz Seifert*	*(Zweitgutachter)*
Professor Dr.	*Hans-Werner Schmidt*	
Professor Dr.	*Georg Krausch*	

This work was financially supported by the "Deutschen Forschungsgemeinschaft-Sonderforschungsbereich 481"

I dedicate this work to my wife
Alla
and thank her for her love and personal support.

Acknowledgement

I want to thank all people who contributed and helped me to make this research work possible at MCI, University of Bayreuth. I have really enjoyed working at the MCI.

Firstly I would like to thank Prof. Hans-Werner Schmidt for the great opportunity to work in his department as well as for the support and encouragement during this thesis.

Many thanks to Privatdozent Dr. Mukundan Thelakkat, our solar cell group leader and my supervisor, for all the brilliant ideas, encouragement, help and for bringing me to the "world of organic synthesis" connected to the "world of electro-optical devices". His generous support allowed me to spend most of my time on research and also to travel to interesting conferences. His advice was most valuable to understand the obtained results and to determine the next steps for the research presented in this thesis.

I want to acknowledge die Deutsche Forschungsgemeinschaft, Sonderforschungsbereich 481 (SFB 481), Project B4, for providing the financial support for this work.

Special thanks goes to Dr. Martin Pfeiffer and Steffen Grundmann for the successful cooperation in the field of solar cells. These guys made the most efficient solar cells I got in this work.

I am grateful to Helmut Hänsel from Department of Physical Chemistry II (University of Bayreuth) for successful cooperation work, which led to two publications. I want to thank Markus Bäte (MCI) for successful cooperation in the field of OLEDs. Markus is responsible for fabrication of all OLEDs present in my work here. I would also thank Dr. Bin Peng (MCI) for providing IPCE measurements and for the tasteful green tea directly from China we drank together. I would also thank Apl. Prof.. Lothar Kador from Department of Experimental Physics IV for providing MOPAC calculations. I am thankful to Dr. Gert Jungmann (MCI) for the synthesis of poly(perylene bisimide), which I have used for testing in polymer solar cells. I must thank Dr. Cristoph Schmitz, who taught me everything he knew about solar cells preparation. I am thankful to Michael Sommer for supporting my research work. As a HIWI he helped me in preparing polymer solar cells I present in this work.

List of Abbreviations and Symbols

Alq_3	– 8-hydroxyquinolinolato aluminium (III)
AM 1.5	– air mass 1.5 global solar spectrum
BCP	– 2,9-dimethyl-4,7-diphenyl-1,10-phenanthroline
BINAP	– 2,2'-bis(diphenylphosphino)-1,19-binaphthyl
C_{60}	– fullerene
CIE	– Commission Internationale de L'Eclairage or International Commission on Illumination
CV	– cyclic voltammetry
DMAc	– N,N-dimethylacetamide
DMF	– N,N-dimethylformamide
DPPF	– 1,1'-bis(diphenylphosphino)ferrocene
DPPP	– 1,3-bis(diphenylphosphino)propane
DSC	– differential scanning calorimetry
DTITN	– 1,3-di-2-thienylbenzo[c]thiophene
DTITNPD	– 1,3-bis(5'-diarylaminothiophene-2-yl)benzo[c]thiophene
EL	– electroluminescence
EQE	– external quantum efficiency
ETL	– electron transport layer
F_4-TCQN	– tetrafluoro-tetracyano-quinodimetane
Fc	– ferrocene
FT-IR	– Fourier transformed infrared spectroscopy
HH coupling	– head-to head coupling
^{1}H-NMR	– proton nuclear magnetic resonance spectroscopy
HOMO	– the highest occupied molecular orbital
HTL	– hole transport layer
HT coupling	– head-to tail coupling
IPCE	– incident photon-to-current conversion efficiency
ITN	– isothianaphthene or benzo[c]thiophene
ITO	– indium tin oxide
LCD	– liquid crystal display
LUMO	– the lowest unoccupied molecular orbital

MDMO-PPV – poly([2-methyl-5(3',7'-dimethyloctyloxy)-p-phenylene vinylene])

*tetra*MeO-TPD – N,N,N'N'-tetrakis(4-methoxyphenyl)-benzidine)

MePTCDI – N,N'-dimethylperylene-3,4,9,10-dicarboxyimide

MEK – methyl ethyl ketone

MPP – maximum power point

MS – mass spectrometry

NMP – 1-methyl-2-pyrrolidinone

NPD – 1-Naphthyl phenyldiamine

NTSC – National Television System Committee

OFET – organic field-effect transistor

OLED – organic light-emitting diode

P3AT – poly(3-alkylthiophene)

P3HT – poly(3-hexylthiophene)

P3OPT – poly(3-(4-octylphenyl)thiophene)

PCBM – [6,6]-phenyl-C_{61}-butyric acid methyl ester

PEDOT-PSS – poly(3,4-ethylenedioxythiophene)-poly(styrenesulfonate)

PL – photoluminescence

PPI – poly(perylene bisimide)

PPV – poly(*p*-phenylene vinylene)

SEC – size exclusion chromatography

$TBAPF_6$ – tetrabutylammonium hexafluorophosphate

THF – tetrahydrofuran

TGA – thermogravimetric analysis

TPD – triphenyldiamine

TT coupling – tail-to tail coupling

ZnPc – zinc phthalocyanine

α	– absorption coefficient [cm^{-1}]	[$I = I° \exp(-\alpha \cdot d)$]
c	– concentration [M]	
d	– cuvett thickness [cm]	
ε	– molar extinction coefficient [$cm^{-1}mol^{-1}dm^{3}$]	[$\varepsilon = \ln 10 \cdot \alpha$]
E_g	– band gap [eV]	
E_g^{opt}	– optical band gap [eV]	
E_g^{ec}	– electro-chemical band gap [eV]	
E_{red1}	– first reduction potential [V]	
E_{ox1}	– first oxidation potential [V]	
E°	– standard potential for a reversible reaction [V]	
E_{pa}	– anodic peak potential [V]	
E_{pc}	– cathodic peak potential [V]	
V_{OC}	– open-circuit voltage [V]	
I_{SC}	– short-circuit photocurrent density [mA/cm^2]	
I_{mpp}	– current density at the maximum power point [mA/cm^2]	
V_{mpp}	– voltage at the maximum power point [V]	
FF	– fill factor [%]	
M_n	– number-average molecular weight [g/mol]	
M_w	– weight-average molecular weight [g/mol]	
M_p	– peak molecular weight [g/mol]	
η_c	– power conversion efficiency [%]	
η_{el}	– maximum electroluminescence efficiency [cd/A]	
N_{El}	– number of generated electrons	
N_{Ph}	– number of incident photons	
P_{In}	– incident power of irradiation [mW/cm^2]	
OD	– optical density (Absorbance)	
λ	– wavelength [nm]	
λ_{max}^{abs}	– wavelength of maximum absorption [nm]	
λ_{max}^{fl}	– wavelength of maximum fluorescence [nm]	
λ_{max}^{el}	– maximum wavelength of electroluminescence [nm]	
$T_{-5\%}$	– onset temperature for a 5 % weight loss [°C]	
T_g	– glass transition temperature [°C]	

Table of contents

1 Introduction

Research on organic semiconducting devices is leaping forward with immense speed. The realisation of durable thin layer electro-optical devices employing organic semiconductors is a result of a real boost in the last few years in the design and development of different types of functional materials for application in organic light-emitting diodes (OLEDs)[1,2], organic solar cells[3,4,5], organic field-effect transistors (OFETs)[6,7,8,9], photorefractive holography[10,11,12], etc. The underlying feature of these applications is the development of a suitable set of materials having properties like charge injection/transport in combination with optical properties such as light absorption or emission. Moreover, these materials also should have matching HOMO/LUMO energy values in order to avoid an energetic barrier for charge injection at the interfaces. Using these materials, which are termed “organic semiconductors”, a multicomponent electro-optical device is designed by taking into consideration the required energetics at the interfaces between two layers or components. The task of the material science community is to understand the complex physical processes in such devices so that the design of new materials tackles some of existing problems and improves the overall performance of organic semiconductor devices. The present Ph. D. thesis does not focus on inorganic materials and devices technologies, but concentrates on the development of tailor-made organic materials and their characterisation as well as determination and comparison of HOMO/LUMO energy values of these materials. Thus, this work is based on the synthesis and characterisation of novel bifunctional organic materials combining hole-transport and emitter/dye functions within one molecule. Moreover, these new hole-transport dyes are successfully applied in solar cells and bright red OLEDs. Anyhow, a brief introduction on the different types of materials and devices is given below to clearly understand the priorities and complexity involved in the design and development of organic materials for electro-optical applications.

1.1 Organic electro-optical devices

Nowadays, electro-optical devices fabricated from organic and polymeric materials are gaining recognition and attention of the electro-optical industrial community. During the last decade, there was an explosion of information pertaining to the field. As a result, organic-based devices are currently experiencing accelerated development efforts as dictated by the optical storage, display and solar cell markets. Advantages of the fabrication of organic materials into electro-optical devices, as well as an enormous information age market potential, have long been recognised. However, only now do these technologies appear to be reaching a critical mass as the next generation in several key technologies. Driving this trend are the continuing and accelerating developments in both manufacturing process technology, including novel nano designs and fabrications, and new materials systems[13].

There are several reasons to use organic materials for application in electro-optical devices. Most important are the peculiar advantages of organic materials:

- in organic devices the materials are usually used as thin amorphous films, which can be processed easily over large areas;
- amounts of organic materials are relatively small (100 nm thick) and large-scale production (chemistry) is easier than for inorganic materials (growth processes of single crystals etc.);
- they can be tuned chemically in order to adjust the separately band gap, charge transport as well as solubility and several other structural properties;
- the vast variety of possible chemical structures and functionalities of organic materials (polymers, oligomers, dendrimers, organo-minerals, dyes, pigments, liquid crystals, etc.) favour an active research for alternative competitive materials with the desired properties.
- the amorphous nature of polymers provides additional advantages in terms of film fabrication;

In order to give an historical outlook about organics for electro-optical applications, the most important technological developments in the field of organic-based electro-optics are summarised in Table 1.

Table 1. Major technological developments in the field of organic-based electro-optics.

Year	Materials or Devices	Company or Institute	Commercial Contribution
1977	Discovery of conducting polymers	*Heeger* – University of California, *MacDiarmid* – University of Pensilvania, *Shirakawa* – University of Tsukuba	Since their discovery, conductive polymers have been used to manufacture versions of many electronic and electro-optics products, including OLEDs in digital displays, flat TV screens, low-static computer monitors. On the horizon are molecular computers using plastic molecules to carry electrical current.
1986	"Tang solar cell" based on low molecular weight organics	*Tang* –Eastman Kodak Company, Rochester, NY	First organic solar cell based on two-layer structure. A power conversion efficiency of 1 % has been achieved.
1987	Vapour deposited thin layer OLED	Eastman Kodak, Rochester, NY	Since the discovery of OLEDs, Kodak researchers have made a number of breakthroughs related to OLED materials, device structure, doping techniques, improved efficiency, thin-film deposition methods and patterning methods, designs and fabrication methods for both passive and active-matrix OLED panels.
1990	Polymer LED based on PPV	Cambridge	First polymer LED in the world utilised using simple structure of ITO/PPV/Al.
2000	The largest active-matrix full colour OLED display (240x320 pixels, diagonal of 5.5 in.)	Eastman Kodak and Sanyo	Important milestone in demonstrating scalability of OLED technology and addressing applications needs beyond hand-held devices; active-matrix OLED displays are expected to replace LCDs in most flat-panel display applications
2001	Flexible plastic solar cells based on conjugated polymer and C_{60}[14]	*Sariciftci* and *Brabec* - Linz Institute for organic Solar cells (LIOS)	This work summarises the progress in a special section of photovoltaic energy conversion: i.e., organic, bulk heterojunction solar cells. With ~3 % power conversion efficiency and large potential for improvement, this approach represents a viable route to realizing large-area plastic solar power conversion technology.
2001	Flexible plastic circuit containing 326 OFETs based on polyimide substrate[6]	Philips Research Laboratories, Einhoven	Step towards the realisation of low-cost, all-polymer, flexible OFETs. Charge carrier mobilities comparable to that of amorphous silicon have been obtained.[15] As a demonstrator functional 15-bit programmable code generators are fabricated.

To get an impression of the latest advances in the electro-optical applications of organic semiconductors, examples of a plastic solar cell, an all-organic transistor and an organic electroluminescent display are shown in Figure 1.

A) 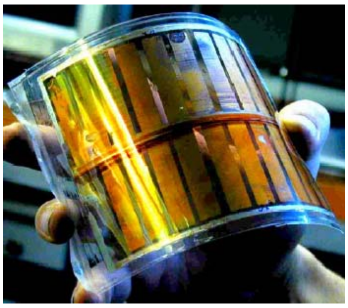 B) 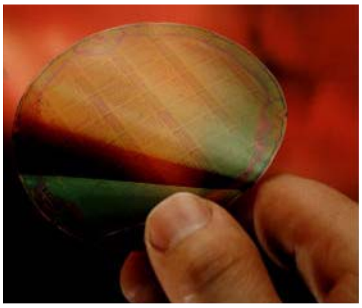 C) 

Figure 1. A) Flexible plastic solar cells based on conjugated polymer and C_{60} (LIOS, Linz Institute for organic Solar cells), B) Flexible plastic circuit containing 326 OFETs based on polyimide substrate (Philips Research Laboratories, Einhoven) and C) 5.5-inch panel thin OLED display with a quarter-VGA resolution (240-320 pixels) and a brightness of 200 cd/m^2 (Sanyo-Kodak). (reference: amob.no/artikkelbilder/kodak_oled.jpg)

General aspects and fundamental principles of OLEDs and photovoltaic cells are briefly introduced in the following.

1.1.1 Organic light-emitting diodes (OLEDs)

The most promising organic-based electro-optic devices are OLEDs. They have recently received a great deal of attention because of their application for a wide range of display applications as well as from the standpoint of scientific interest. They are attractive because of low voltage driving, high brightness, capability of multicolour emission by the selection of emitting materials and easy fabrication of large-area and thin-film devices.[16] Following the reports on OLEDs using single crystals of anthracene[17], recent pioneering works on OLEDs using low molecular-weight organic materials and a conjugated polymer have triggered extensive research and development within this field. Recent years have witnessed significant progress with regard to brightness, multi- or full-colour emission, and durability and thermal stability of OLEDs.

OLEDs fall into two competing technologies based on the materials used:

- polymers; solution processing methods
- low molecular weight materials; vapour deposition methods

Small molecule devices are fabricated using vacuum evaporation techniques, whereas polymer structures can be applied using spin-casting or ink-jet techniques. The screen-printing technique has recently been introduced and is presumed to be applicable to both polymer and small molecule devices.

The typical structure of molecule OLEDs consists of single or multiple layers of organic thin films sandwiched normally between the transparent indium tin oxide (ITO) coated glass and vacuum-evaporated metals with low work function such as magnesium/silver (Mg/Ag) or aluminium (Al) as represented in Figure 2. The operation of OLEDs involves injection of holes and electrons from the ITO and metal electrodes respectively as well as transport of injected charge carriers. Finally, a recombination of holes and electrons in the emission layer generates an electronically excited state in the molecule, followed by luminescent emission. Generally, layered devices consisting of charge transport and emitting layers can more readily achieve charge balance than single-layer devices. A suitable combination of charge transporting and emitting materials in layered devices reduces the energy barrier for the injection of charge carriers from the electrodes. The charge transport layer also acts as a blocking layer against the injection of either holes or electrons from the adjoining layer and their subsequent escape from the device. In order to achieve high performance in OLEDs, it is necessary to attain charge balance. In an ideal case, there should only be a negligible energy barrier for charge injection at each interface leading to balanced charge transport and efficient recombination in the emitter layer.

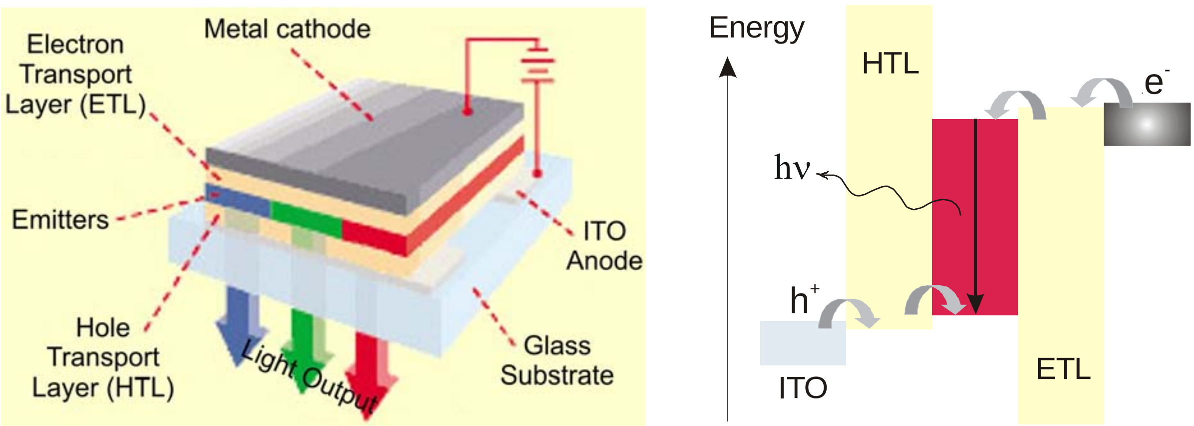

Figure 2. Schematic representation of an OLED and the energy level diagram of the materials involved in it. (reference: www.fotoline.ch/FOTOintern/02-19/oled.jpg)

Due to spin statistics, theoretically only a quarter of the excitons produced by electrical charge injection are singlet excitons and, therefore, by using fluorescent dyes (singlet emitter), the maximum efficiency of OLEDs is limited to 25 %. Recently reports have shown that this rule can not be strictly applicable for conjugated polymers in which efficiency higher than 25 % may be attainable.[18]

For more detailed information about the principles, mechanisms and physics of OLEDs, excellent and comprehensive discussion can be found in the monographs by Greenham and Friend[19] as well as Ishii et al.[20]

Thus, the performance of OLEDs is related to three main technological issues:

- colour range
- electroluminescence efficiency
- reliability or stability

The colour of OLEDs depends on the molecular compositions of the organic interface. The luminance efficiency can be improved by incorporating phosphorescent dyes as dopants in an emitting layer and, thus, exploiting the energy transfer from the singlet state of the host to the triplet state of the phosphorescent emitter to obtain electrophosphorescence.[21] But this concept demands the use of additional layers/components of host and blocking materials and the realisation of an almost perfect match of energy levels in the various materials involved in order to guarantee a high degree of energy transfer to the triplet emitter. Moreover, phosphorescent emitter has to be doped into a host material to avoid any triplet-triplet annihilation and the recombination zone has to be confined to the doped layer. This has been successfully demonstrated in devices prepared by vapour deposition of low molar mass compounds as well as doped systems in polymer blends.[22,23] This is, at present, one of the most attractive strategies to obtain highly efficient devices with emission in the green to red region. The reliability of OLEDs and other electro-optical devices, is a key source for the sceptical approach in the photonics community. The main cause of the reliability problem is the degradation of organic molecules. Many groups are addressing this issue and one solution is to introduce stabilising agents and efficient sealing methods. Another reliability problem relates to deterioration of the active cathode. Engineering tools have been used to deal with this issue.

For the fabrication of high-performance OLEDs, an understanding of basic processes, such as charge injection from the electrodes, charge transport, recombination of charge carriers to generate the electronically excited-state molecule as well as development of new materials with high performance and judicious choice of the combination of emitting and charge transporting materials and the combination of emitting and luminescent dopant molecules, are of vital importance. For this purpose, not only emitting materials but also charge transporting materials are also required. Both polymers and small molecules are candidates for materials in OLEDs.

The materials for OLEDs should meet the following requirements[24]:

- possess a suitable ionisation potential and electron affinity in order to match energy levels for the injection of charge carriers at electrode/organic material and organic material/organic material interfaces
- permit the formation of a uniform film without pinholes
- morphological stability
- thermal stability
- electrochemical stability
- high luminescence for emitting materials.

In addition, doping of luminescent compounds has been shown to be an effective method for attaining high brightness and desirable emission colour.

The most important materials required for OLED technology are red, green and blue emitters. It is possible to get any other colour by using a combination of red, green and blue (RGB). Concerning the class of emitter materials,

- metal chelates like 8-quinolinolato aluminium (III) (Alq_3), porphyrine metal complexes, rare earth metal-organic complexes of Eu, Ru, Tb etc.[25,26],
- small organic molecules like triphenyldiamines (TPDs), oligothiophenes, rubrene, oxidiazoles, triazoles, porphyrines, perylenes, coumarines, nile red etc.,
- polymers like polyfluorenes, poly(vinyl carbazole), poly(TPD)s, poly(phenylene vinylene)s (PPVs), derivatives of poly(thiophene), etc.

and different combinations of these molecules are used in OLEDs[27,28,29,45]. Chemical structures of some materials showing good performance in OLEDs are represented in Figure 3. Emitting colour in organic materials can be tuned from blue to green, yellow, orange and even red by incorporation of different substituents as it was shown for the case of PPV and thiophene derivatives[30,31].

Red emitters

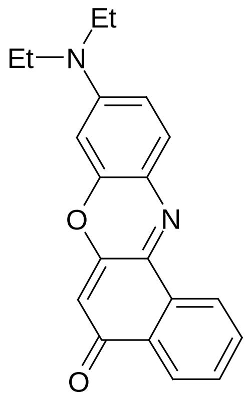

Nile red

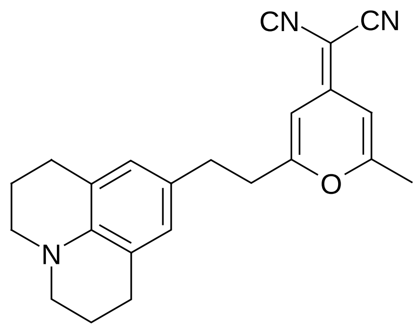

DCM dye

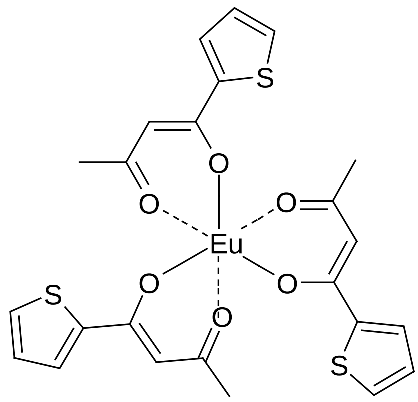

Eu(acac)$_3$

Green emitters

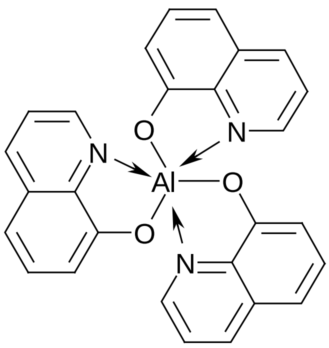

Alq$_3$

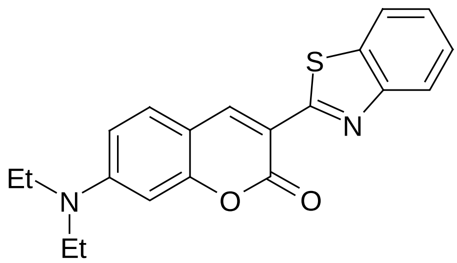

Coumarin-6

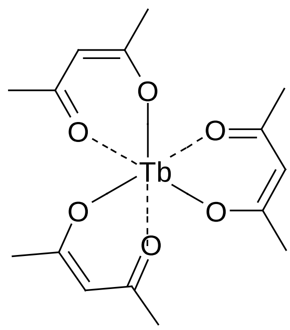

Tb(acac)$_3$

Blue emitters

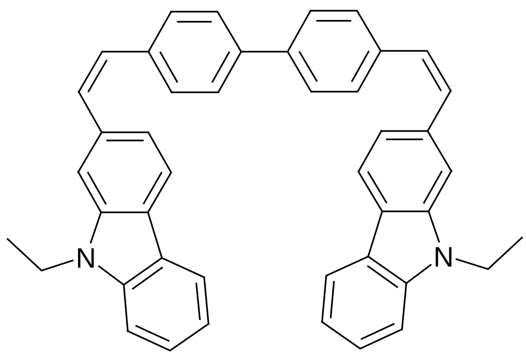

Carbazole derivative

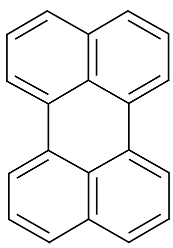

Perylene

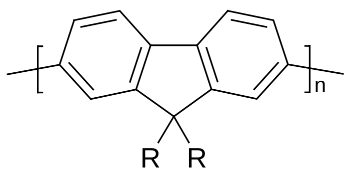

Polyfluorenes

Figure 3. Chemical structures of some emitters used in OLEDs.

1.1.2 Organic solar cells

Depending on the material type used, solar cells can be divided into inorganic, organic and hybrid solar cells, where the hybrid solar cells are fabricated from both organic and inorganic materials. The conversion efficiency of organic photovoltaic devices is still lower than that of inorganic photovoltaic devices[32]. The reason for this may be attributed to low photogeneration efficiency of charge carriers and to high electrical resistivity of organic materials, which stems from the low mobility and low density of free carriers.

In the case of organic and hybrid solar cells, there are at least four different approaches depending on the method by which the interface between p-type (donor) and n-type (acceptor) semiconductors are created at which charge separation takes place; I) multi-layer vapour deposited cells (*Tang cell*), II) bulk heterojunctions cells, prepared by spin-coating of a polymer/polymer or polymer/low molecular weight compound blend (*Plastic solar cell*), III) solar cells in which large band gap electron transport inorganic semiconductor sensitised with monomolecular organic dye layer (*Graetzel cell*)[33], IV) solar cells prepared from blend of conjugated polymer and nanoparticles of low band gap inorganic electron transport semiconductor (*poly(3-alkylthiophene)/CdSe cell*)[34].

Multi-layer solar cells benefit from separated charge transport layers that ensure connectivity with correct electrode and give the separated charge carrier only a small chance to recombine with its counterpart. The disadvantage of these solar cells is the small interface area, which allows only excitons of a thin layer to reach interface between layers and become dissociated. However, this disadvantage can be overcome by co-evaporation of dye and charge transport material. Use of co-evaporation allows achieving heterojunction photoactive layer within multi-layer solar cells. Schematic illustration of a multi-layer solar cell and the energy level diagram of components involved in it are shown in Figure 4. Since the report of solar conversion efficiencies of up to 1 % in 1986 in molecular flat-layer solar cells based on copper phthalocyanine/perylene tetracarboxylic derivative, further improvement of this system in year 2001 using copper phthalocyanine/fullerene[35] showed overall conversion efficiency of 3.6 %. The improvement comparing flat-layer solar cells, discussed above, is attributed to the electron transport properties of fullerene.

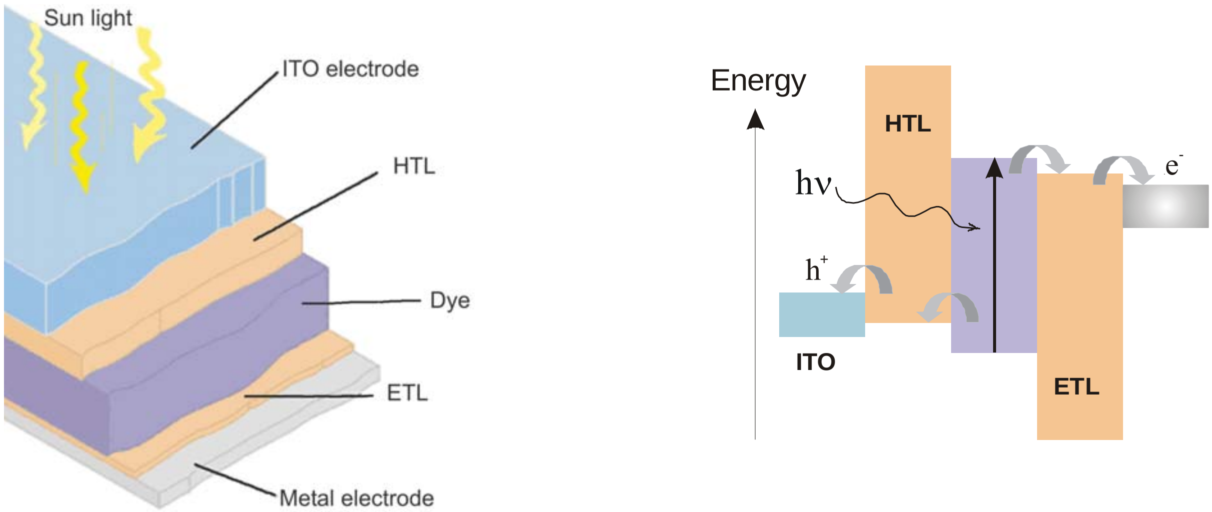

Figure 4. Schematic representation of a three-layered organic solar cell and the energy level diagram of the same. (reference: www.appliedfilms.com/Precision2)

In contrast to multi-layer cells, the bulk heterojunction solar cells exhibit a large interface area and most excitons reach the interface area, but charge carriers have a large chance to recombine and only a part of them can reach electrodes. The schematic representation of plastic solar cell is given in Figure 5.

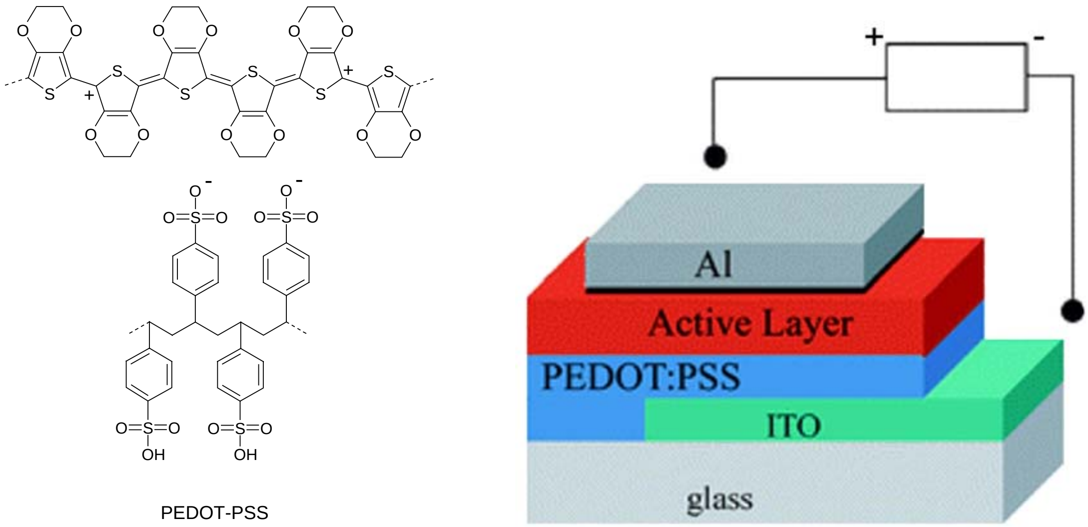

Figure 5. Structure of a plastic solar cell. Active layer consist of a blend of conjugated polymer and fullerene derivative, poly(ethylenedioxythiophene)-poly(styrene-sulfonate) (PEDOT-PSS) used as hole-injection layer. (reference: www.ipc.uni-linz.ac.at/os/index_os.html)

The 3 % overall conversion efficiency was reported in 2001 for “plastic solar cells” with improved bulk heterojunctions (interpenetrating network) of soluble PPV derivative, poly([2-methyl-5(3’,7’-dimethyloctyloxy)-p-phenylene vinylene]) (MDMO-PPV), and soluble fullerene derivative, [6,6]-phenyl-C_{61}-butyric acid methyl ester (PCBM). A slight improvement of this system up to a 3.5 % overall conversion efficiency was achieved in 2003 by replacing MDMO-PPV with poly(3-hexylthiophene) (P3HT)[36]. Better light harvesting with P3HT compared to MDMO-PPV may be attributed to a better performance of the solar cell, fabricated using P3HT. Additionally, the P3HT exhibits morphological advantage on annealing which also contributes to higher photocurrent.

“Graetzel cell”, which is known as dye-sensitised TiO_2 solar cell, consists of mesoporous TiO_2 layer and a monolayer of organic dye chemisorbed on it. In 1991, O’Regan and Graetzel have reported such a solar cell, based on Ru-dye and I_2/KI liquid electrolyte as a hole conductor, with overall conversion efficiency of about 10 %. Nevertheless, the use of liquid electrolyte makes this cell unsuitable for application due to low stability. The stability of this cell was improved using solid organic hole conductor to replace the liquid electrolyte. But the efficiency becomes smaller in replacing the liquid with solid hole conductor. In 2002, an all-solid-state TiO_2 dye sensitised solar cell with an efficiency of 3.2 % was reported[37]. A schematic representation of a solid state TiO_2 dye-sensitised solar cell is shown in Figure 6.

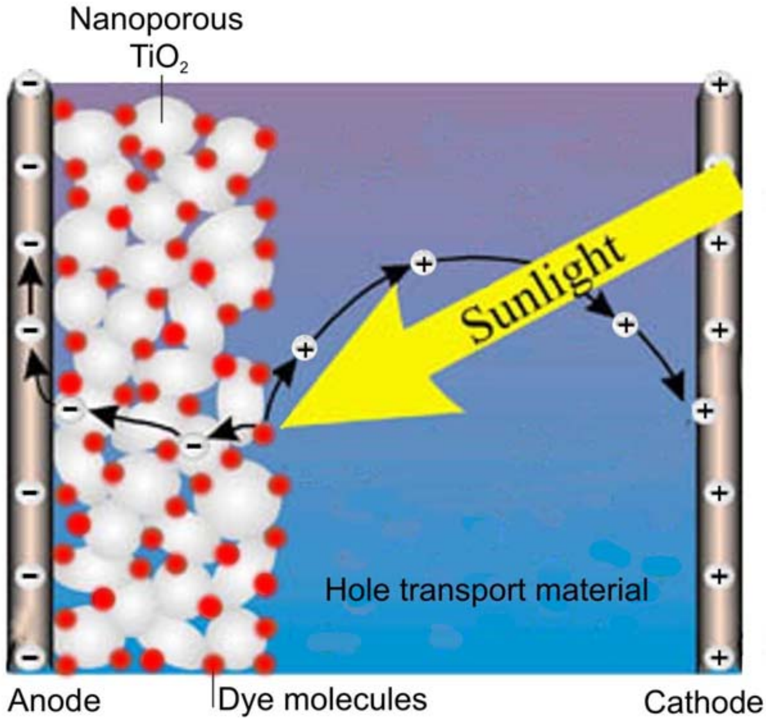

Figure 6. Schematic representation of dye-sensitised TiO_2 solar cell. (reference: www.delftoutlook.tudelft.nl/info/images%5CACF58D.JPG)

Another concept of a hybrid solar cell is a blend system involving both conjugated low band gap polymer and an inorganic electron acceptor semiconductor. This approach combines the easy processability of polymer materials with the advantageous absorption profile of inorganic materials. Additionally, the inorganic materials show good transport, which can be

optimised by tuning their size. A power conversion efficiency of 1.7 % has been demonstrated for such devices using P3HT and CdSe nanoparticles34.
The working principle of an organic solar cell, which is almost the reverse of an OLED, again demands the adaptation of energy levels of functional materials in such a way that there is a direct charge transport towards the electrodes. A prerequisite is charge separation after creation of electron and hole from the exciton produced in the dye. The major difference between an OLED and a solar cell is the magnitude of the field at which the charge transport occurs. In an OLED, fields as high as 10 to 100 $MV\cdot cm^{-1}$ are involved which makes the charge injection and transport into the emitter layer easier. However, only fields of less than two orders of magnitude exist in a solar cell, which makes it difficult to transport the charges away from the absorption layer in to the electrodes.
Recently, Gregg and Hanna[38] proposed a new model of an excitonic solar cell, describing all types of organic solar cells. The driving force for the charge transport is assigned to the chemical potential gradient, formed by the charge generation at the interface. The charges move away from this interface to the opposite electrodes. In contrast to classical inorganic solar cells, the built-in field in the organic solar cells is not limiting the open-circuit potential (V_{OC}), but the photoinduced quasi Fermi level difference of electron and hole. Thus, the energetic difference between the HOMO of the donor and the LUMO of the acceptor has to be considered as the limitation for the V_{OC}. The complicated physic processes involved in transformation of solar energy into electricity in organic photovoltaic devices can be simply divided into four steps:

1) Absorption of light, which leads to excitons generation;
2) Diffusion of excitons to the semiconductor/dye interface (great interface is needed due to small exciton diffusion length in organic materials of ~10 to 20 nm)
3) Charge separation at the interfaces (exact match in energy levels of materials involved is necessary);
4) Charge transport to the electrodes.

Considering the fact that light-emitting films of plastic materials have been realised, there is also a chance to achieve photovoltaic conversion in such materials.[39] There is no short-term ambition to replace silicon, or thin film technologies (crystalline and amorphous silicon, copper indium diselenide)[40], but to develop a long-term technology based on organic materials with almost unlimited availability. Before these cells become practical, which at the moment still looks far away, the efficiency will have to be increased further. The long-term stability and protection against environmental influences are also significant challenges. Organic materials bear this potentially. Thus, progress in organic photovoltaics requires new materials with improved properties:

- Low band gap materials with high optical coefficients are required for efficient photon harvesting and possibility to fabricate thin layer device
- Materials with high charge mobilities are required for efficient charge transport

Nowadays, the lack of sufficient and optimum absorption of solar light is found to be the major problem in organic solar cells. Extremely high optical absorption coefficients are possible with organic materials, which offers the possibility for the production of very thin solar cells of about 100 nm thickness, which is far below ~1 mm thick inorganic solar cells, and, therefore, only very small amounts of materials are needed. As an example, chemical structures of some organic dyes/pigments, used in photovoltaic devices, are represented in Figure 7.

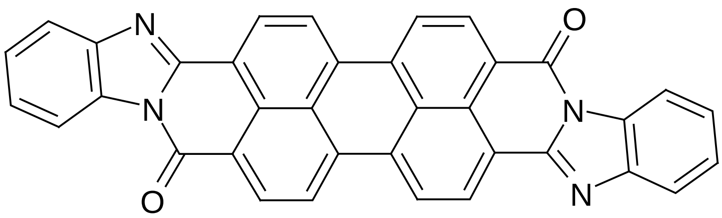

Perylene derivative

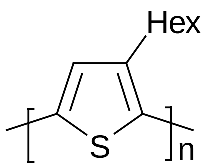

poly(3-hexylthiophene)

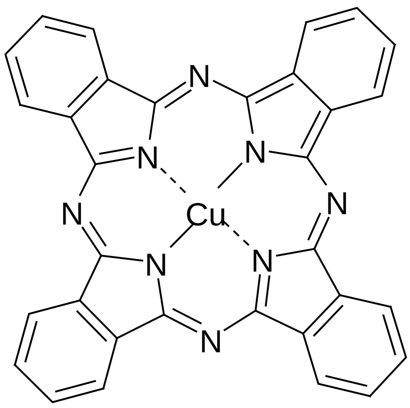

Cupper phthalocyanine (CuPc)

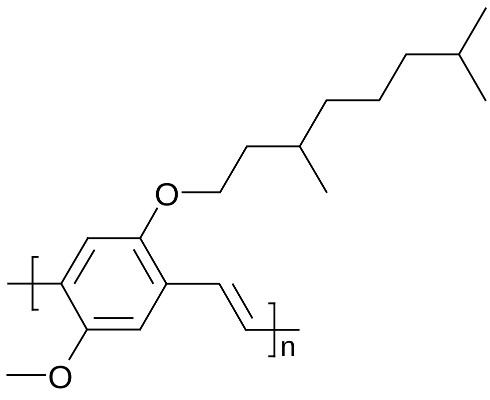

MDMO-PPV

Figure 7. Chemical structures of some dyes/pigments used in organic solar cells.

A preferred strategy of improving overall conversion efficiency of organic solar cells is to replace dyes in photovoltaic devices, which do not absorb further than 700 nm (band gap ~1.8 eV), with others that absorb further into red (band gap < 1.8 eV). The need for low band gap organic dyes to improve light harvesting leading to higher overall conversion efficiency of organic solar cells is clearly shown in Figure 8, in which air mass 1.5 global solar spectrum (AM 1.5)[41] is illustrated in order to compare it with absorption of blend (1:4) of P3HT and PCBM , which is the standard system in a polymer solar cell.

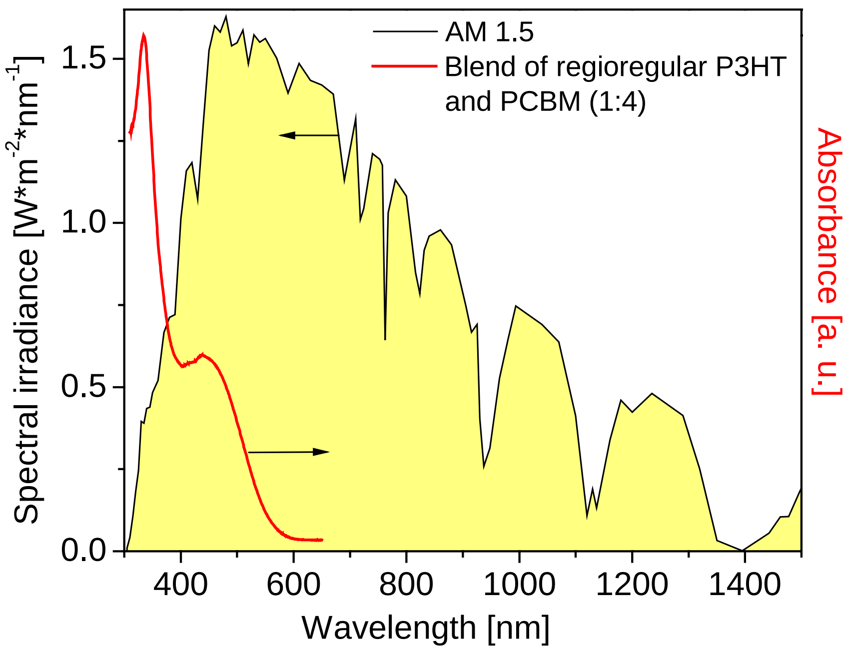

Figure 8. Global spectral irradiance AM 1.5 and absorption of P3HT+PCBM (1:4 wt/wt %) active layer in a polymer solar cell. (reference: http://rredc.nrel.gov/solar/spectra/am1.5/)

1.2 Organic semiconductors

In contrast to inorganic materials that consist of covalent or ionic bonds of atoms over the entire field of solids, organic materials are based on independent molecules and characterised by weak intermolecular interactions. Therefore, designs of organic materials can be readily performed on the molecular level. In particular, organic π-electron systems have received attention as potential photo- and electroactive materials. The task of material development encompasses a suitable selection of structural units either with charge transport property or optical properties in addition to the necessary mechanical, thermal and electrochemical properties. The fundamental requirement for all these organic materials is the ability to form stable and smooth films either via vapour deposition or by solution casting methods. This requirement can be fulfilled either by amorphous low molecular weight compounds of soluble high molecular weight polymers. The hole injection/transport or the electron injection/transport properties have to be incorporated into the molecular structure by selecting electron-rich moieties (p-type materials or donors) or electron-deficient moieties with high electron affinity (n-type materials or acceptors) respectively. The examples of hole transport units are represented in Figure 9. The building molecular units for obtaining materials with electron transport properties is shown in Figure 10.

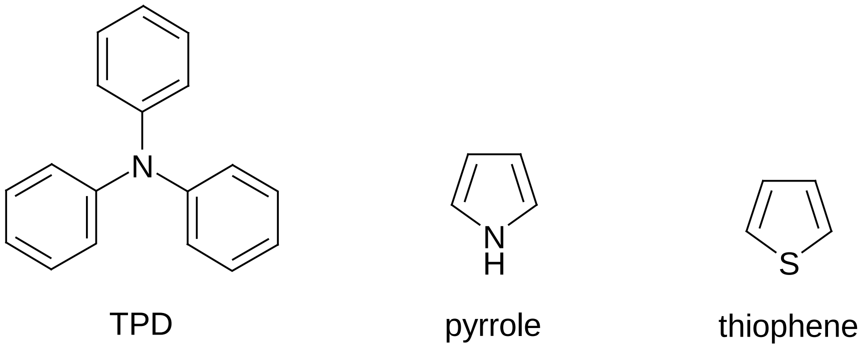

Figure 9. Chemical structures of some electron-rich moieties for building hole transport materials.

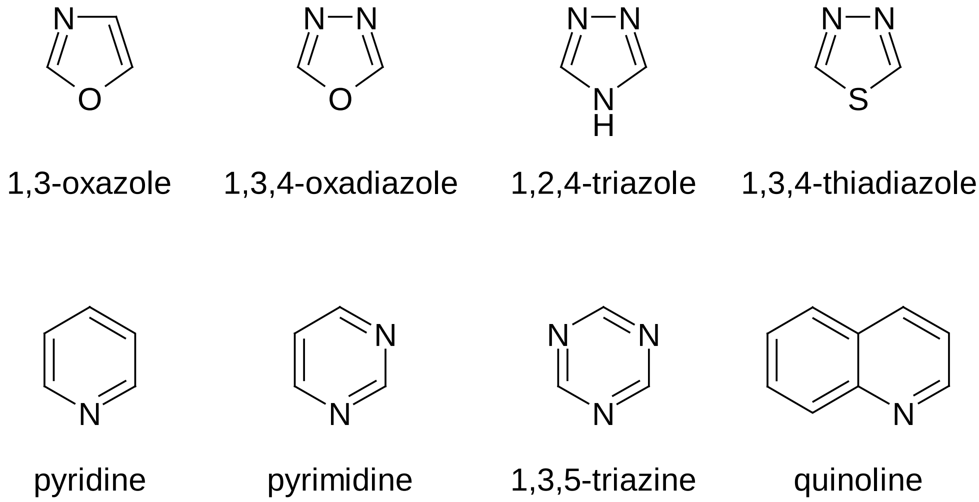

Figure 10. Chemical structures of some electron-deficient moieties for building electron transport materials.

Transport and mobility of organic materials requires knowledge of the charge species. Energy levels of the charge species are usually determined by cyclic voltammetry measurements in solution. Unlike the situation in inorganic materials, primary photo-excitations in organic materials do not directly lead to free charge carriers in general, but to coulombically bound electron-hole pairs, called excitons. One possibility of breaking these excitons into charge carriers is the combination of materials with suitable energy levels for efficient charge separation. In small molecules, charged species are localised spatially, they are simply the cation (positive) and anion (negative) radicals. In polymers, the electron-phonon coupling leads to the so-called polarons which are charges dressed by a reorganisation of the lattice[42]. Polarons may be regarded as defects in conjugated polymer chains, as an example, schematical representation of a polythiophene polaron is shown in Figure 11. Such defect stabilises the charge which is self trapped as a consequence of lattice deformation.

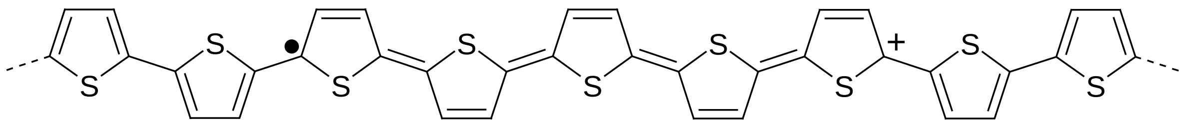

Figure 11. Charged polaron in polythiophene.

1.2.1 Low molecular weight materials

Low molecular-weight organic compounds generally tend to crystallise readily, and hence, they usually exist as crystals below their melting points. Although it had been reported that amorphous or quasi-amorphous films of polycyclic aromatic hydrocarbons are formed by vacuum deposition at a low temperature[43] and a few organic compounds form amorphous glasses at ambient temperatures[44], little attention had been paid to amorphous glasses of low molecular-weight organic compounds until the late 1980s.

The creation of low molecular-weight organic compounds that readily form stable amorphous glasses above room temperature, which are referred as “amorphous molecular materials" or “molecular glasses”, and their structures, reactions, properties, functions and applications has been studied for last three decades by a group headed by Shirota[45]. This work may open up a new field of organic materials science that deals with molecular glasses as distinct from covalently bonded inorganic glasses. Moreover, such amorphous molecular materials may constitute a new class of organic functional materials.

Amorphous molecular materials or molecular glasses are of interest because of the following aspects. They are in a thermodynamically non-equilibrium state and hence may exhibit glass-transition phenomena usually associated with amorphous polymers. The T_g of molecular glasses is understood as the temperature at which molecular motions of a group of molecules, which are caused by intramolecular bond rotations, start to take place, resulting in a change in the position of the gravity of molecules. It is thought that they assume a variety of states such as the amorphous glass, supercooled liquid, and crystal. They may be characterised by the presence of free volume and by the disorder of both intermolecular distance and orientation. They may form uniform, transparent amorphous thin films by vapour deposition and spin-coating methods. In contrast to single crystals and liquid crystals, which show anisotropic properties, amorphous molecular materials may exhibit isotropic properties as well as homogeneous properties due to the absence of grain boundaries. In contrast to polymers, they are pure materials with well-defined molecular structures and definite molecular weights without any distribution.

Nevertheless, low molecular weight materials, which tend to crystallise, are also used in electro-optical devices. For example, tris-8-hydroxyquinoline aluminium (Alq_3) is widely used as electron transport material and green emitter for fabrication of high performance OLEDs. Moreover, perylene derivatives, which carry electron transport and dye function, were successfully used for preparation of fully deposited multi-layer solar cells.

1.2.2 Conjugated organic polymers

In the late 1970s, conjugated polymers were proclaimed as futuristic new materials that would lead to the next generation of electronic and optical devices. It now appears with the discoveries of, for example, organic transistors[46], polymer light-emitting diodes (OLEDs) and solar cells that new technologies are imminent. It has become apparent, from this large body of work, that extensive delocalisation of electrons along the polymer backbone is necessary for a polymer to behave as semiconductor or even as an electrical conductor. This delocalisation of electrons may occur through the interaction of π-electrons in a highly conjugated chain or by a similar interaction of π-electrons with nonbonded electrons of heteroatoms such as sulphur and nitrogen in the backbone. In that way electrochemical polymerisation of aromatic compounds such as thiophene[47], furan, indole[48], carbazole, azulene, pyrene[49], and benzene[50] conjugation has been rapidly extended. Polypyrrole, polyaniline and their derivatives are the most commonly used conjugated polymers because of their relatively superior stability[51]. Other examples include poly(p-phenylene vinylene)s (PPVs), polyfluorenes and polyalkylthiophenes. For some time the application of conjugated polymers has been limited due to their intractability and insolubility, especially in the doped state. This problem was overcome by the use of substituted monomers[52,53] which not only produced processable polymers, but also allowed the polymers obtained to be fully characterised by chemical and physical methods. Conjugated polymers are also widely exploited because of their special characteristics such as low densities, mechanical strength, ease of fabrication, flexibility in design, stability, resistance to corrosion and low cost.

Over the last decade, organic polymeric thin films for photonic applications have been a rapidly growing research area. Conjugated polymers[42,54] are the classes of plastic materials, in which semiconducting characteristics can be observed as given in Figure 12. Conjugated polymers become conducting in the doped state. These are polymers that possess a delocalised π-electron system along the molecular backbone. This system confers semiconducting properties to the polymer and gives it the ability to support positive and negative charge carrier along the polymer chain.

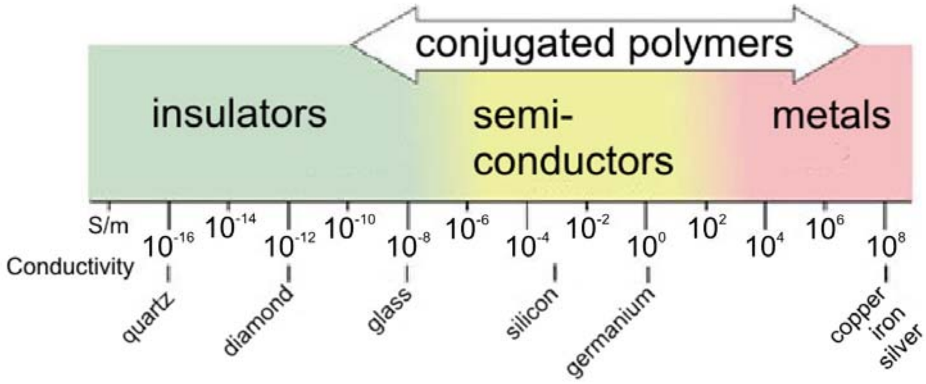

Figure 12. Conductivity of conjugated polymers compared to that of other materials, from quartz (insulator) to copper (conductor). Polymers may also have conductivities corresponding to those of semiconductors. (reference: www.c-science.com/txt/images/2000/001107scns1.jpg)

The electronic and optical properties of π-conjugated polymers result from a limited number of states around the highest occupied and the lowest unoccupied levels. According to the band theory, the highest occupied band, which originates from the HOMO of each monomer unit, is referred to as the valence band and the corresponding lowest unoccupied band originating from the LUMO, as the conduction band. The evolution of bands in a conjugated polymer during its formation by monomer addition is shown in Figure 13.

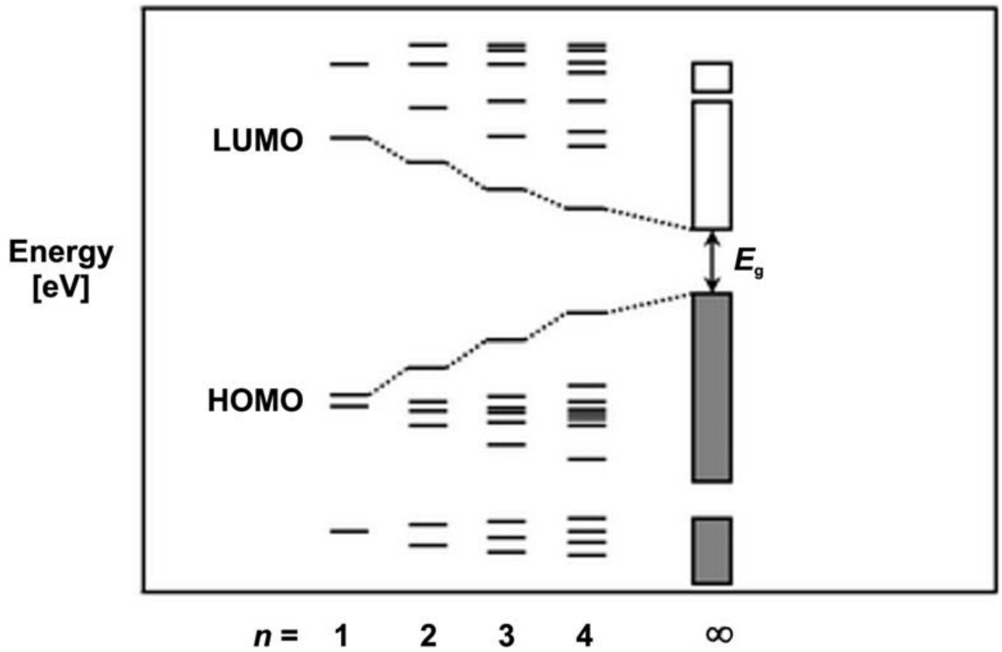

Figure 13. Band formation during the polymerisation of a conjugated monomer into a π-conjugated polymer.[55]

The longer the conjugation on the backbone, the smaller the band gap (E_g). It was generally found that the band gap decreases with increasing conjugation length, approaching a finite value for infinite conjugation length. Torsion between the adjacent rings partially interrupts the conjugation and leads to an effective increase of the band gap.

Due to the fact that the framework of this Ph. D. is based on the synthesis and characterisation of hole transport polymers carrying dye function, a more detailed introduction in chemistry of electron-rich polymers such as polytriphenylamines and polythiophenes as well as low band gap polymers (E_g <1.8 eV) is given below:

Polytriphenylamines

Triarylamine derivatives are well known photoconductors with appreciably high hole transport mobility. The structural unit of triphenylamine responsible for the photoconductive and hole transporting property can be covalently bound with one another or can be attached to a polymer backbone through substituents to obtain a wide variety of low molecular weight compounds as well as polymers. Due to the electron-donating nature of the nitrogen atom in triarylamines, they act as hole-transport materials in various applications like xerography, light emitting diodes, solar cells, photorefractive systems, etc.[56] The wide variety of electro-optical applications require the necessary material properties like thermal stability, non-crystallinity or amorphous film-forming nature and electrochemical reversibility in addition to high electronic-grade material purity. The uses of these compounds in various applications are described in the appropriate contexts.

Two basic properties of the triarylamine unit are the easy oxidizability of the nitrogen centre and its ability to transport positive charge centres via the radical cation species. The creation of positive charges by absorption of light with suitable wavelength and the drift mobility of holes under an applied external field have been extensively studied by Borsenberger et al.[57] and Heun et al.[58] in a variety of TPA derivatives using the time-of-flight method. In amorphous vapour deposited films of low molecular weight TPD derivatives, hole transport mobilities up to 10^{-2} $cm^2 \cdot V^{-1} \cdot s^{-1}$ have been observed[59]. For polymers doped with such TPDs (about 25 wt.-%) hole transport mobilities up to 10^{-3} $cm^2 \cdot V^{-1} \cdot s^{-1}$ have also been achieved[60]. Under the influence of an applied electric field, the transport mechanism for such disordered organic systems is assumed to be a hopping process.

The general synthetic routes to poly(triphenyldiamines) poly(TPD)s are described below and represented in Scheme 1.

First attempts to synthesise main-chain polymeric triarylamines by an Ullmann reaction from diarylaminobiphenyls and diiodides resulted in oligomeric mixtures and insoluble products.[61] A modified Ullmann procedure[62] with 18-crown-6 as phase-transfer catalyst and using diiodides was adopted in our group[63] for the synthesis of soluble and film-forming triarylamine polymers with appreciable high molecular weights. The polymeric TPD with ether spacing[64] was effectively applied as a hole injecting and transport layer in multi-layer OLEDs[65]. This polymer was also employed as a hole transport material in single polymer blend layer devices in combination with a substituted poly(p-phenylene-ethynylene)[66] as emitter.

On the other hand, Hartwig et al.[67] have reported oligomeric and polymeric triarylamines by Pd-catalysed polymerisation of diarylaminobiphenyls and dibromides. The usual method to obtain triarylamines is using a catalyst like $Pd(dppf)Cl_2$ or $Pd(OAc)_2$ or $Pd_2(dba)_3$ in combination with phosphine ligands such as $P(o\text{-tolyl})_3$, dppf [1,1'-bis(diphenylphosphino)ferrocene], BINAP [2,2'-bis(diphenylphosphino)-1,19-binaphthyl] or even $(t\text{-Bu})_3P$ and carry out the reaction under strong basic conditions in benzene or toluene. There are two basic problems in adapting this method for the synthesis of polymers. The first is phosphine arylation resulting in incorporation of phosphorous atoms into polymer chains, which leads to end-capping of chains by phosphine. The second is hydrodehalogenation of aryl halide limiting the formation of high molecular weight polymers. Moreover, the concurring cyclization reactions leading to cyclic oligomers again limit the molecular weight of the polymers[67a]. These difficulties were partially overcome by Hartwig et al. by a suitable selection of phosphine ligands and starting the reaction from "oligomeric monomers". With this modified procedure they obtained some high molecular weight poly(triarylamine)s with meta- and para-linkages[67b].

Suzuki coupling between dibromotriarylamine and phenylene-1,4-diboronic ester also resulted in a sparingly soluble poly(triarylamine) with low molecular weight possessing highly efficient blue photoluminescence[68].

All synthetic methods for preparation of polymeric triarylamines described above are illustrated in Scheme 1.

Scheme 1. Synthetic methods for poly(triphenyldiamines), poly(TPD)s.

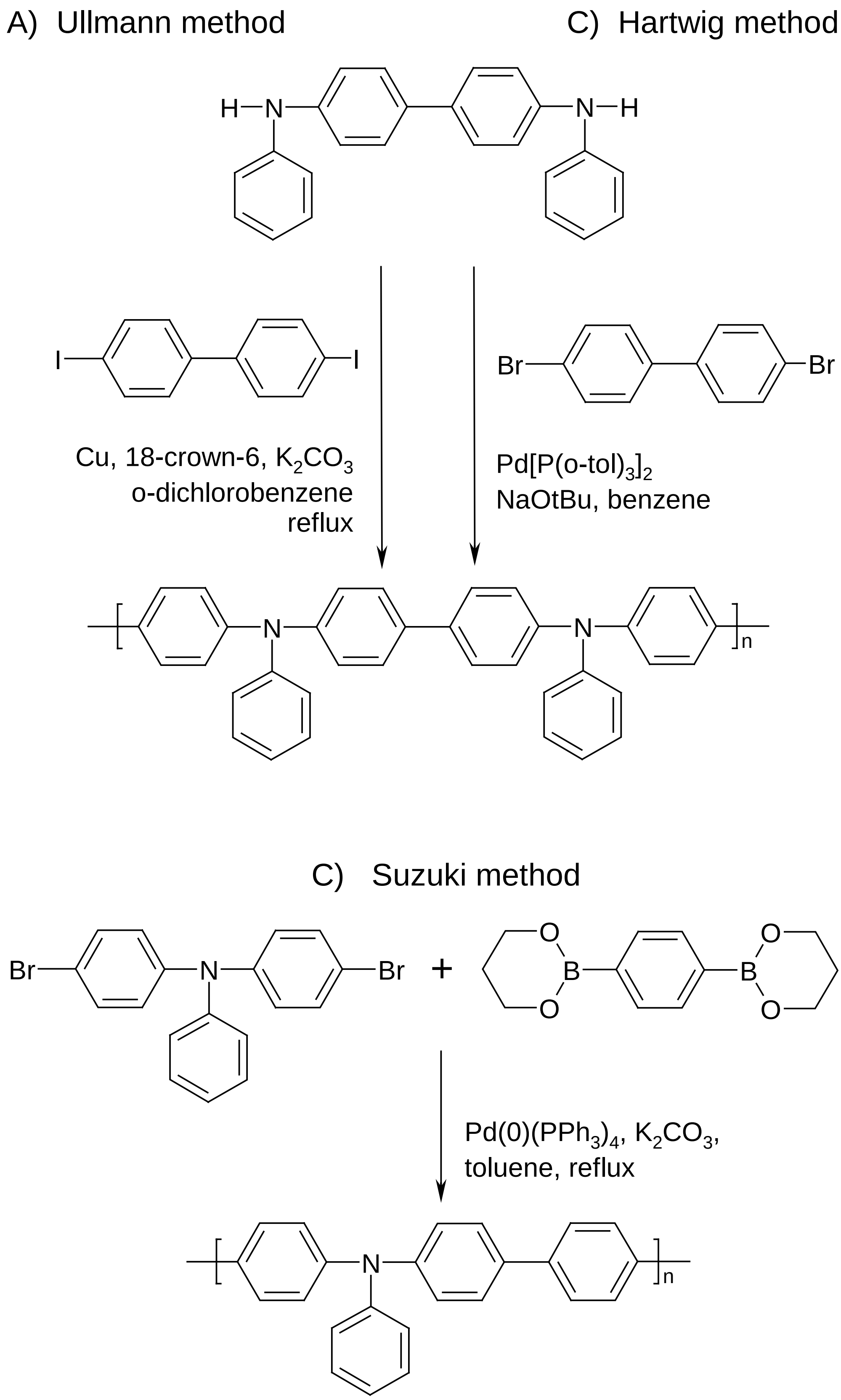

In order to optimise the hole injection and transport properties of emissive polymers, the triarylamine units were incorporated into classical emissive polymers like PPV or poly(9,9-

dialkylfluorenes) to obtain alternating copolymers[69] with a wide range of structures and resulting electronic properties. The copolymers of triarylamine and 9,9-dialkylfluorenes[63,70] were found to exhibit high hole transport mobilities in the range of 10^{-4} to 10^{-3} $cm^2 \cdot V^{-1} \cdot s^{-1}$ as measured by time-of-flight method at a field of 2.56105 $V \cdot cm^{-1}$. Kim et al.[71] reported the first triarylamine-distyrylbenzene emissive copolymers with solubilizing ether and urethane spacers. Later, a series of differently substituted distyrylbenzene units were incorporated as co-monomers in order to obtain copolymers with emission in the desired visible range as well as maintaining the good hole injection and hole transport properties of triarylamine polymers[72].

Thus, the well-known class of triarylamine compounds, which are excellent hole transport compounds, were presently applied in xerography. Nowadays, they slowly finds its way into other electro-optical applications like OLEDs, organic solar cells, photorefractive holography, etc. Such wide application spectrum of triarylamines can be attributed as being due to the feasibility of structural modification and incorporation of this moiety into other functional polymers. On the other hand the concept of copolymers opens up an intelligent way of incorporating different functionalities into one polymer maintaining the good hole injection and hole transport properties of triarylamines.

Polythiophenes

Polythiophenes are an important representative class of conjugated polymers that form some of the most environmentally and thermally stable materials that can be used as electrodes[73], sensors[74], transistors[75], polymer LEDs[76], solar cells etc. Polythiophene and its derivatives work very well in some of the above applications and less impressively in other devices. Creative new design and development strategies of new polythiophenes has led to interesting new materials and enhanced performance in certain devices. The ability of molecular designers to begin understanding how to gain control over the structure, properties, and function in polythiophenes continue in order to make the synthesis of polythiophenes a critical subject in the development of new advanced materials.

Pure polythiophene without side chains is neither soluble nor fusible. Once the polymer is prepared, it’s not possible to further process the obtained film or powder. However, side chains, which give solubility and fusibility to the polymer, can be attached to the thiophene ring. The most widely used polymer is the poly(3-hexylthiophene) (P3HT).

Since 3-alkylthiophene is not a symmetrical molecule, the band gap and conductivity of poly(3-alkylthiophene)s are strongly dependent on regioregularity of these polymers. There are three relative orientations available when two thiophene rings are coupled between the 2- and 5- positions as given in Figure 14. The first of these is head-to-tail (HT) coupling, the second is head-to-head (HH) coupling and the third is tail-to-tail (TT) coupling. HT coupling of 3-alkyl thiophene plays key role in the synthesis of regioregular polymer. If HH and TT couplings take place, the irregular polymer will be obtained. Regioregular polymer has lower band gap and higher conductivity compared to irregular one.

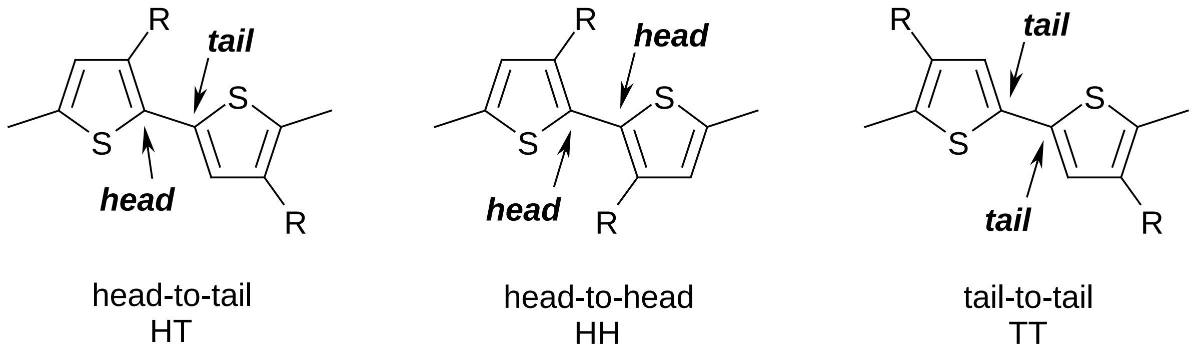

Figure 14. Possible couplings between two 3-alkylthiophenes along the polymer chain.

Polymerisation of 3-alkylthiophenes can be carried out in many different ways as given in Scheme 2 and these methods have recently been excellently described by R. D. McCullough[77] and Katz et al.[78] The most commonly used methods are the following:

1) Electropolymerisation of the monomers, mostly for the preparation of films of insoluble polymers. Electropolymerisation of 3-alkylthiophenes giving irregular polymers, with approximately 70% of the HT-coupling.[79]

2) Grignard coupling of 2,5-diiodo-substituted 3-alkylthiophenes gives random polymers, with approximately 50–60% of the HT-coupling.[80]

3) Polymerisation with $FeCl_3$[81] which is simple, is generally known to give irregular polymers, approximately 70–80% HT, although exceptions with regioselective polymerisation exist.[82] The formed polymers are in the doped state and must be dedoped before they become soluble and fusible.

4) The McCullough method giving regioselective polymerisation, based on a Grignard type of reaction. The regioregularity is generally 98% HT. McCullough and co-workers have recently described a simplified method based on Grignard coupling.[83]

5) Rieke has developed a method for preparing regioregular 3-alkylthiophenes using zinc and a special catalyst ($Ni(dppe)Cl_2$).[84] The HT content in the polymer is also generally 98% HT.

6) Two other methods for preparing regioregular polymers via Pd-catalysed polymerisation of 3-alkylthiophenes using Suzuki[85] or Stille[86] coupling instead of Grignard coupling have also been developed.

Scheme 2. Synthetic methods for regioregular and regiorandom poly(3-alkylthiophene)s.

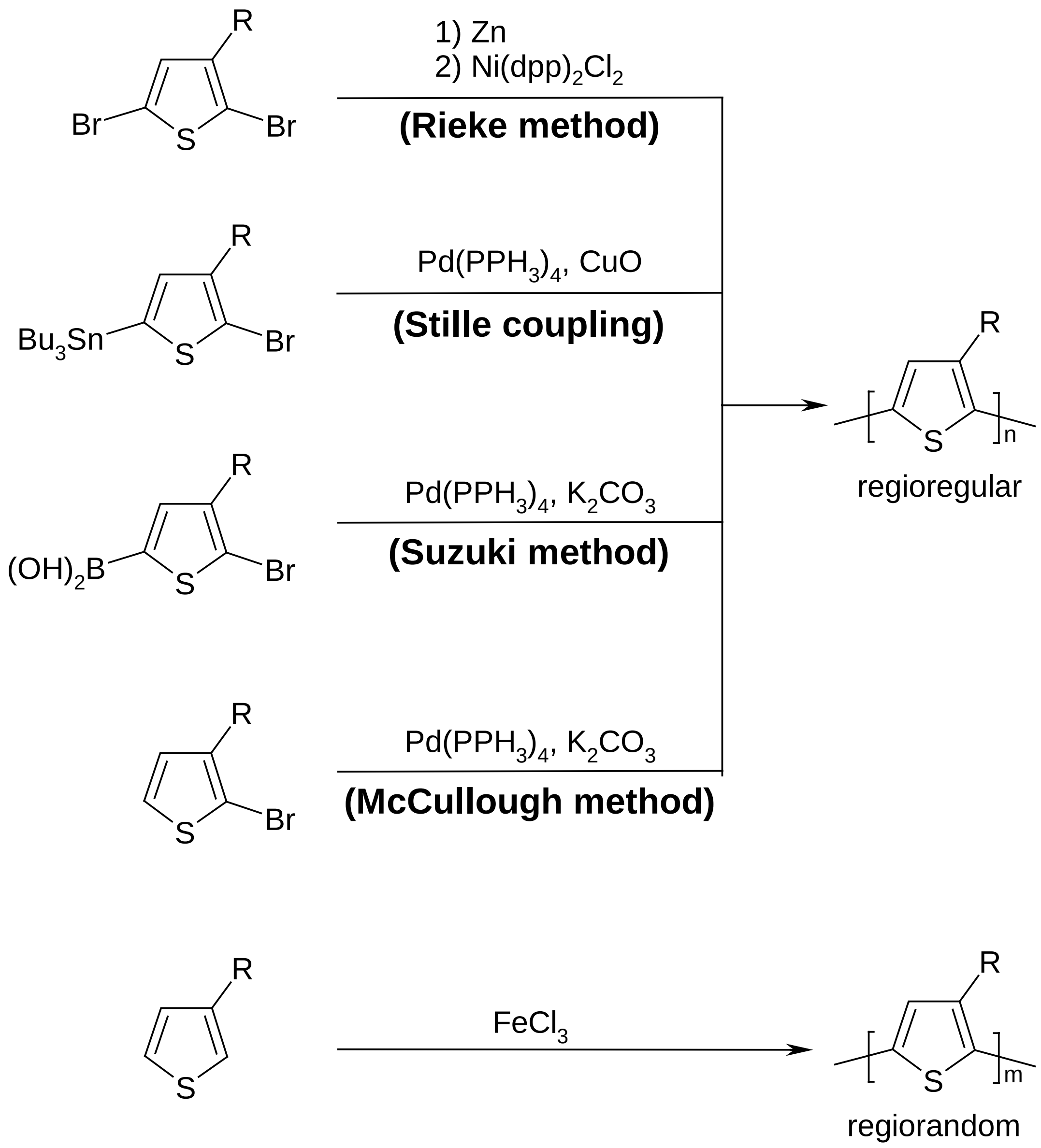

Low band gap polymers

An ongoing research goal for application of conducting polymers in solar cells has been the reduction of the energy band gap (E_g) so that the absorption of the undoped polymer shifts from the green towards the red region of the electromagnetic spectrum. In 1992 Roncali published an excellent review about amazing properties of low band gap thiophenes derivatives[87]. In this review, synthetic principles for band gap control are presented in such a way as to get low band gap materials based on thiophenes.

The efficiency of polymer based bulk heterojunction devices could also be steadily increased using low band gap polymers, which absorb further into red and, thus, overlap with the solar spectrum efficiency. Despite considerable innovative developments in the field of conducting polymers, only few low band gap polymers (E_g < 1.8 eV) are known[87,**88**]. Since the first synthesis of polyisothianaphthene (poly(ITN)) as a low band gap conducting polymer was reported[**89**], variously substituted analogues of poly(ITN)s were obtained by oxidative polymerisation of the corresponding ITN derivatives. Poly(ITN) was one of the first examples of this class of materials with a band gap of 1 eV. Moreover, the low band gap polymers were successfully used in solar cells[**90**,**91**] and red/near-IR OLEDs[**92**,31]. Figure 15 shows the chemical structures of some of these polymers.

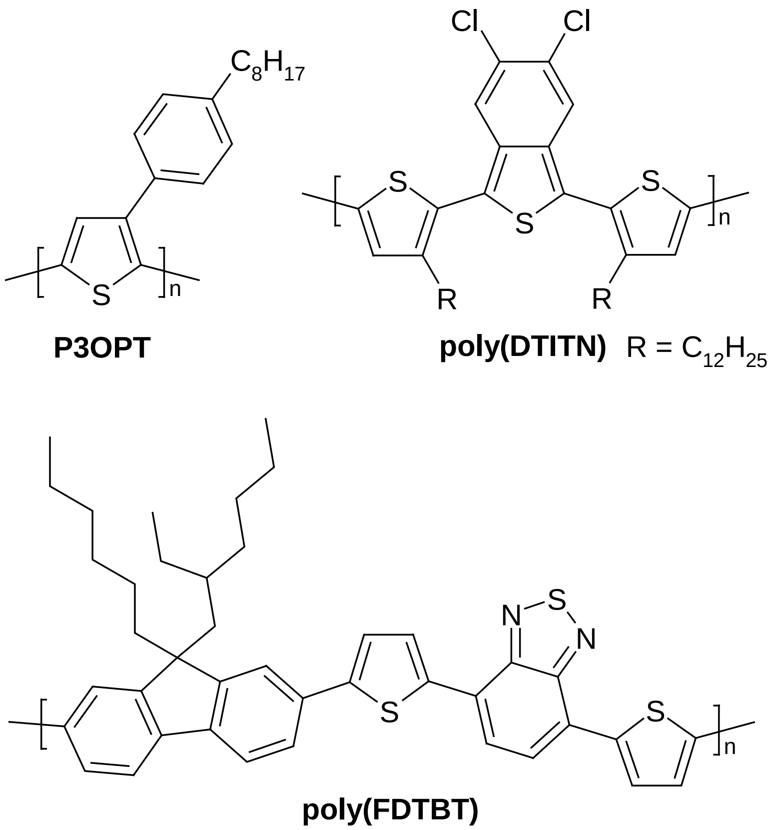

Figure 15. Chemical structures of low band gap polymers used in plastic solar cells. P3OPT – poly(3-(4-octylphenyl)thiophene); poly(DTITN) – poly(1,3-dithienylisothianaphthene); poly(FDTBT) - poly(2,7-(9-(2'-ethylhexyl)-9-hexyl-fluorene)-alt-5,5-(4',7'-di-2-thienyl-2',1',3'-benzothiadiazole)).

2 Motivation and aim

During the last two decades, the field of synthesis and characterisation of functional molecules with extended π-electron delocalisation gained more attention. Among the development of new applications using organic semiconducting materials, organic light emitting diodes and displays are today entering the market. Furthermore, the combination of conjugated polymers with fullerenes enabled the fabrication of inexpensive and flexible large-area solar cells and photodetectors. For many of the electro-optical applications, a balanced transport of holes and electrons is important. Electron deficient molecules like perylenebisimide and fullerene have been found as excellent electron transport materials for photovoltaic applications. In contrast to the solar cells, the mostly used electron transport material in OLED technology is Alq_3. Moreover, dye functionality such as absorption (solar cells) or emission (OLEDs) is also required.

The aim of present Ph. D. thesis is the synthesis and characterisation of bifunctional materials combining the hole transport property and dye functionality. Thus, the strategy of this work is obtaining novel hole transport dyes. These materials should also possess environmental stability to be helpful for electro-optical applications.

For the purpose described above, the following candidates were chosen as building blocks for desired hole transport dyes. Nowadays, the triphenylamines are well known as good hole conductors due to their ability to form stable radical cation under photoexcitation. However, triphenylamines are characterised by a large band gap. Another candidate is isothianaphthene (ITN). Its polymer analogue, poly(ITN) is characterised by a band gap as low as 1 eV. Additionally, the well-known stable ITN derivative, dithienylisothianaphthene (DTITN) can be utilised for the light harvesting in solar cells. Thus, triphenylamine and 1,3-dithienylisothianaphthene building blocks were chosen for obtaining new class of materials, called dithienylisothianaphthene phenyldiamines (DTITNPDs). The synthesis of low molar mass as well as polymeric DTITNPDs is the main aim of this work. In the synthesis of these new polymers care should be taken to introduce solubilising groups so that the resulting polymers are soluble and, hence, solution processable. Additionally, influence of substituents onto the different properties of DTITNPDs should be studied in order to obtain materials with desired optical and electronic properties. HOMO energy level in triphenyldiamines and LUMO energy levels in thiophenes can be varied depending on substituents. Tuning of energy levels should allow decreasing of the band gap and better matching of HOMO/LUMO levels of these molecules to those of electron transport compounds.

In order to study the influence of incorporation of triphenylamine moieties into dithienylisothianaphthene on the energy levels of resulting molecules, theoretical calculations were carried out. The MOPAC calculations of HOMO/LUMO distribution of DTITN and DTITNPD (delocalisation of HOMO/LUMO) were performed using theoretical MOPAC calculations in the gas phase. All computer simulation and semi-empirical molecular orbital calculations were carried out by Privatdozent Dr. Lothar Kador from Department of Experimental Physics IV, University of Bayreuth using MOPAC version 6.0 and CERIUS version 6.0 software.

Results of MOPAC calculation of HOMO/LUMO values and a graphical representation of HOMO distribution for basic units **DTITN** and **DTITNPD** are given below. In DTITN, both HOMO and LUMO are distributed among ITN and thiophene rings.

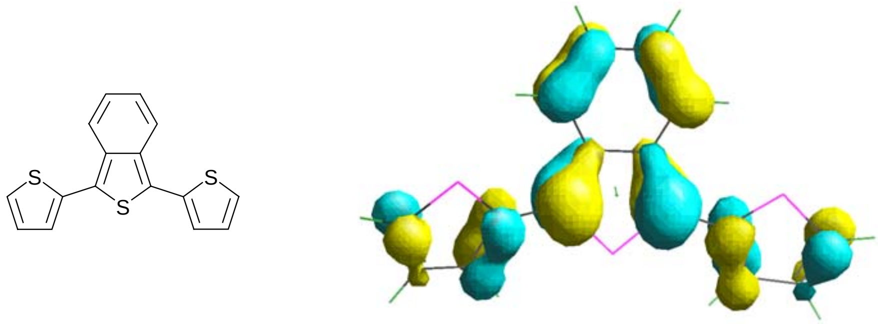

Figure 16. Graphical representation of HOMO distribution for DTITN as a result of MOPAC calculations.

Now the question here was to estimate the influence of introduction of diphenylamine groups into a DTITN moiety on HOMO and LUMO resulting in DTITNPD. The molecular orbital calculations of the DTITNPD were carried out, and the result is given below.

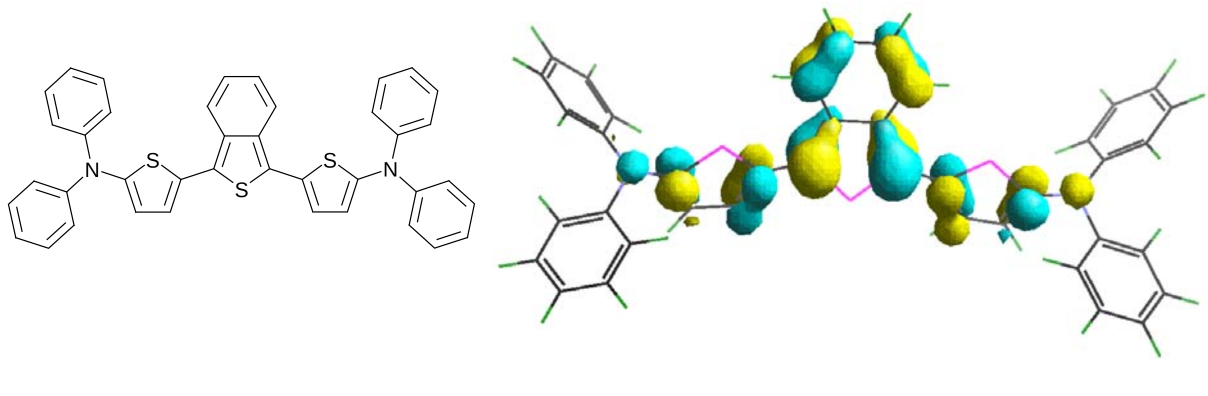

Figure 17. Graphical representation of HOMO distribution for DTITNPD from MOPAC calculations.

It can be clearly seen that the HOMO distribution in DTITNPD is more delocalised than in DTITN. This should help to transfer and transport the holes created by absorption of photons in a better way in DTITNPD than in DTITN. As expected, the LUMO energy distribution is not influenced by the introduction of diphenylamine groups and it is concentrated on the DTITN part of the molecule due to high electronegativity of ITN group (LUMO distribution not shown here). Thus, theoretical calculations showed that introducing triphenylamine units into DTITN should lead to novel DTITNPD with improved hole transport properties and lower band gap due to more delocalised electron density in the HOMO of DTITNPD.

The properties of DTITNPDs can be studied using different techniques described below. Absorption and emission can be examined using UV-Vis and fluorescence spectroscopy. HOMO/LUMO energy levels and electro-chemical stability can be examined using cyclic voltammetry. Thermal stability can be studied using TGA measurements and important parameter like T_g can be observed using DSC.

If the novel DTITNPDs should possess low band gap nature ($E_g < 1.8$ eV), they can be tested as hole transport dyes in organic solar cells. In the case that they would exhibit bright red photoluminescence, such compounds may be used as red-emitters with improved transport property in OLEDs.

Thus, the main aim of this work is to design a suitable synthetic strategy to combine DTITN and triarylamine units into low molecular weight compounds as well as polymers. After a successful synthesis and characterisation of these novel materials, some of the suitable candidates may also be tested in appropriate devices.

3 Monomers

In sections 3.1 and 3.2, the synthesis and characterisation of 1,3-di-2-thienylbenzo[c]thiophenes (DTITNs) as monomers for the ferric chloride oxidative polymerisation are highlighted. Synthesis and characterisation of di(halogeno)-1,3-di-2-thienylbenzo[c]thiophenes and bis(secondary amine)s for polycondensation are described in sections 3.3 and 3.4.

3.1 Synthesis of 1,3-di-2-thienylbenzo[c]thiophenes (DTITNs **1-3**)

In this chapter, synthesis of the monomers, 1,3-di-2-thienylbenzo[c]thiophenes (DTITNs) **1-3** is described. The synthetic strategy of compounds **1-3** is given in Scheme 3. The properties of **1-3** are compared in section 3.2. The preparation of **1** was used as a model reaction for the synthesis of monomers **2** and **3**. Compound **1** was also used for the synthesis of 1,3-bis(5-halogeno-2-thienyl)benzo[c]thiophenes. The substituents in **2** and **3** were introduced to get soluble polymers via oxidative polymerisation.

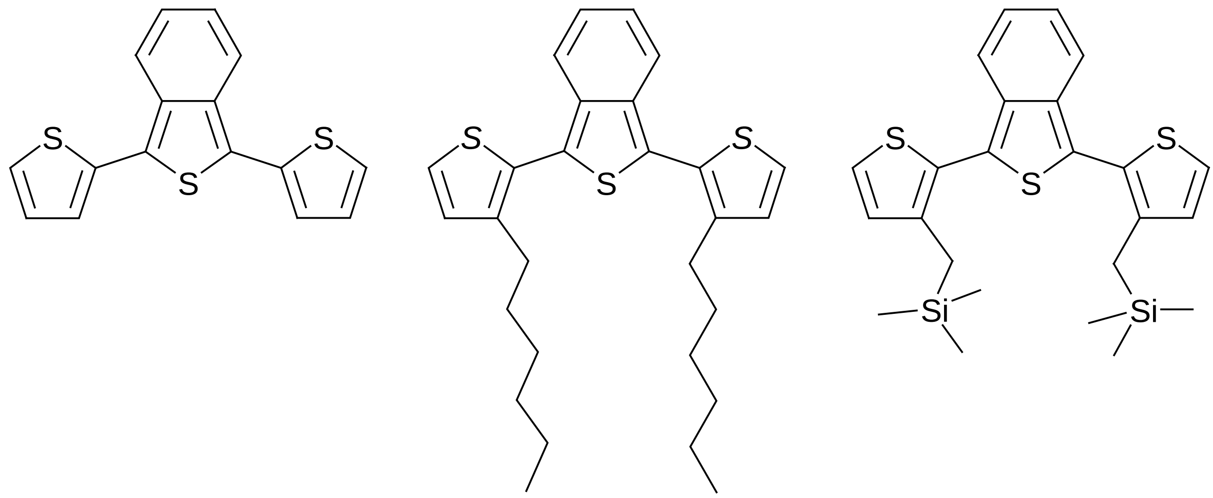

1 **2** **3**

*Figure 18. 1,3-di-2-thienylbenzo[c]thiophenes **1-3**.*

Generally, DTITNs are prepared by the ring close reaction of dithienyl phenyl diketones using sulfirising reagents like diphosphorpentasulfide P_2S_5 or Lawesson's reagent. Compounds **1-3** were prepared from 3-alkylsubstituted-2-bromothiophenes by Grignard reaction with a dithioester followed by ring closure. For the synthesis of compound **1**, commercially available

2-bromothiophene was used. First, diketones, carrying substituents at 3-position of thiophene ring, were isolated after Grignard reaction. These diketones were then converted by ring-closure reaction with a sulfirising Lawesson's reagent into target compounds **1-3** with yields of 66 %, 81 % and 88 % respectively. The dithioester, reported above, was synthesised by esterification of 2-mercaptopyridine using phthaloyl dichloride. The starting compounds, 3-substituted-2-bromothiophenes were synthesised by a two-step procedure. The first step was a coupling of 3-bromothiophene via Kumada reaction to obtain 3-alkylsubstituted thiophenes. The second step was a standard bromination of 3-alkylsubstituted thiophenes with N-bromosuccinimide.

The oxidative polymerisation of unsubstituted 1,3-di-2-thienylbenzo[c]thiophene **1** by anhydrous ferric chloride led only to an insoluble dark powder, containing dimer, trimer and tetramer of **1** as reported by Mohanakrishnan et al.[93] Due to this fact, only monomers **2** and **3**, carrying solubilising substituents, were used for oxidative polymerisation.

Scheme 3. Synthesis of 1,3-di-2-thienylbenzo[c]thiophenes ***1-3***.

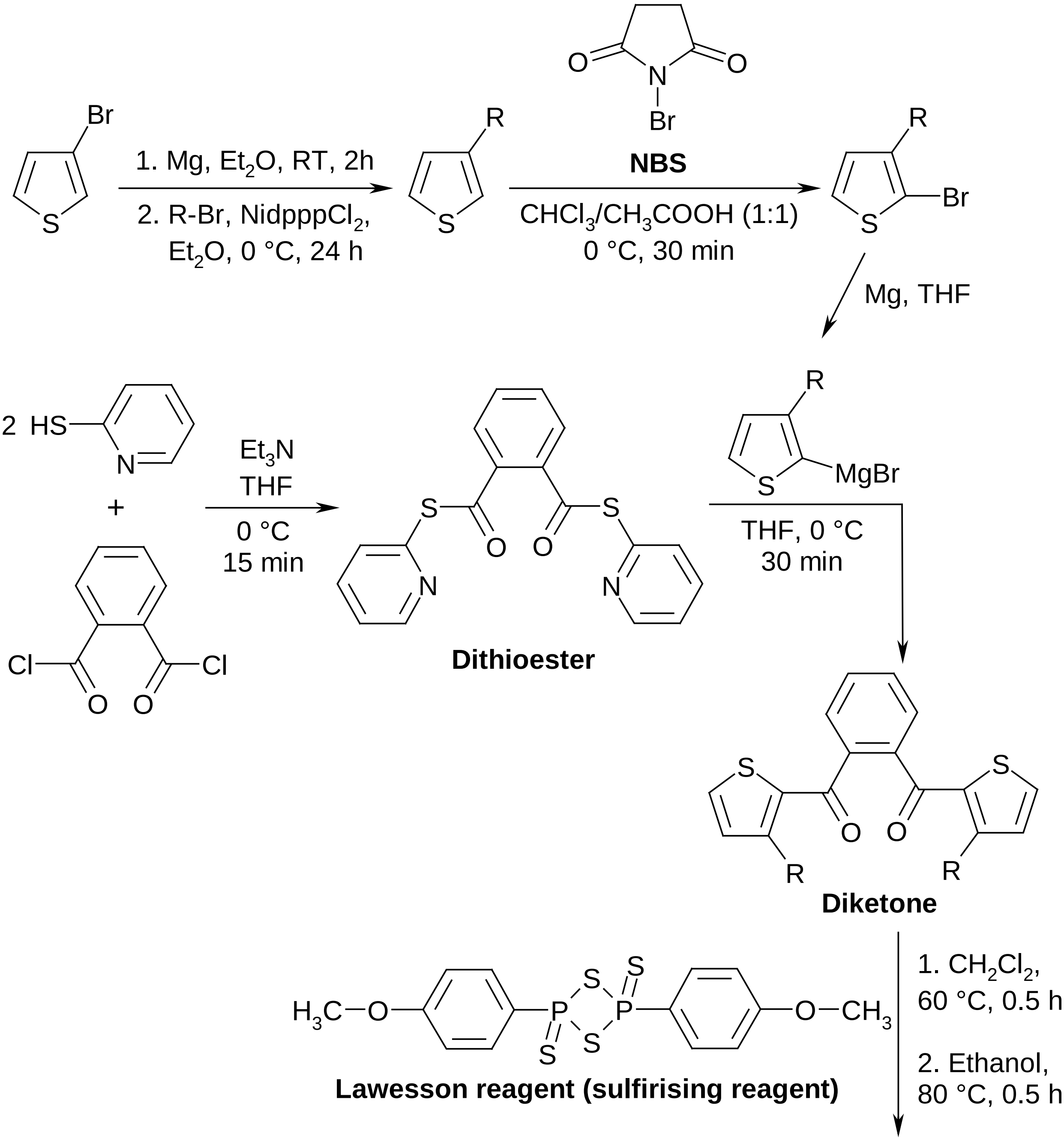

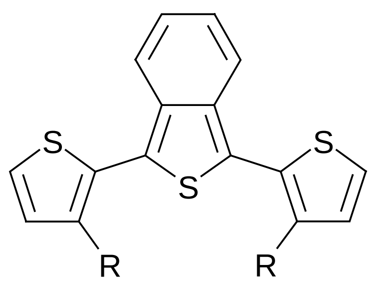

1-3

Monomer	**1**	**2**	**3**
R	H	n-hexyl	(trimethylsilyl)methyl

3.2 Characterisation

3.2.1 Proton Nuclear Magnetic Resonance (^{1}H-NMR) and Fourier Transformed Infrared (FT-IR) spectroscopy

1,3-di-2-thienylbenzo[c]thiophenes **1-3** were characterised by proton NMR spectroscopy. The details, such as chemical shifts and integral of resonance signals, are given in the experimental part. As an example, a ^{1}H-NMR spectrum of monomer **2** is shown in Figure 19.

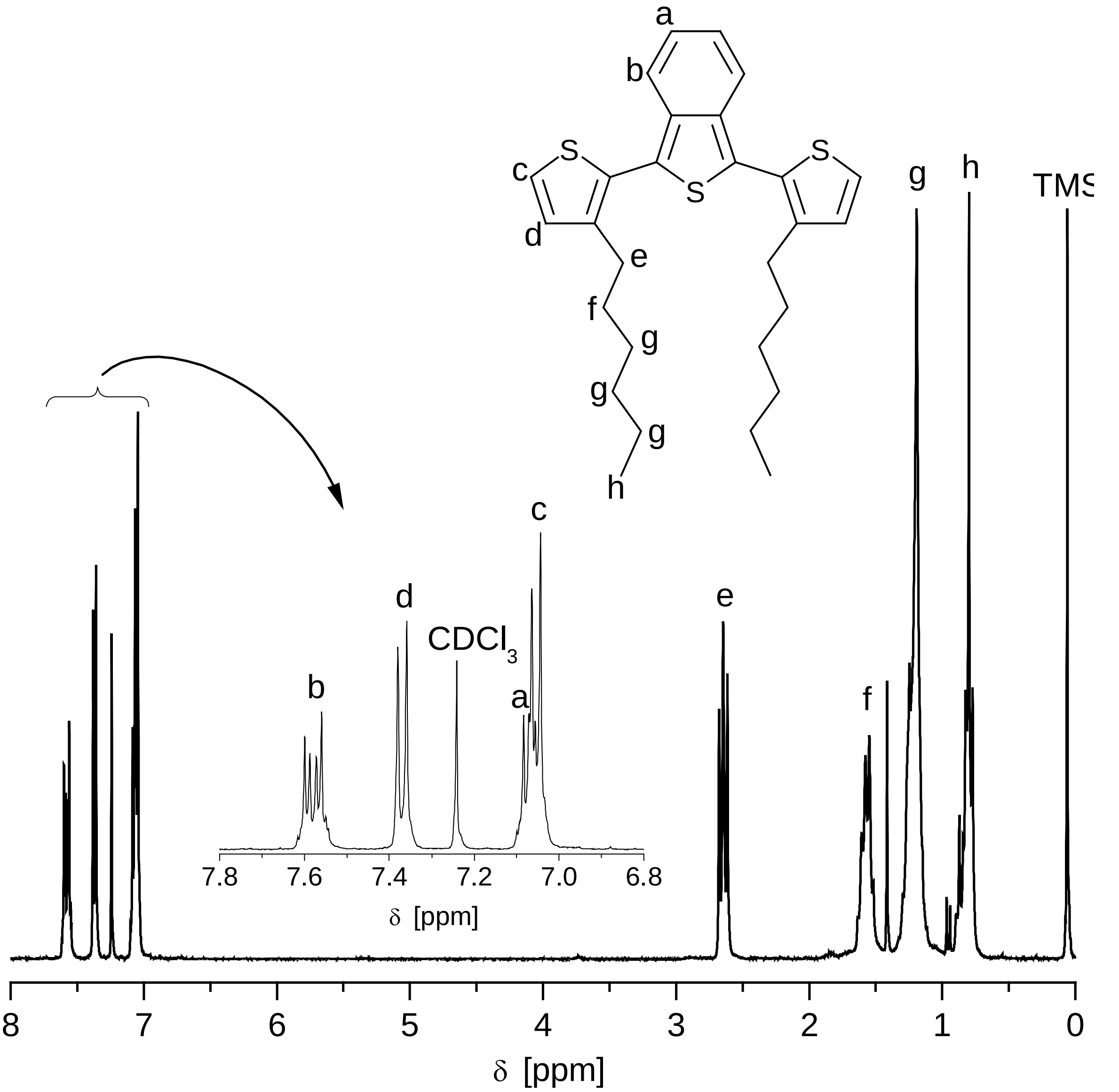

*Figure 19. ^{1}H-NMR spectra (250 MHz, $CDCl_3$, 25 °C) of compound **2**.*

NMR signals from methyl protons **h** were detected in a region of 0.5 to 1.0 ppm. Methylene protons **g** shows the resonance signals in a region of 1.0 to 1.5 ppm, and then follows the resonance signals of methylene protons **f**. The methylene protons **e**, which are close to the thiophene ring, show resonance at about 2.6 ppm. NMR signals from protons, belonging to heterocyclic conjugated system, were observed in a region of 7 to 8 ppm. Two characteristic multiplets **a** and **b** belonging to benzo[c]thiophene protons were detected at 7.05 and 7.60 ppm. Two characteristic doublets **c** and **d** from thiophene protons are also obtained at about 7.0 and 7.4 ppm. Compounds **1** and **3** were characterised in a similar manner (spectra not shown).

FT-IR data for monomers **1-3** are given in the experimental part. Characteristic C-H stretchings of thiophene ring at regions of 740 cm^{-1} and of 1500 cm^{-1} were observed for all of these compounds. The strong IR absorption at 2956, 2926 and 2856 cm^{-1} due to C-H stretching in hexyl side chains was detected for DTITN **2**, carrying hexyl groups. The strong signals at 2955 and 2893 cm^{-1} due to C-H stretching in (trimethylsilyl)methyl side chains were also observed in DTITN **3**, carrying (trimethylsilyl)methyl substituents.

3.2.2 Optical properties via UV-Vis and Fluorescence spectroscopy

The optical properties of monomers **1-3** were studied by measuring UV-Vis and fluorescence spectra in solution (n-hexane), and the data are summarised in Table 2. The absorption spectra of compounds **1-3** are given in Figure 20.

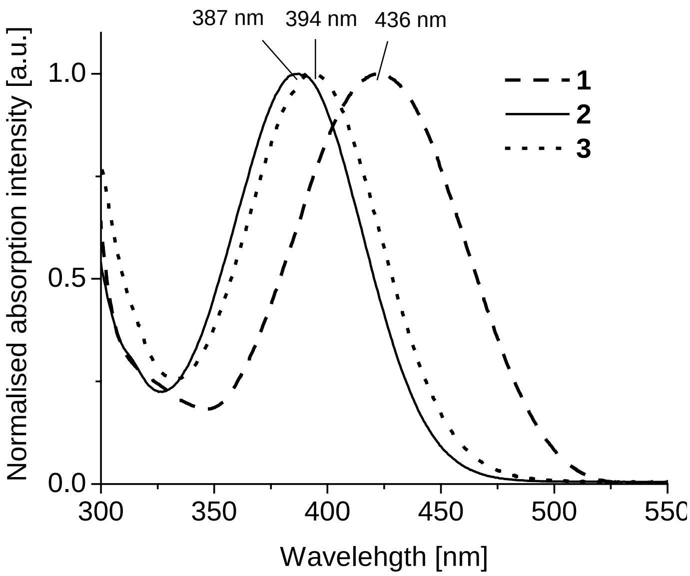

*Figure 20. UV-Vis spectra of 1,3-di-2-thienylbenzo[c]thiophenes **1-3** measured in n-hexane.*

1,3-di-2-thienylbenzo[c]thiophenes, **1-3** show an absorption spectra with one absorption band in the visible region. Compounds **2** and **3** have similar absorption with maxima, close to each other at 387 and 394 nm, and absorption edges at 444 and 456 nm respectively. Unsubstituted 1,3-di-2-thienylbenzo[c]thiophene **1** shows a red shift in the absorption spectra of about 50 nm compared to compounds **2** and **3**, which carry hexyl and (trimethylsilyl)methyl substituents respectively. This can be explained as follows. The steric hindrance due to the two hexyl substituents in monomer **2** and two (trimethylsilyl)methyl substituents in monomer **3** causes a stronger torsion around the C-C inter thiophene ring bonds, which leads to a lower conjugation. Optical band gap energies (E_g^{opt}) of corresponding 1,3-di-2-thienylbenzo[c]thiophenes **1-3,** calculated from absorption edges by putting tangents on the absorption shoulder, are 2.49, 2.79 and 2.72 eV respectively (see Table 2).

Fluorescence spectra of monomers **1-3** measured in n-hexane solutions are shown in Figure 21. 1,3-di-2-thienylbenzo[c]thiophenes **1-3** show greenish-yellow fluorescence. The fluorescence spectra of monomers **1-3** are very similar with maxima at 530, 517 and 522 nm respectively.

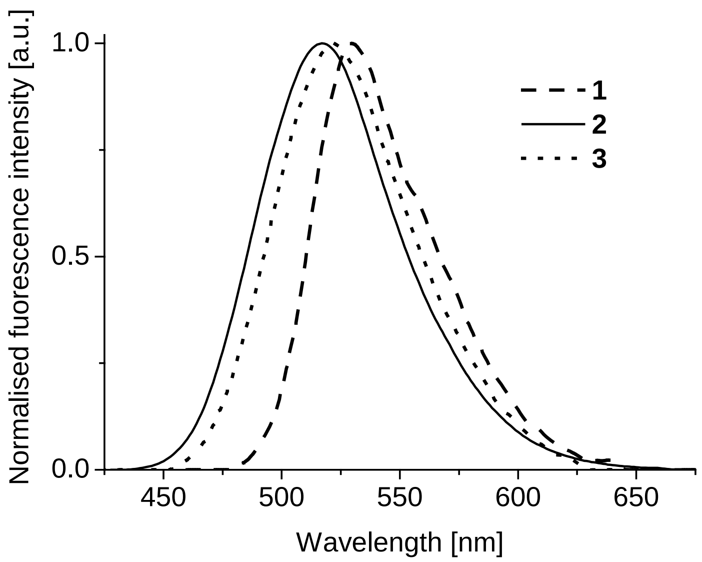

*Figure 21.Fluorescence spectra of 1,3-di-2-thienylbenzo[c]thiophenes **1-3** measured in n-hexane.*

*Table 2. Optical properties of 1,3-di-2-thienylbenzo[c]thiophenes **1-3** measured in n-hexane.*

Monomer	**UV-Vis absorption**				**Fluorescence**
	λ_{max}^{abs} [nm]	E_g^{opt} (from λ_{max}^{abs}) [eV]	Absorption edge [nm]	E_g^{opt} (from edge) [eV]	λ_{max}^{fl} [nm]
1	436	2.84	497	2.49	530
2	387	3.16	444	2.79	517
3	394	3.11	456	2.72	522

λ_{max}^{abs} – wavelength of maximum absorption [nm]
E_g^{opt} – optical band gap
λ_{max}^{fl} – wavelength of maximum fluorescence [nm]

3.2.3 Cyclic Voltammetry (CV)

The electrochemical stability and the reversibility of the redox processes of 1,3-di-2-thienylbenzo[c]thiophenes **1-3** were studied using cyclic voltammetry (CV). The measurements were carried out using a glassy carbon electrode in a solution of carefully dried THF containing 0.1 M tetrabutylammonium hexafluorophosphate ($TBAPF_6$) at room temperature. The potentials were measured against $Ag/AgNO_3$ as the reference electrode and each measurement was calibrated with the ferrocene/ferrocenium (Fc) redox system as internal standard[94]. The HOMO and LUMO energy values of the compounds were determined from the first oxidation and the first reduction potentials (E_{ox1} and E_{red1}) respectively, by taking the value of -4.8 eV as a HOMO energy level for the Fc with respect to zero vacuum level as described by Pommerehne et al.[95] Electrochemical properties of monomers **1-3** are summarised in Table 3.

Electrochemical stability of all these compounds was examined by measuring repeated cycles of redox processes. 1,3-di-2-thienylbenzo[c]thiophenes **1-3** show completely reversible reduction steps and irreversible oxidation steps for the entire scanning rate in a region of 50 $mV{\cdot}s^{-1}$ to 500 $mV{\cdot}s^{-1}$. Monomers **1-3** show first reduction potentials (E_{red1}) of -2.17, -2.48 and -2.38 V vs. ferrocene respectively and similar oxidation behaviour with the first oxidation potentials (E_{ox1}) of 0.46, 0.54 and 0.60 V respectively as shown in Figure 22.

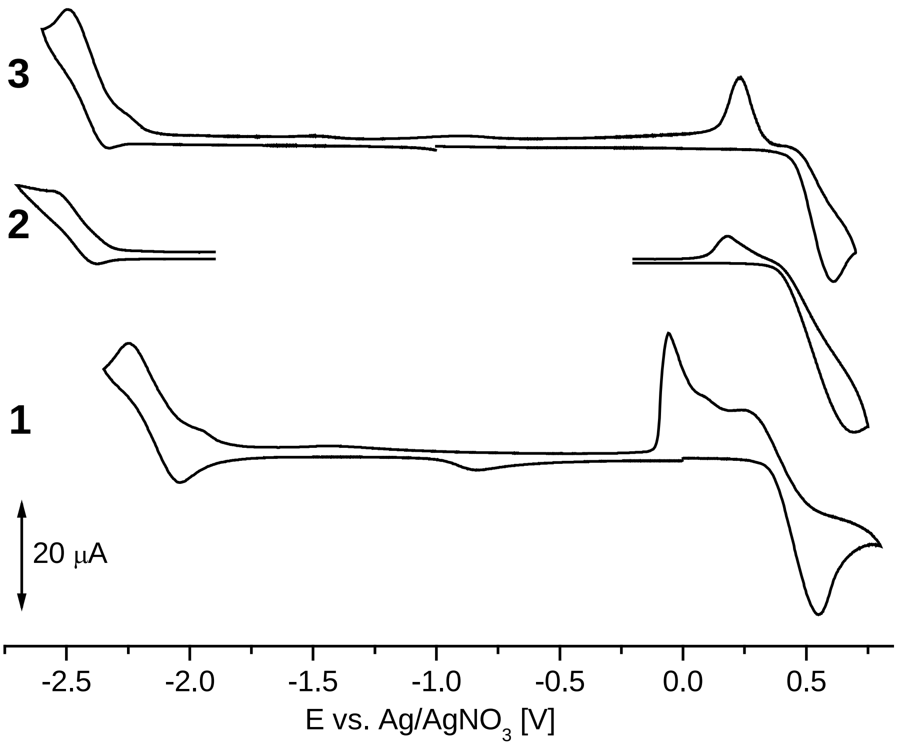

*Figure 22. Cyclic voltammograms of 1,3-di-2-thienylbenzo[c]thiophenes **1-3**.*

As an example, the repeated cyclic voltammograms, measured at a scanning rate of 50 $mV \cdot s^{-1}$, showing irreversible oxidation behaviour of compound **1** is given in Figure 23. The first cycle of oxidation to a radical monocation takes place at a potential of 550 mV vs. $Ag/AgNO_3$. This radical cation undergoes chemical reaction and a reduction peak at about 340 mV vs. $Ag/AgNO_3$ is observed on back reduction of radical cation. In the second cycle, a new oxidation step below the E_{ox1} from the 1st cycle is observed, which is also reversible, indicating the formation of some electrochemically stable oligomers. The same electrochemical behaviour was observed in the cyclic voltammograms of monomers **2** and **3**. This result also indicates that compounds **1-3** can be oxidatively polymerised. This behaviour is common to thiophenes which do not carry substituents at 2-position.

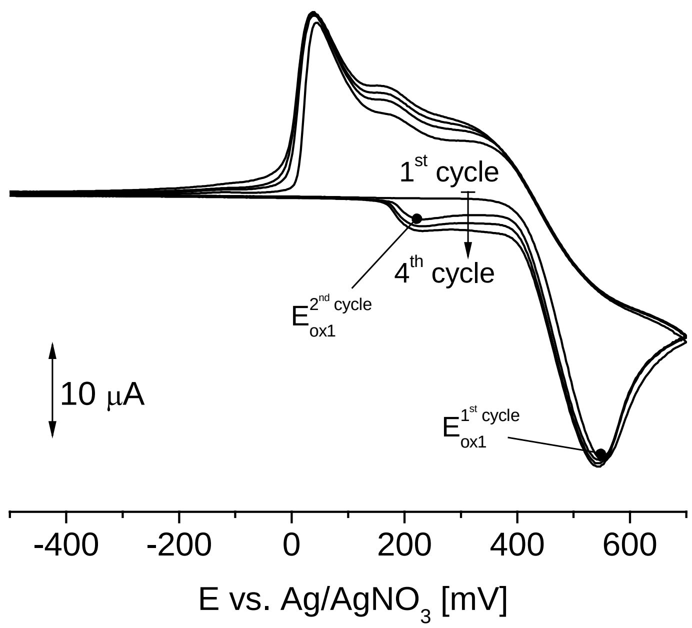

Figure 23. Cyclic voltammogram with four repeated scans of 1,3-di-2-thienylbenzo[c]thiophene ***1*** *in THF at room temperature.*

The corresponding HOMO and LUMO values for all of these compounds, determined from the first oxidation and reduction potentials with respect to ferrocene/ferrocenium (Fc) as an internal standard, are presented in Table 3. Monomers **1-3** have similar HOMO values of about -5.3 eV and LUMO values of -2.63, -2.32 and -2.42 eV respectively. This result clearly shows that LUMO levels in 1,3-di-2-thienylbenzo[c]thiophenes can be appreciably manipulated by introducing substituents at 3-position of thiophene ring. Moreover, it also indicates that the substituents at 3-position on outer thiophene rings make the molecules less electronegative and increases reduction potential. The electrochemical band gap (E_g^{ec}) values, given in Table 3, were calculated using the difference between HOMO and LUMO levels of compounds **1-3**. These values have a difference of about 0.25 eV with the optical band gap

(E_g^{opt}) values obtained from absorption band edges that were measured in solution (see Table 3).

*Table 3. Electrochemical properties of 1,3-di-2-thienylbenzo[c]thiophenes **1-3**.*

Monomer	$^*E_{ox1}$ [V]	HOMO [eV]	$^*E_{red1}$ [V]	LUMO [eV]	E_g^{ec} [eV]	E_g^{opt} [eV]
1	0.46	-5.26	-2.17	-2.63	2.63	2.49
2	0.54	-5.34	-2.48	-2.32	3.02	2.79
3	0.60	-5.40	-2.38	-2.42	2.98	2.72

* - calculated vs. ferrocene
E_{ox1} and E_{red1} – first oxidation and reduction potentials respectively
E_g^{ec} – electrochemical band gap
E_g^{opt} – optical band gap

3.3 Synthesis of 1,3-bis(5-halogeno-2-thienyl) benzo[c]thiophenes **4, 5**

For the purpose of metal-catalysed coupling reactions, halogeno derivatives of DTITN are required. Therefore, the dibromo derivative **4** and the diiodo derivative **5** were synthesised. The synthetic procedure for 1,3-bis(5-bromo-2-thienyl)benzo[c]thiophene **4** and 1,3-bis(5-iodo-2-thienyl)benzo[c]thiophene **5** is given in Scheme 4. Compounds **4** and **5** were synthesised by halogenation of DTITN **1** using N-bromosuccinimide and N-iodosuccinimide respectively. Synthesis of di(bromothienyl)benzo[c]thiophene **4** was already reported by Mitschke et al.[96] using DMF as a solvent at –20 °C. In this work, compound **4** was prepared using $CHCl_3$ and acetic acid (5:1) mixture as a solvent at -40 °C with an yield of 70 %. Four different methods were tried for the iodination of DTITN **1** to get novel diiodo compound **5** (see experimental part under section 11.8.2). The conventional iodination methods using KI/KIO_3 and 1,1-bis(trifluoroacetoxy)iodobenzene did not yield the desired product. But only iodination with N-iodosuccinimide in DMF at –55 °C yielded 52 % of di(iodothienyl)benzo[c]thiophene **5**.

*Scheme 4. Synthesis of 1,3-bis(5-halogeno-2-thienyl)benzo[c]thiophenes **4, 5**.*

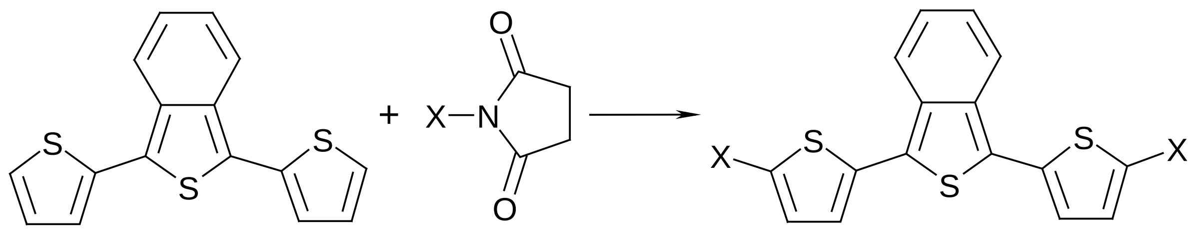

1

4: X = Br
5: X = I

3.3.1 Characterisation by ^{1}H-NMR and FT-IR spectroscopy

^{1}H-NMR spectrum of 1,3-bis(5-iodo-2-thienyl)benzo[c]thiophene **5** is shown in Figure 24. Protons, belonging to heterocyclic conjugated system, showed resonance signals in a region of 7 to 8 ppm. Two characteristic multiplets **a** and **b,** belonging to benzo[c]thiophene, were detected at 7.15 and 7.85 ppm. Two characteristic doublets **c** and **d** from outer thiophene rings were also obtained at about 7.0 and 7.25 ppm. 1,3-bis(5-bromo-2-thienyl)benzo[c]thiophene **4** was characterised in a similar manner.

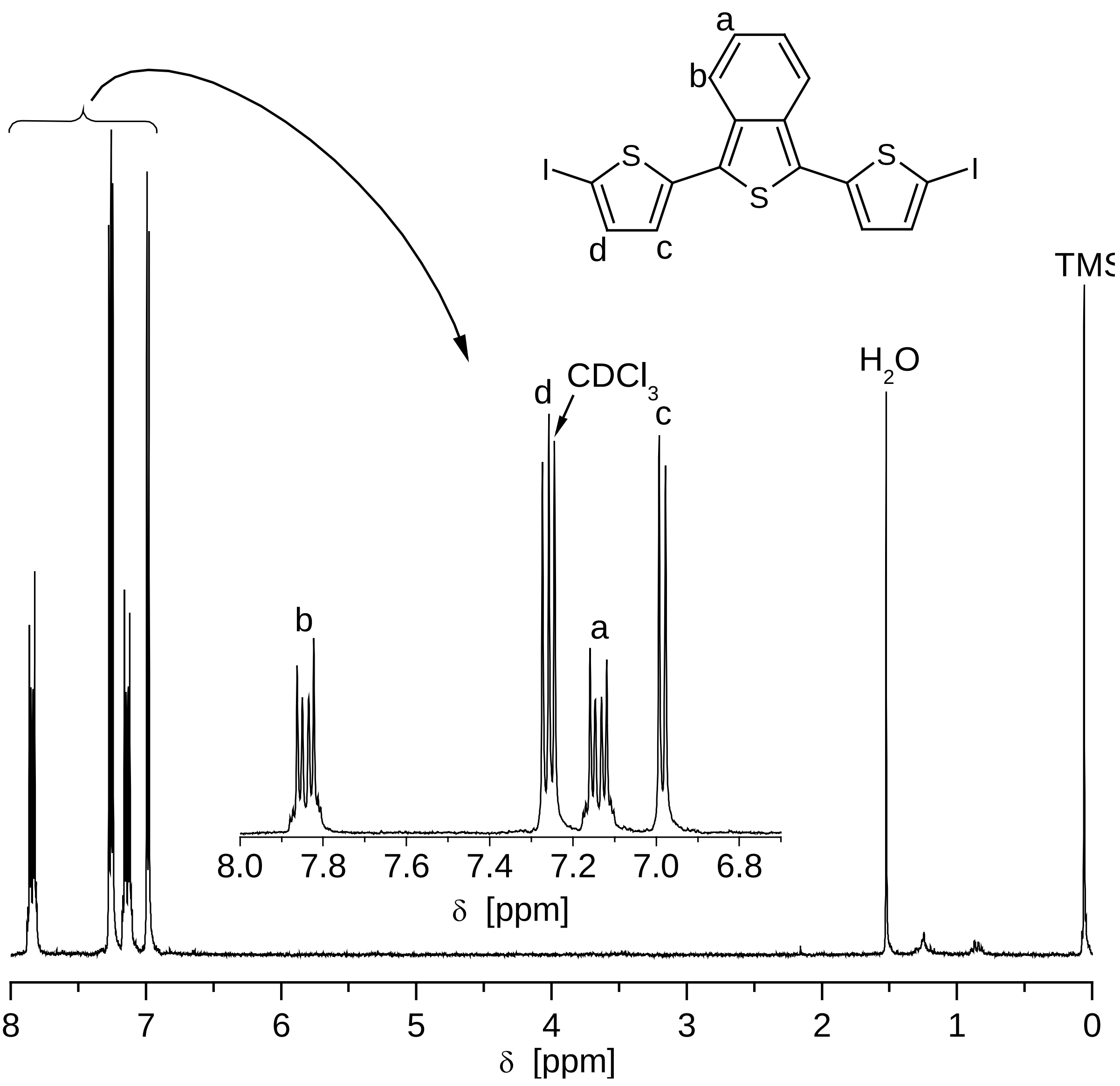

Figure 24. ^{1}H-NMR spectra (250 MHz, $CDCl_3$, 25 °C) of compound ***5****.*

Characteristic C-H stretchings of thiophene ring at about 730 cm^{-1} and at about 1530 cm^{-1} were observed in FT-IR spectra of monomers **4** and **5**.

3.4 Synthesis of 4,4´-diarylamino biphenyls **6, 8** and 4,4´-diarylamino biphenylether **7**

In this part, the synthesis of diarylaminobiphenyls is described. A synthetic pathway is given in *Scheme 5*. The bis(secondary amine)s **6-8** were synthesised via Pd-catalysed C-N coupling between anilines and diiodides by refluxing them with Pd(dppf)Cl_2 in combination with DPPF and *t*-BuONa as a base, in toluene for 16 h as shown in *Scheme 5*.

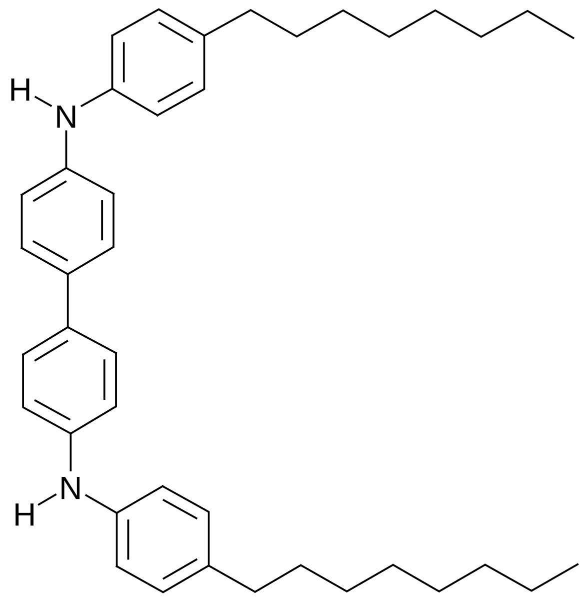

6

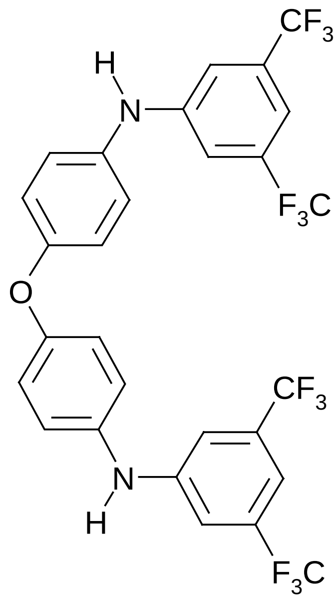

7

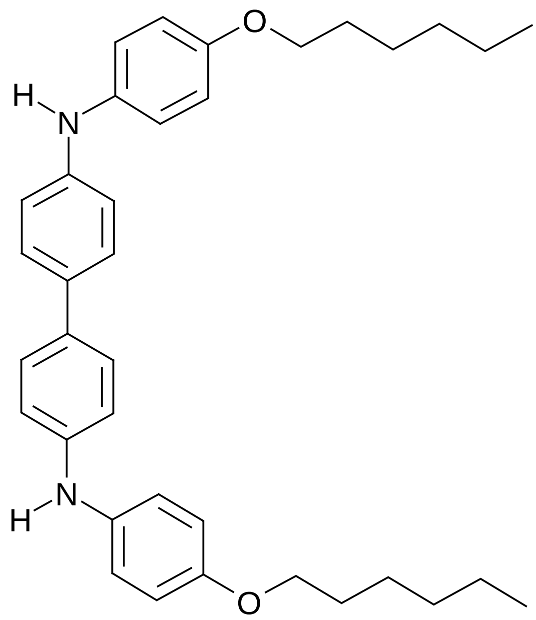

8

Figure 25. Chemical structures of 4,4´-diarylaminobiphenyls ***6, 8*** *and 4,4´-diarylamino biphenylether* ***7****.*

The groups of Buchwald[97] and Hartwig have intensively and independently investigated Pd-catalysed amination of aryl halides, and an optimised procedure[98] of theirs was adopted here. For obtaining bis(secondary amine)s **6-8** in good yields, an excess amount of aniline was used, which avoided the formation of doubly substituted side products of aniline.

Scheme 5. Synthesis of 4,4′-diarylaminobiphenyls ***6***, ***8*** *and biphenylether* ***7****.*

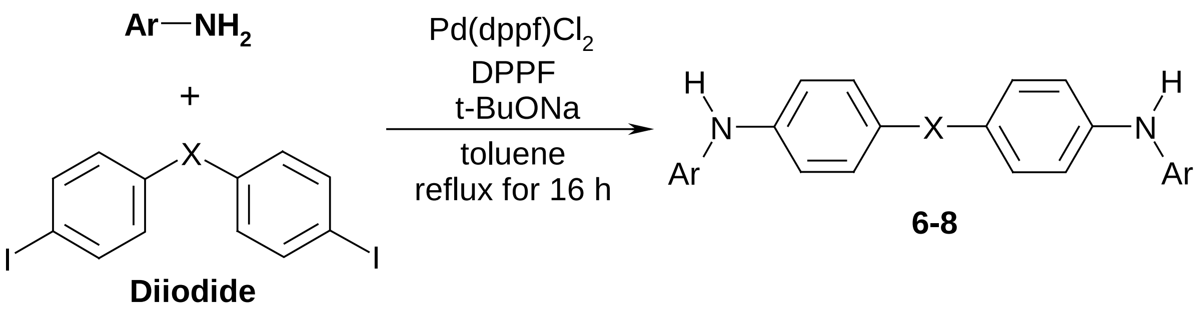

Reagents \ Products	6	7	8
Diiodides	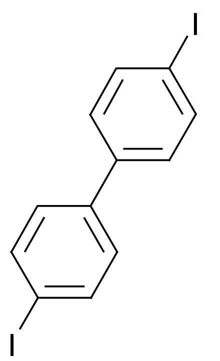	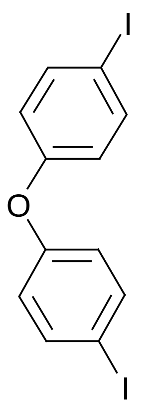	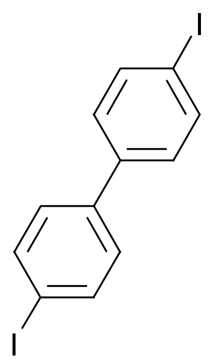
Ar—NH$_2$	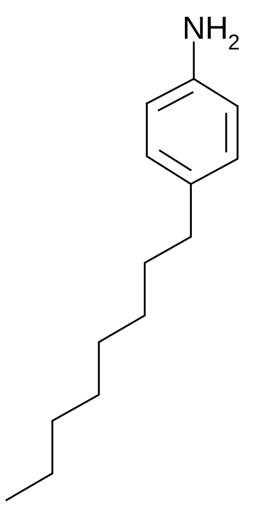	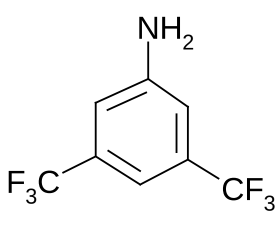	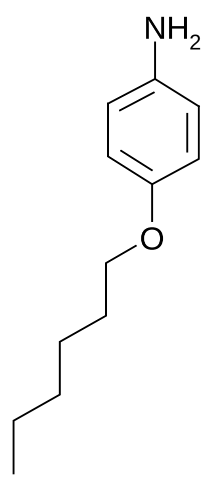

4,4´-Diarylaminobiphenyl **6**, carrying hexyl substituents**,** was synthesised from 4,4'-diiodobiphenyl and p-octylaniline. 4,4´-Diarylaminobiphenylether **7**, carrying trifluoromethyl substituents, was obtained from 4,4'-(bisiodobiphenyl)ether and 3,5-(bistrifluoromethyl)aniline. 4,4´- Diarylaminobiphenyl **8**, carrying hexyloxy substituents, was prepared by a coupling of 4,4'-diiodobiphenyl with p-hexyloxyaniline. Washing with concentrated HCl and water, followed by reprecipitation from concentrated THF solution into methanol, carried out the final purification of monomers **6** and **8**. Monomer **7** was purified by column chromatography with cyclohexane/ethylacetate (5:1) as eluent. In this way, the target bis(secondary amine)s **6-8** were obtained in relatively good yields of 46, 60 and 79 % respectively.

The substituents, hexyl, hexyloxy and bis(trifluoromethyl) groups were selected in such a way that the electronic properties, polarity and solubility of the resulting polymers can be varied and the structure-property relationships could be elucidated. The use of biphenyl ether and biphenyl segments allows studying the conjugation effect of an ether group in the main chain of the resulting polymer (see chapter 1).

3.4.1 Characterisation by ^{1}H-NMR and FT-IR spectroscopy

^{1}H-NMR spectra of compound **6** as an example is shown in Figure 26. The triplet signal from methyl protons **i** was detected at about 1.0 ppm. Methylene protons **h** and **g** shows multiplet signals in region of 1.0 to 2.0 ppm. Additionally, methylene protons **f**, which are close to phenyl ring, show resonance at about 2.5 ppm. Resonance signals from aromatic protons were observed in a region of 7 to 7.5 ppm. Two characteristic doublets **a** and **b,** belonging to core phenyl rings, are detected at about 7.0 ppm. Two characteristic doublets **c** and **d** from phenyl rings, carrying octyl substituents, are also obtained at about 7.1 and 7.3 ppm. A characteristic singlet, belonging to amino protons, was observed at about 5.0 ppm. Compounds **7** and **8** were characterised by ^{1}H-NMR in a similar manner.

The strong IR absorptions at 3405-3420 cm^{-1} due to characteristic N-H stretching and the characteristic C-N stretching of amine at 1250-1314 cm^{-1} were observed in bis(secondary amine)s **6-8**. Additionally, monomers **6** and **7** exhibit characteristic aliphatic absorptions at around 2855, 2925 cm^{-1} (C-H stretching) and monomer **8** exhibits IR absorptions at 1378, 1168 and 1139 cm^{-1} due to characteristic C-F stretching.

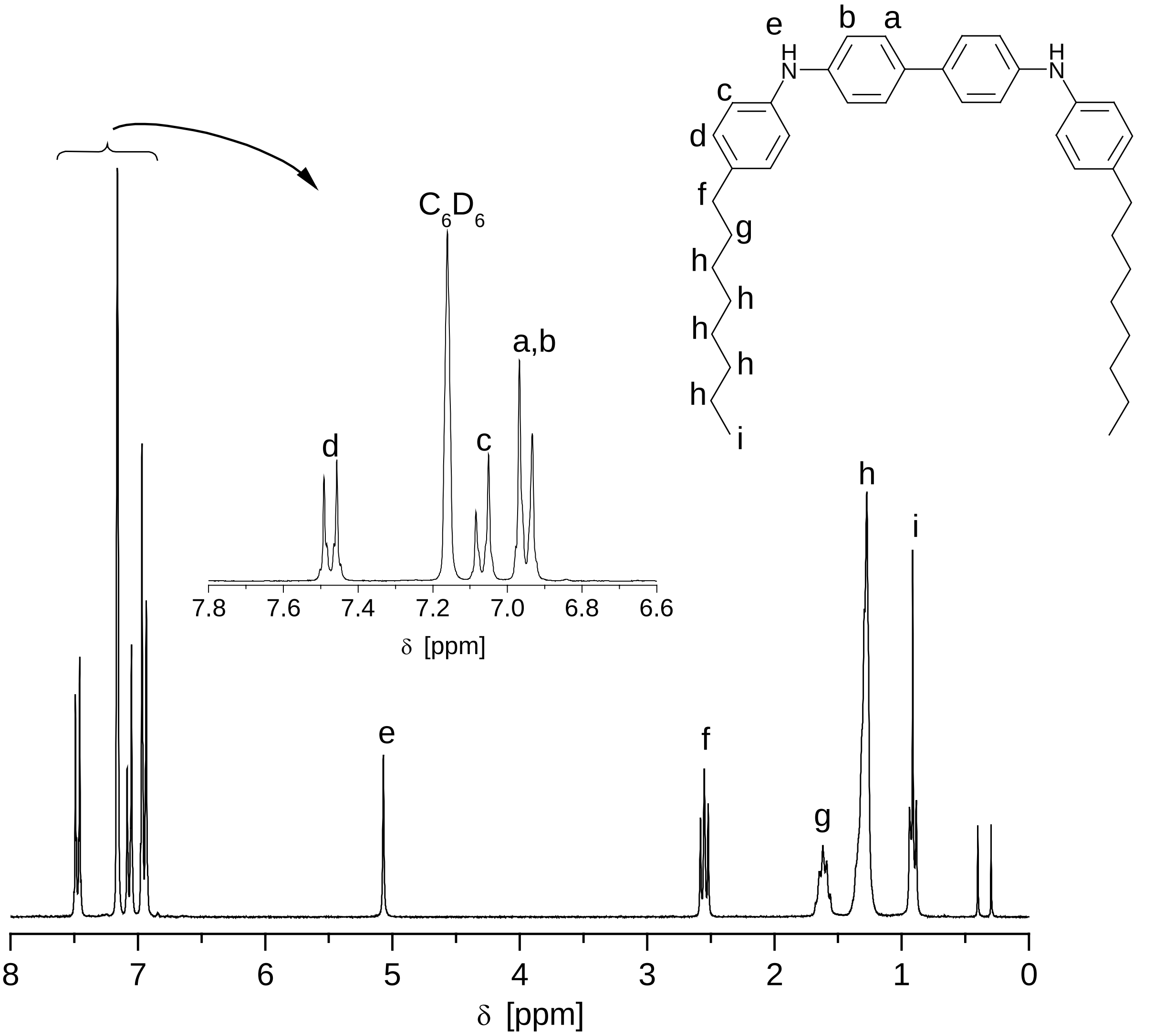

*Figure 26. [1]H-NMR spectra (250 MHz, C_6D_6, 25 °C) of compound **6**.*

4 Model compounds carrying benzo[c]thiophene (ITN) and triarylamine groups

In this chapter, a novel class of compounds, generally termed dithienylisothianaphthene phenyldiamines (DTITNPDs), is presented. The synthesis and characterisation of DTITNPDs are described here. The synthetic strategy of these low molecular weight dithienylisothianaphthene phenyldiamines is highlighted in section 4.1. The optical, thermal and electrochemical properties of these model compounds are compared in section 4.2.

4.1 Synthesis of 1,3-bis(5'-diarylaminothiophene-2-yl)benzo[c]thiophenes (DTITNPDs **9-11**) and [2,2'-bithiophene]-5,5'-diarylamine **12**

An isothianaphthene moiety was successfully incorporated into oligothiophenes containing triarylamine units via Pd-catalysed amination of di(bromothienyl)isothianaphthene **4**, resulting in a new class of compounds, dithienylisothianaphthene phenyldiamines. These model compounds combine the efficient hole-transport property of the triarylamines and the low band gap nature of the isothianaphthene unit. Dithienyl phenyldiamine **12**, which does not carry any ITN unit, was also prepared in order to compare its properties with DTITNPDs **9-11**.[99]

The synthetic strategy of the compounds **9-12** is given in *Scheme 6*. Palladium-catalysed amination of arylhalides, developed and studied in detail by *Buhwald et al*.[97] and *Hartwig et al.* for the preparation of secondary amines as well as triarylamines, was used here to obtain the target molecules in good yields. The starting dibromo compounds, 1,3-bis(5-bromo-2-thienyl)isothianaphthene **4** and 5,5-dibromo-2,2'-bithienyl **4'**, and three different secondary amines, carrying different substituents, were used to get model compounds **9-12**. DTITNPDs **9-11** were synthesised by coupling 1,3-bis(5-bromo-2-thienyl)isothianaphthene **4** with dimethoxydiphenylamine, di(trifluoromethyl)phenyl-phenylamine and N-(2-naphthyl)aniline respectively. After final purification by column chromatography the model compound **9** was isolated in a 58 % yield as a deep violet-red solid, compound **10** was isolated in a 77 % yield as a bright fluorescent red powder and DTITNPD **11** was isolated in a 28 % yield as a deep red solid. Synthesis of di(trifluoromethyl)phenyl-phenylamine, used for the preparation of **10**, was carried out via Pd-catalysed amination of 1-iodo-3,5-bis(trifluoromethyl)benzene and aniline.

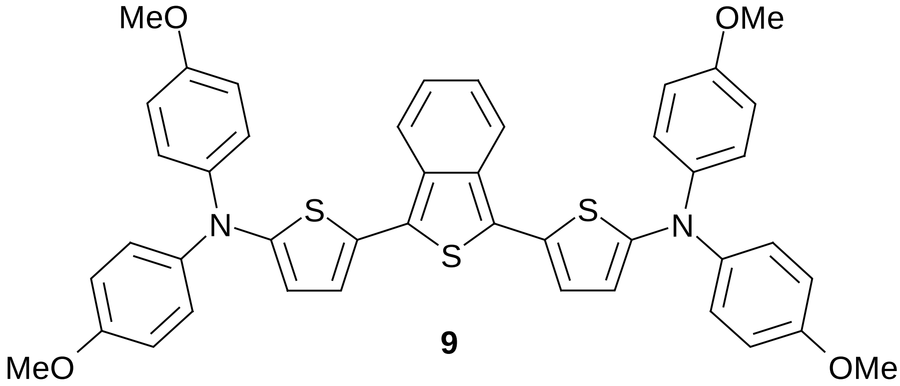

9

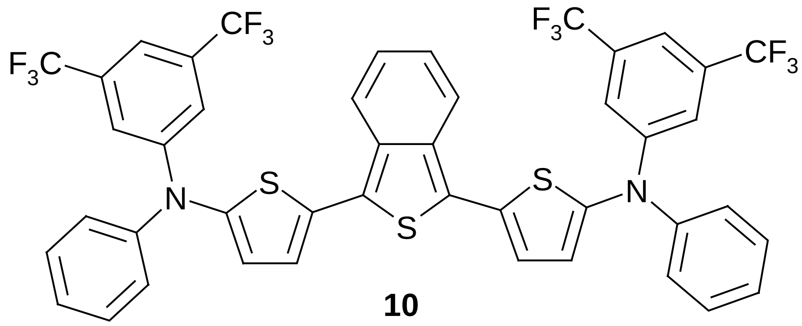

10

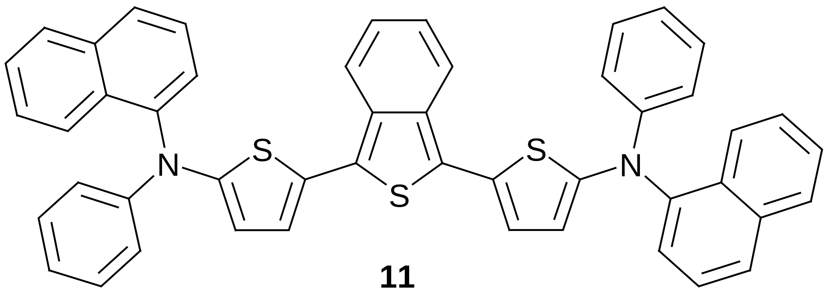

11

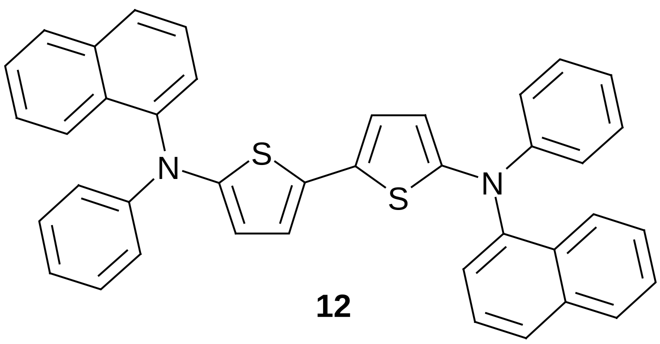

12

Figure 27. Chemical structures of model dithienylisothianaphthene phenyldiamines ***9-11*** *and dithienyl phenyldiamine* ***12****.*

Preparation of dithienyl phenyl-naphthylamine **12** by coupling of 5,5-dibromo-2,2'-bithienyl **4'** with N-(2-naphthyl)aniline yielded 50 % of a yellow solid. Synthesis of compound **12** was already reported by Wong et al.[100] Synthesis of 1,3-bis(5-bromo-2-thienyl)isothianaphthene **4** is given in section 3.3.

Scheme 6. Synthesis of low molecular weight dithienylisothianaphthene phenyldiamines (DTITNPDs) ***9-11*** *and dithienyl phenylamine* ***12****.*

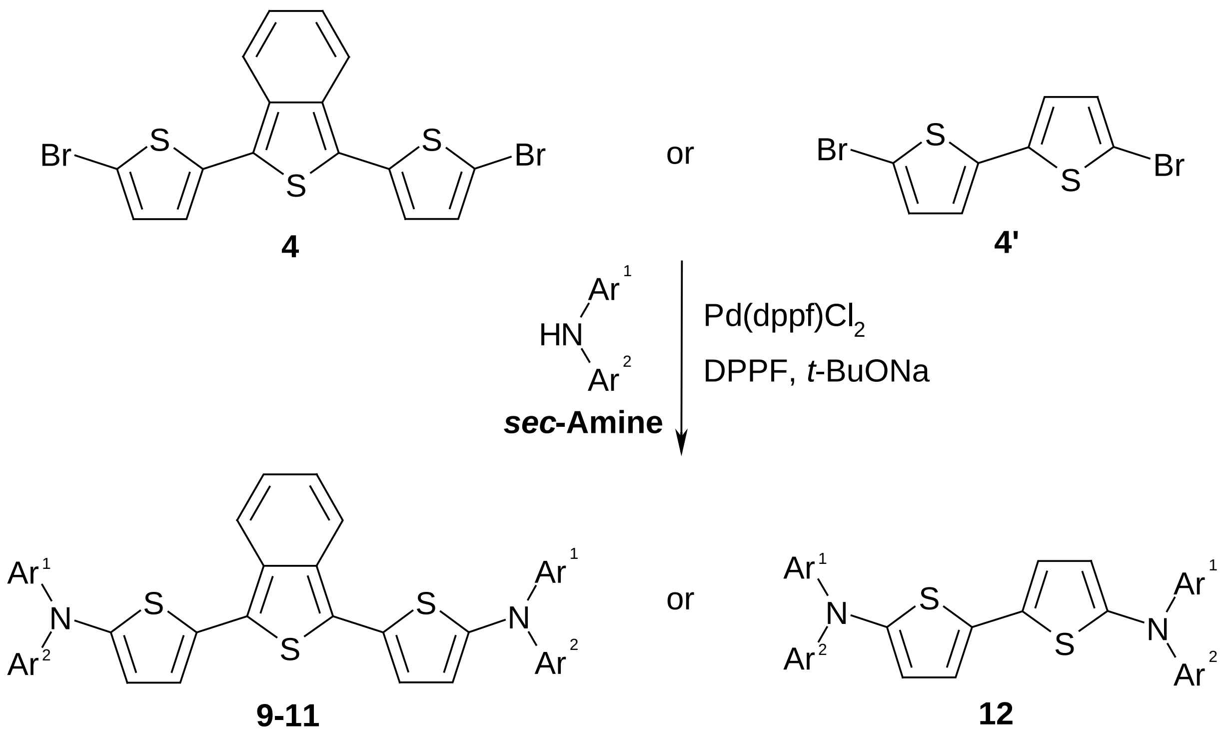

Products / Reagents	9	10	11	12
Dibromo-thiophenes	**4**	**4**	**4**	**4'**
***sec*-Amines**	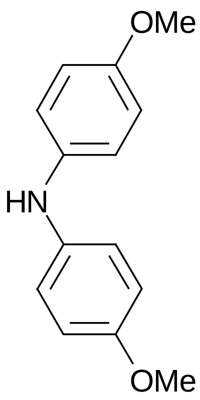	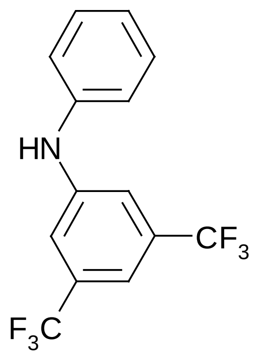	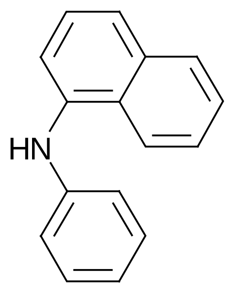	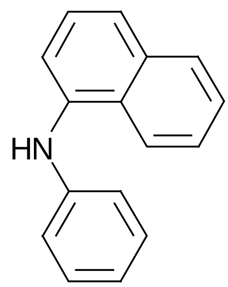

4.2 Characterisation

4.2.1 ¹H-NMR and FT-IR spectroscopy

The ^{1}H-NMR spectra of compound **9** as an example is shown in Figure 28. NMR signals from methyl protons were observed at 3.28 ppm. Two characteristic multiplets **a** and **b** belonging to benzo[c]thiophene were detected at 6.78 and 7.94 ppm respectively. Two characteristic doublets **c** and **d** from thiophene were also obtained at 6.98 and 6.48 ppm respectively. Phenyl protons are characterised by two doublets **e** and **f** at 6.73 and 7.19 ppm respectively. All other model compounds were characterised in a similar manner. The details are given in the experimental part (see sections 11.10 and 11.11).

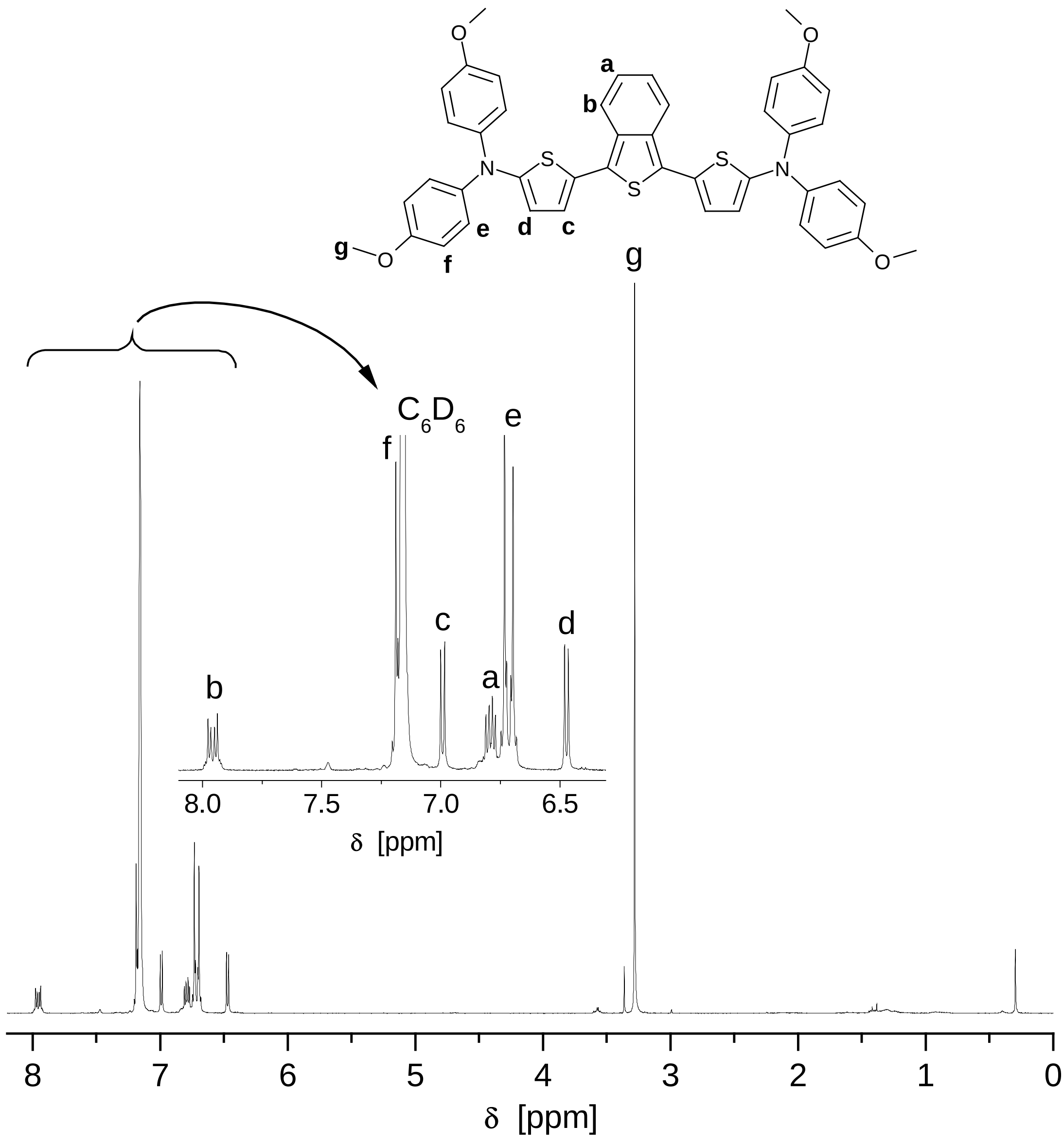

*Figure 28. ^{1}H-NMR spectra (250 MHz, C_6D_6, 25 °C) of dithienylisothianaphthene phenyldiamine **9**.*

In contrast to starting secondary amines, the strong IR absorptions at 3405-3419 cm^{-1} in the compounds **9-12** due to characteristic N-H stretching in secondary amines disappeared completely and absorptions at 1231-1384 cm^{-1} appear due to the characteristic C-N stretching of amines. Additionally, all these compounds exhibited characteristic aromatic absorptions at 3044-3064 cm^{-1} (C-H stretching) and at 1592-1615 cm^{-1} (C-C stretching). Characteristic C-H stretchings of thiophene ring at 1491-1503 cm^{-1} and 743-878 cm^{-1} were also observed in the products. Moreover, characteristic absorptions at 1377 and 1133 cm^{-1} due to aliphatic CF_3 stretching were obtained in IR spectra of model compound **10**.

4.2.2 Optical properties via UV-Vis and Fluorescence spectroscopy

In the following paragraph the electronic absorption and photoluminescence (PL) spectra of model compounds **9-12** in solution as well as in the thin film obtained by spin-coating from chloroform onto glass substrates are discussed. The influence of substitution pattern, conjugation length, and intermolecular interaction is investigated.

UV-Vis and fluorescence in solution

The absorption and fluorescence spectra of compounds **10-12** were measured in cyclohexane. The measurements of **9** were carried out in dioxane due to its poor solubility in cyclohexane. These absorption spectra are given in Figure 29.

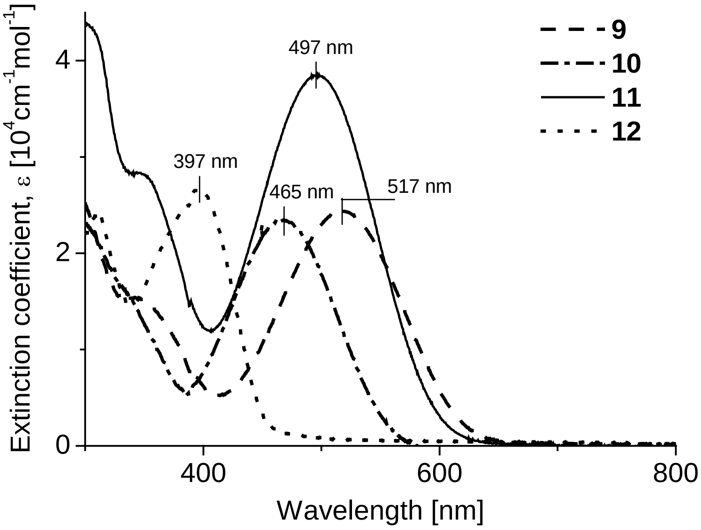

*Figure 29. UV-Vis spectra of **9-12** measured in solution (**9**: dioxane, **10-12**: cyclohexane) at concentrations of about $5 \cdot 10^{-6}$ M.*

The model compounds **9-11** with an ITN group in the middle show extended absorption in the visible range with a red shift of 100 nm compared to **12** without an isothianaphthene group. In order to use these model compounds as strongly absorbing dyes, for example, in solar cells, the molar extinction coefficient needs to be high enough. Compound **11** shows the highest value of 38600 $cm^{-1}mol^{-1}dm^3$, which is in the same range as many of the light harvesting dyes like perylene bisimides and Ru-bipyridyl dyes presently used in solar cells. Dyes **9** and **10** possess similar molar extinction coefficient (ε) values of about 24000 $cm^{-1}mol^{-1}dm^3$. E_g^{opt} of the corresponding compounds **9-12**, calculated from absorption edges by putting tangents on the absorption shoulder, are 2.01, 2.25, 2.08 and 2.76 eV respectively (see Table 4).

The fluorescence spectra of **9-12** measured in dilute solutions are shown in Figure 30. The fluorescence measurements of all these compounds were performed under similar conditions by excitation at λ_{max}^{abs} obtained from the absorption spectra. Dithienylisothianaphthene phenyldiamines **9-11** show red emissions at 640, 585 and 610 nm respectively and dithienyl phenyldiamine **12** shows greenish-yellow emission at 464 nm. This result shows a difference of about 150 nm between fluorescence emission maxima λ_{max}^{fl} of red dyes **9-11** compared with the yellow dye **12**. Moreover, the emission wavelength can be tuned by varying the substituents as can be seen from the fluorescence spectra of **9-11**.

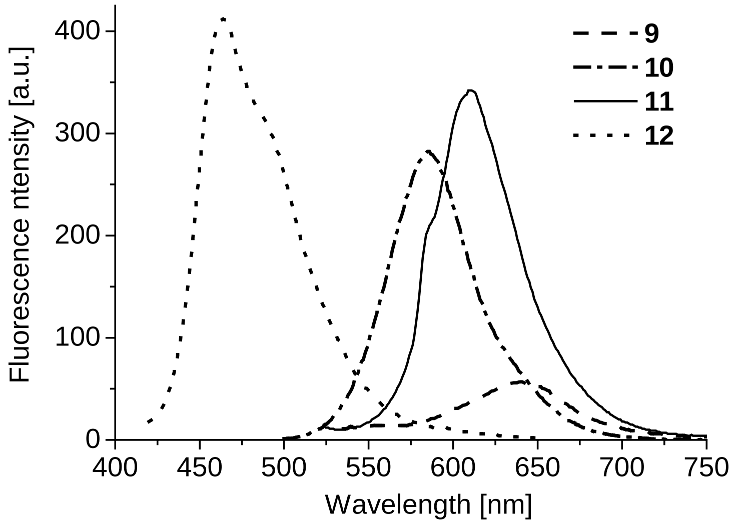

*Figure 30. Fluorescence spectra of **9-12** measured in solution (**9** in dioxane, **10-12** in cyclohexane) at concentrations of about $5 \cdot 10^{-6}$ M.*

Incorporating of the isothianaphthene into the core of dithienyl phenyldiamines leads to the new class of materials, dithienylisothianaphthene phenyldiamines (DTITNPDs). With an aim to study the properties of these new materials, the optical properties of compound **11** carrying ITN group and compound **12** without any ITN group are compared here. Model compounds **11** and **12** have similar chemical structures (except the presence of ITN group in **11**), which allow minimising the influence of substituents on properties of these compounds. Thus, DTITNPD **11** compared to dithienyl isothianaphthene **12** showed red shift of λ_{max}^{abs} of 100 nm with decreasing the band gap from 2.8 eV to 2.1 eV. A red shift of λ_{max}^{fl} from greenish-yellow emission at 464 nm to red emission at 610 nm was also observed. Moreover, compound **11** had a higher extinction coefficient at λ_{max}^{abs} than compound **12** with values of $3.9 \cdot 10^4$ $cm^{-1}mol^{-1}dm^3$ and $2.7 \cdot 10^4$ $cm^{-1}mol^{-1}dm^3$ for **11** and **12** respectively. Thus, incorporating of low band gap ITN moiety into dithienyl phenyldiamines led to a new class of red hole-transport dyes, dithienylisothianaphthene phenyldiamines with higher extinction coefficients and broader absorption in the visible range.

*Table 4.Optical properties of model compounds **9-12** measured in solution.*

Compound	Concentration $[10^{-6}$ M]	**Absorption**				**Fluorescence**
		λ_{max}^{abs} [nm]	ε (at λ_{max}^{abs}) $[cm^{-1}mol^{-1}dm^3]$	Absorption edge [nm]	E_g^{opt} (from edge) [eV]	λ_{max}^{fl} [nm]
9	7.28	517	24400	618	2.01	640
10	4.95	465	23500	560	2.25	585
11	4.90	497	38600	595	2.08	610
12	6.79	397	26600	449	2.76	464

λ_{max}^{abs} – absorption maxima
λ_{max}^{fl} – fluorescence maxima
ε - molar extinction coefficient
E_g^{opt} – optical band gap

Optical properties of low molecular weight DTITNPDs **9-11** were also compared to those of DTITNs **1-3** in order to understand the influence of incorporation diarylamine groups into 5-positions of thiophenes in dithienylisothianaphthenes leading to low band gap dithienylisothianaphthene phenyldiamines. DTITNPDs **9-11** were compared to DTITN **1** which does not carry any substituents. An amazing red shift of λ_{max}^{abs} more than 100 nm was observed with a lowering of the band gap from 2.5 eV up to 2.0 eV from compound **1** to compounds **9-11**. Even a larger red shift of λ_{max}^{fl} of more than 150 nm was observed from **1** to **9-11** (compare Table 2 and Table 4). Thus, introducing diarylamine groups into low molecular weight dithienylisothianaphthenes drastically improves the optical properties of these compounds, resulting in low band gap hole-transport dyes, dithienylisothianaphthene phenyldiamines. Thus, the concept of bringing together the ITN group and the diarylamine group into one compound is a successful strategy in order to achieve low band gap hole transport dyes with red emission.

UV-Vis and fluorescence in the thin film

Optical absorption and emission studies of dyes **9-11** in thin films were performed with an aim to study the suitability of these model compounds for application in thin film electro-optical devices such as OLEDs and solar cells. The absorption spectra measured in thin film are given in Figure 31. Absorption maxima of **9-11** are 537, 484 and 522 respectively. All these compounds show similar absorption coefficients in the range of 30000 cm^{-1}. Moreover, E_g^{opt} of dyes **9-11** measured from absorption in film are 1.75, 2.06 and 1.89 eV respectively (see Table 5). All E_g^{opt} values measured in thin film show a bathochromic shift of about 0.2 eV compared to those measured in solution (see also Table 4). Such a low ITN band gap and well known hole-transport properties of triaryl amines, combined in one molecule, make model compounds **9-11** suitable for application in solar cells as hole-transport dyes.

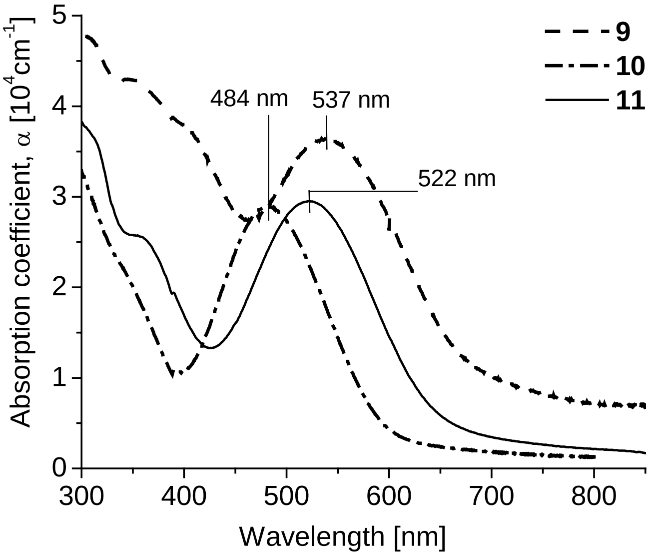

*Figure 31. UV-Vis spectra of **9-11** measured in thin film obtained by spin-coating from $CHCl_3$.*

Fluorescence spectra of dithienylisothianaphthene phenyldiamines **9-11**, measured in the thin film, are illustrated in Figure 32. The fluorescence study was carried out using excitation wavelength at λ_{max}^{abs}. Red emission of **9** was observed at 647 nm. The λ_{max}^{fl} of compound **9** in thin film correlates with those measured in solution (640 nm) as given in Table 4. Compound **10** showed bright red emission at 613 nm in film with a red shift of about 30 nm compared to that measured in solution (see Table 4). Model compounds **11** and **12** did not show any emissions in thin film. The bright photoluminescence of DTITNPD **9**, observed in a solid state, makes this compound suitable for potential application as a red-emitter in OLEDs. The testing results of red-emitter **10** are described in chapter 1.

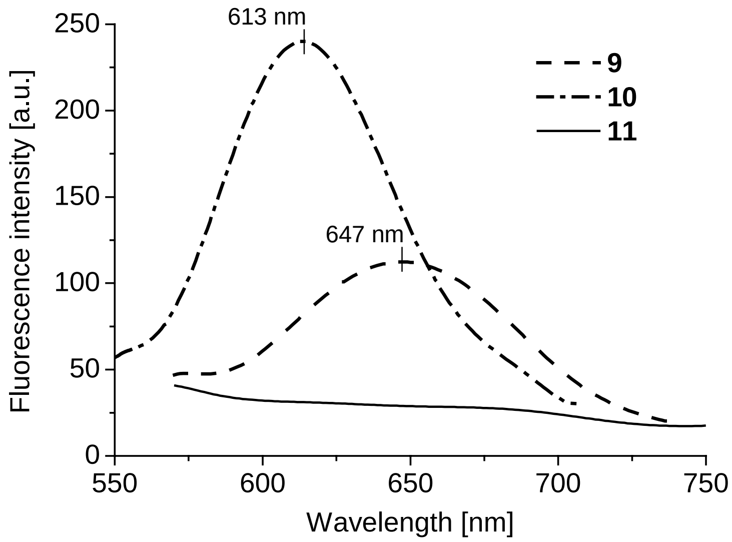

*Figure 32. Fluorescence spectra of **9-11** measured in thin film spin-coated from $CHCl_3$.*

Regarding the red shifted fluorescence of thin films compared to the solution spectra, a very good theoretical overview is given by Cornil et al.[101] The red shift of fluorescence can be attributed to packing effects, excimer formation, geometry and lattice relaxation, all leading to a lowering of energy of the vibronic relaxed lowest singlet excited state in strongly interacting molecules.

*Table 5. Optical properties of model compounds **9-11** measured in thin film.*

Compound	Absorption				Fluorescence
	λ_{max}^{abs} [nm]	α (at λ_{max}^{abs}) [cm^{-1}]	Absorption edge [nm]	E_g^{opt} (from edge) [eV]	λ_{max}^{fl} [nm]
9	537	36400	710	1.75	647
10	484	28900	601	2.06	613
11	522	29500	655	1.89	*-

α - absorption coefficient
E_g^{opt} – optical band gap
** - fluorescence was not observed*

The comparison between absorption spectra of each of DTITNPDs **9-11**, measured in solution and in thin film, is illustrated in Figure 33. Absorption peaks of these compounds, measured in thin films, became broader than those observed from measurements in solution. A strong broadening of the vibronic band was observed in compound **9**, carrying methoxy substituents. Absorption spectra of compound **10** showed only slight broadening of absorption peak due to less interaction owing to the hydrophobic nature of trifluoromethyl substituents that are present in this compound. The behaviour of compound **11** is similar to that of compound **10**.

The red shifts of about 20 nm were also observed in the absorption maxima of compounds **9-11** measured in thin film compared to measurements performed in solution.

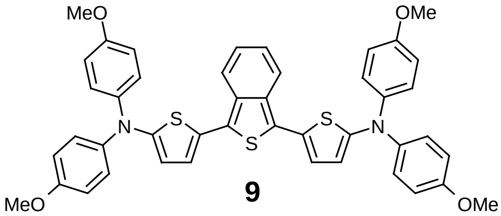

9

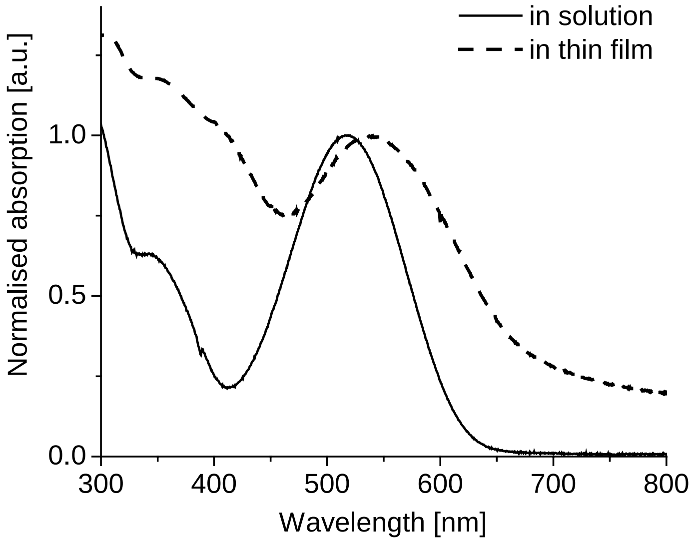

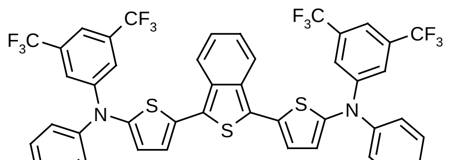

10

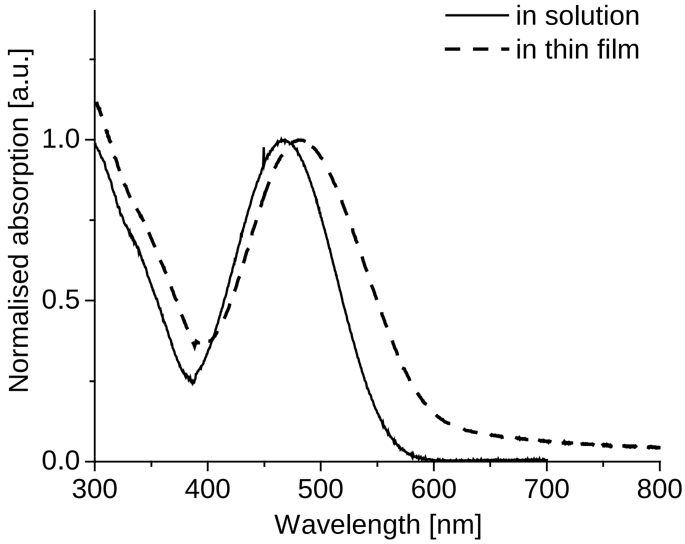

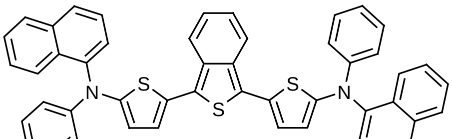

11

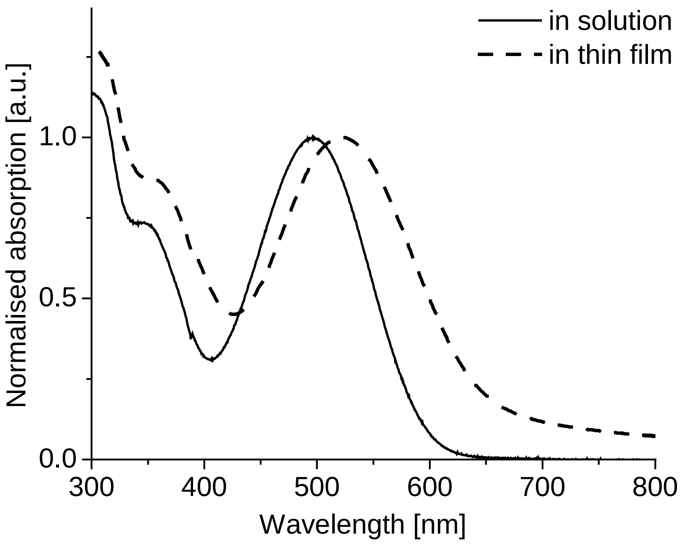

*Figure 33. Comparing of UV-Vis spectra of model compounds **9-11** measured in solution and in thin film.*

The absorption spectrum broadening of **9** in the thin film compared to that of solution and the red shift observed in the solid state for all the compounds, indicates aggregation of molecules in the solid state. Kasha et al. can explain the aggregation behaviour observed in film by means of the molecular exciton model[102,103], which is illustrated below.

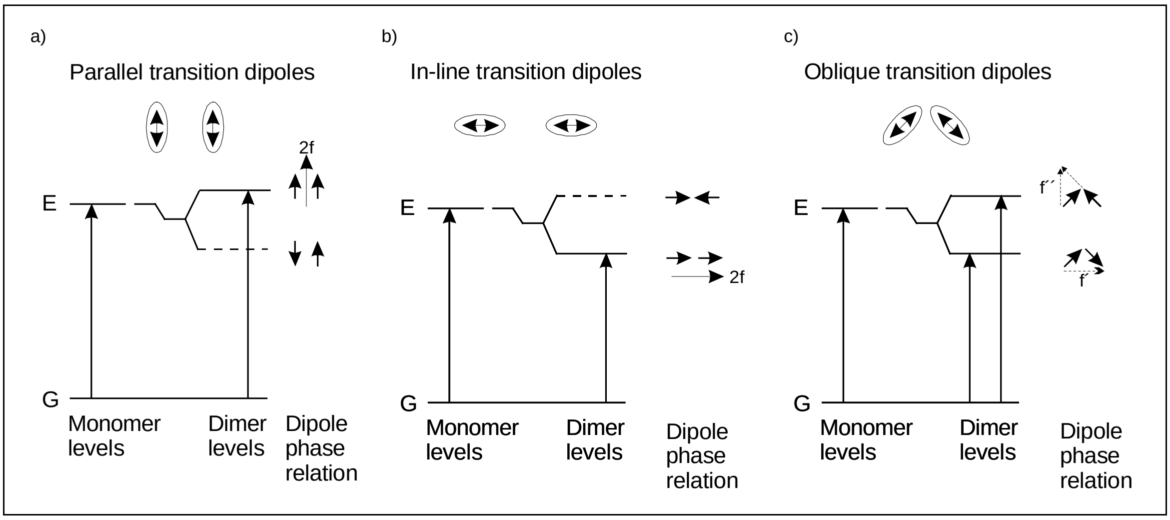

Figure 34. Exciton band energy diagram for a molecular dimer, or double molecule, with a) parallel transition dipoles (H-aggregation), b) in-line transition dipoles (J-aggregation), and c) oblique transition dipoles; G = ground state, E = excited state, f = resulting transition dipole moment

The ovals correspond to the molecular profile, and the double arrow indicates the polarisation axis for the molecular electronic transition considered. The transition moment is given by the vector sum of the individual transition dipole moments in the compound molecule. Thus, transitions from ground state to exciton state having out-of-phase arrangement are forbidden, while transitions from the ground state to exciton state having in-phase arrangement are allowed. The out-of-phase dipole arrangement corresponds electrostatically to a lowering of energy, lying lower than the van der Waals displaced states of the component molecules. In-line transition dipoles occur in π-conjugated molecules but for the geometrical axes of the molecule parallel, with transition dipoles polarised along the short axis of a unit molecule. The cases of in-line transition dipole moment orientation (H-aggregation) resulting in blue-shifted absorption and oblique transition dipoles resulting in band splitting are not discussed in detail here, but given in reference. In-line transition dipoles, resulted in red-shifted absorption, lead to the exciton level diagram as shown in Figure 34b. This kind of orientation is also known as J-aggregation. Subsequently, the red-shifts in absorption spectra of model compounds **9-11**, discussed above, gives an indication that these compounds have a tendency to form J-aggregates when in a solid state.

4.2.3 Cyclic Voltammetry (CV)

The electrochemical stability and the reversibility of the redox processes of model compounds **9-12** were studied using CV. All measurements were performed in a solution of carefully dried THF. The redox potentials were measured against $Ag/AgNO_3$ as a reference electrode and each measurement was calibrated as usual with the standard ferrocene/ferrocenium (Fc) redox system. Cyclic voltammograms of compounds **9-12** are given below.

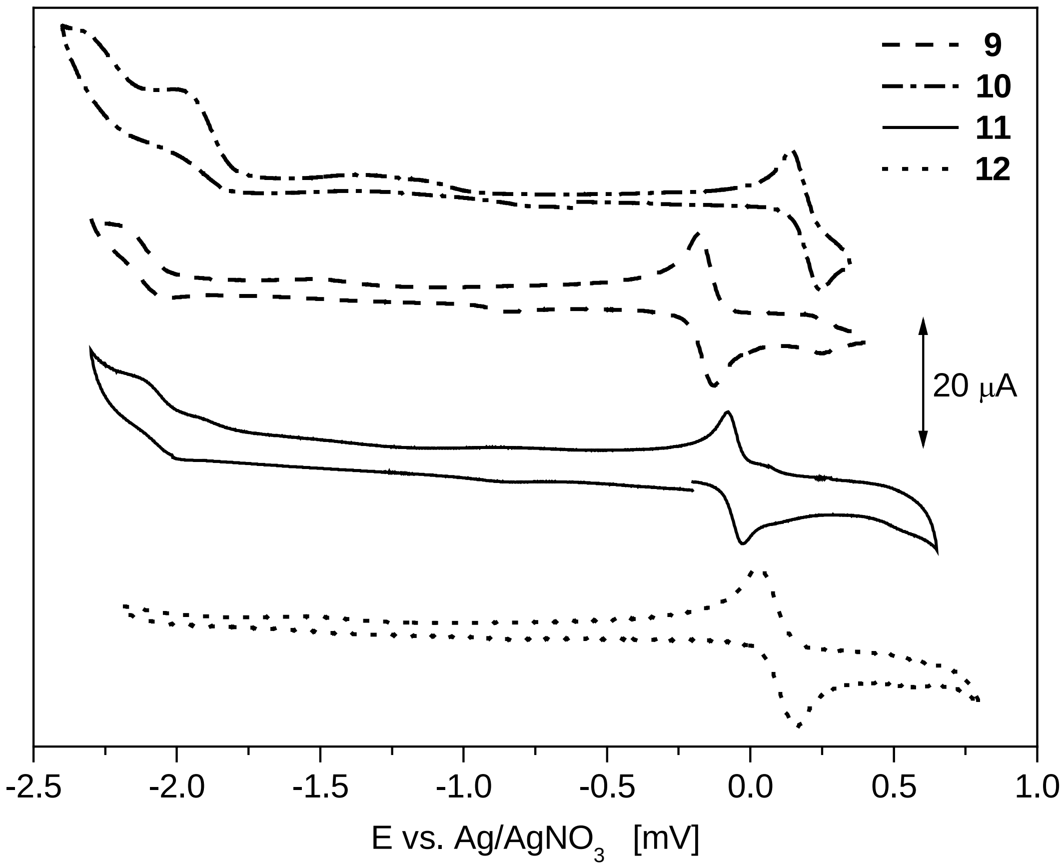

Figure 35. Cyclic voltammograms of ***9-12*** *measured at 50 $mV{\cdot}s^{-1}$ scanning rate in THF.*

The electrochemical stability of model compounds was examined by measuring repeated cycles of redox processes for the scanning rates of 50 $mV{\cdot}s^{-1}$ to 500 $mV{\cdot}s^{-1}$. Model compounds **9-11** showed completely reversible reduction and oxidation steps and compound **12** showed a completely reversible oxidation step and no reduction up to –2.5 V vs. $Ag/AgNO_3$.

E_{ox1} of -0.19, +0.26, +0.09 V and +0.05 V were observed from CV measurements and HOMO levels of -4.61, -5.06, -4.89 eV and -4.85 eV were calculated from corresponding E_{ox1} for compounds **9-12** respectively. The highest LUMO value was obtained for compound **9** carrying four methoxy substituents. The HOMO levels variation in DTITNPDs **9-11** due to the influence of substituents is in full agreement with the data, obtained by comparing series of triphenyldiamines[104]. A comparison of the HOMO values of dithienylisothianaphthene phenyldiamine **11** with ITN group and dithienyl phenyldiamine **12** without ITN group indicates, that the introduction of an ITN group into the core of dithienyl phenyldiamine does not affect the HOMO level of these molecules. Compounds **9-11** showed similar reduction behaviour with E_{red1} of -2.20, -2.01 and -2.12 V vs. ferrocene respectively. LUMO levels of model compounds **9-11**, calculated from E_{red1}, are -2.60, -2.79 and -2.68 eV respectively. The E_g^{ec} values of **9-11** are 2.01, 2.27 and 2.21 eV respectively as given in Table 6. E_g^{ec} and E_g^{opt} of **9** and **10**, obtained from cyclic voltammetry and UV-Vis spectroscopy respectively, show values of 2.01 and of about 2.26 eV respectively, and the band gap energy for model compound **11** shows a small difference of 0.13 eV.

*Table 6. Electrochemical properties of **9-12**.*

Compound	E_{ox1} [V]	HOMO [eV]	E_{red1} [V]	LUMO [eV]	E_g^{ec} [eV]	E_g^{opt} [eV]
9	-0.19	-4.61	-2.20	-2.60	2.01	2.01
10	0.26	-5.06	-2.01	-2.79	2.27	2.25
11	0.09	-4.89	-2.12	-2.68	2.21	2.08
12	0.05	-4.85	^{a}-	^{a}-	^{a}-	2.76

E_{ox1} – first oxidation potential
E_{red1} – first reduction potential
E_g^{ec} – electrochemical band gap
E_g^{opt} – optical band gap measured in solution
^{a} – reduction was not detected

In order to compare the HOMO and LUMO energy values of low molecular weight dithienylisothianaphthenes and dithienylisothianaphthene phenyldiamines, DTITN **1** and DTITNPD **11** were chosen. Introducing phenyl-naphthylamine groups in to the 5-positions of thiophenes in DTITN **1** results in DTITNPD **11**. Comparison of model compounds **1** and **11** without any substituents avoids the influence of substituent on energy levels of these molecules, and it also minimises steric hindrance in inter C-C bonds between thiophenes rings which carry substituents. The band gap was reduced from 2.6 eV to 2.2 eV by increasing the HOMO energy value from about -5.3 eV to -4.9 eV in **1** to **11** respectively, keeping the LUMO levels of **1** and **11** almost constant with values of about -2.6 eV as illustrated in Figure 36. This indicates that the LUMO value is generally decided by the central ITN group. The result obtained comparing energy levels of DTITN **1** and DTITNPD **11** is in the full agreement with the theoretical calculations performed for these molecules (see chapter 1).

In conclusion, incorporating diarylamino groups into dithienylisothianaphthenes leads to the new class of compounds, dithienylisothianaphthene phenyldiamines, which have improved electro-optical properties such as lower band gap and strong red emission. Thus, the hole-transport dyes, DTITNPDs **9-11** are promising candidates for application in solar cells as absorbing dyes and as red-emitters in OLEDs.

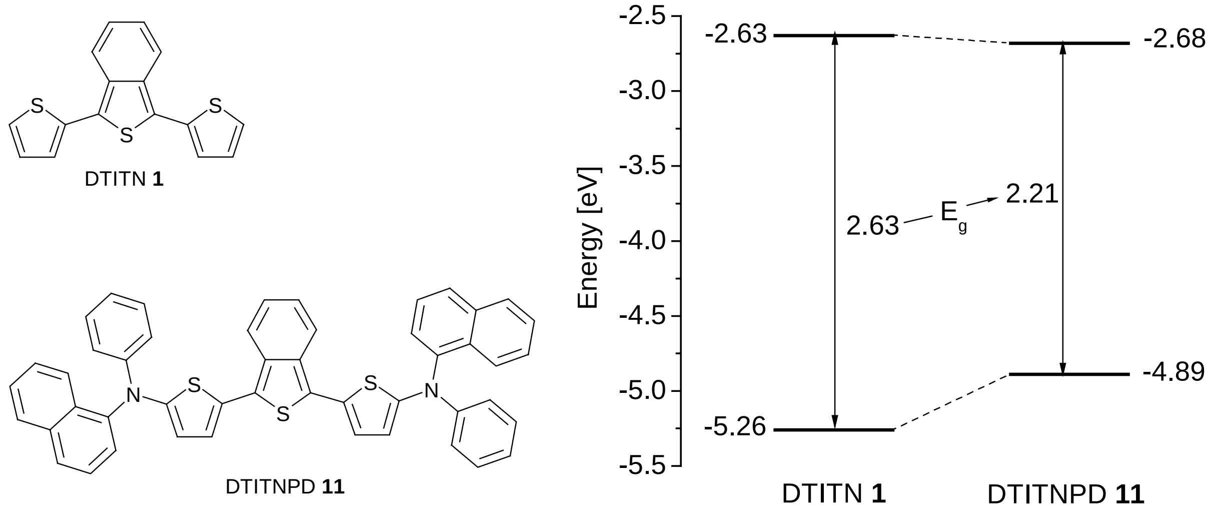

*Figure 36. Energy levels diagram of DTITN **1** and DTITNPD **11**, obtained from CV measurements in carefully dried THF.*

4.2.4 Thermal properties

The thermal properties of **9-12** were examined by differential scanning calorimetry (DSC) and thermogravimetric analysis (TGA) measurements. TGA of **9-12** were carried out at a heating rate of 10 K·min^{-1} by heating in the range from 30 to 560 °C in alumina pan under nitrogen atmosphere. All the compounds **9-12** showed similar thermal stability with the onset temperatures for a 5 % weight loss ($T_{-5\%}$) of 315, 332, 330 and 335 °C respectively. At a temperature of 560 °C, compound **9** was the most stable with about 50 % weight left, compound **11** had 30 % of its weight left and compounds **10** and **12** had only 15 % of their weights left as shown in Figure 37.

DSC measurements of **9-12** were performed in order to study influence of different substituents present in these compounds on their glass transition temperature and melting point values. All measurements were carried out at 10 K·min^{-1} heating rate under nitrogen atmosphere. Thermal properties of **9-12** are summarised in Table 7.

The compounds **9-12** exhibit glass transition temperature (T_g) at 54, 48, 71, 57 °C and melting peaks at 229, 183, 186, 208 °C respectively. A higher T_g value of **11** compared to **12** indicates the rigidity of the ITN unit, which was introduced into the core of dithienyl phenyldiamine **12**, resulting in DTITNPD **11**.

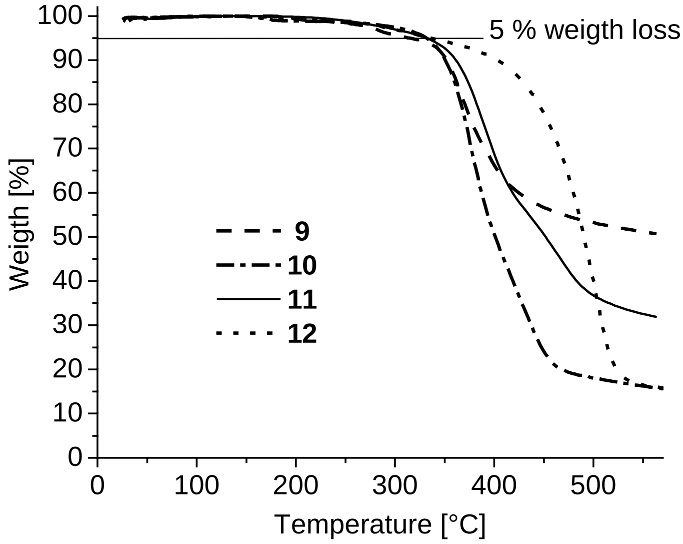

Figure 37. TGA measurement of ***9-12*** *at 10 K·min^{-1} heating rates under N_2 flow.*

Generally, DSC curves of all these compounds did not show T_g on the 1st heating cycle. On all other cooling and heating cycles T_g was observed for compounds **9-12**. There are large differences in the thermal transition and crystallisation behaviour of these compounds. Compound **9** is more crystalline in nature than **10-12**. The second heating curve of **9** exhibited a T_g, crystallisation peak and melting peak. Third heating also showed a T_g, crystallisation peak and melting peak. Such thermal behaviour of **9** shows that this compound has a tendency to crystallise on heating above its T_g. On the other hand, the metastable glassy state of **10-12** can be obtained by cooling down from above the melting point. There is no further crystallisation on the heating and cooling cycles of these compounds. As an example, the DSC heating and cooling curves of compound **12** are shown in Figure 38. Both second and third heating curves of **12** exhibited only a T_g and no melting and crystallisation behaviour. Compounds **10** and **11** also showed similar behaviour to compound **12** with no melting and no crystallisation behaviour on second and further heating and cooling cycles between -40 °C and 250 °C at 10 K·min^{-1}.

Thus, the compounds **9-12** showed a difference in their thermal properties as observed with DSC. Compound **9** exhibited recrystallisation above T_g, whereas compounds **10-12** showed no crystallisation in all heating and cooling cycles after cooling down from melt.

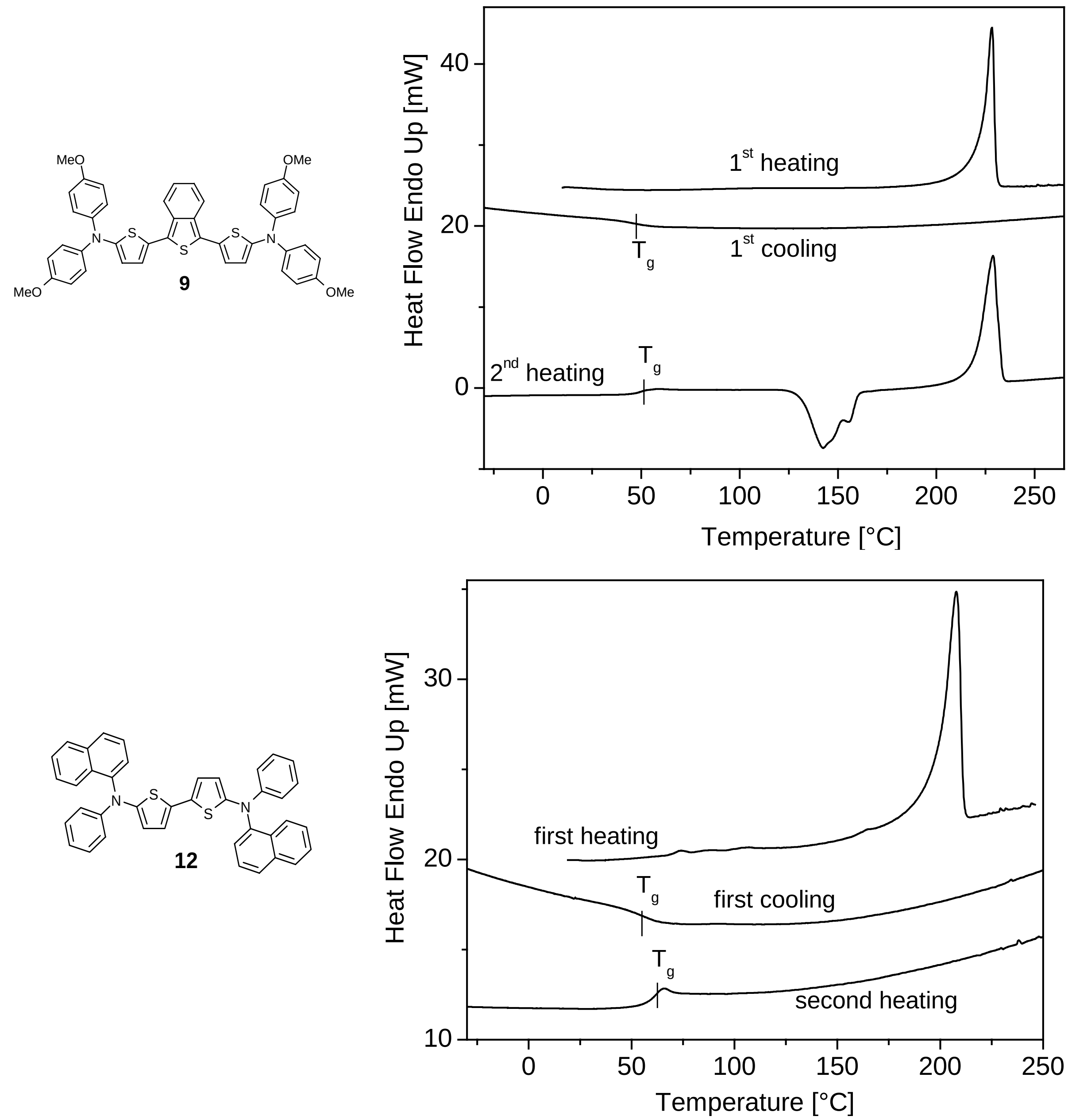

*Figure 38. DSC measurement of model compounds **9** and **12** at 10 K·min^{-1} under N_2 flow.*

*Table 7. Thermal properties of **9-12** studied using TGA and DSC at heating/cooling rate of 10 K·min^{-1} under nitrogen atmosphere.*

Compound	TGA	DSC	
	$T_{-5\%}$ [°C]	T_g [°C]	Melting peak [°C]
9	315	54	229[a]
10	332	48	183[b]
11	330	71	186[b]
12	335	57	208[b]

[a] – in all heating steps
[b] - only in first heating step

5 Polymers carrying 1,3-di-2-thienylbenzo[c]thiophene group in main chain

The synthesis, characterisation and properties of a poly(dithienylisothianaphthene)s, poly(DTITN)s are described in this section. These polymers are characterised by the presence of a low band gap isothianaphthene unit in the main chain.

From a comparative experimental and theoretical study of short-chain model compounds[105], the ground electronic state of poly(isothianaphthene), poly(ITN) has been proven to possess a quinoid structure with double bonds between the monomeric units. This means that polyITN has a very rigid polymer backbone, which explains its low solubility[106]. Only the oligomeric fraction becomes soluble to some extent in organic solvents. In this respect an aromatic geometry like in polythiophene should be more promising because of the higher mobility of the polymer backbone. Because ITN is a highly reactive compound[107], such a copolymer should be synthesised through polymerisation of an oligomer in which the reactive ITN unit is stabilised. Since substituents in the 1,3-positions of benzo[c]thiophene are known to stabilise these systems[108], 1,3-di-2-thienylisothianaphthene **1** could be an excellent candidate for this purpose.

When symmetrically substituted with solubilising side chains, monomeric DTITN can be used for oxidative polymerisation using ferric chloride. The resulting polymer is regioregular both in substitution and composition of the monomeric units. For substituted polythiophenes, regioregularity has been proven to be crucial for optimum material properties such as conductivity[109]. The usual polymerisation procedure[110] is to add the monomer quickly to a suspension of $FeCl_3$ in chloroform and then to stir the mixture for some hours. Adding the $FeCl_3$ slurry slowly to the monomer dissolved in chloroform could increase the molecular weight of the polymers.[111] This allows a much softer and more selective polymerisation and there is no large excess of $FeCl_3$ at the beginning of the polymerisation. This favours the growth of the polymer chains instead of the growth of new chains, and thus favours the production of high molecular weight products. The possible propagation mechanism of $FeCl_3$ oxidative polymerisation involves a radical reaction[112] as given in Scheme 7.

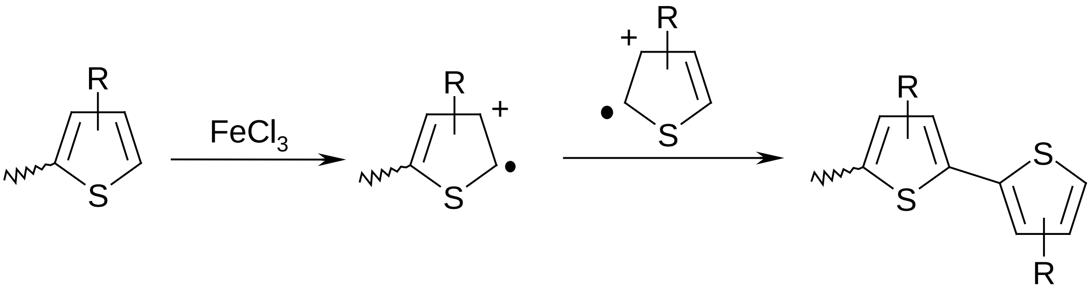

Scheme 7. Proposed propagation mechanism for the regiorandom polymerisation of 3-alkylthiophene involving radical reaction.

Because the regularity of the copolymer is a direct result of the molecular structure of the monomer, this material can be classified as a "formal" copolymer. Poly(1,3-di-2-thienylisothianaphthene) can thus be considered as a formal copolymer of bithiophene and isothianaphthene units. The band gap is expected to have a value between those of polythiophene and polyITN.

5.1 Synthesis of poly(1,3-di-2-thienylbenzo[c]thiophene)s (poly(DTITN)s **13, 14**)

Several synthetic routes to obtain poly(DTITN) can be found in literature. Four groups almost simultaneously published their synthesis at the beginning of the nineties[107,113]. Only recently, a more general synthetic route was developed with a higher overall yield and with possibilities for easy derivatisation[114]. Moreover, $FeCl_3$ oxidative polymerisations of 1,3-di-2-thienylisothianaphthene derivatives with different substituents at 3-position in thiophenes rings and at 5,6-positions in benzo[c]thiophenes have been reported by Vangeneugden et al.[115] As discussed above, polymerisation with $FeCl_3$ is generally known to give irregular polymers, with approximately 70-80% of head-to-tail coupling of 3-alkylsubstituted thiophenes. Regioregular poly(3-alkylthiophene)s compared to irregular poly(3-alkylthiophene)s showed lower band gap, higher conductivity and better performance in electro-optical devices. In order to avoid the formation of an irregular polymer, the synthetic strategy of monomers was chosen in such a way as to obtain molecules with a symmetric structure. The preparation of symmetric monomers **2** and **3** is described in section 3.1. The chemical structures of poly(DTITN)s **13** and **14**, synthesised in this work, are given in Figure 39.

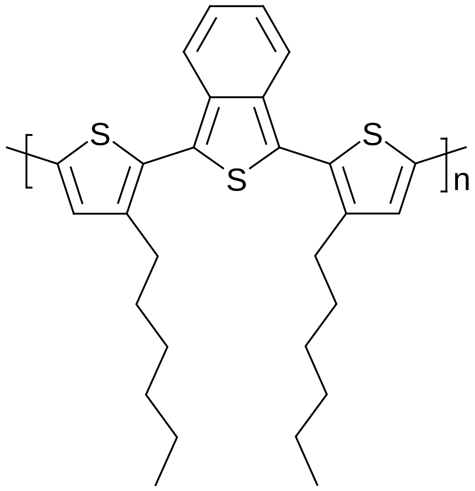

13

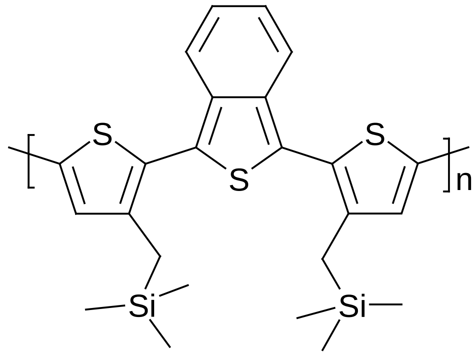

14

*Figure 39. Chemical structures of poly(1,3-bis(2-thienyl)benzo[c]thiophene)s **13** and **14**.*

The syntheses of poly(DTITN)s **13** and **14** via $FeCl_3$ oxidative polymerisation from monomers **2** and **3** respectively are given in Scheme 8. The polymerisations were carried out by adding four times excess of the $FeCl_3$ slurry slowly to the corresponding monomer dissolved in chloroform. The polymers **13** and **14** were obtained from the reaction mixture in a doped state as deep blue solids with the Fe content of 0.43 % and 0.091 % respectively after precipitation of reaction mixtures in hexane. Large Fe content in the polymer **13** makes this polymer unsuitable for application in opto-electronic devices. Moreover, Taka et al.[116] has shown that Fe impurities strongly affect solubility and processability of poly(3-octylthiophene), prepared by ferric chloride polymerisation. Therefore, multi-step purification procedure was undertaken to decrease the Fe content. The poly(1,3-bis(3-hexyl-2-thienyl)benzo[c]thiophene)s **13** and **14** were dedoped using an improved purification procedure (see experimental part, section 11.12.1) in order to achieve brown polymers with an Fe content of only 0.013 % and 0.09 % respectively. Reducing of Fe content in the poly(1,3-bis(3-(trimethylsilyl)methyl-2-thienyl)benzo[c]thiophene) **14** was not possible due to insolubility of this polymer in common organic solvents.

It should be noted, that polymer **13** was only partially soluble in common organic solvents like THF (see experimental part, section 11.12.1). About 79 % of the overall yield was soluble in THF. All further analyses of poly(DTITN) **13** were performed using this fraction, which is soluble in THF. Nevertheless, poly(DTITN)s **13** and **14** were obtained after purification in yields of about 49 % and 59 % respectively as brown solids. Characterisation of polymer **14** was also done using THF soluble fraction.

*Scheme 8. Schematic representation of polymerisations of DTITNs **2** and **3** via $FeCl_3$ oxidative polymerisation.*

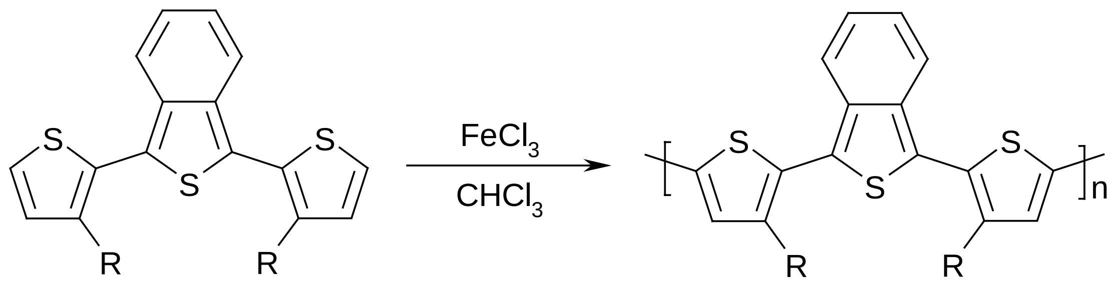

2; R = n-C_6H_{13}
3; R = -CH_2-$Si(CH_3)_3$

13; R = n-C_6H_{13}
14; R = -CH_2-$Si(CH_3)_3$

On the other hand, $FeCl_3$ oxidative polymerisation of unsubstituted 1,3-bis(2-thienyl)isothianaphthene **1** only led to insoluble dark powder, containing dimer, trimer and tetramer of **1**.

5.2 Characterisation

SEC analysis and all spectroscopic analyses, except FT-IR spectroscopy, of poly(1,3-bis(3-hexyl-2-thienyl)benzo[c]thiophene) **13** and poly(1,3-bis(3-(trimethylsilyl)methyl-2-thienyl)benzo[c]thiophene) **14** were done with the THF soluble fractions of these polymers. The rest of polymer **13** was insoluble even in NMP, DMAc etc. Whereas the polymer **14** showed good solubility in chlorobenzene.

5.2.1 ^{1}H-NMR and FT-IR spectroscopy

Polymer **13** exhibited broad proton signals in aromatic region of 7.0 to 7.8 ppm. Broad resonance signals from aliphatic protons were also observed in the range from 0.7 to 2.8 ppm. Furthermore, a characteristic ^{1}H-NMR signal from –C**H$_2$**–Ph aliphatic protons at 2.70 ppm was present in polymer **13**.

Characteristic absorptions due to C-H stretching of thiophene ring at 1444-1453 cm^{-1} and at 745-746 cm^{-1} were observed in polymers **13** and **14**. Additionally, these polymers exhibited characteristic aromatic absorptions at 3060 and 3050 cm^{-1} (C-H stretching), at 1641 and 1636 cm^{-1} (C-C stretching). Moreover, characteristic aliphatic absorptions at 2854-2858 and 2917-2952 cm^{-1} due to C-H stretching presented in the IR spectra of polymers **13** and **14**.

5.2.2 Size Exclusion Chromatography (SEC)

In general, the SEC data obtained against polystyrene standards for polythiophenes have to be taken as relative values. It has been reported by Yue et al.[117] that extensive aggregation occurs in regioregular poly(3-alkylthiophenes), P3ATs and this can lead to exaggerated molecular weight values in the SEC. In order to avoid possible aggregation of polymers **13** and **14**, SEC measurements of these polymers were performed using THF containing 0.25 wt. % of tert-butyl ammonium bromide as eluent.

The SEC elution diagram of poly(DTITN) **13** is represented in Figure 40. This polymer exhibited an M_n of 9160 g/mol, M_w of 26390 g/mol, M_p of 11240 g/mol and relatively low polydispersity index of 2.9.

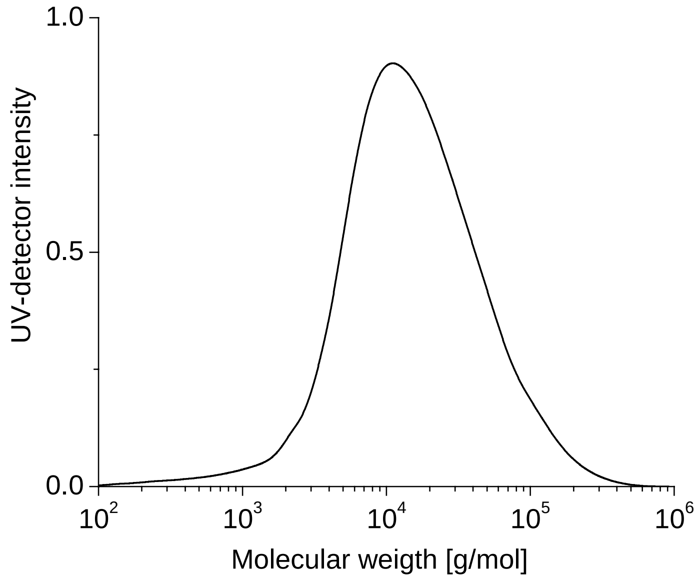

*Figure 40. SEC eluogram of polymer **13** performed against polystyrene standards by using THF, containing 0.25 wt. % of tert-butyl ammonium bromide, as eluent at room temperature.*

The SEC eluogram of polymer **14** obtained from the THF soluble oligomeric fraction of this polymer is illustrated in Figure 41. The main peak on this eluogram belongs to unreacted monomer **3**, the second peak can be explained as a dimer of **3** and the rest are oligomers, containing a tail of polymer fraction up to 10000 g/mol. All data obtained from SEC measurements of poly(DTITN)s **13** and **14** are summarised in Table 8.

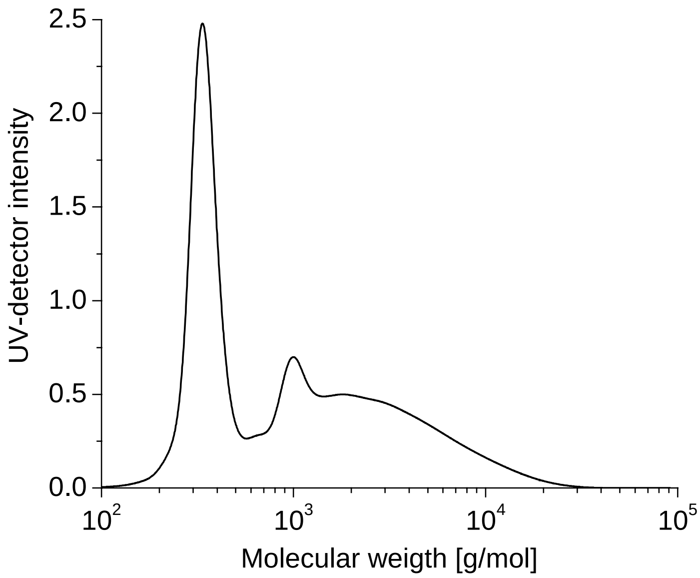

Figure 41. SEC eluogram of oligomeric fraction of polymer ***14*** *performed against polystyrene standards using THF containing 0.25 wt. % of tert-butyl ammonium bromide as eluent at room temperature.*

Table 8. SEC data determined (relatively to polystyrene standards) with THF containing 0.25 wt. % of tert-butyl ammonium bromide as eluent.

Polymer	M_n [g/mol]	M_w [g/mol]	M_p [g/mol]	PDI
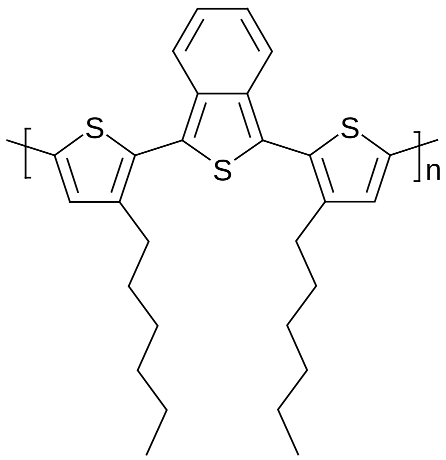 **13**	9160	26390	11240	2.9
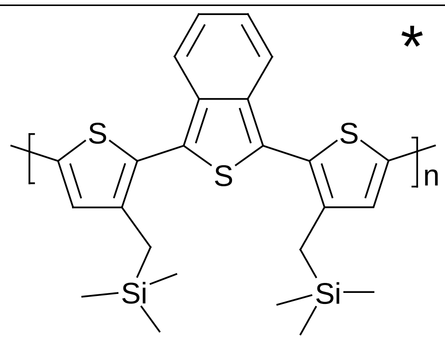 * **14**	580	2000	340	3.44

**- oligomeric fraction*

5.2.3 Optical properties via UV-Vis and Fluorescence spectroscopy

UV-Vis spectroscopy measurements of polymers **13** and **14** were carried out in both solution and thin film, prepared by spin-coating from chlorobenzene. UV-Vis spectra of monomers **2** and **3** are also included for comparison of the absorption spectra of these monomers with the resulting polymers **13** and **14** respectively.

The normalised absorption spectra of DTITN **2**, measured in cyclohexane, and poly(DTITN) **13**, measured in both thin film and chlorobenzene due to its poor solubility in cyclohexane is given in Figure 42. Absorption maxima of polymer **13** in film did not show any shift compared to the spectrum obtained from the solution. On the other hand, broadening of absorption spectra of polymer **13**, measured in thin film, compared to that, measured in chlorobenzene, can be an indication of aggregation of polymer molecules in film.

A red shift of 60 nm from λ_{max}^{abs} from 387 nm to 447 nm was observed from a low molecular weight DTITN **2** to poly(DTITN) **13** respectively.

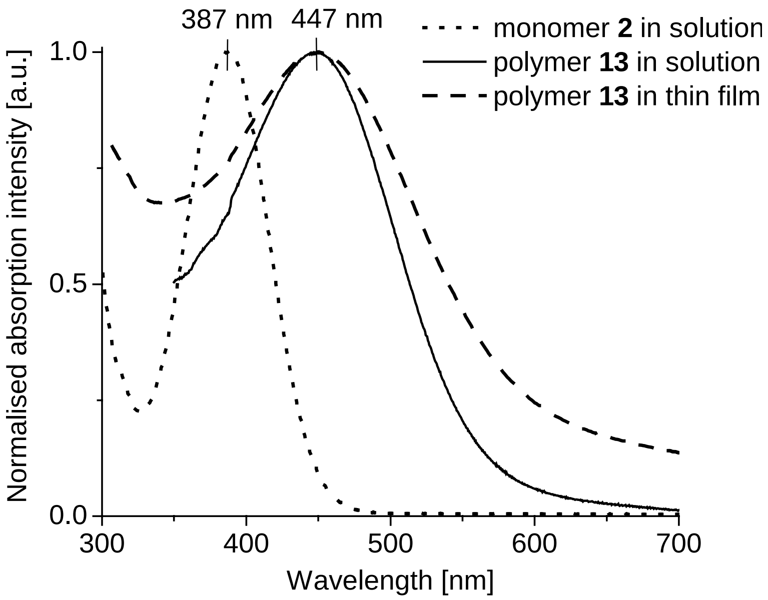

*Figure 42. Normalised absorption spectra of monomer **2**, measured in solution (cyclohexane), and poly(DTITN) **13**, both measured in solution (chlorobenzene) and in thin film.*

A comparison of λ_{max}^{abs} of polymer **14** measured in THF and in thin film showed a red shift of 10 nm and a broadening of the absorption spectra.

UV-Vis spectra of monomer **3** and oligomeric fraction of polymer **14** were compared in a similar manner as above in Figure 43. Absorption spectra of DTITN **3** and poly(DTITN) **14** showed λ_{max}^{abs} of 393 and 446 nm measured in cyclohexane and THF respectively. Thus, the red shift of about 50 nm was observed by comparing the absorption of compound **3** with the oligomeric fraction of polymer **14**. This red shift is similar to that observed in polymer **13**. Such red shifts, observed in polymers **13** and **14**, indicate that an increasing conjugation length from a monomeric molecule to a polymeric molecule can be achieved in 3-substituted DTITNs even though the 3-substituent disturbs the conjugation due to a large torsional angle between the C-C bonds belonging to the thiophene rings.

Both polymers **13** and **14** exhibited band gaps of about 2 eV as calculated from the UV-Vis measurement in thin film by putting tangents on the absorption shoulder (see Table 9). Such a band gap energy of about 2 eV was already observed in the regioregular poly(3-alkylthiophene)s, which does not carry any low band gap ITN group. In this respect, it was expected to observe a band gap lower than 2 eV for poly(1,3-bis(2-thienyl)benzo[c]thiophene)s. This can be explained as being due to steric hindrance between inter thiophene ring C-C bonds, due to the presence of bulky substituents such as hexyl and (trimethylsilyl)methyl groups in poly(DTITN)s **13** and **14** respectively. The increasing of conjugation in the main chain polymers can be overcome by attaching solubilising groups not to 3-position of thiophene ring, but to 5,6-positions of isothianaphthene. In this respect, a new series of main chain polymers, poly(dithienylisothianaphthene phenyldiamine)s **15-17**, represented below (see section 6.1), were synthesised with solubilising groups attached to phenyl rings, and not to the thiophene group.

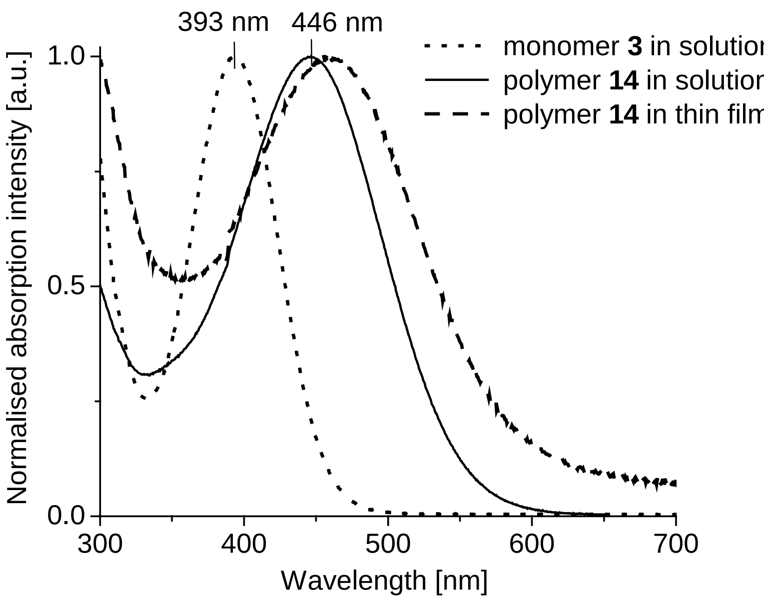

*Figure 43. Normalised absorption spectra of monomer **3**, measured in solution (cyclohexane), and oligomeric fraction **14** both measured in solution (THF) and in thin film*

The photoluminescence of polymer **13** measured in solution ($CHCl_3$) is given in Figure 44. Polymer **13** exhibited fluorescence in solution with a maximum at 596 nm on excitation with a wavelength of 450 nm. No photoluminescence was detected in the thin film of this polymer prepared with a spin coating of its chlorobenzene solution. The photoluminescence spectra of monomer **2**, measured in n-hexane, had a greenish-yellow fluorescence with a maximum at 517 nm. Thus, red shift of emission maxima of 80 nm was observed compared to that of the monomer.

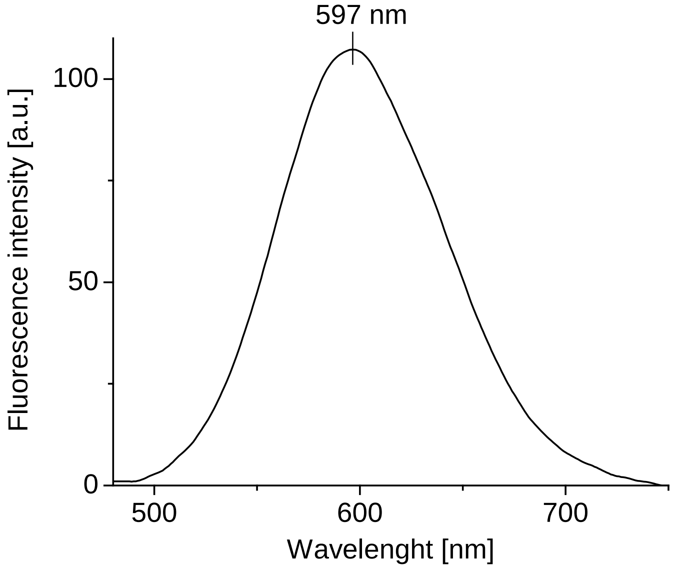

*Figure 44. Fluorescence spectra of polyDTITN **13** (10.8 mg/L) measured in chloroform from excitation wavelength at 450 nm.*

The photoluminescence of polymer **14** was not measured due to its insolubility in common organic solvents.

Optical properties of polymers **13** and **14**, measured in both solution and thin film, are summarised in Table 9.

*Table 9. Optical properties of polyDTITNs **13** and **14** via UV-Vis and fluorescence spectroscopy measured in solution and in thin film.*

Compound	**UV-Vis absorption**						**Fluorescence**	
	λ_{max}^{abs} [nm]		**Edge [nm]**		**E_g^{opt} [eV]**		**λ_{max}^{fl} [nm]**	
	solution	film	solution	film	solution	film	solution	film
13	447[a]	447	560	612	2.21	2.03	597	-[c]
14 (oligomers)	446[b]	456	548	592	2.26	2.09	-[d]	-[d]

E_g^{opt} – optical band gap, calculated from by putting tangents on absorption shoulder
[a] – measured in chlorobenzene
[b] - measured in THF
[c] – not detected
[d] – not measured

5.2.4 Cyclic Voltammetry (CV)

The electrochemical stability and the reversibility of the redox processes of poly(dithienylisothianaphthene) **13** were studied using CV (see Figure 45). The cyclic voltammogram was measured in a solution of carefully dried THF vs. $Ag/AgNO_3$ as reference electrode and each measurement was calibrated with the standard Fc redox system. Polymer **13** exhibited completely reversible one oxidation and one reduction potentials on a cyclic voltammogram measured at scanning rate in a region of 50 to 500 $mV \cdot s^{-1}$. E_{ox1} of 0.16 V and E_{red1} of -2.12 V vs. Fc were obtained from CV measurement. HOMO and LUMO energy values of this polymer are -4.96 and -2.68 eV respectively.

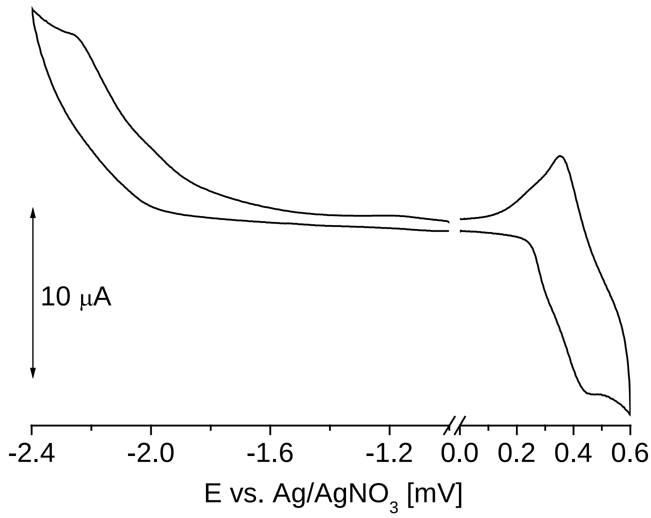

Figure 45. Cyclic voltammogram of polyDTITN ***13*** *measured in THF against $Ag/AgNO_3$ as reference electrode at scanning rate of 50 $mV \cdot s^{-1}$.*

The E_g^{ec} value of polymer **13** was calculated as a difference between HOMO and LUMO values obtained from CV. The E_g^{ec} and E_g^{opt} of this polymer, obtained from THF and from chlorobenzene solutions respectively, showed similar values of about 2.25 eV as given in Table 10. These values were also compared to those of the monomer **2**. In polymer, both HOMO and LUMO values are lowered, thus resulting in a lower band gap for the polymer.

In order to elucidate this, HOMO and LUMO energy bands of monomer **2** and its polymer **13**, are plotted in Figure 46. An increasing conjugation length in polymer **13** compared to model compound **2** led to lowering of the band gap of about 0.7 eV. A comparison of energy levels of DTITN **2** and poly(DTITN) **13** also shows an increase in HOMO values from -5.34 to -4.96 eV and increase in LUMO values from -2.68 to -2.32 eV respectively. The evolution of energy bands obtained by comparing conjugated monomer **2** with main chain conjugated polymer **13** with decreasing E_g is in full agreement with band theory (see Figure 13, section 1.2.2).

*Table 10. Electrochemical properties of the polymer **13** obtained from cyclic voltammetry measured in THF vs. Ag/AgNO$_3$ as reference electrode and calibrated vs. ferrocene.*

Compound	E_{OX1} vs. Fc [V]	HOMO [eV]	E_{RED1} vs. Fc [V]	LUMO [eV]	E_g^{ec} [eV]	E_g^{opt} [eV]
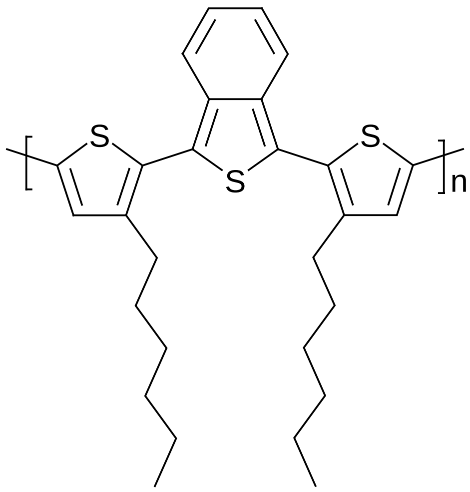 **13**	0.16	-4.96	-2.12	-2.68	2.28	2.21
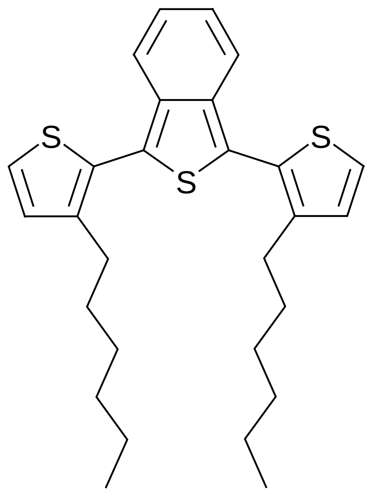 **2**	0.54	-5.34	-2.48	-2.32	3.02	2.79

E_g^{ec} – electrochemical band gap
E_g^{opt} – optical band gap

In conclusion, comparing the electrochemical and optical properties of compounds **2** and **13**, it can be shown that polymerisation of DTITN **2** with symmetrical structure led to solution processable polymer **13**, which has a much lower band gap and improved energy band values compared to its monomeric analogue. Nevertheless, the band gap of 2.28 eV, obtained for poly(DTITN) **13**, is in the range of a band gap values of 2.0-2.5 eV, obtained for low molecular weight (DTITNPD)s **9-11**. In order to get poly(DTITN) with lower band gap, the solubilising groups should be attached to the 5- and 6-positions of benzo[c]thiophenes. Such synthetic strategy should lead to a lower band gap conjugated polymer without strong steric hindrance of solubilising groups, which can disturb the planarity of the molecule.

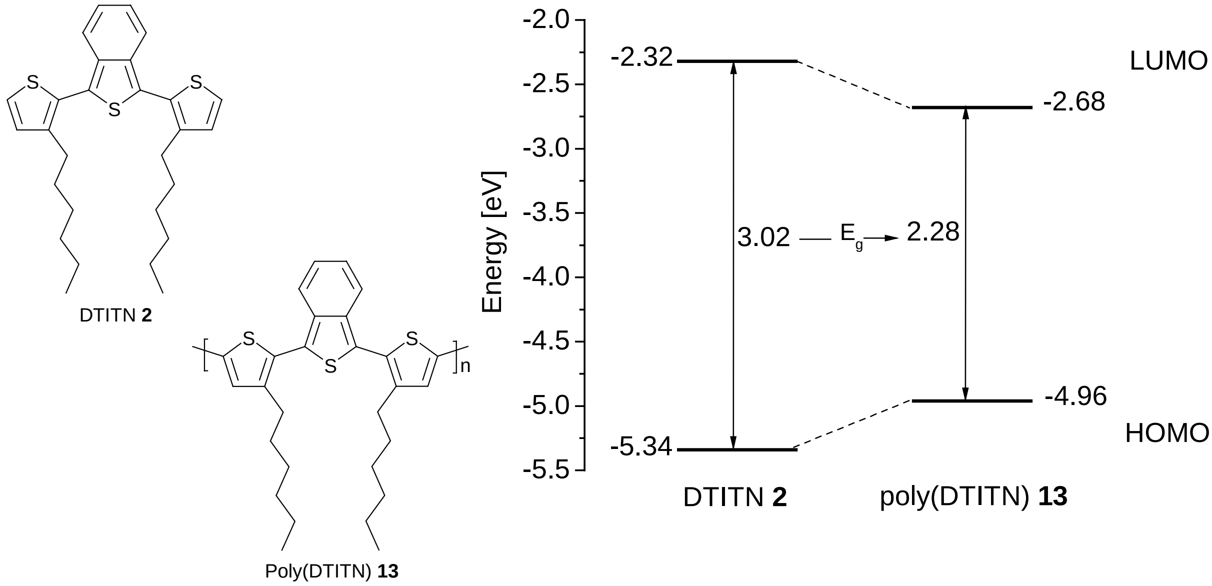

*Figure 46. Energy bands diagram of monomer **2** and its polymer **13**, obtained from CV measurements at 50 mV·s^{-1} scanning rate.*

5.2.5 Thermal properties via TGA and DSC

Thermal properties of polymers **13** and **14** were examined using TGA and DSC measurements. TGA measurements were carried out at a 10 K·min^{-1} heating rate under N_2 atmosphere. The TGA curves showing dependence of weight loss on temperature for all three polymers are represented in Figure 59. The $T_{-5\%}$ values of 315 and 352 °C were observed for poly(1,3-bis(2-thienyl)isothianaphthene)s **13** and **14** respectively. Poly(DTITN) **14** showed higher thermal stability than poly(DTITN) **13** as indicates the difference of their $T_{-5\%}$ value of about 40 °C.

Thermal properties of the polymers **13** and **14** were also studied by measuring three heating and cooling cycles of DSC at a scanning rate of 10 K·min^{-1} under N_2 atmosphere. Poly(DTITN)s **13** and **14** exhibited T_g of 90 and 111 °C respectively. Thus, a higher rigidity of (trimethylsilyl)methyl substituents in polymer **14** compared to flexible hexyl side groups in the polymer **13** shifts Tg from 90 to 111 °C respectively. No melting peak was observed for these polymers in any of the heating and cooling steps of DSC measured in a range from -40 to +250 °C. Characteristic onset temperatures $T_{-5\%}$ and Tg values of polymers **13** and **14** are given in Table 11.

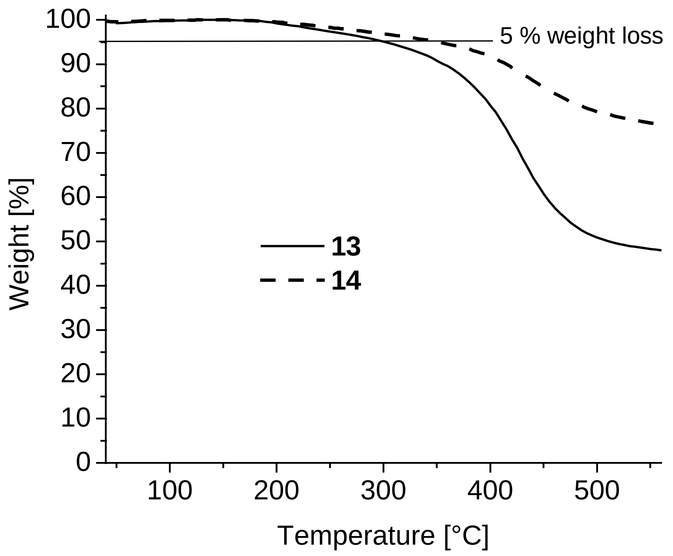

*Figure 47. TGA of polymers **13-14** performed at 10 K·min^{-1} heating rates under N_2 atmosphere.*

*Table 11. Thermal properties of poly(DTITN)s **13** and **14** via TGA and DSC measured at 10 K·min^{-1} heating rate under N_2 atmosphere.*

Polymer	**TGA**	**DSC***
	$T_{-5\%}$ [°C]	T_g [°C]
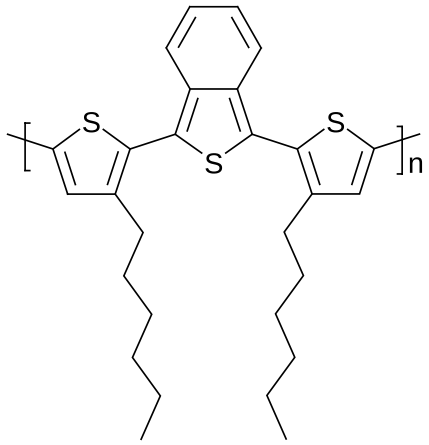 **13**	315	90
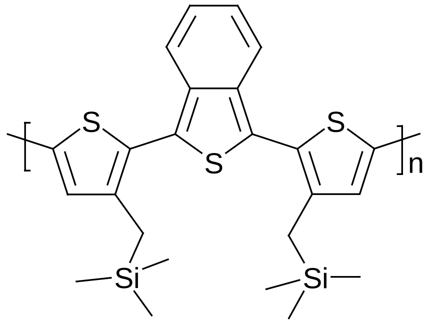 **14**	352	111

** - no melting peak was observed for each polymer in a three heating and cooling steps of DSC measured in a range from -40 to +250 °C.*

6 Polymers carrying triarylamine and 1,3-di-2-thienylbenzo[c]thiophene groups in the main chain

The synthesis, characterisation and properties of a new class of hole-transport dyes, (poly-dithienylisothianaphthene phenyldiamine)s (poly(DTITNPD)s), are highlighted in this chapter. These polymers are characterised by the presence of a low band gap isothianaphthene and hole transport triarylamine units in the main chain. The new polymers, reported here, exhibited improved thermal stability and higher glass transition temperatures. The optical, thermal and electrochemical properties were studied and compared to poly(DTITN)s without having triarylamine groups in the main chain. The incorporation of ITN group into the main chain of a polytriarylamine caused an appreciable lowering of the band gap energy of up to 1.6 eV. This resulted in light harvesting hole-transport dyes having fewer mismatches with the solar spectrum. Moreover, these polymers exhibit reversible redox behaviour and possess HOMO values of about -4.7 eV and LUMO values of about -2.9 eV.

6.1 Synthesis of poly(1,3-bis(5'-diarylaminothiophene-2-yl)benzo[c]thiophene)s (poly(DTITNPD)s **15-17**)

The synthetic strategy of these new polymers is chosen in such a way as to obtain hole-transport, low band gap materials, which can also be solution processable. In order to avoid steric hindrance of solubilising substituents as it was observed for poly(DTITN)s **13** and **14**, the side groups in the new poly(DTITNPD)s were attached to phenyl rings in the phenyldiamine part of these polymers. A modified Ullmann polycondensation reaction using a phase transfer catalyst was utilised to prepare these polymers. Due to the above discussed side reactions by Pd-catalysed coupling, the modified Ullmann procedure with diiodo dithienylisothianaphthene **5** was chosen to prepare the target polymers (see section 1.2.2, page 17). The synthetic route was selected in such a way as to obtain relatively high molecular weight poly(DTITNPD)s **15-17** in good yields (see Scheme 9). Polymerisation from dibromo compounds via this modified Ullmann method was tested and it led to an oligomeric mixture with a molecular weight of less than 3000 g/mol.

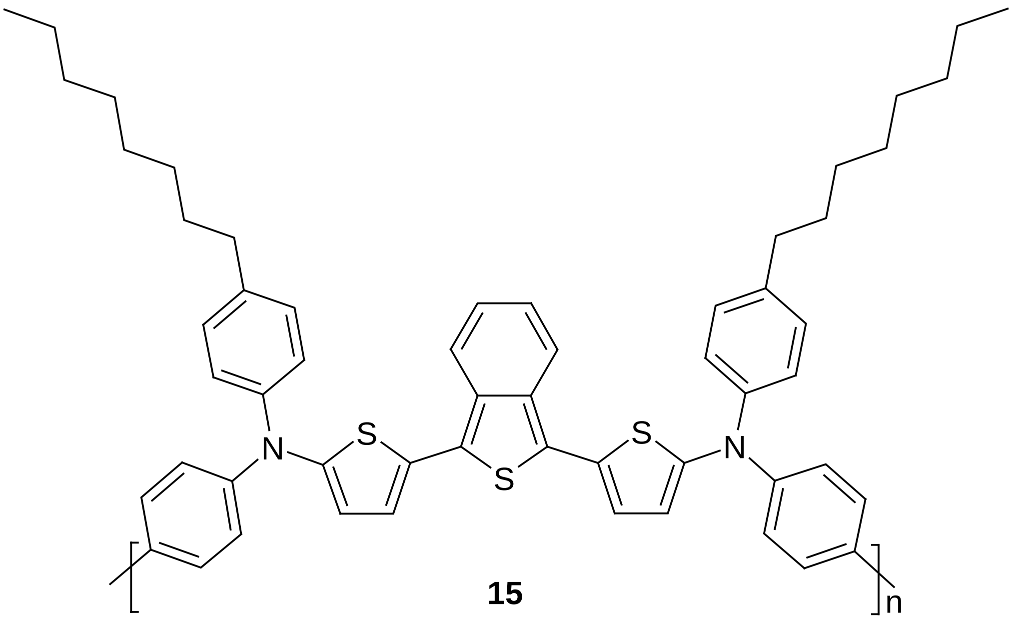

15

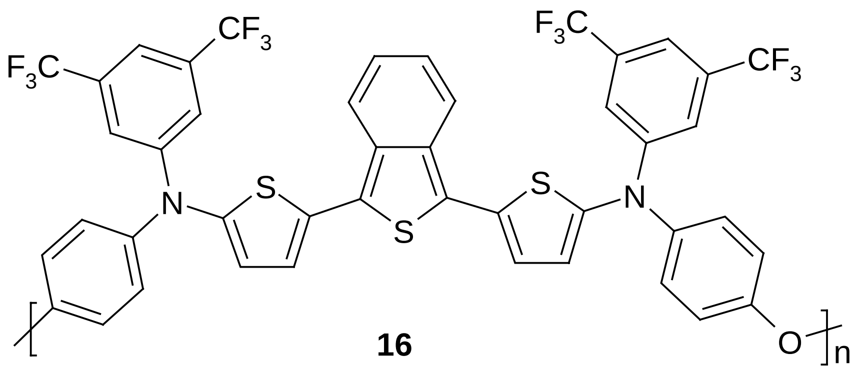

16

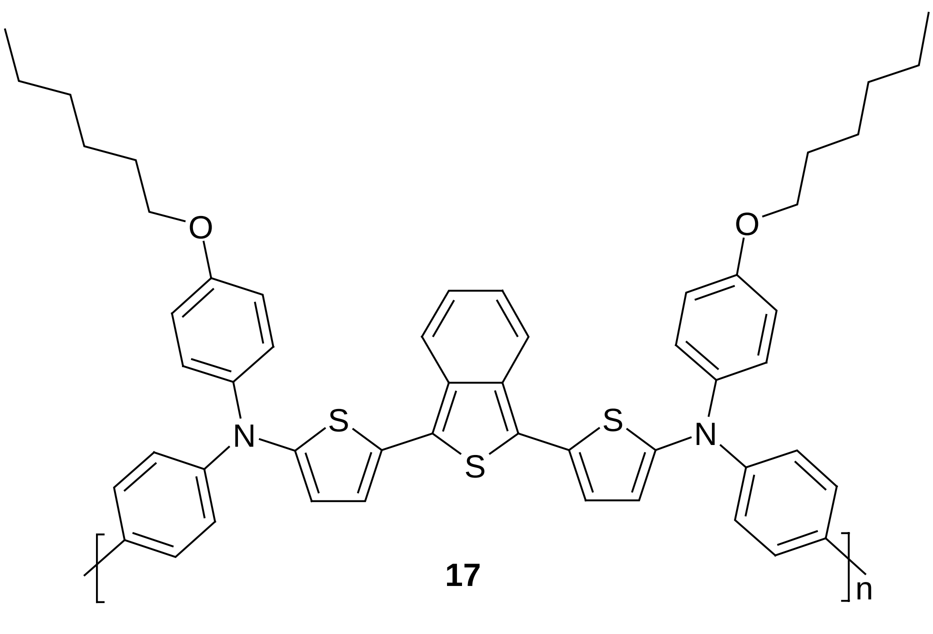

17

Figure 48. Chemical structures of poly(1,3-bis(5'-diarylaminothiophene-2-yl)benzo[c]thiophene)s ***15-17***.

The schematic representation of polycondensation reaction of 1,3-bis(5-iodo-2-thienyl)benzo[c]thiophene **5** with bis(secondary amine)s **6-8** via the modified Ullmann method is given in Scheme 9. The poly(DTITNPD)s **15-17** were obtained as dark-brown solids in yields of 63, 78 and 43 % respectively. In order to get materials with high purity for further application in electro-optic devices, each polymer was purified by repeated reprecipitation, at least 3 times. All the polymers possess solubility in common organic solvents, such as $CHCl_3$, THF, toluene and xylene. Polymers **15** and **17** formed thin and stable amorphous films of high optical clarity by solution casting on glass substrates. The trifluoromethyl groups were introduced into polymer **16** with an aim to obtain hydrophobic material with selective wetting property on substrates. Accordingly, it was found that polymer **16** formed amorphous films only on hydrophobic substrates, obtained by silylation of glass substrates.

The synthesis of 1,3-bis(5-iodo-2-thienyl)isothianaphthene **5** from 1,3-di-2-thienylisothianaphthene **1** is given in Scheme 4 under section 3.3. The preparation of a series of bis(secondary amine)s **6-8** through the Pd-catalysed coupling of corresponding diiodobiphenyls and anilines is presented in Scheme 5 (see section 3.4).

*Scheme 9. Polycondensation of 1,3-bis(5-iodo-2-thienyl)isothianaphthene **5** with bis(secondary amine)s **6-8** via modified Ullmann procedure resulting in poly(1,3-bis(5'-diarylaminothiophene-2-yl)benzo[c]thiophene)s **15-17**.*

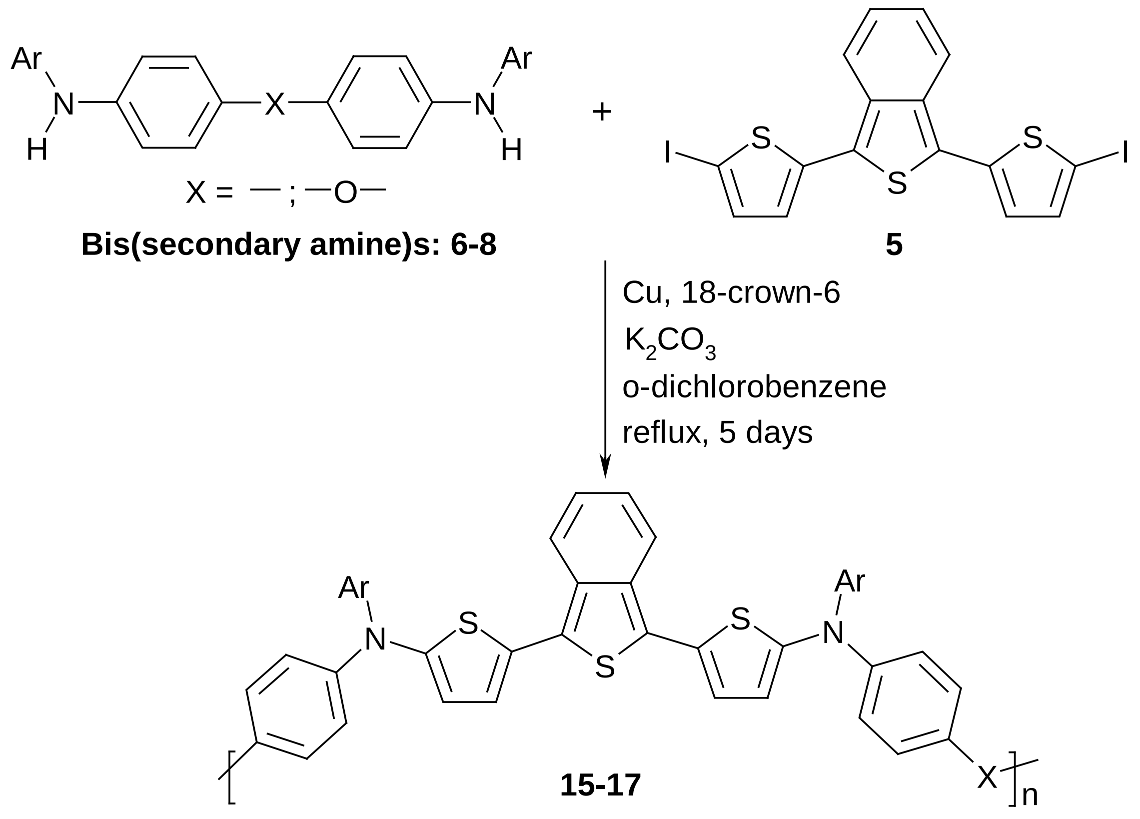

Diarylaminobiphenyls	**Poly(DTITNPD)s**
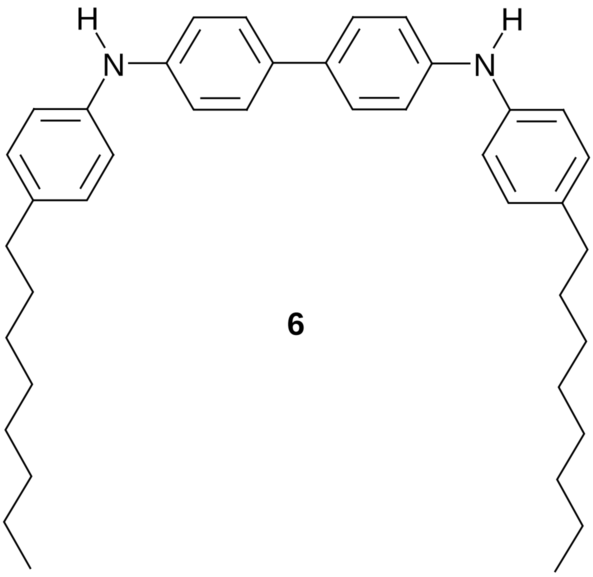 **6**	**15**
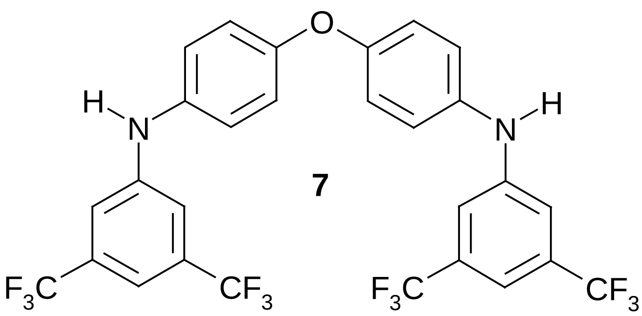 **7**	**16**
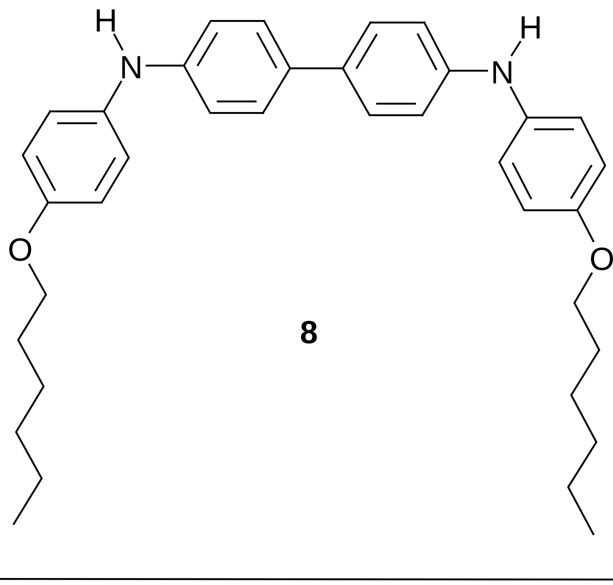 **8**	**17**

6.2 Characterisation

6.2.1 ^{1}H-NMR and FT-IR spectroscopy

All these polymers showed broad proton signals in ^{1}H-NMR spectra. Polymer **16** exhibited only phenyl and thienyl proton signals in the aromatic region of 6.8 to 8.0 ppm and no signals in aliphatic region. Polymers **15** and **17** showed signals from aliphatic protons in the range from 0.8 to 4.0 ppm, additional to aromatic protons similar to polymer **16**. Furthermore, characteristic ^{1}H-NMR signal from –C$\mathbf{H_2}$–Ph aliphatic protons was presented at 2.53 ppm in polymer **15**, and polymer **17** showed a characteristic signal belonging to –C$\mathbf{H_2}$–O aliphatic protons at 3.88 ppm.

In polymers **15-17**, the strong IR absorptions at 3405-3419 cm^{-1} due to N-H stretching in monomers **6-8** disappeared completely and the characteristic C-N stretching of amine at 1250-1314 cm^{-1} and characteristic absorptions due to C-H stretching of thiophene ring at 1492-1495 and at 742-746 cm^{-1} were observed in the products. Additionally, these polymers exhibited characteristic aromatic absorptions at 3029-3064 cm^{-1} (C-H stretching), and at 1603-1617 cm^{-1} (C-C stretching). Moreover, characteristic aliphatic absorptions at 2851-2858, 2924-2928 cm^{-1} due to C-H stretching were present in IR spectra of polymers **15** and **17**.

6.2.2 Size Exclusion Chromatography (SEC)

By each polycondensation, the reaction progress was monitored by size exclusion chromatography (SEC) by taking out aliquots and doing SEC at different time intervals. The SEC elution curves for the reaction between monomers **8** and **5** resulting in polymer **17** are shown in Figure 49. The curve A of Figure 49 illustrates the eluograms of monomers; curve B represents the product obtained after 3 days of reaction and curve C shows the polymer obtained after 5 days of reaction. It can be clearly seen that the discrete oligomers up to the pentamer stage, that were formed in 2-3 days get converted into high molecular weight polymers with prolonged time of polymerisation. Similar results were obtained for the polycondensations of **6** and **7** with **5** resulting in appreciably high molecular weights of **15** and **16**.

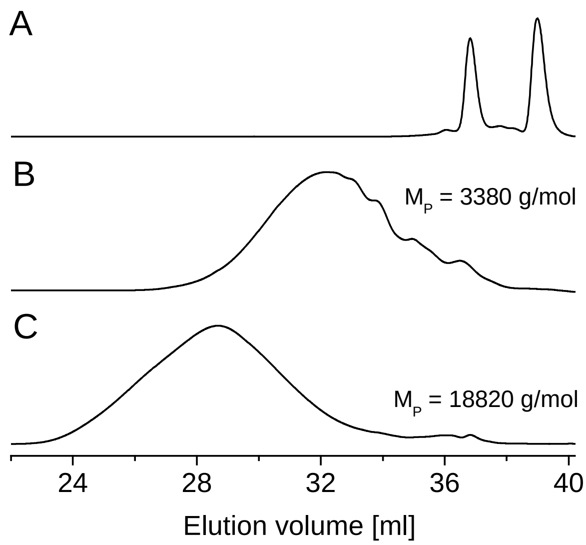

*Figure 49. Monitoring of the polycondensation of monomers **8** and **5** via modified Ullmann procedure using SEC with polystyrene as standard and THF containing 0.25 wt.% of* tert-*butyl ammonium bromide as eluent. SEC eluogram (A) of starting monomers **8** and **5**, (B) precipitated product after 3 days reaction time, (C) precipitated polymer after 5 days reaction time.*

The SEC data for all the polymers with polystyrene as standard and THF containing 0.25 wt.% of *tert*-butyl ammonium bromide as eluent is given in Table 12. The polymers **15-17** exhibited M_n of 10480, 5980 and 7240 g/mol respectively. As expected for polycondensation, the polydispersity varies over a wide range between 4 and 12 depending on the reactivity and concentration of monomers.

The M_w for **15-17** were observed as 127520, 47540 and 28990 g/mol respectively. The highest molecular weight (M_w = 127520 g/mol) was obtained for the polymer **15** carrying octyl groups and the lowest molecular weight (M_w = 28990 g/mol) was observed in the polymer **17** with hexyloxy groups, which is in agreement with the degree of solubility of corresponding monomers **6** and **8**, carrying octyl and hexyloxy side groups and the resulting polymers respectively, in reaction media. In order to study the effect of monomer concentration on the polycondensation reaction, polymer **15** was also prepared using the same polymerisation method, but under more diluted reaction conditions (0.09 M instead 0.15 M). The resulting polymer is denoted as **15a** and it had a lower molecular weight of M_n = 7730 g/mol, M_w = 23180 g/mol and a narrow molecular weight distribution of 3. The low polydispersity of this polymer can be explained as being due to an efficient removal of the oligomers by repeated reprecipitation, which allowed removing oligomers from low molecular weight polymer **15a**, which was not so successful for polymer **15**.

*Table 12. SEC data of polymers **15-17** determined (relatively to polystyrene standards) with THF containing 0.25 wt. % of tert-butyl ammonium bromide as eluent.*

Polymer	M_n [g/mol]	M_w [g/mol]	M_p [g/mol]	PDI
15	10 480	127 520	146 580	12.1
15a	7730	23180	12470	3.0
16	5 980	47 540	45 280	7.9
17	7 240	28 990	18 820	4.0

6.2.3 Optical properties via UV-Vis and Fluorescence Spectroscopy

The optical properties of poly(1,3-bis(5'-diarylaminothiophene-2-yl)benzo[c]thiophene)s **15-17** were studied by measuring UV-Vis spectra both in solution ($CHCl_3$) and in thin films prepared by spin-coating from $CHCl_3$.

The normalised UV-Vis absorption spectra of these polymers, measured in $CHCl_3$, are illustrated in Figure 50. Polymers **15-17** showed two vibronic bands in absorption spectra. Absorption maxima of poly(DTITNPD)s **15** and **16** are 505 and 538 nm respectively, whereas polymer **17** shows a very broad absorption from 440 to 520 nm with a long wavelength absorption shoulder at about 520 nm. The polymers **15-17** show extended absorption up to 700 nm in $CHCl_3$ with E_g^{opt} values of 1.77, 1.81 and 1.90 eV respectively as calculated from absorption edge wavelengths.

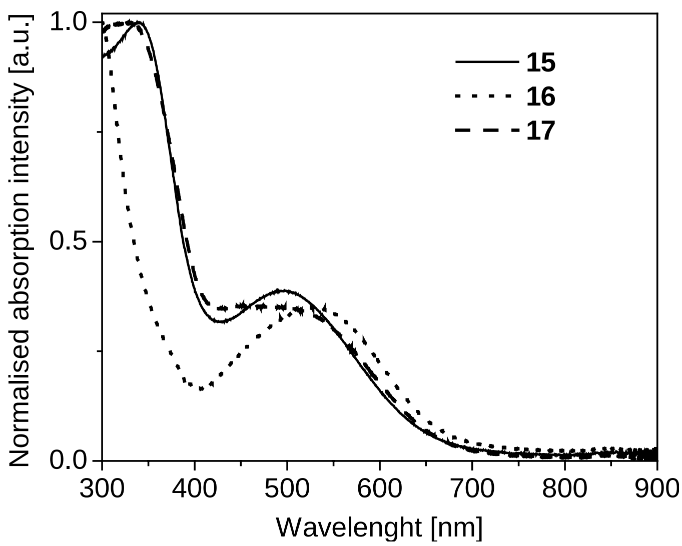

*Figure 50. Normalised absorption spectra of poly(DTITNPD)s **15-17** measured in chloroform.*

The UV-Vis spectra of these polymers, measured in thin film, are illustrated in Figure 51. All the polymers **15-17** show similar absorption spectra in thin film with two vibronic bands. But polymer **15** has the highest absorption coefficient compared to polymers **16** and **17**. The absorption of polymers **15-17** extends up to 750 nm with E_g^{opt} values (as calculated from absorption edge) of 1.71, 1.66 and 1.68 eV respectively. Such a low band gap nature (~1.7 eV) makes the polymers suitable for application in polymeric solar cells. The longest wavelengths of absorption maxima (λ_{max}^{abs}) of poly(dithienylisothianaphthene phenyldiamine)s **15-17** in the visible region are 523, 545 and 530 nm respectively. Thus polymer **17** exhibits broadening of absorption both in solution as well as in solid state, indicating aggregation behaviour.

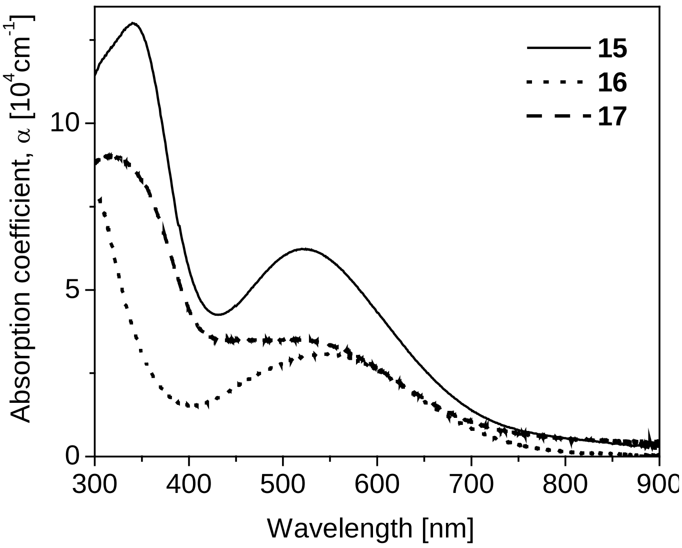

*Figure 51. UV-Vis spectra of poly(DTITNPD)s **15-17** measured in film.*

Moreover, the absorption spectra of these polymers measured in thin film showed a bathochromic shift of about 10-20 nm compared to absorption measured in solution ($CHCl_3$) as given in Table 13. Such bathochromic shift was also observed in the case of low molecular weight (dithienylisothianaphthene phenyldiamine)s **9-11** (see section 4.2.2). This shift of λ_{max}^{abs} may be attributed to solvent effect or it can also be explained by Kasha's molecular exciton model for J-aggregates as illustrated in Figure 34 (see page 53) for the case of model compounds **9-11**.

The photoluminescence spectra of polymers **15-17** measured in $CHCl_3$ are illustrated in Figure 52. The polymers **15-17** showed similar red fluorescence with corresponding maxima at 584, 582 and 579 nm using an excitation wavelength of 500 nm. The fluorescence spectra of these macromolecules were also measured in thin film in order to study photoluminescence properties of poly(dithienylisothianaphthene phenyldiamine)s **15-17** as potential emitters for

OLEDs. But no fluorescence from these polymers was observed in thin film, which can be explained as being due to concentration quenching effect arising in solid state.

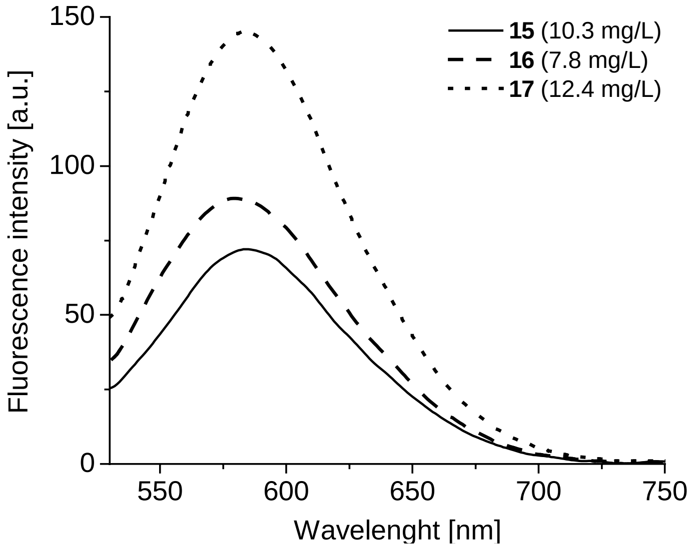

*Figure 52. Fluorescence spectra of poly(DTITNPD)s **15-17** measured in chloroform with concentrations of 10.3, 7.8 and 12.4 mg/L respectively at 500 nm excitation wavelength.*

The results of the optical study of polymers **15-17** measured both in solution and in the thin film are summarised in a Table 13.

*Table 13. Optical properties of poly(dithienylisothianaphthene phenyldiamine)s **15-17** via UV-Vis absorption measured in solution ($CHCl_3$) and in thin film and fluorescence measured in solution ($CHCl_3$).*

Polymer	**UV-Vis absorption**							**Fluorescence**
	λ_{max}^{abs} [nm]		**α [cm^{-1}]**	**Edge [nm]**		**E_g^{opt} [eV]**		**λ_{max}^{fl} [nm]**
	$CHCl_3$	film	film	$CHCl_3$	film	$CHCl_3$	film	$CHCl_3$
15	505	523	62300	700	725	1.77	1.71	582
16	538	545	30800	685	745	1.81	1.66	584
17	520	530	35200	653	740	1.90	1.68	579

α – absorption coefficient at λ_{max}^{abs}
E_g^{opt} – optical band gap as calculated from λ_{edge}
T_g – glass transition temperature
$T_{-5\%}$ – onset temperature at 5 % weight loss

The absorption measured in both solution and thin film of low molecular weight DTITNPDs **9** and **10,** carrying alkoxy and trifluoromethyl substituents respectively, was compared with poly(DTITNPD)s **17** and **16**, which also carry alkoxy and trifluoromethyl side groups respectively. But there is one small difference between the chemical structures of polymer **16,** in which the repeating units are interconnected via an ether linkage, and model compound **10**. Absorption maxima of compound **10**, carrying electron-withdrawing trifluoromethyl groups, was blue-shifted by about 50 nm compared to compound **9**, carrying electron-donating alkoxy groups as given in Table 5 under section 4.2.2. It was expected that a similar blue shift would be observed in the maximum absorption of polymer **16** compared to polymer **17**. But maximum absorption of **16** is shifted slightly towards longer wavelengths compared to **17** (see Table 13). The red shift in **16** can be explained as being due to the presence of the oxygen atom introduced between two phenyl rings, which avoids torsion around the inter ring bonds, leading to a longer conjugation. Moreover, ether linkage also brings more electron density to this polymer.

Polymers **15-17**, carrying diphenylamine and dithienylisothianaphthene groups, were also compared with polymer **13**, which has only dithienylisothianaphthene group in the main chain and no diphenylamine group (see section 5.1 for chemical structure). Poly(DTITNPD) **15** showed a red shift of about 70 nm compared to polyDTITN **13** as illustrated below.

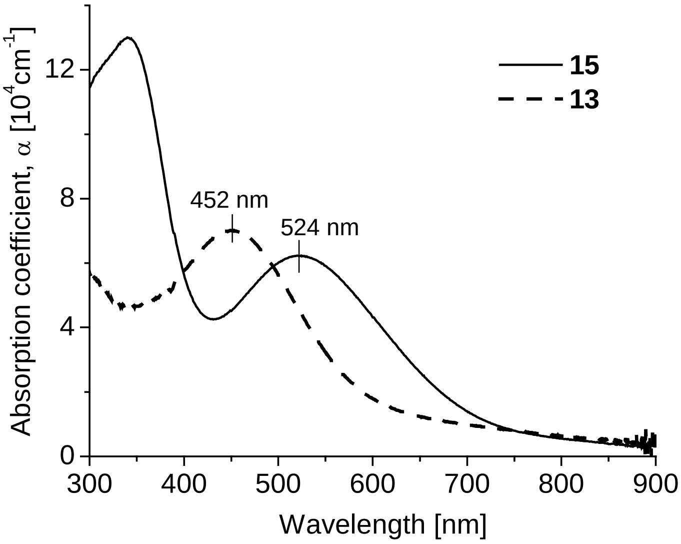

*Figure 53. Comparison of UV-Vis spectra of polyDTITN **13** without any phenyldiamine groups and poly(DTITNPD) **15**.*

This result indicates that the incorporation of the triaryldiamine unit into the main chain of a polyDTITN leads to longer conjugation. A similar result was also obtained in the case of low molecular weight compounds DTITNPDs **9-11** compared to DTITNs **1-3** as discussed in section 4.2.2. Additionally, the steric hindrance due to the two hexyl substituents attached to the thiophenes rings in polymer **13** causes stronger torsion around the inter ring bonds which leads to a lower conjugation. On the other hand, octyl side groups, attached to the phenyl rings of polymer **15**, should not sterically disturb the planarity of this polymer. Thus, the strategy of introducing dithienylisothianaphthene and diphenylamine groups into one molecule has paid off considerably in terms of extended conjugation and in turn broader absorption.

6.2.4 Cyclic Voltammetry (CV)

The electrochemical stability and the reversibility of the redox processes of poly(dithienylisothianaphthene diamine)s **15-17** were studied using CV. The redox potentials were measured in a solution of carefully dried THF vs. Ag/AgNO$_3$ as reference electrode and each measurement was calibrated with the standard Fc redox system. Cyclic voltammograms of polymers **15-17** showing reduction are given in Figure 54, and CV curves of these polymers showing oxidation are given in Figure 55.

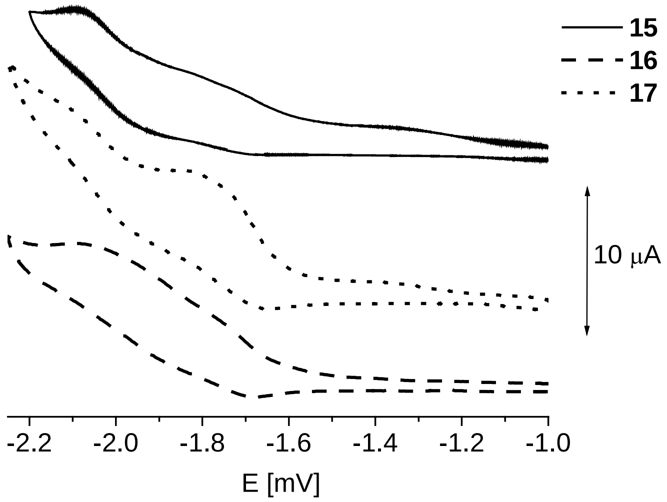

Figure 54. Cyclic voltammograms showing reduction of poly(DTITNPD)s **15-17** *measured in THF vs. Ag/AgNO$_3$ at 50 mV·s^{-1} scanning rate.*

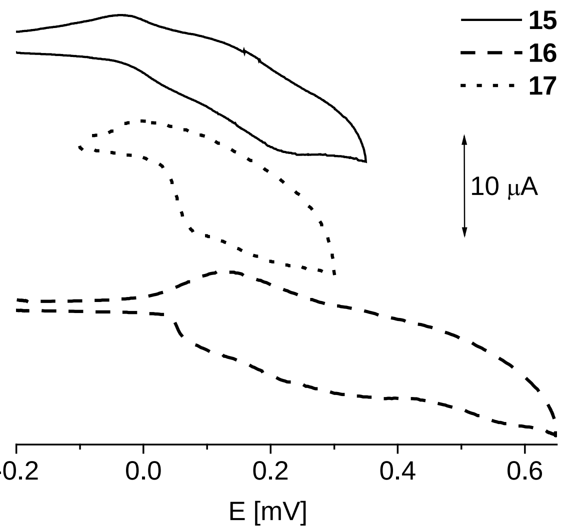

Figure 55. Cyclic voltammograms showing oxidation of poly(DTITNPD)s **15-17** *measured in THF vs. Ag/AgNO$_3$ at 50 mV·s^{-1} scanning rate.*

Electrochemical stability of polymers **15-17** was examined by measuring repeated cycles of redox processes for the scanning rate of 50 $mV \cdot s^{-1}$ to 500 $mV \cdot s^{-1}$. Similar to their model compounds, these polymers are also stable for these scanning rates. Poly(dithienylisothianaphthene phenyldiamine)s **15-17** showed similar oxidation behaviour with completely reversible two oxidation steps. It is known in literature, that poly(phenyldiamine)s always exhibit two oxidation steps in cyclic voltammogram, whereas the reduction steps are usually not observed, because of low electron affinity of these polymers. Polymers **15-17** also showed similar reduction behaviour with completely reversible two reduction steps. These oxidation and reduction steps were broad as expected for the macromolecules with high molecular weight distribution (PDI of **15-17** > 3). The E_{ox1} values corrected against Fc for compounds **15-17** are -0.13, -0.10 and 0 V respectively. The HOMO energy levels of **15-17** are at about -4.7 eV and are given in Table 14. Polymers **15-17** showed distinct reduction E_{red1} at about -1.9 V vs. Fc with the LUMO energy values of -2.9 eV. This indicates, that these new polymers have higher electron affinity than their corresponding analogue with DTITN group. The E_g^{ec} values of these polymers were calculated as a difference between HOMO and LUMO values obtained from CV. The E_g^{ec} and E_g^{opt} of these polymers, obtained from THF and from $CHCl_3$ respectively, showed similar values of about 1.8 eV (see Table 14).

*Table 14. Electrochemical properties of the polymers **15-17** obtained from cyclic voltammetry measured in THF vs. Ag/AgNO$_3$ as reference electrode and calibrated vs. Fc.*

Polymer	E_{ox1} vs. Fc [V]	HOMO [eV]	E_{red1} vs. Fc [V]	LUMO [eV]	E_g^{ec} [eV]	E_g^{opt} [eV]
15	-0.13	-4.67	-1.88	-2.92	1.75	1.77
16	-0.10	-4.70	-1.88	-2.92	1.78	1.81
17	0	-4.80	-1.85	-2.95	1.85	1.90

E_g^{ec} – electrochemical band gap
E_g^{opt} – optical band gap from measurements in chloroform

Electrochemical properties of new poly(DTITNPD)s, carrying diarylamine groups in the main chain, were compared here to those of poly(DTITN)s, which do not carry any diarylamine groups. In this way, energy band diagrams of poly(DTITN) **13** and poly(DTITNPD) **15**, carrying hexyl and octyl groups respectively, are represented in Figure 56. It was discussed above in section 4.2.3, that low molecular weight (DTITNPD) **11** exhibited lower band gap than low molecular weight DTITNs **1** due to the decreasing of LUMO levels in DTITNPDs compared to DTITN, keeping the HOMO levels of both constant (see Figure 36). A similar result was observed when comparing the electrochemical and optical properties of poly(DTITN) **13** and poly(DTITNPD) **15**, where the band gap was lowered from 2.3 to 1.8 eV with decreasing the LUMO energy values from -2.7 eV up to -2.9 eV respectively (compare Table 10 under section 5.2.4 and Table 14). Moreover, the HOMO levels of poly(DTITNPD)s **15** were increased from -5.0 eV to -4.7 eV compared to poly(DTITN) **13**. Decreasing of HOMO levels in poly(DTITNPD) **15** compared to poly(DTITN) **13** is not in agreement with data, obtained by comparing DTITNPD **11** with DTITN **1**. This disagreement can be explained as follows. The disturbance of the planarity in poly(DTITN) **13** due to steric hindrance of hexyl side groups, attached into 3-positions of thiophenes, leads to lower conjugation, keeping the LUMO level high. On the other hand, octyl groups, attached into *para* position of phenyl rings of diarylamines in polymer **15**, do not disturb planarity of this polymer leading to longer conjugation, which brings decreasing LUMO level of polymer **15** compared to polymer **13**.

Thus, the synthetic strategy, chosen for preparation of poly(DTITNPD)s **15-17** led to low band gap polymers with improved HOMO and LUMO energy levels.

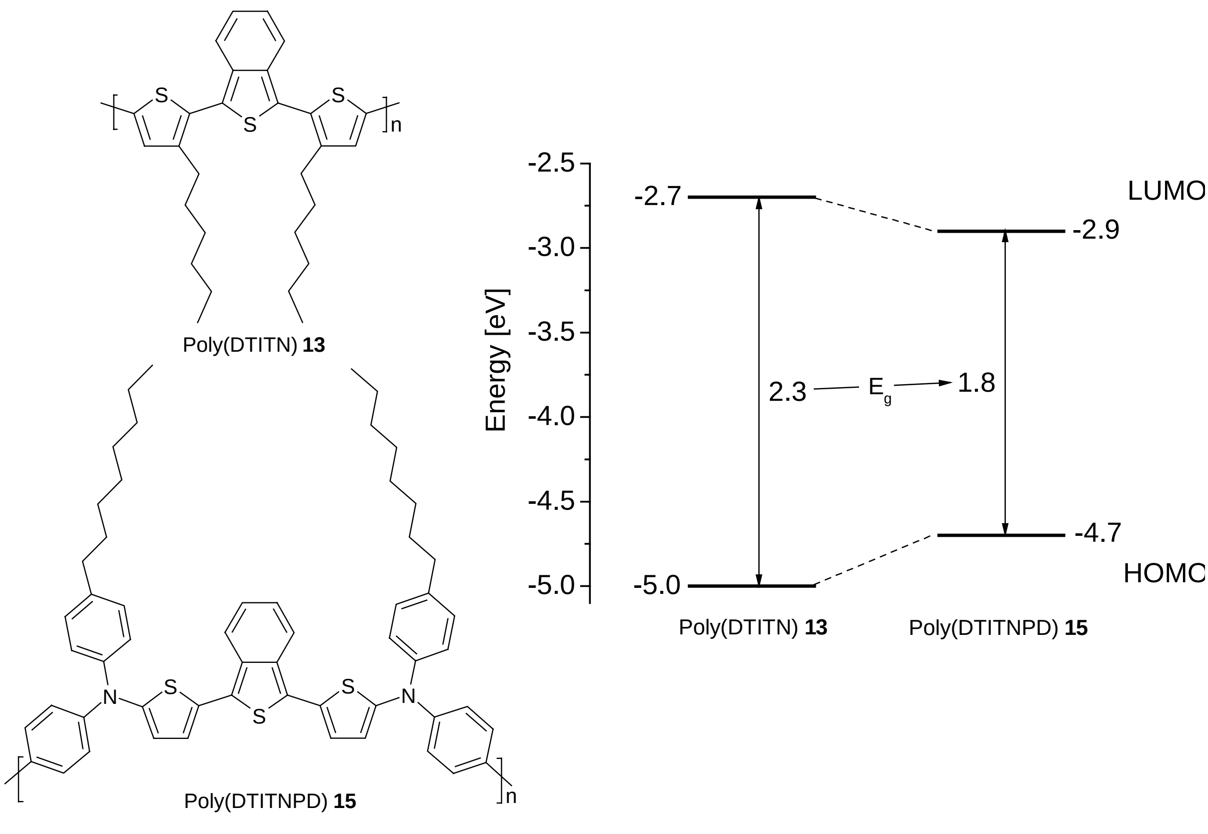

Figure 56. Comparison of HOMO and LUMO energy levels and band gaps, obtained from CV measurements of poly(DTITN) ***13*** *with poly(DTITNPD)* ***15****.*

It is also very interesting from scientific point of view to compare electrochemical properties of low molecular weight and polymeric DTITNPDs. The chemical structures of low molar mass and polymeric DTITNPDs are different; there are no full analogues available. But, in general, low molecular weight and polymeric DTITNPDs **9-11** and **15-17** exhibited HOMO values in the range of -5.0 to -4.6 eV with lowering of the band gaps from 2.1±0.1 eV to about 1.8 eV respectively. Relatively constant HOMO values of all of these polymers indicates that increasing conjugation length in DTITNPDs does not affect the HOMO level of these molecules (compare Table 6 under section 4.2.3 and Table 14), and lowering of the band gap is mainly due to decreasing of LUMO energy bands in poly(DTITNPD)s **15-17** compared to DTITNPDs **9-11**.

Nevertheless, model compound **10** and polymer **16** were chosen, as an example, to compare their electrochemical properties, because both of these compounds carry four electron-poor trifluoromethyl substituents per unit (see Figure 57). As expected, the decreasing of LUMO value in **16** compared to **10** from -2.79 to -2.92 eV respectively by 0.13 eV was observed. The large increasing of the HOMO level from –5.06 to -4.70 eV, comparing compounds **10** and **16** respectively, can be explained as being due to influence of an oxygen atom introduced into the main chain of polymer **16**. It was already shown, that DTITNPD **9** carrying electron-donor methoxy substituents compared to DTITNPD **10** carrying electron-acceptor trifluoromethyl substituents showed an increase in the HOMO value of about 0.4 eV (see Table 6 under section 4.2.3). Thus, lowering of the band gap in the polymer **16** compared to compound **10** was observed from 2.27 to 1.78 eV respectively by about 0.5 eV.

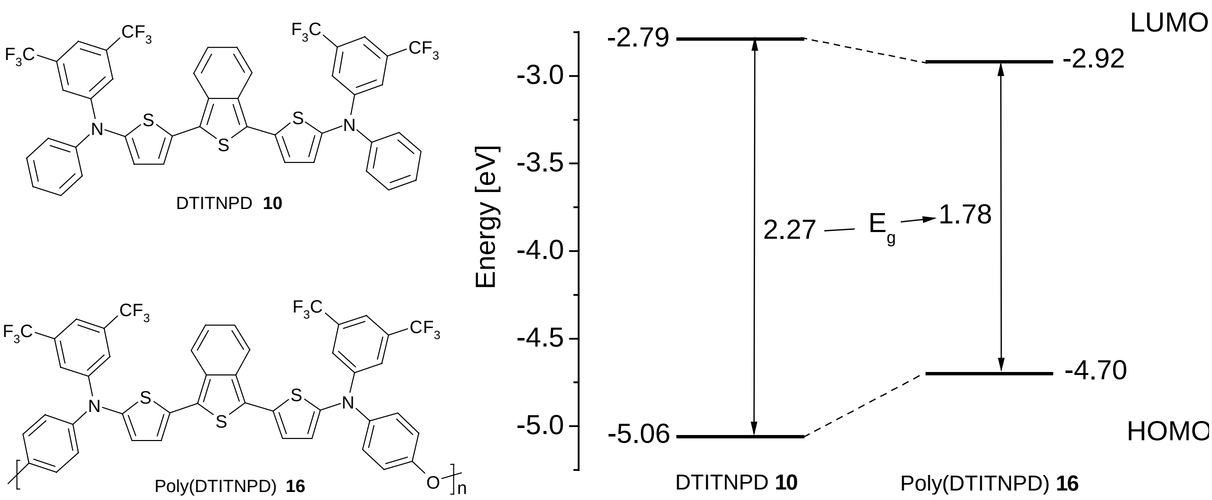

*Figure 57. Comparison of HOMO and LUMO energy levels and band gaps, obtained from CV measurements of DTITNPD **10** with poly(DTITNPD) **16**.*

Electrochemical properties of model compound **9** and polymer **17** were also compared, because these compounds carry corresponding electron-rich methoxy and hexyloxy substituents. As expected, the LUMO value was decreased from -2.60 eV to -2.95 eV comparing model compound **9** with polymer **17** respectively due to increased of conjugation of polymer compared to model compound. The HOMO value of DTINTPD **9** was surprisingly higher than that of poly(DTINTPD) **17**, -4.61 eV and -4.80 eV respectively. Its can be explained due to the fact that compound **9** carries more electron-donating substituents per unit than polymer **17**. Corresponding four methoxy groups and two hexyloxy groups are present in **9** and **17**. Nevertheless, polymer **17** exhibited lower band gap value of about 0.15 eV than model compound **9**.

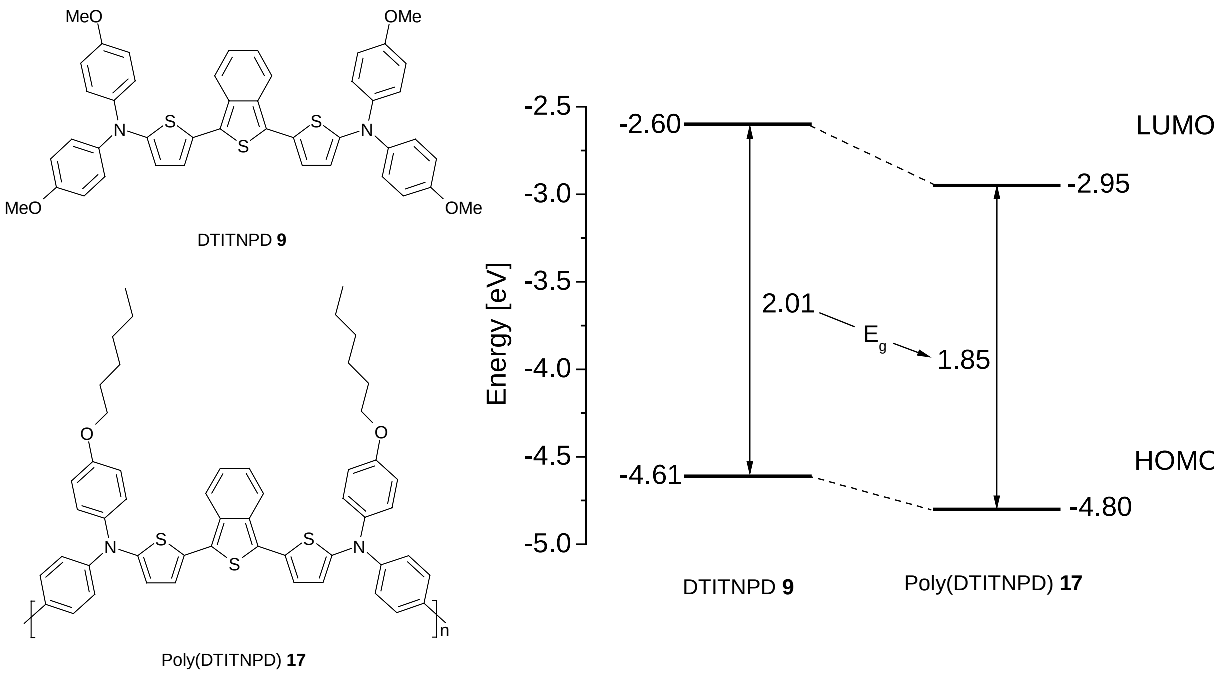

*Figure 58. Comparison of HOMO and LUMO energy levels and band gaps, obtained from CV measurements of DTITNPD **9** with poly(DTITNPD) **17**.*

6.2.5 Thermal properties via TGA and DSC

TGA and DSC measurements were performed for polymers **15-17** in order to study their thermal properties. All measurements were carried out at 10 K·min^{-1} heating rates under N_2 atmosphere. The TGA curves showing weight loss vs. temperature for all the three polymers are given in Figure 59. Characteristic onset temperatures for a 5 % weight loss ($T_{-5\%}$) are shown in Table 15. Poly(1,3-bis(5'-diarylaminothiophene-2-yl)benzo[c]thiophene)s **15-17** showed $T_{-5\%}$ of 381, 393 and 385 °C respectively. Poly(DTITNPD) **16** showed a slightly higher $T_{-5\%}$ value of about 10 °C compared to poly(DTITNPD)s **15** and **17**. This indicates better thermal stability of polymer **16**, carrying trifluoromethyl side groups, than polymers **15** and **17**, carrying octyl and hexyloxy side groups respectively.

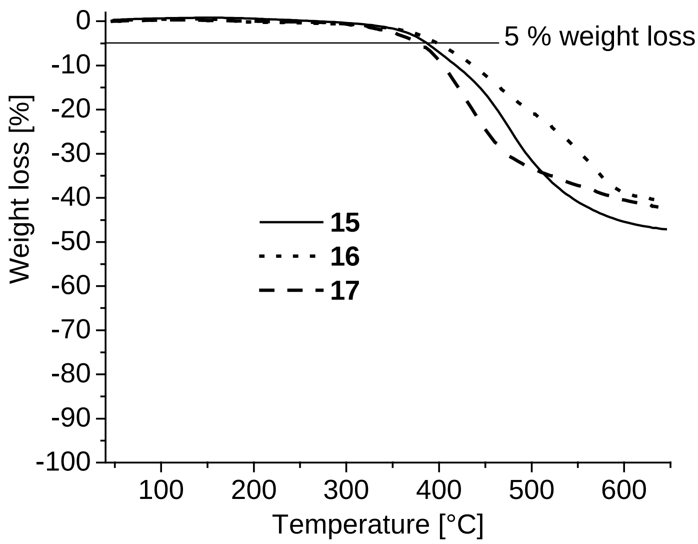

Figure 59. TGA of polymers ***15-17*** *performed at 10 K·min^{-1} heating rate under N_2 atmosphere.*

The second heating curves obtained from DSC for **15-17** are shown in Figure 60. Polymers **15-17** exhibited T_g of 130, 108 and 132 °C respectively, depending on the substituents. No melting peak was observed for any polymer in any of the heating and cooling steps of DSC measured in a range from -40 to +280 °C.

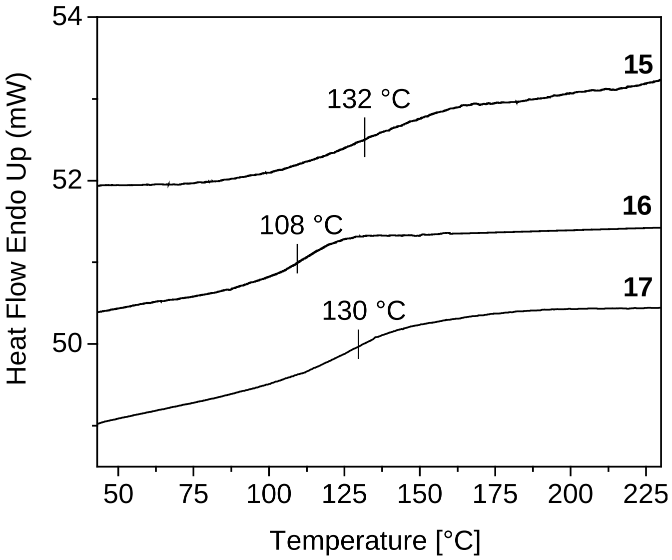

*Figure 60. Second heating curves obtained from differential scanning calorimetry of polymers **15-17** (measured at 10 K·min^{-1} heating rate under N_2 atmosphere).*

On comparison of T_g values of poly(DTITNPD)s **15-17** with polyDTITNs **13** and **14,** an improvement of more than 30 °C is observed here (compare Table 11 and Table 15). Higher T_g values of polymers **15-17** compared to polymers **13** and **14** indicate the higher rigidity of DTITN unit in combination with triarylamine units in polymers **15-17**. As is the case with thermal stability, T_g is also improved in polymers **15-17** due to the incorporation of ITN and triarylamine groups into the polymer main chain. The low T_g value in polymer **13** can also be attributed to the higher weight percentage of the side groups compared to the DTITN part as well as being due to the high torsion of C-C bond between substituted thiophenes in the main chain arising from the steric effect of the large alkyl substituents.

The thermal property data of polymers **15-17** such as $T_{-5\%}$ and T_g obtained from TGA and DSC measurements are presented in Table 15.

*Table 15. Thermal properties of poly(DTITNPD)s **15-17** obtained from TGA and DSC measurements at 10 K·min^{-1} heating rate under N_2 atmosphere.*

Polymer	DSC*	TGA
	T_g [°C]	$T_{-5\%}$ [°C]
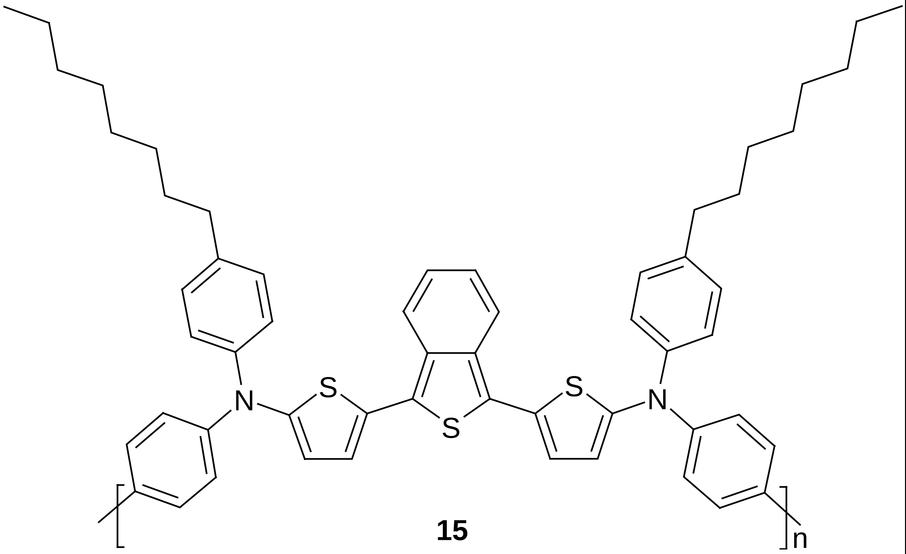 **15**	132	381
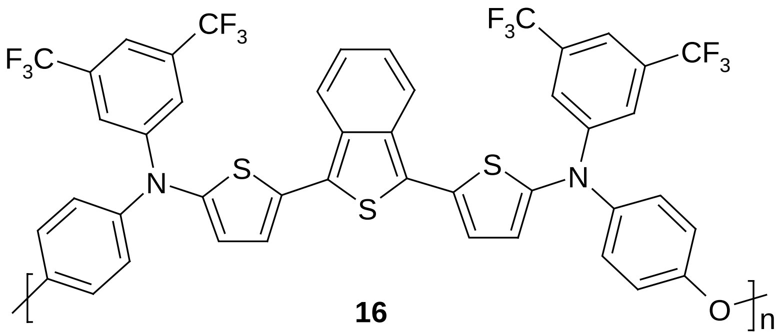 **16**	108	393
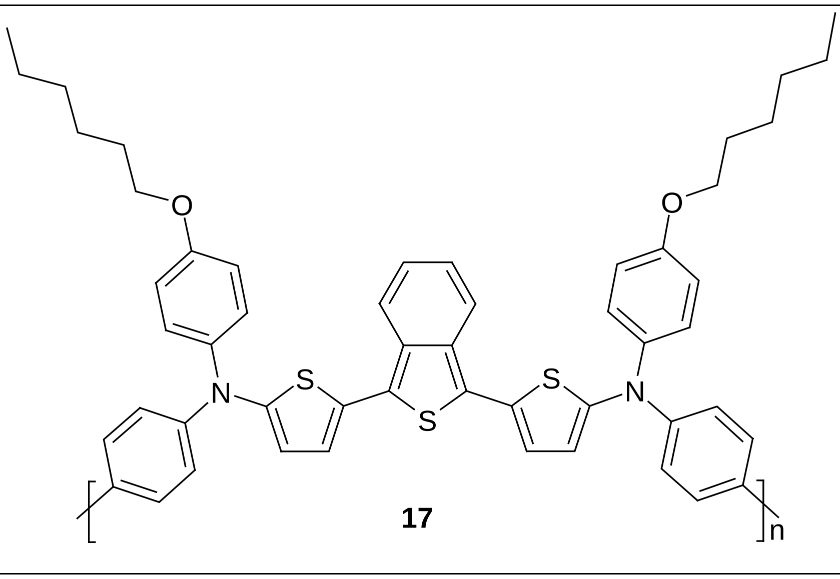 **17**	130	385

** - no melting peak was observed for any polymer in any heating and cooling curves of DSC measured in a range from -40 to +280 °C.*

7 Application in organic solar cells

In order to study the possibilities of potential application of novel hole transport dyes synthesised in this work, some of these materials were tested in combination with electron transport materials in multi-layer cells as well as polymer blend solar cells. Two different types of electron transport materials were used: 1) low band gap perylenebisimide derivatives and 2) wide band gap fullerene derivatives.

This chapter consist of three sections. In the first one, preparation and characterisation of multi-layer solar cells from low molar mass compounds by vapour deposition are described. Second and third sections describe polymer solar cells containing blends of a low molar mass compound with a polymer. Low molecular weight as well as polymeric hole transport compounds, synthesised in this work, were used in combination with low molecular weight and polymeric electron transport compounds.

All vapour deposited solar cells were fabricated in cooperation with the group headed by Dr. Martin Pfeiffer at Institut für Angewandte Photophysik, Technische Universität Dresden, Germany.

All polymer blend solar cells were prepared using spin-coating technique of the active materials in cooperation with Michael Sommer at the Department of Macromolecular Chemistry I, University of Bayreuth.

It should be noted that the emphasis of this Ph. D. thesis is on design, synthesis and characterisation of novel hole transport dyes and not on engineering task such as solar cells optimisation. Therefore, only the first results obtained from non-optimised solar cells using some of these compounds as examples are given below.

7.1 Multi-layer solar cells using vapour deposition technique

For testing materials in multi-layer solar cells, vapour depositable compounds are required. The best candidates for use in such solar cells are small molar mass compounds, DTITNPDs **9-11**. As an example, dithienylisothianaphthene phenyldiamine **10** was chosen as a hole transport dye.

The concept, used here in multi-layered solar cells, is based on co-evaporation of two organic compounds, an electron-rich HTM (eg: **10**) and a high electron affinity material (ETM) such as perylenebisimide or fullerene in order to create a high internal interface between these two components at which charge separation takes place. Moreover, the doping concept in photovoltaic devices allows increasing the conductivity of the wide gap hole transport layers (HTL) and electron transport layers (ETL) by more than four orders of magnitude[118]. These doped layers were used as charge transport layers. In addition to this mixed layer concept, pure multi-layers of HTM and ETM were also studied as active layers. The strong acceptor molecule tetrafluoro-tetracyano-quinodimetane (F_4-TCQN) was used for p-type doping of hole transport materials like zinc-phthalocyanine (ZnPc) and amorphous N,N,N'N'-tetrakis(4-methoxyphenyl)-benzidine) (*tetra*MeO-TPD)[119]. Dopant concentration up to 30 mol.% was used in these solar cells.

The two different cell structures tested in multi-layer cells are given in Figure 61.

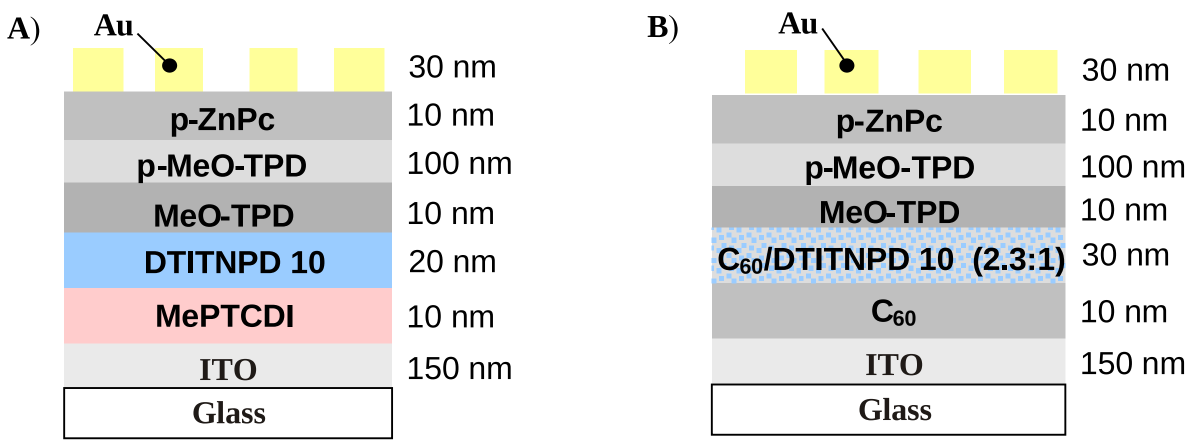

Figure 61. Schematic representation of cell structure of vapour deposited solar cells using DTITNPD ***10*** *and electron acceptors:* ***A)*** *MePTCDI and* ***B)*** *C_{60}.*

Active layer for light absorption and charge separation in **type A**) solar cells consisted of two layers containing low band gap electron transport material, N,N'-dimethylperylene-3,4,9,10-dicarboxyimide (MePTCDI) and model compound **10.** The **type B**) cells blend layer prepared by co-evaporation of fullerene and hole transport dye **10** in combination with a pure C_{60} layer as charge transport layer. Moreover, both solar cells had additional layers containing *tetra*MeO-TPD, p-doped *tetra*MeO-TPD and p-doped ZnPc as charge transport layers. All organic layers were placed between two electrodes, indium tin oxide (ITO) and vapour deposited Au. The chemical structures of all compounds used in these solar cells are given in Figure 62.

The cell configuration and layer thicknesses of individual layers are in accordance with a standard test structure developed in IAPP, TU Dresden. All the measurements were also carried out at IAPP in the group of Dr. Martin Pfeiffer and I acknowledge the help and co-operation of this group in this regard.

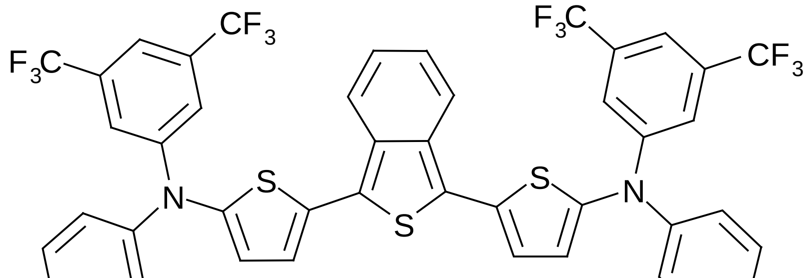

10

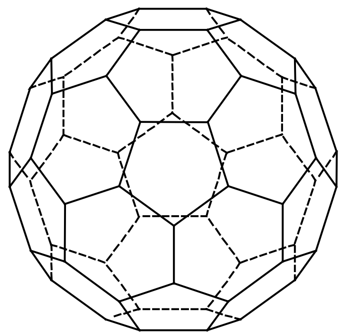

C_{60}

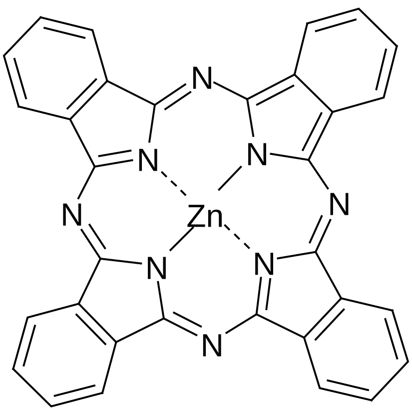

ZnPc

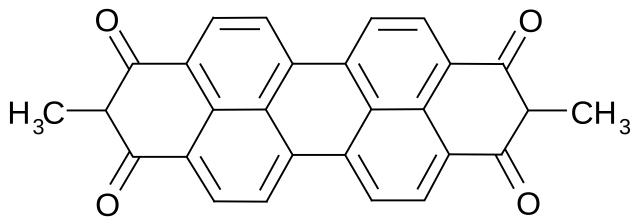

MePTCDI

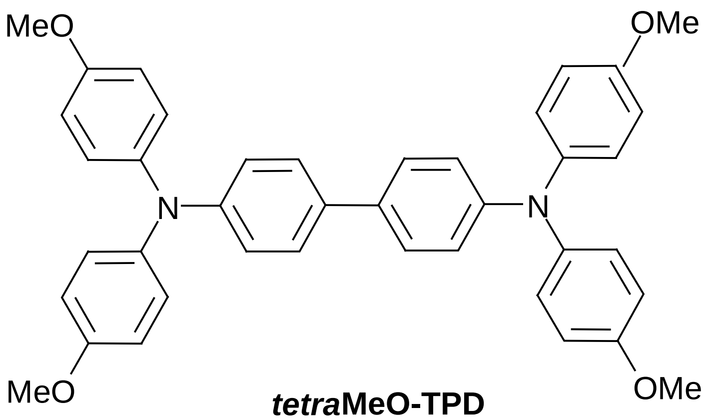

***tetra*MeO-TPD**

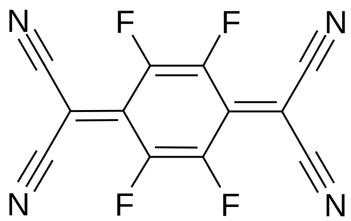

F4-TCQN
(Dopant)

Figure 62. Chemical structures of compounds used in vapour deposited solar cells.

7.1.1 Current-Voltage characteristics

I-V characteristics of multi-layer solar cell types **A**) and **B**) were obtained after measurements in the dark and using standard Xe-lamp white light with the AM 1.5 filter resembling solar spectra under 127 mW/cm^2 illumination intensity. All measurements were performed *in situ* under inert atmosphere. The graphic representation of I-V measurement is illustrated in Figure 63 and I-V characteristics are given in Table 16.

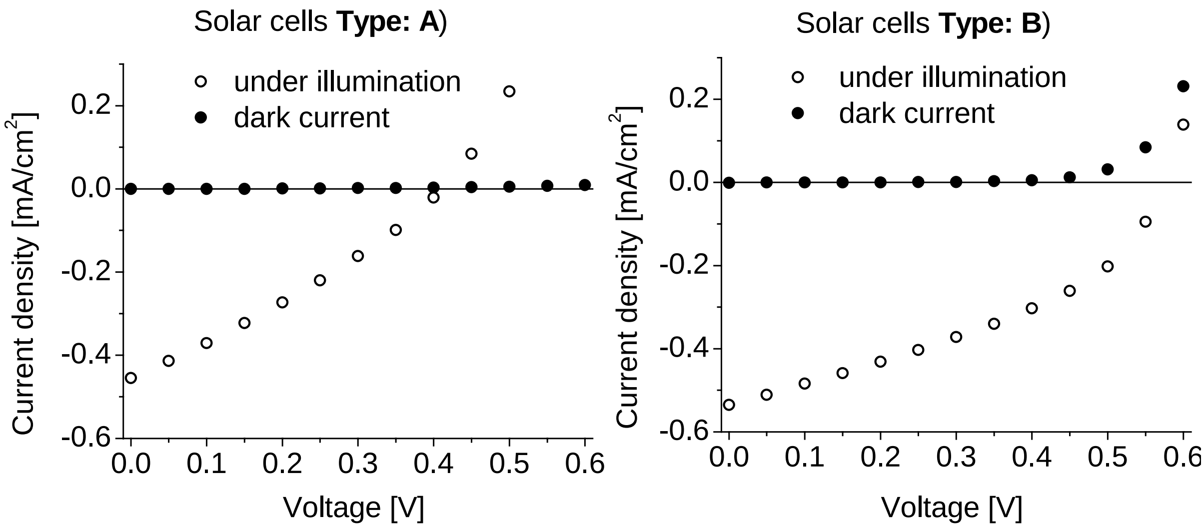

*Figure 63. Current-voltage characteristics of solar cells of type **A**) and **B**) prepared by vapour deposition of DTITNPD **10** as hole-transport material and electron-transport materials, **A**) - MePTCDI and **B**) – C_{60}.*

Comparison of devices **A** and **B** showed similar short-circuit current density (I_{SC}) values of -0.45 and -0.53 mA/cm^2, open-circuit voltage (V_{OC}) from 0.41 to 0.58 V, fill factor (FF) from 30 to 39 % and overall conversion efficiency (η_c) from 0.04 to 0.10 %. Thus, better performance of solar cells **B** compared to solar cells **A** can be attributed to better electron transport property of C_{60} compared to MePTCDI. Moreover, bulk-heterojunction coevaporated layer of C_{60} and **10** in multi-layer cells **B** can lead to better charge separation at the C_{60}/DTITNPD **10** interface due to larger interface then in **type A**) cells.

*Table 16. I-V characteristics of multi-layer solar cells **A** and **B**.*

Solar cells type	I_{SC} [mA/cm^2]	V_{OC} [V]	FF [%]	η_c [%]
A (MePTCDI/**10**)	-0.45	0.41	30	0.04
B (C_{60} + **10**)	-0.53	0.58	39	0.10

I_{SC} – short-circuit current
V_{OC} – open-circuit voltage
FF – fill factor
η_c – power conversion efficiency

7.2 Polymer blend solar cells with DTITNPD **9** and poly(perylene bisimide) (PPI)

In this section, a combination of low molecular weight hole transport dye **9** and low band gap electron transport poly(perylene bisimide) (PPI) was used for testing in polymer blend cells. Plastic solar cells were prepared by spin-coating solutions DTITNPD **9** and PPI in chloroform onto cleaned ITO substrate followed by deposition of Al electrode in high vacuum. It should be noted that poly(perylene bisimide) used here was synthesised by Gert Jungmann within the framework of his Ph. D. thesis[120] and kindly made available here. The schematic representation of plastic solar cells **C** based on DTITNPD **9** and PPI is given below.

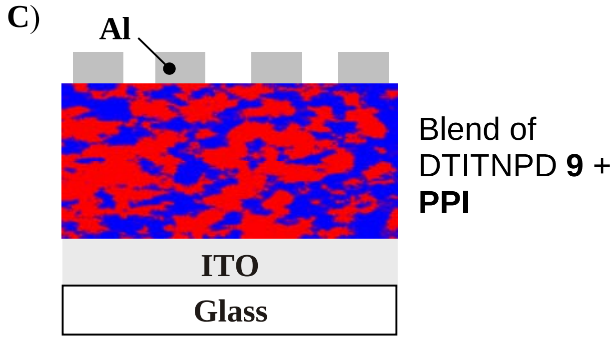

*Figure 64. Schematic representation of plastic solar cells **C** prepared from model compound **9** and poly(perylene bisimide) (PPI).*

The chemical structures of organic materials used in solar cells **C** are given below. Influence of blend compositions and variation of thicknesses on I-V characteristics of these cells were studied. Blend composition of 1:3 wt/wt % (solar cells **C**.I) of compound **9** and PPI respectively with a thickness of 100 nm was studied. Additionally, blend composition of 1:1 wt/wt % (solar cells **C**.II) of the compounds, **9**:PPI with thicknesses of 100, 150 and 200 nm was also studied.

In order to study the suitability of HTM/ETM components that can be used in solar cells, the fluorescence quenching experiment in thin film was used.

Thus, fluorescence quenching can be an indication of electron transfer from one component to another, which is very essential for a solar cell. The fluorescence quenching is dependent on energy levels (HOMO/LUMO) of compounds used. The fluorescence of PPI was fully quenched, when **9** and PPI were blended together, and the blend was excited at the λ_{max}^{abs} of PPI (see Figure 66).

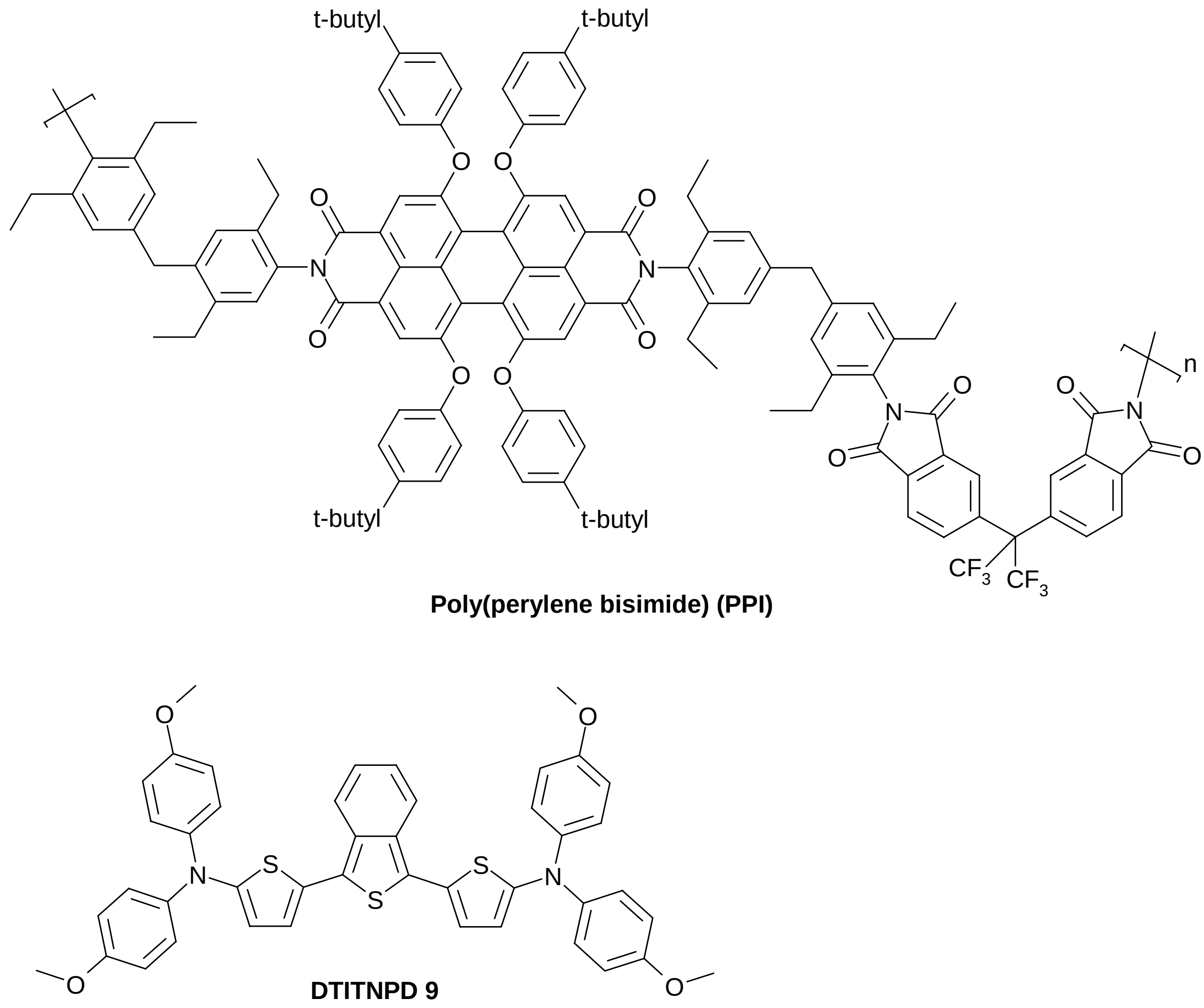

*Figure 65. Chemical structures of DTITNPD **9** and polyperylenebisimide (PPI).*

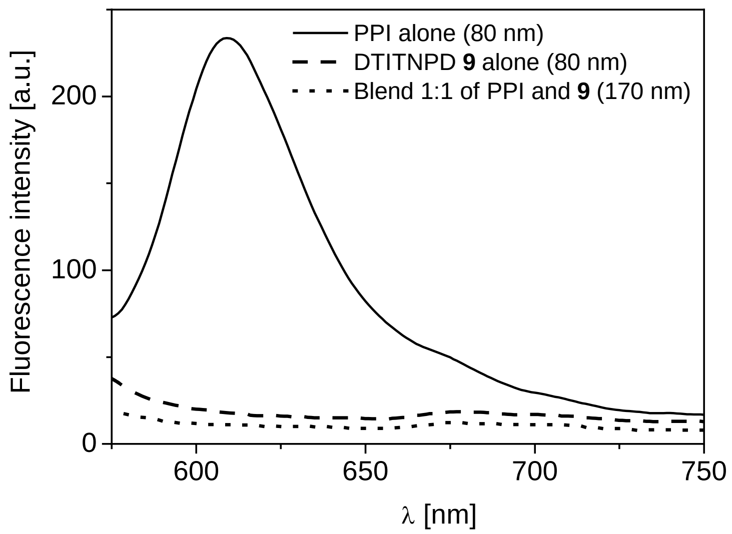

*Figure 66. Fluorescence quenching of PPI in blends of PPI with DTITNPD **9** (excitation at λ_{max}^{abs} of PPI: 588 nm).*

The proposed mechanism of fluorescence quenching in PPI by compound **9** is represented in Figure 67. The vacant position in HOMO orbital of excited state PPI will be occupied due to the electron transfer from the HOMO of **9** to the HOMO of PPI and this presents the radiative decay of excited PPI state which is observed as photoluminescence (PL) quenching. Another concurring effect is always the energy transfer from PPI to **9**. In which case, the band gap of **9** should fit into the band gap of PPI, which is not the case here. Therefore, the observed PL-quenching in such blends can be attributed to electron transfer phenomenon.

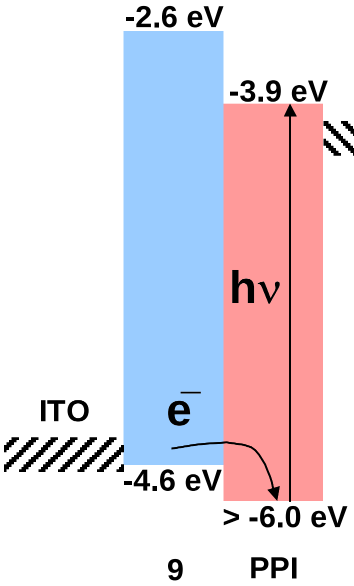

Figure 67. Energy level diagram of components involved in solar cells ***C****.*

The thicknesses of blends used in these solar cells were measured by Decktak and were also controlled by UV-Vis spectroscopy. As an example, the dependence of absorption of active layer with blend composition 1:1 on blend thicknesses is given below.

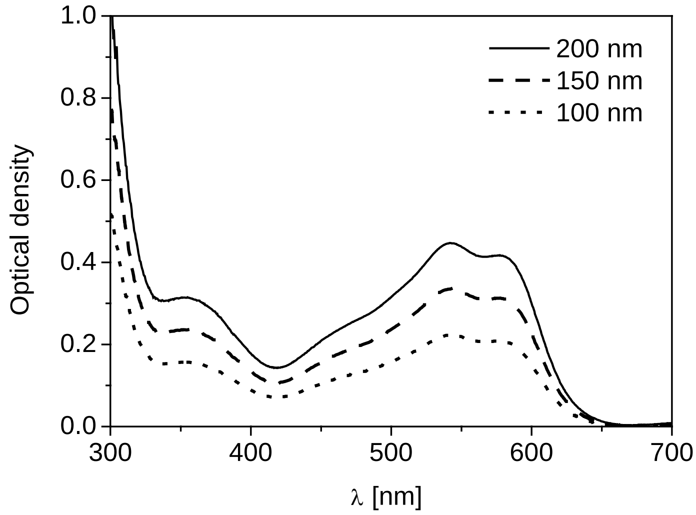

Figure 68. UV-Vis spectra of active layer blends with different thicknesses used in plastic solar cells, ***C****- type with blend composition 1:1 of DTITNPD* ***9*** *and PPI.*

7.2.1 Current-Voltage characteristics

I-V characteristics of plastic solar cells of **C-type** were measured in the dark and using standard Xe-lamp white light under AM 1.5 solar spectra conditions and using 77 mW/cm^2 illumination intensity. All measurements were performed in air. The I-V characteristics are illustrated in Figure 69.

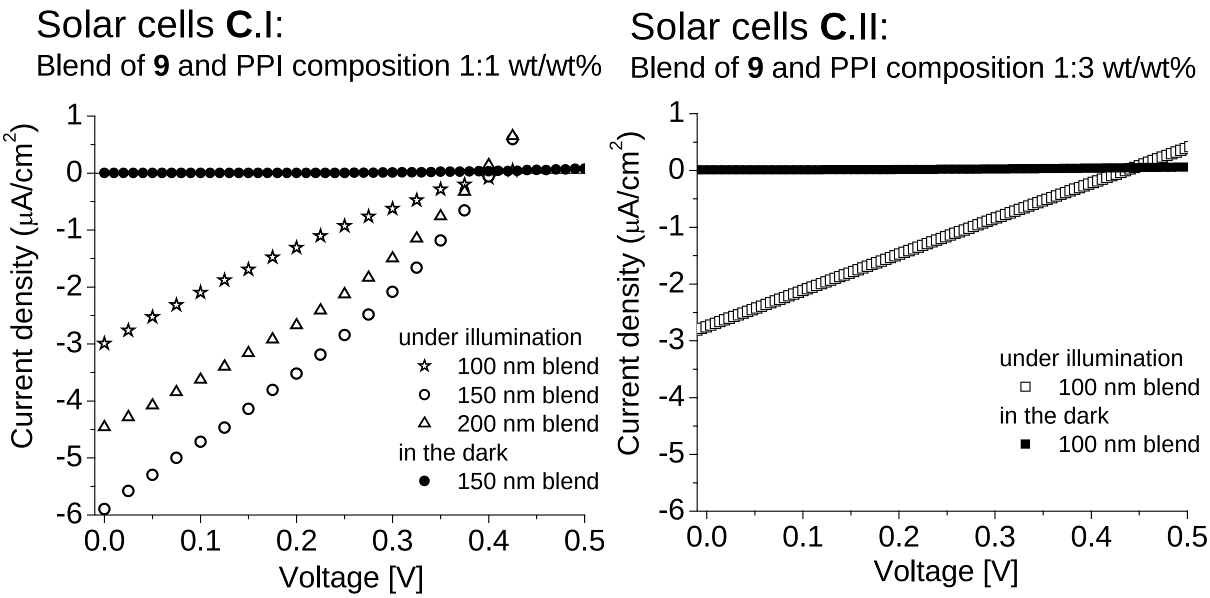

*Figure 69. I-V characteristics of plastic solar cells **C** measured in the dark (filled symbols) and using Xe-lamp solar light simulator (open symbols) for the AM 1.5 illumination with the power of light of 77 mW/cm^2.*

Comparison between solar cells **C**.I and **C**.II with the same photoactive blend thickness but with different blend compositions of 1:1 and 1:3 respectively showed only slight changes in I-V characteristics (see Table 17). But dramatic changes were observed by thickness variation of blend layer within the solar cells **C**.I, where the blend thicknesses of 100, 150 and 200 nm were used. I_{SC} of 3.5 μA/cm^2, V_{OC} of 0.35 V, FF of 24 % and η_c of $0.38\cdot10^{-3}$ % were obtained, when the blend thickness of 100 nm was used. All these parameters were improved further using 150 nm thick photoactive blend layer. I_{SC} was raised by ~1.7 times from -3.5 to -5.9 μA/cm^2. Such raising of short-circuit current density value can be attributed to more efficient photon harvesting by the thicker blend layer. Slight improvement of V_{OC} from 0.35 to 0.43 V and FF from 24 to 29 % were also obtained with overall conversion efficiency of $0.96\cdot10^{-3}$ %, which is more than two times large than that obtained using 100 nm thick blend layer. Another situation was observed from comparison of solar cells **C**.I prepared using blend layers with thicknesses of 150 nm and 200 nm, where all measured I-V parameters were slightly worse, except FF, which was increased from 29 to 32 %. No further increase of I_{SC}

due to larger number of absorbed photons by 200 nm blend can be realised due to charge transport problems, morphology reason etc. in thick layers. A further improvement may be achieved if the morphology phase separation in blends can be controlled by thermal annealing methods.

Table 17. I-V characteristics of plastic solar cells ***C****.*

Solar cells	Blend thickness [nm]	I_{SC} [μA/cm^2]	V_{OC} [V]	FF [%]	η_c [10^{-3} %]
C.I	100	-3.5	0.35	24	0.38
	150	-5.9	0.43	29	0.96
	200	-4.5	0.39	32	0.73
C.II	100	-2.8	0.44	25	0.40

7.3 Polymer blend solar cells with poly(DTITN) **13** and [6,6]-phenyl-C_{61}-butyric acid methyl ester (PCBM)

This section describes the preparation and characterisation of plastic solar cells (**type D**) prepared using solution processable polymeric hole transport dye, poly(DTITN) **13** and low molecular weight fullerene derivative, which does not absorb in the visible region. Thus, poly(DTITN) **13** was chosen as an example in combination with [6,6]-phenyl-C_{61}-butyric acid methyl ester (PCBM). For the solar cell fabrication, cleaned ITO glass was covered with poly(3,4-ethylenedioxythiophene)-poly(styrenesulfonate) (PEDOT-PSS) as hole-injection layer prepared by spin-coating from PEDOT-PSS aqueous solution. After the PEDOT film had dried overnight, a photoactive blend layer was prepared by spin-coating a solution of polymer **13** and PCBM (1:4 wt/wt %) in chlorobenzene, followed by deposition of Al electrode at about 10^{-5} bar vacuum. The schematic representation of plastic solar cells of **D-type** is given in Figure 70 and chemical structures of polymer **13** and PCBM are illustrated in Figure 71.

In order to study and compare the thermal annealing effect, plastic solar cells of **D-type** were treated at 90 °C (T_g of poly(DTITN) **13)** for 2 h under N_2 flow after cell preparation and before I-V characterisation. Padinger et al. have demonstrated that I-V characteristics of plastic solar cells based on poly(3-hexylthiophene) (P3HT) and PCBM were improved drastically in overall conversion efficiency from 0.4 % to 2.5 % by a postproduction thermal treatment of these solar cells.

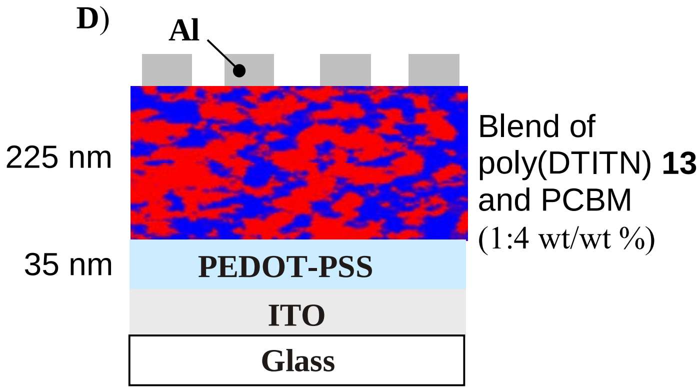

Figure 70. Schematic representation of plastic solar cells ***D*** *structure.*

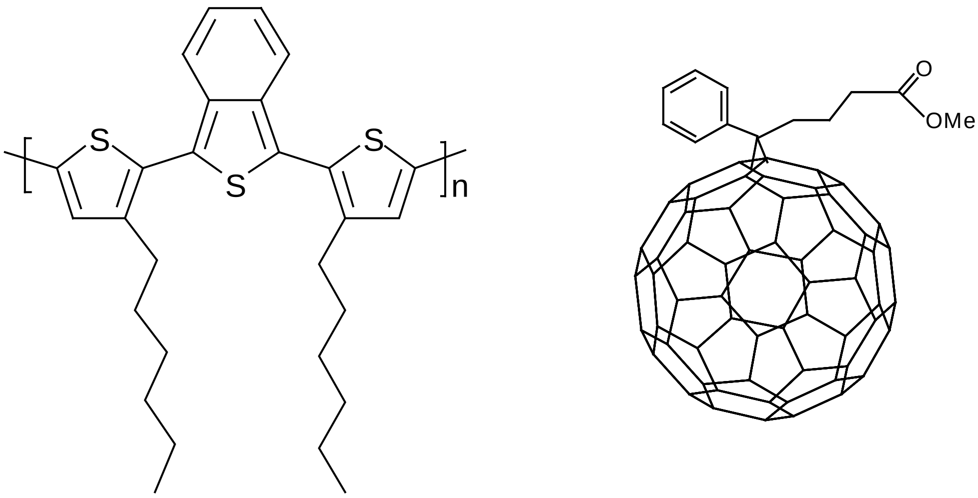

Poly(DTITN) 13 **PCBM**

Figure 71. Chemical structures of compounds used in active layer blend for solar cells ***D*** *preparation.*

7.3.1 Current-Voltage characteristics

Then I-V measurements of both cells thermally untreated (solar cells **D**.I) and thermally annealed (solar cells **D**.II) cells were performed. A comparison of I-V characteristics of solar cells **D**.I and **D**.II is given in Figure 72. The photovoltaic cells without any postproduction treatment (circles) have V_{OC} 0.46 mV, a I_{SC} 0.28 mA/cm^2 and a FF of 27 %. The overall conversion efficiency of this solar cell is 0.05 %. If is heated at 90 °C for 2 h under inert atmosphere (squares) the V_{OC} raises to 0.49 V and I_{SC} decreases to 0.24 mA/cm^2. The fill factor for this cell has the value of 26 %. Therefore the conversion efficiency of solar cells **D**.II after postproduction treatment is 0.04 %. A comparison of untreated and treated plastic solar cells **D** shows no large difference in these cells performance. This is also an indirect clue about the good stability of such cells, which do not show any degradation effect under air and under thermal stress (without encapsulation). It should also be pointed out that no additional advantage was observed by thermal treatment unlike the P3HT/PCBM cells.

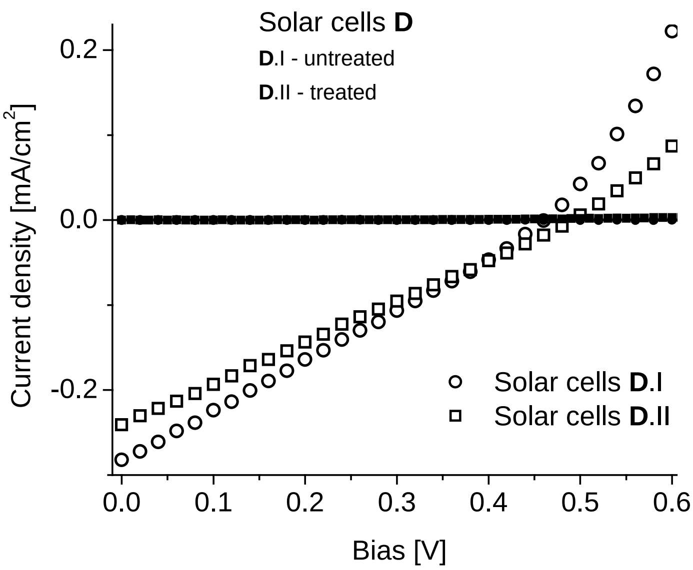

*Figure 72. I-V measurement of plastic solar cells **D** obtained in the dark (filled symbols) and with AM1.5 solar light simulator illumination (open symbols) at 77 mW/cm^2 power of light. Where solar cells **D**.I and **D**.II are untreated and treated at 90 ° for 2 h under N_2 flow respectively.*

All data obtained from I-V measurement of solar cells D are summarised in Table 18.

*Table 18. I-V characteristics of plastic solar cells **D** obtained in the dark and with solar light simulator illumination at 77 mW/cm^2.*

Solar cells	Remarks	I_{SC} [mA/cm^2]	V_{OC} [V]	FF [%]	η_c [%]
D.I	Untreated	-0.28	0.46	27	0.05
D.II	Treated at 90 ° for 2 h under N_2 flow	-0.24	0.49	26	0.04

7.3.2 Characterisation via IPCE or External quantum efficiency (EQE)

All IPCE characterisations of solar cells were performed in cooperation with Dr. Bin Peng (Macromolecular Chemistry I, University of Bayreuth).

In Figure 73 the results of the IPCE (incident photon-to-current conversion efficiency) measurements for untreated solar cells **D**.I were compared to absorption spectrum of polymer **13** alone and to absorption spectrum of polymer **13** and PCBM blend with composition 1:4 respectively. Generally, IPCE spectrum exhibits a value of more than 9 % in the region of 314 to 654 nm. The external quantum efficiency of IPCE for this device (open squares) showed a maximum of ~40 % at 350 nm and a second maximum of 15 % at 540 nm. Actually, it was expected to observe an overlap of IPCE spectrum of untreated solar cell **D** with absorption spectrum of active layer. But surprisingly photons harvesting at 540 nm (second maximum of IPCE) contribute more towards photocurrent. This can be an indication of some kind of charge transfer complex formation between hole transport polymer **13** and electron transport PCBM.

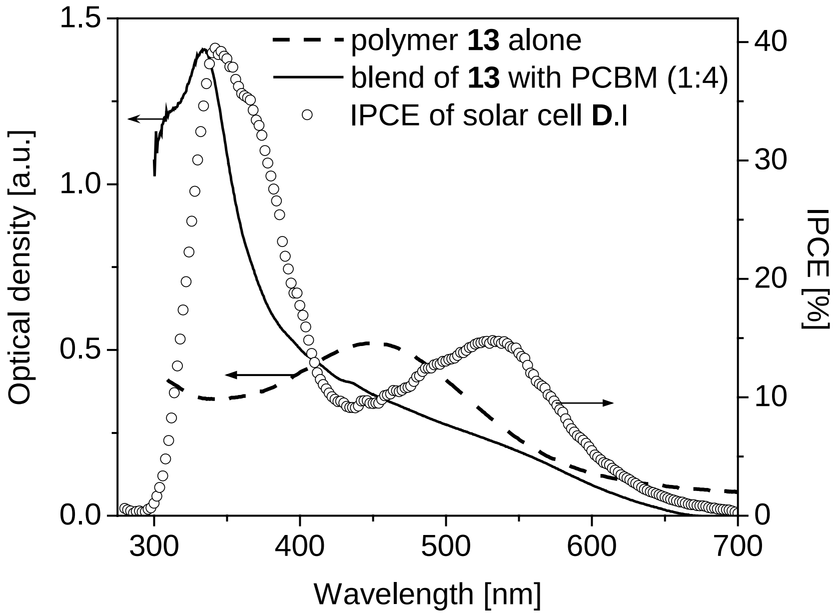

*Figure 73. Photoaction spectra of solar cells **D**.I (untreated).*

8 Application in organic light emitting diodes (OLEDs)

Since Kodak's and Cambridge's seminal reports, organic light emitting diodes (OLEDs) continue to attract broad attention due to their potential applications in various displays. For full-colour applications, the development of pure red-, green- and blue-emitting materials with sufficiently high luminous efficiency, proper chromaticity and stability is required. While pure green emitting materials[121] with good stability strength have been achieved, pure blue- and red-emitting materials are still required. Due to the fact that new low molecular weight and polymeric dithienylisothianaphthene phenyldiamines developed here are emitting in red region, here I focus on red OLEDs. Red-emitting materials largely remain crystalline and require cumbersome doping methods in OLED fabrications. The most commonly used red-emitters include pyran containing compounds such as DCM, DCM2[122], DCJT[123] and DCJTB (see Figure 3, page 8), porphyrine compounds[21,124] and europium chelate complexes[125]. These dyes generally exhibit enhanced aggregation property due to π-π interaction[126] or strong charge transfer character[127]. This leads to the degradation of the film quality and fluorescence quenching. Consequently, all the afore mentioned red-emitting materials are used as dopants in small amounts in Alq_3 (0.5 to 2 % wt/wt), except the europium chelate complexes. In such devices, careful control of the dopant concentration is a very critical since non-efficient energy transfer from the host will result in a mixture of two emission profiles and contribute to an unsaturated emission.

In order to avoid fluorescence quenching in electroluminescence (EL) emitter was doped in the host material and used as emitting layer in OLEDs. However, the OLEDs with emitting layer based on pure layer of red-emitter were also fabricated for comparison with OLEDs based on doped emitting layer. Moreover, different device configuration using additional layers like NPD, Alq_3 or BCP were also prepared and tested.

The preparation and characterisation of multi-layer red OLEDs was done in cooperation with Markus Bäte (Macromolecular Chemistry I, University of Bayreuth). These OLEDs were prepared using combinatorial vapour deposited technique[128] available at MCI.

The low molecular weight DTITNPD **10** was chosen as an example for testing it as hole transport red-emitter in multi-layer OLEDs. Comparing vapour depositable DTITNPDs **9-11**, the compound **10** showed the brightest red photoemission in the solid state.

All of the devices described below have multi-layer structures with the organic layers placed between indium tin oxide (ITO) and LiF/Al electrodes. The area of each OLED cell is typically 20 mm^2.

Figure 74 lists the molecular structures of the organic materials used for OLEDs fabrication. These organic materials exhibit different functionalities such as emitting and/or charge transport properties.

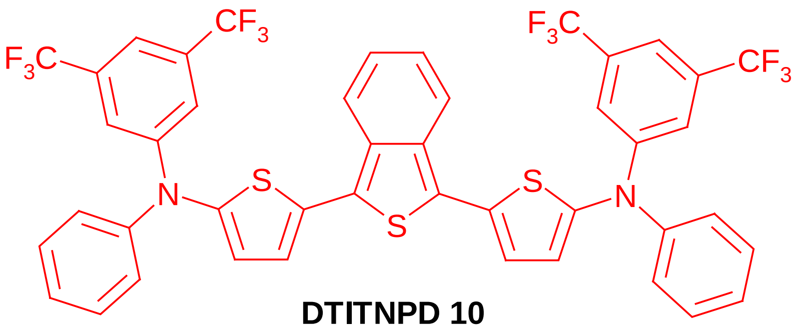

DTITNPD 10

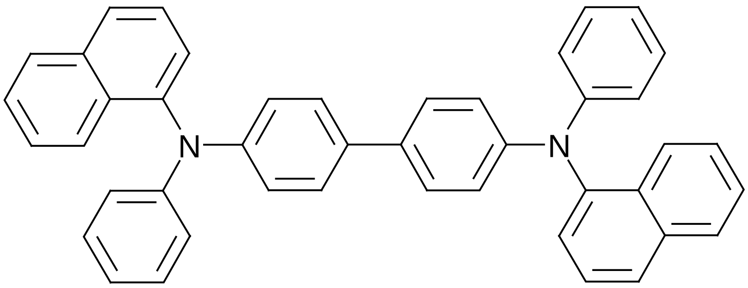

NPD

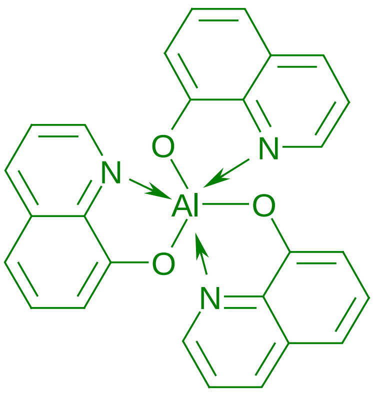

Alq_3

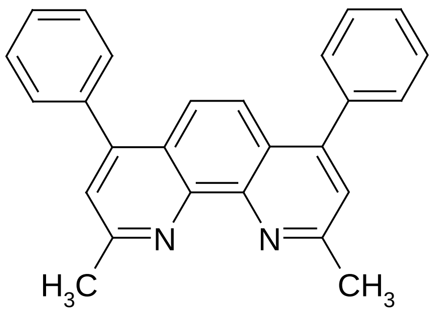

BCP

*Figure 74. Chemical structures of organic materials used in OLEDs **A** and **B**.*

NPD is α-naphthyl-phenyldiamine, BCP is 2,9-dimethyl-4,7-diphenyl-1,10-phenanthroline and Alq_3 is aluminium tris(8-hydroxyquinoline).

NPD belongs to the class of aromatic diamines that have been extensively studied in connection with their applications in xerography[129]. They are generally characterised by their ability to transport holes but not electrons.

Alq_3 belongs to a well-known class of metal chelates[130] and is characterised as electron transport green-emitter. The stability and fluorescence properties of metal chelates have been studied extensively[131]. Alq_3 is one of the most fluorescent and stable molecules in this class and has also the ability to form smooth thin films. Numerous red or green fluorescent organic molecules have been found to be useful as dopants in Alq_3 as host.

The BCP layer was widely used as hole blocking and exciton blocking layer[132] in OLEDs.

8.1 OLEDs with emitting layer based on pure DTITNPD **10**

Type A and B devices

Generally all of the undoped devices have emitting zone consisting of DTITNPD **10** single layer. Depending on the presence of an additional hole transport layer of NPD, all these OLEDs are divided into OLEDs **A** without any NPD layer and OLEDs **B**, which include additional NPD layer. In order to achieve high luminance efficiency device, the general structures of OLEDs **A** and **B** were varied giving substructures **A.1** to **A.4** and **B.1** to **B4** depending on the presence of electron transport layer of Alq_3 and/or buffer layer of BCP. The configurations of OLEDs **A-types** are schematically illustrated below.

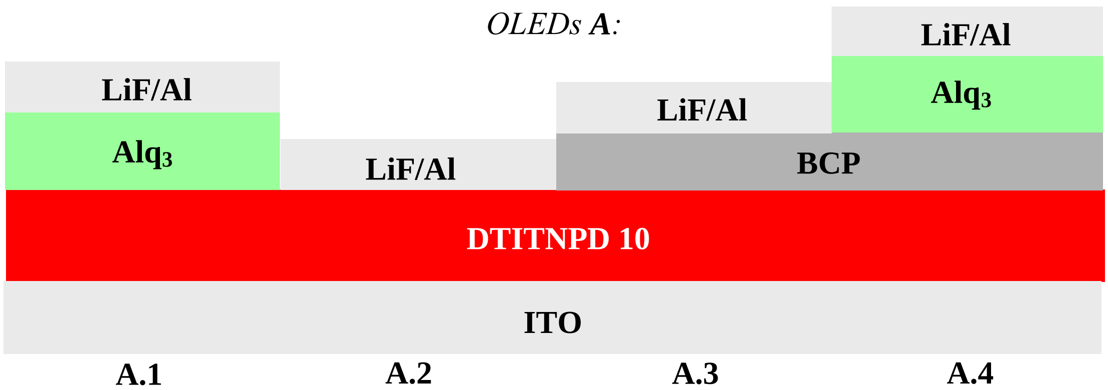

*Figure 75. Structures of red OLEDs **A** based on undoped red-emitting layer of DTITNPD **10**.*

The devices **A.1** to **A.4** are based on organic layers **10**/Alq_3, **10** alone, **10**/BCP and **10**/BCP/Alq_3 respectively. In the case of OLEDs **B.1** to **B.4**, their structures consist of similar organic layers as in **A.1** to **A.4**, but with an additional NPD layer underneath eg: **B.1:** NPD/**10**/Alq_3, **B.2:** NPD/**10**, **B.3:** NPD/**10**/BCP and **B.4:** NPD/**10**/BCP/Alq_3. It should be noted that thickness of each organic layer used in EL devices **A** and **B** are kept constant. The organic layers of 50 nm thick NPD, 60 nm thick red-emitter **10**, 6 nm thick BCP and 20 nm thick Alq_3 as well as 1 nm thick LiF layer were used in undoped OLEDs of **A** and **B** types. The configurations of OLEDs **B-types** are schematically illustrated below.

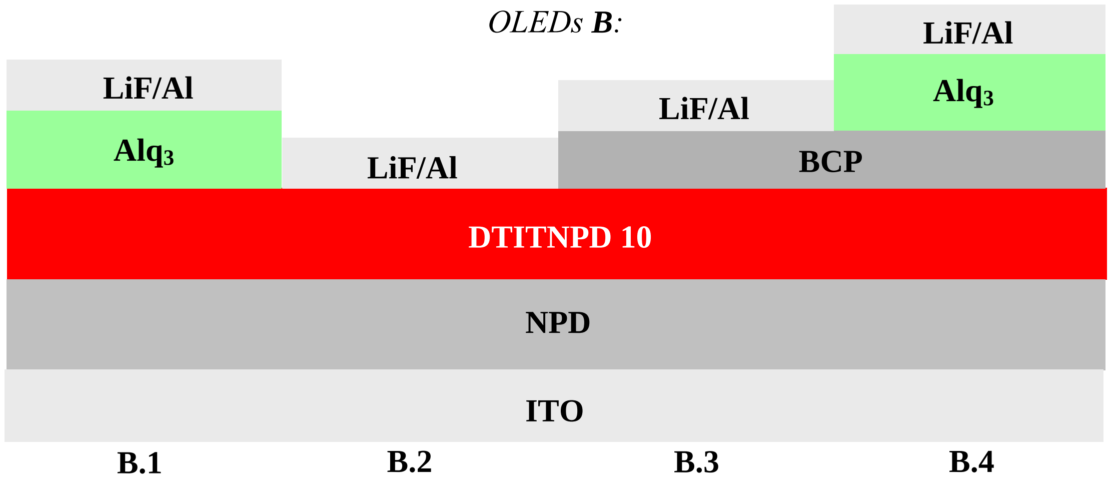

OLEDs	A.1	A.2	A.3	A.4	B.1	B.2	B.3	B.4
LiF	1 nm							
Alq_3	20 nm	-		20 nm	20 nm	-		20 nm
BCP	-		6 nm		-		6 nm	
DTITNPD **10**	60 nm							
NPD	-				50 nm			

*Figure 76. Structures of red OLEDs **B** based on undoped red-emitting layer of DTITNPD **10**.*

8.1.1 Current-bias (I-V), luminance-bias and electroluminescence (EL) characterisation

The I-V characteristics of these OLEDs are given in Figure 77. Influence of additional electron transport Alq_3, hole transport NPD and exciton blocking BCP layers on operating current density and luminescence values of OLEDs **A** and **B** was studied. The devices without Alq_3 layer such as **A.2** and **B.2, A.3** and **B.3** had current densities of about 52 and 26, 33 and 21 mA/cm^2 respectively at the operating voltage of 10 V. In contrast to that, the devices with additional Alq_3 layer such as **A.1** and **B.1**, **A.4** and **B.4** exhibited much lower corresponding values of 3 and 5, 14 and 0.5 mA/cm^2 at the operating voltage of 10 V. The lowering of current density values indicates better performance in OLEDs leading to devices with higher efficiency values.

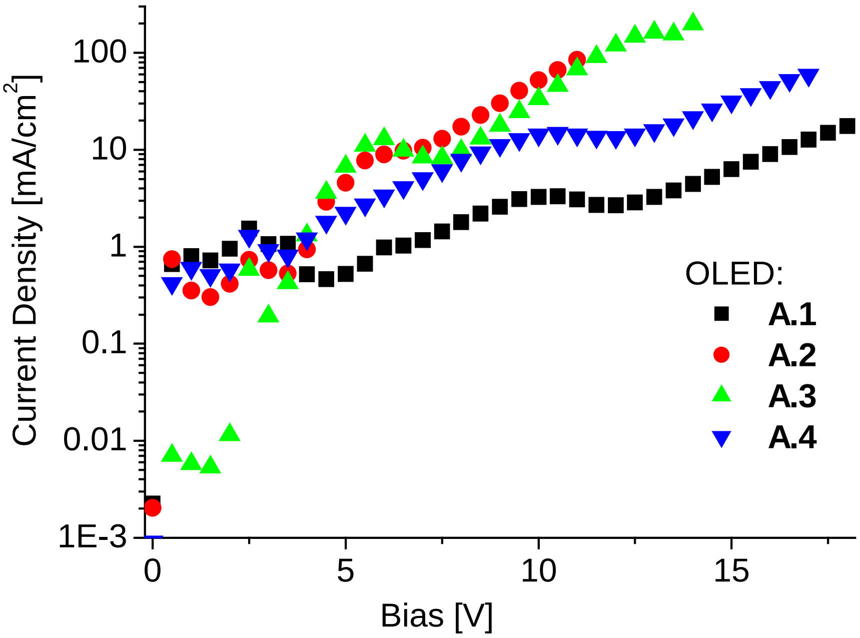

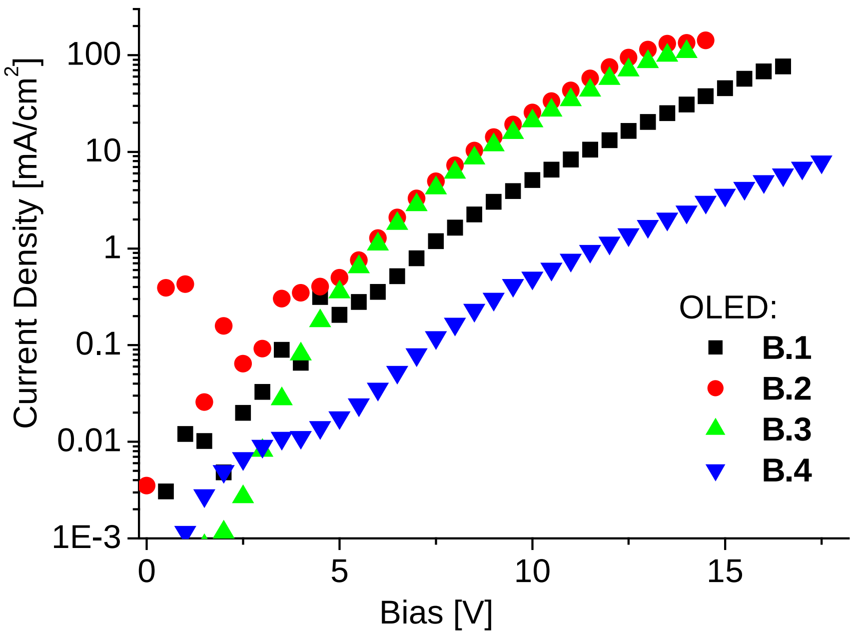

*Figure 77. I-V characteristics of the OLEDs **A.1** to **A.4** (top graph) and **B.1** to **B.4** (bottom graph).*

Comparison of the OLEDs **A.1** to **A.4** without NPD layer and OLEDs **B.1** to **B.4** including NPD layer also showed decreasing of current densities in the latter devices, except **A.1** and **B.1** (see Table 19). Thus, the use of hole transport NPD layer as well as electron transport Alq_3 layer allowed large improving of current densities values due to the negligible energy barriers between organic layers in these OLEDs. The influence of thin exciton-blocking BCP layer on I-V characteristics of OLEDs **A** and **B types** was not considerable.

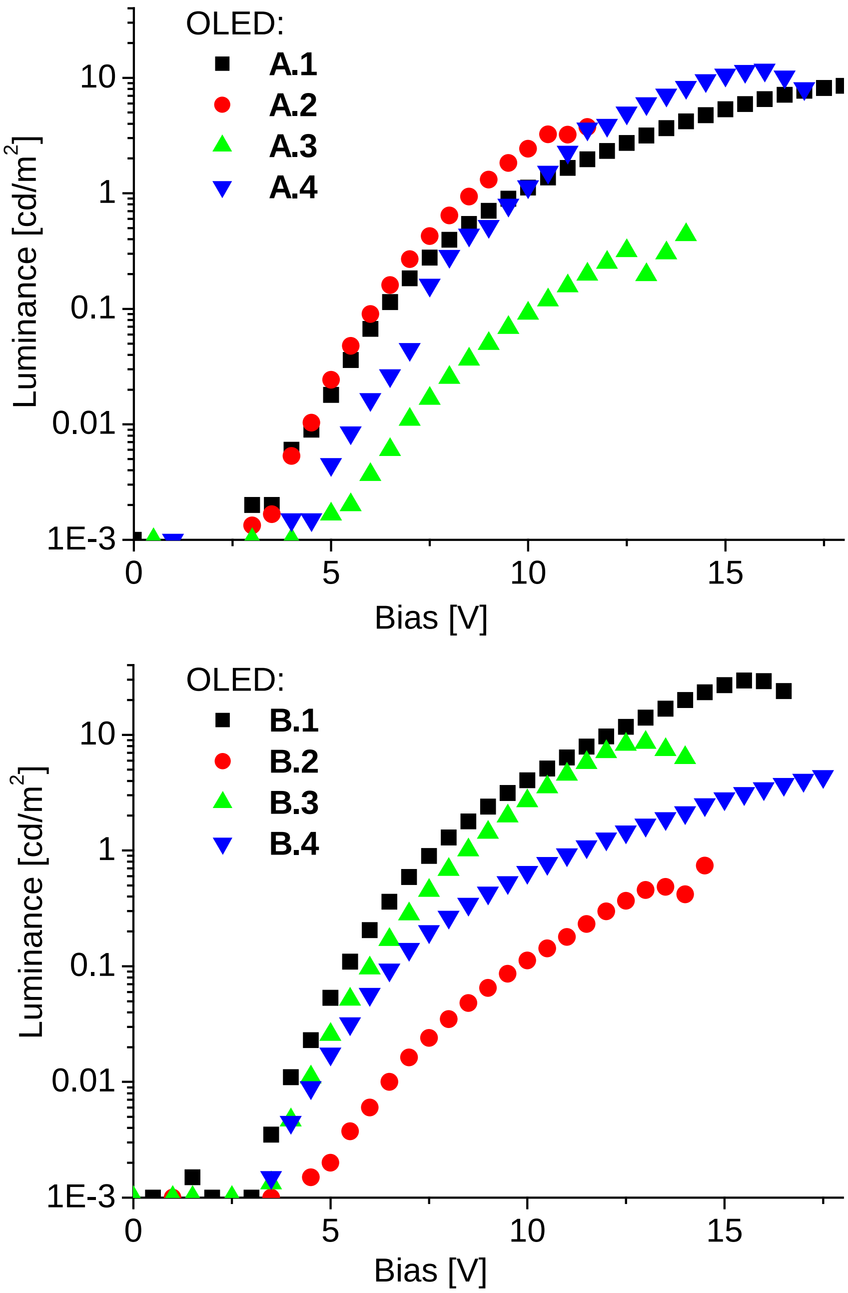

*Figure 78. Luminance-bias characteristics of the OLEDs **A.1** to **A.4** (top graph) and **B.1** to **B.4** (bottom graph).*

The luminance-bias characterisation of OLEDs **A** is represented in Figure 78. Generally, all of these devices showed very weak luminance. The maximum luminescence value of 29 cd/m^2 was obtained in device **B.1** at 16 V operating voltage. The OLEDs **A.1** to **A.4** exhibited luminance values of 1.1, 2.4, 0.1 and 1.1 cd/m^2 respectively at operating bias of 10 V. Whereas the OLEDs **B.1** to **B.4** showed luminescence values of 4.0, 0.1, 2.7 and 0.6 cd/m^2 at operating bias of 10 V. There is no clear influence of device structure on its luminance-bias characteristics for pure **10** as emitter layer. This is an indication that in pure red emitter **10** (100 %) there is non-radiative decay or quenching effects.

Generally, the OLEDs **A.1**, **A.4**, **B.1** and **B.4** containing Alq_3 layer showed better performance than OLEDs **A.2**, **A.3**, **B.2** and **B.3** (see Figure 79). The incorporation of an additional electron transport layer of Alq_3 improved the performance of OLEDs. This indicates that red-emitter **10** carries hole transport property. Thus, the bifunctional DTITNPD **10** can be classified as hole transport red-emitter.

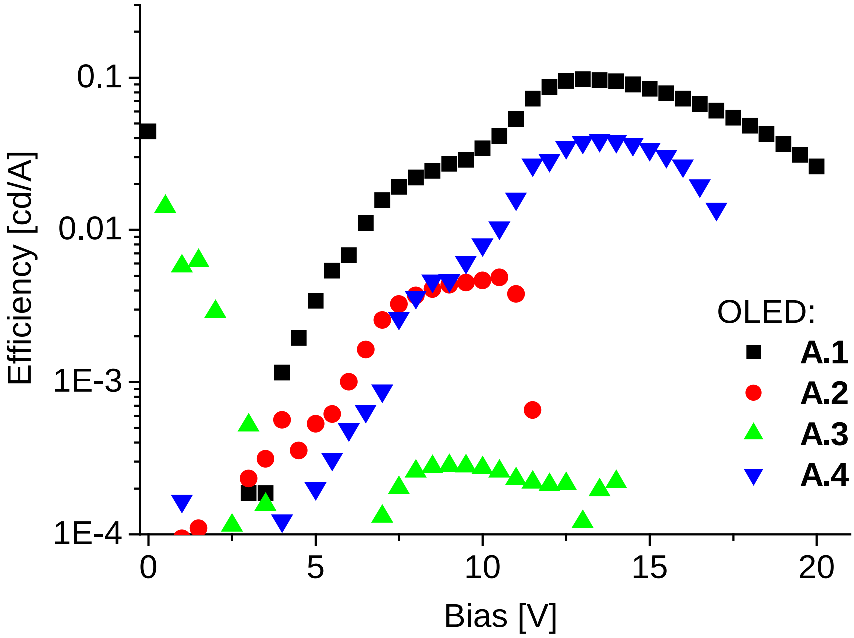

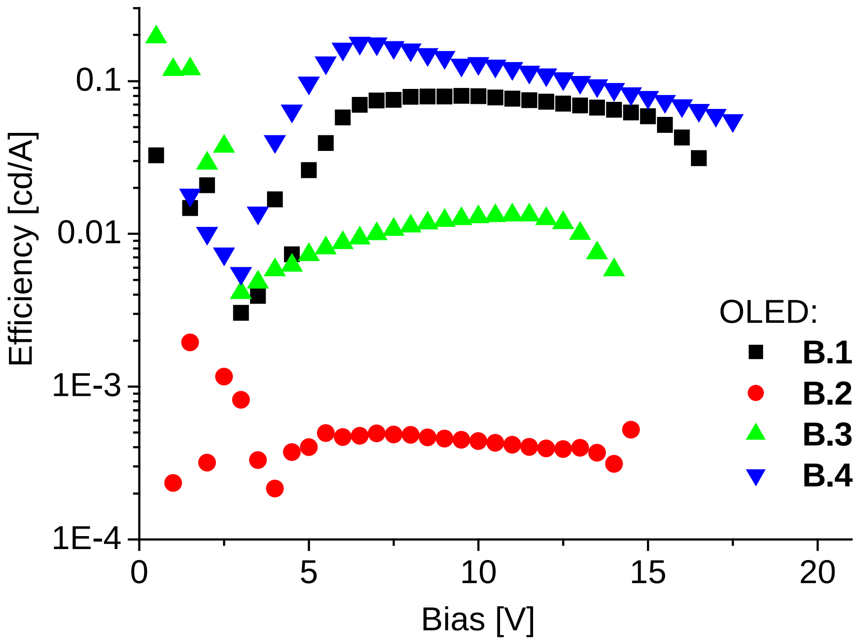

*Figure 79.A. Luminance efficiency of the OLEDs **A.1** to **A.4** (top graph) and **B.1** to **B.4** (bottom graph) plotted vs. bias.*

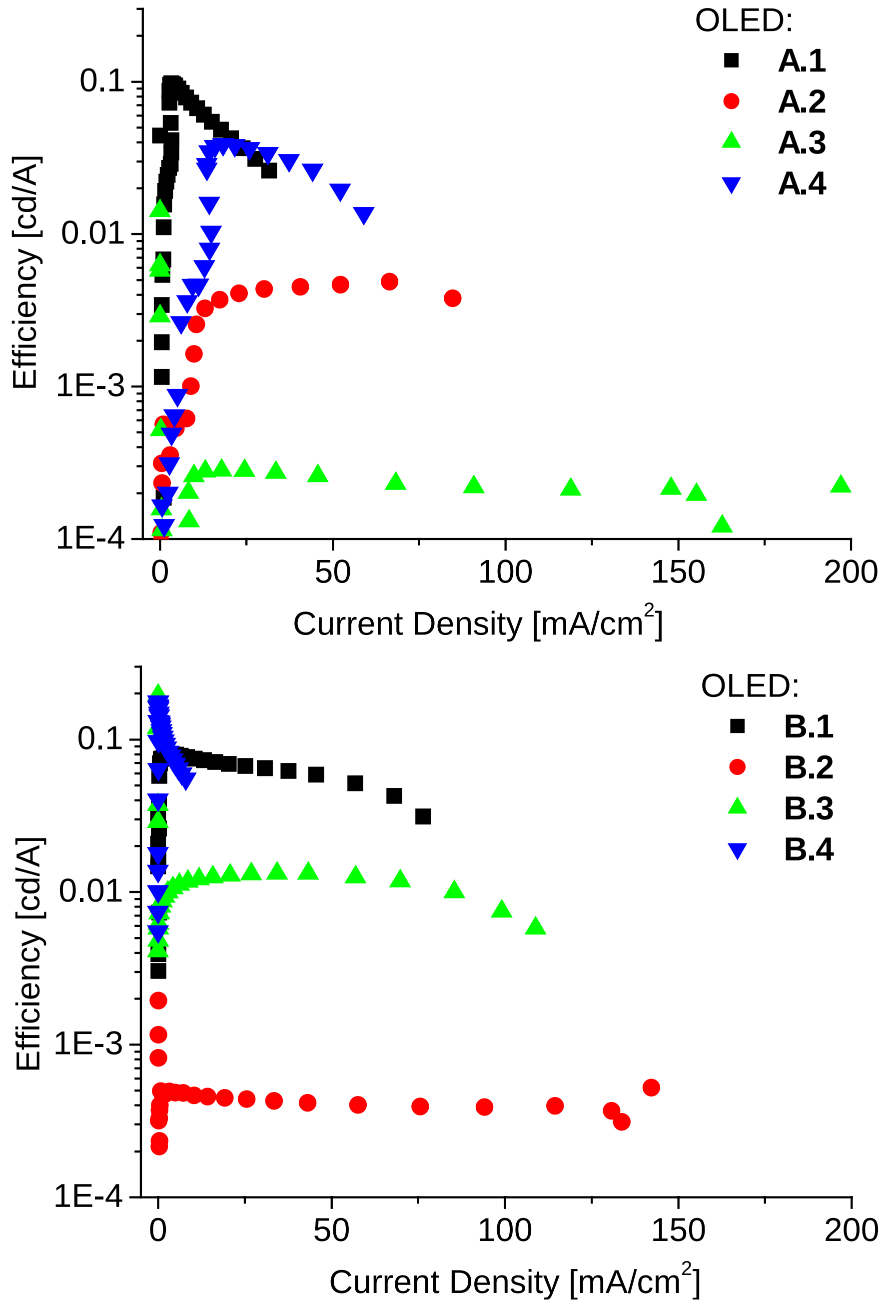

Figure 79.B. Luminance efficiency of the OLEDs ***A.1*** *to* ***A.4*** *(top graph) and* ***B.1*** *to* ***B.4*** *(bottom graph) plotted vs. current density.*

The electroluminescence (EL) spectral characteristics of OLEDs **A** and **B** were performed. Influence of Alq_3 layer on electroluminescence spectra of these OLEDs was studied. Figure 80 lists the normalised EL curves of OLEDs **A.1**, **B.1** (with Alq_3) and **B.3** (without Alq_3) at 10 V operation bias. The EL spectrum of **B.3** showed red emission with the maximum at 608 nm corresponding to the PL peak of this compound at 613 nm (see chapter 4.2.2, Table 5). The EL spectrum maxima of devices **A.1** and **B.1** were 595 and 599 nm respectively, which are slightly shifted towards shorter wavelength compared to **B.3**. Additional small luminescence peaks at 500 nm were also observed in EL spectra of OLEDs **A.1** and **B.1**. This result can be attributed to the presence of Alq_3 layer, which is a well-known green emitter, in **A.1** and **B.1** types. Nevertheless, nice red electroluminescence was obtained in all OLEDs of **A** and **B types** containing undoped emitting layer of DTITNPD **10**, but with low efficiency.

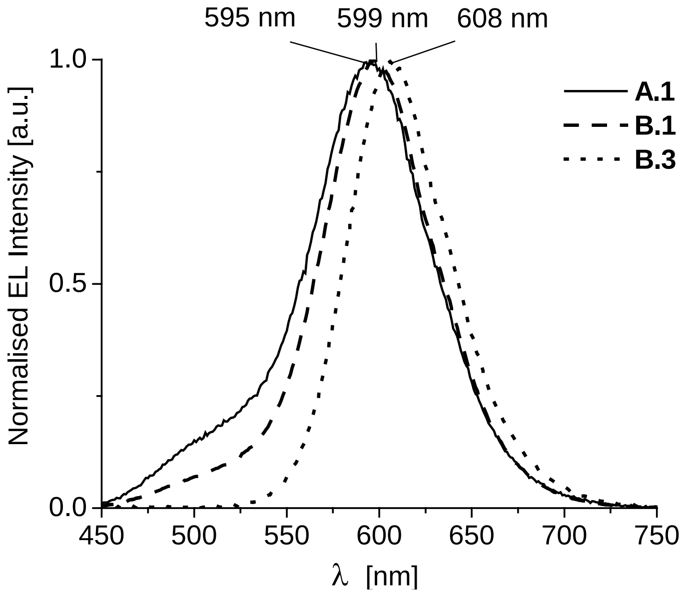

Figure 80. Comparison of the normalised electroluminescence measured at 10 V of OLEDs ***A.1*** *(**10**/Alq_3),* ***B.1*** *(NPD/**10**/Alq_3) and* ***B.3*** *(NPD/**10**/BCP) using solid, dash and dot lines respectively.*

Table 19. EL characteristics of undoped OLEDs **A** *and* **B** *based on DTINTPD* **10** *emitting layer.*

OLEDs	**Current density[a] [mA/cm^2]**	**η_{el} [cd/A]** (Current density [mA/cm^2], Bias [V])	**λ_{max}^{el} [nm][a]**
A.1	3	0.10 (3.3, 13)	595
A.2	52	0.005 (52.3, 10)	602
A.3	33	0.003 (17.8, 9)	610
A.4	14	0.04 (15.9, 13)	613
B.1	5	0.08 (1.64, 8)	599
B.2	26	0.005 (3.3, 7)	607
B.3	21	0.01 (34.3, 11)	608
B.4	0.5	0.18 (0.05, 6.5)	607

[a] – measured at operation bias of 10 V
η_{el} – maximum electroluminescence efficiency
λ_{max}^{el} – wavelength of maximum electroluminescence

As expected, the red OLEDs **A** and **B** based on undoped emitting layer showed very low EL intensity due to the fluorescence quenching. The use of doped emitting layers is a well-known concept for obtaining high luminescence efficiency values in OLEDs. In order to improve the performance of red OLEDs involving **10** as emitter, the most luminescent OLED **B.1** was chosen as a model system. Therefore, the structure of EL device in **B.1**, which consist of organic layers NPD/**10**/Alq_3, was modified by doping emitter **10** in electron transport layer of Alq_3 by co-evaporation. In this way, a series of concentrations of **10** in Alq_3 was achieved resulting in OLEDs of **C-type**. The structure and characterisation of OLEDs **C-type** based on Alq_3 doped with DTITNPD **10** as emitting layer are described in the next section.

8.2 OLEDs with DTITNPD **10** doped in Alq_3 as emitter layer

Type C devices (**10** doped in Alq_3)

Generally, the OLEDs **C** consist of NPD layer and **10** doped in Alq_3 as emitter placed between ITO and LiF/Al electrodes. Typical configuration of EL devices of **C-type** containing doped emitting layer is ITO / NPD (50 nm) / **10** doped in Alq_3 (80 nm) / LiF (1 nm) / Al as given in Figure 81. The doping level of DTITNPD **10** increases from 0 to 8 %, in which 0 % doped OLED is a reference TPD/Alq_3 device emitting green colour.

*OLEDs **C**:*

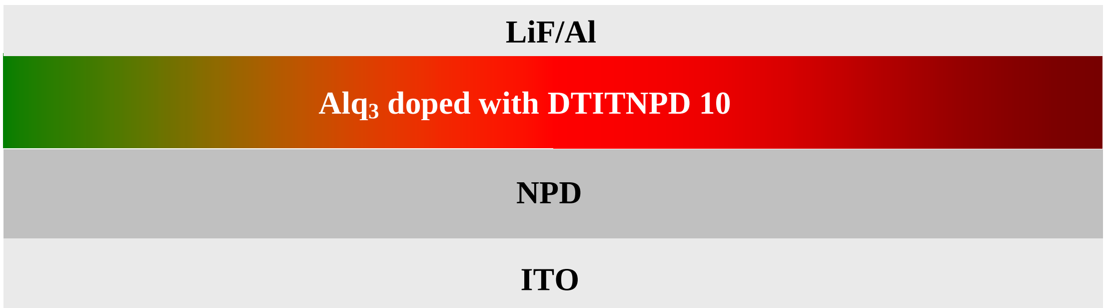

OLEDs	C.1	C.2	C.3	C.4	C.5	C.6	C.7	C.8	C.9	C.10
LiF	1 nm									
Doped Alq_3	80 nm									
red-emitter **10** concentration	0 %	1 %	2 %	3 %	4 %	4 %	5 %	6 %	7 %	8 %
NPD	50 nm									

*Figure 81. Configuration of OLEDs **C** based on red-emitter **10** doped in Alq_3 host layer.*

Depending on the concentration of **10** in the Alq_3, the OLEDs **C** were divided into 10 structures (**C.1** to **C.10**) with the concentrations of **10** in Alq_3 being 0, 1, 2, 3, 4, 4, 5, 6, 7 and 8 % respectively. OLEDs **C.1-type** with 0 % red-emitter showed green EL corresponding to Alq_3 emission. OLEDs **C.5** and **C.6** are similar with 4 % red-emitter **10** concentration in Alq_3 layer each. Dependence of device performance on the red-emitter **10** concentrations in OLEDs **C** is discussed below.

8.2.1 Current-bias (I-V), luminance-bias and electroluminescence (EL) characterisation

Figure 82 represents the I-V characteristics of OLEDs of **C-type**. A decrease of the current density in EL devices **C** with increasing red-emitter **10** concentration was observed in these devices. OLEDs **C.1** to **C.10** exhibited current densities of 219, 132, 13.5, 3.16, 1.67, 0.98, 0.59, 0.46, 0.25 and 0.16 mA/cm^2 respectively at 10 V operating bias.

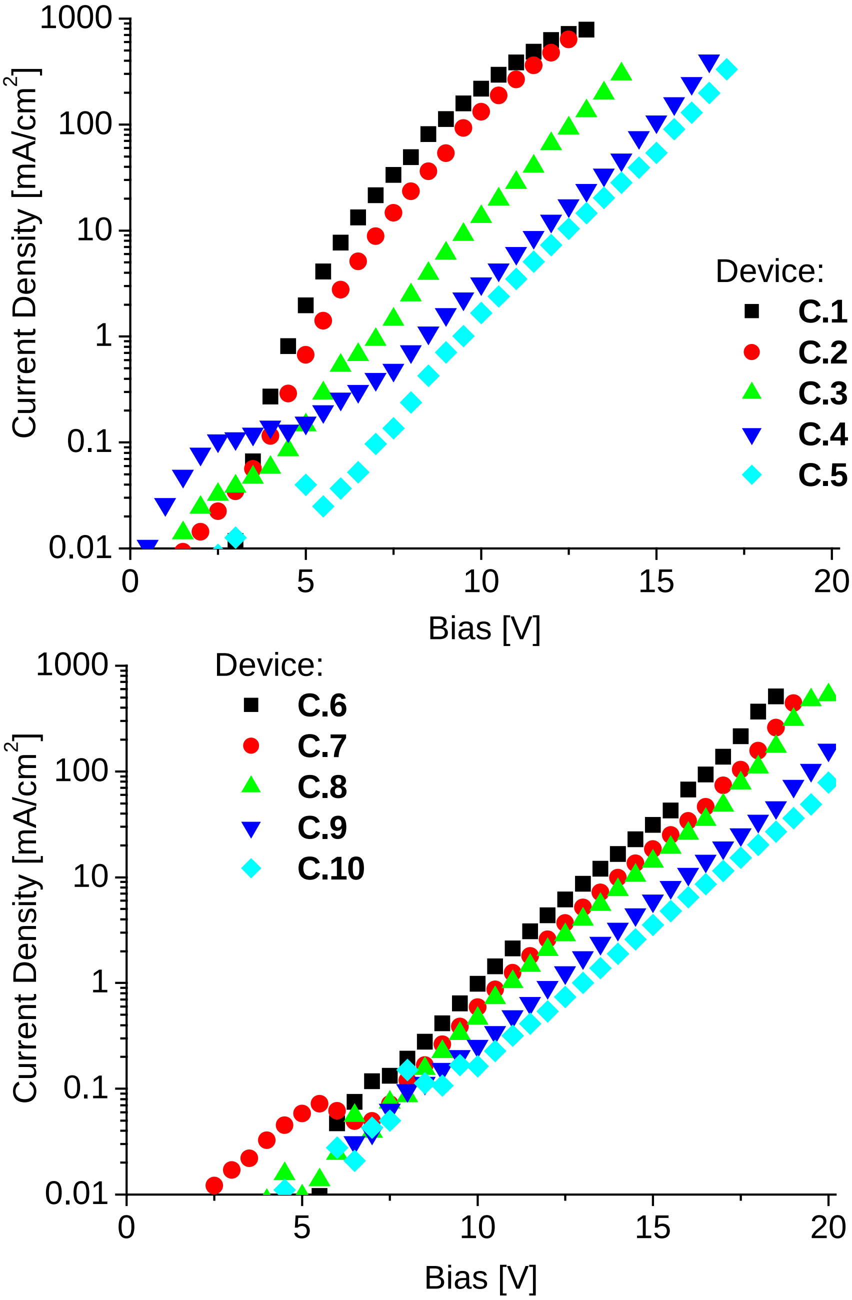

*Figure 82. I-V characteristics of the OLEDs **C.1** to **C.5** (top graph) and **C.6** to **C.10** (bottom graph).*

Luminance intensities of these devices are plotted vs. bias as given in Figure 83. Luminance intensities of 8262, 4031, 431, 73.6, 41.6, 26.1, 15.8, 10.9, 3.71 and 1.69 cd/m^2 at operating bias of 10 V were obtained in OLEDs **C.1-C.10** respectively. The dependence of luminance intensity on red-emitter **10** concentration showed lowering of luminance intensity with raising red-emitter **10** content in Alq_3 layer. Theoretically, the lowering of current density values with increasing red-emitter **10** content as described above should lead to higher luminance intensity. Practically, opposite situation was observed. Thus, the decrease of luminance with raising red-emitter concentration in OLEDs **C** can be attributed to the EL quenching due to concentration effect.

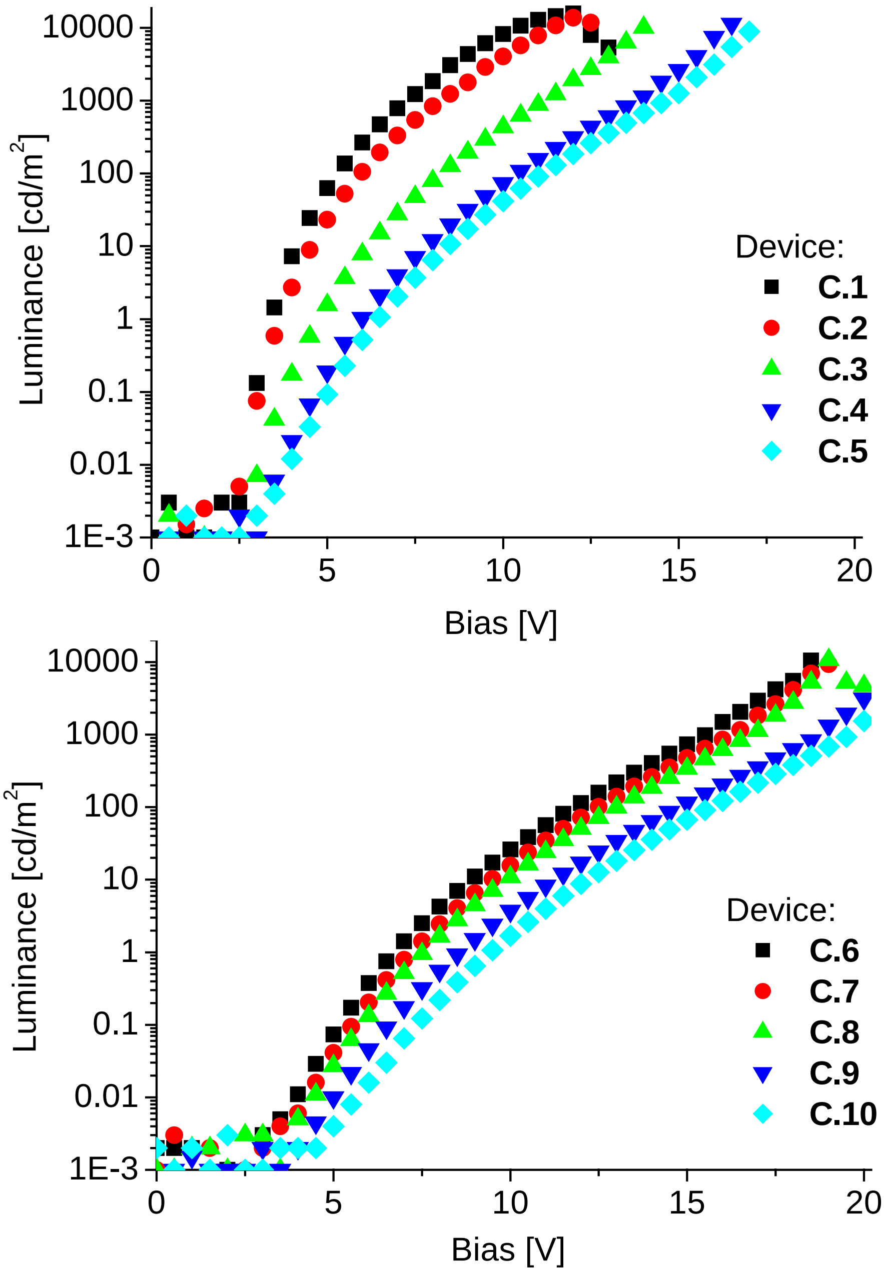

*Figure 83. Luminance-bias characteristics of the OLEDs **C.1** to **C.5** (top graph) and **C.6** to **C.10** (bottom graph).*

EL efficiencies of doped devices **C** plotted vs. bias and current density are represented in Figure 84. Generally, efficiency of these EL cells is decreasing with increasing red-emitter **10** concentration. OLEDs **C.1** and **C.2** showed maxima efficiency of about 4 cd/A, devices **C.3** exhibited a maximum efficiency at more than 3 cd/A. Then follows **C.4** to **C.8** with maxima efficiency at about 2.5 cd/A. Finally, values of about 2 cd/A were observed in **C.9** and **C.10**.

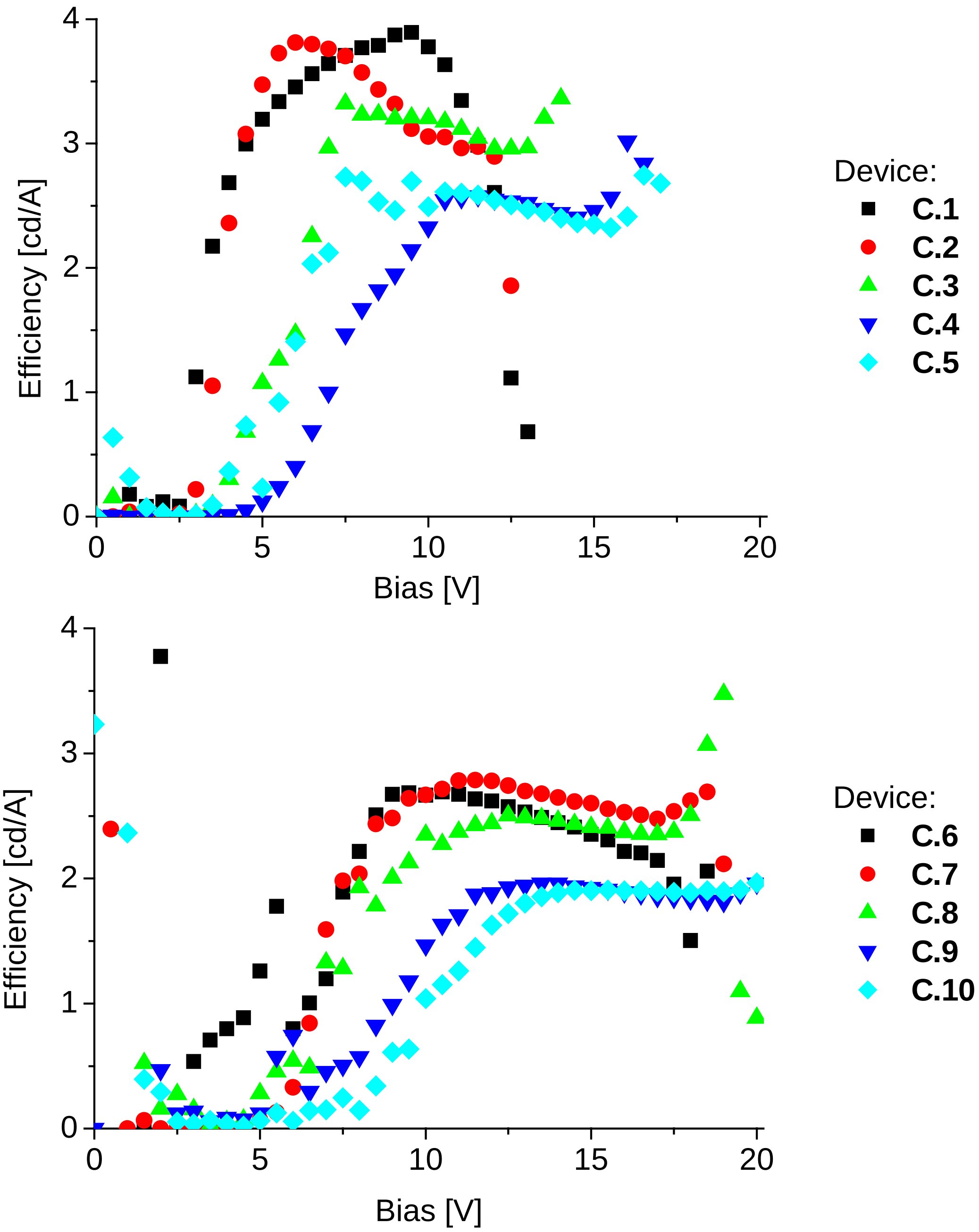

Figure 84.A. Electro-luminance efficiency of the OLEDs ***C.1*** *to* ***C.5*** *(top graph) and* ***C.6*** *to* ***C.10*** *(bottom graph) plotted vs. bias.*

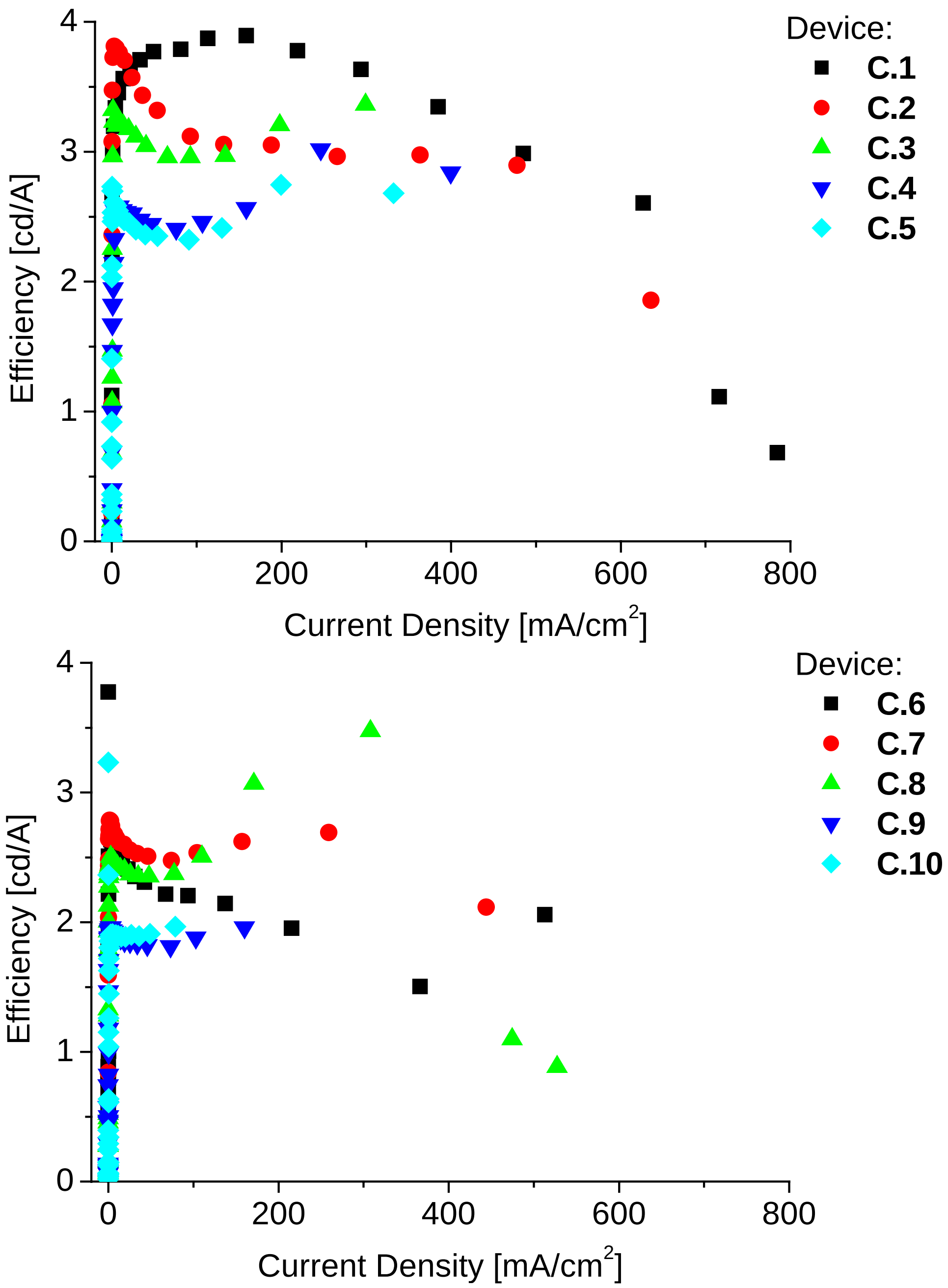

Figure 84.B. Electro-luminance efficiency of the OLEDs ***C.1*** *to* ***C.5*** *(top graph) and* ***C.6*** *to* ***C.10*** *(bottom graph) plotted vs. current density.*

Figure 85 plots the normalised EL intensities as a function of the wavelength measured at 6 V for all cells. The NPD/Alq_3 cell (**C.1**) showed typical green EL from Alq_3 at 518 nm maximum wavelength. The dramatic changes in EL spectra of these OLEDs with red-emitter concentration of 1 % were observed, where the EL was switched from green (**C.1**, 0 % of **10**) to orange-red (**C.2**, 1 % of **10**) with maximum wavelength at 584 nm indicating efficient energy transfer from Alq_3 to red-emitter **10**. Moreover, the OLEDs **C.3** to **C.10** exhibited red electroluminescence with maximum at 595 nm for **C.3**, with maxima at 601 nm for OLEDs

C.4, **C.5** and with maxima at 605 nm for OLEDs **C.6** to **C.10.** All red emissions arise from excited state of **10**.

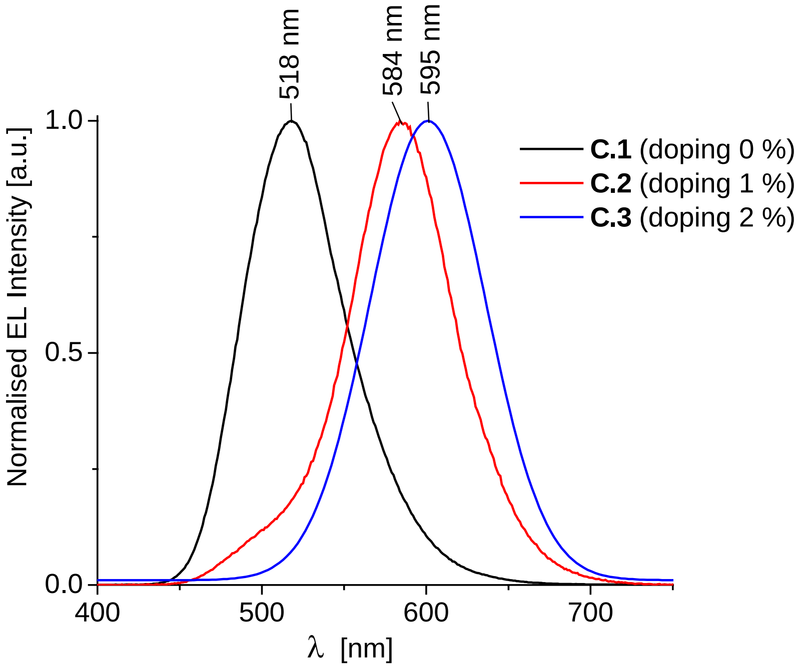

Figure 85. Comparison of the normalised electroluminescence of OLEDs ***C.1*** *to* ***C.5*** *measured at 6 V.*

All measured and calculated EL characteristics of OLEDs of **C-type** are collected in Table 20. The CIE chromaticity coordinates for the green OLED (**C.1**) and the most efficient red OLED (**C.2**) are presented graphically below. CIE coordinates for pure red from different standards such as NTSC, EBU (PAL/SECAM) and SMPTE are also given for a comparison. Thus, it can be seen that the most efficient device **C.2**, ITO / NPD (50 nm) / 1% **10** in Alq_3 (80 nm) / LiF (1 nm) / Al shows almost the required pure EL colour of emission.

*Table 20. EL characteristics of OLEDs **C** based on DTINTPD **10** doped in Alq_3 emitting layer.*

OLEDs	Red-emitter 10 concent-ration [%]	EL intensity[a] [cd/m^2]	Current density[a] [mA/cm^2]	η_{el} [cd/A] (Current density [mA/cm^2], Bias [V])	λ_{max}^{el} [nm] [b]	CIE chromaticity coordinates[c] [x, y] (Bias [V])
C.1	0	8262	219	3.9 (158, 9.5)	518	0.371, 0.547 (6.5 V)
C.2	1	4031	132	3.8 (2.77, 6)	584	0.656, 0.341 (6.5 V)
C.3	2	431	13.5	3.3 (1.44, 7.5)	595	0.656, 0.344 (9 V)
C.4	3	73.6	3.16	2.58 (8.67, 11.5)	601	0.606, 0.394 (12 V)
C.5	4	41.6	1.67	2.73 (0.14, 7.5)	601	0.645, 0355 (12 V)
C.6	4	26.1	0.98	2.69 (1.44, 10.5)	602	0.623, 0.375 (12 V)
C.7	5	15.8	0.59	2.79 (1.81, 11.5)	-[d]	-[d]
C.8	6	10.9	0.46	2.50 (2.84, 12.5)	604	0.653, 0.347 (15 V)
C.9	7	3.71	0.25	1.96 (2.39, 13.5)	605	0.655, 0.345 (17 V)
C.10	8	1.69	0.16	1.90 (2.59, 14.5)	605	0.661, 0.338 (17 V)

[a] – measured at operation bias of 10 V
η_{el} – maximum electroluminescence efficiency
λ_{max}^{el} – wavelength of maximum electroluminescence
[b] – measured at operation bias of 6 V
[c] – 1931 Commission Internatiobnal de l´Eclairage
[d] – not measured

In conclusion, the red OLED based on low molar mass organic compounds were fabricated. The luminance intensity and efficiency of undoped red EL devices was drastically improved using doping concept. Moreover, it was reported earlier[133] that half-life time of undoped green OLED containing organic layers of NPD/Alq_3 was improved from 4200 h to 7500 h by using a doping concept. Thus, the concept of using novel DTITNPD **10** as red-emitter for fabrication of pure red OLEDs like **C.2** and **C.3** with brightness maxima of 13830 at 12 V and 10060 cd/m^2 at operating bias of 14 V respectively were successfully realised.

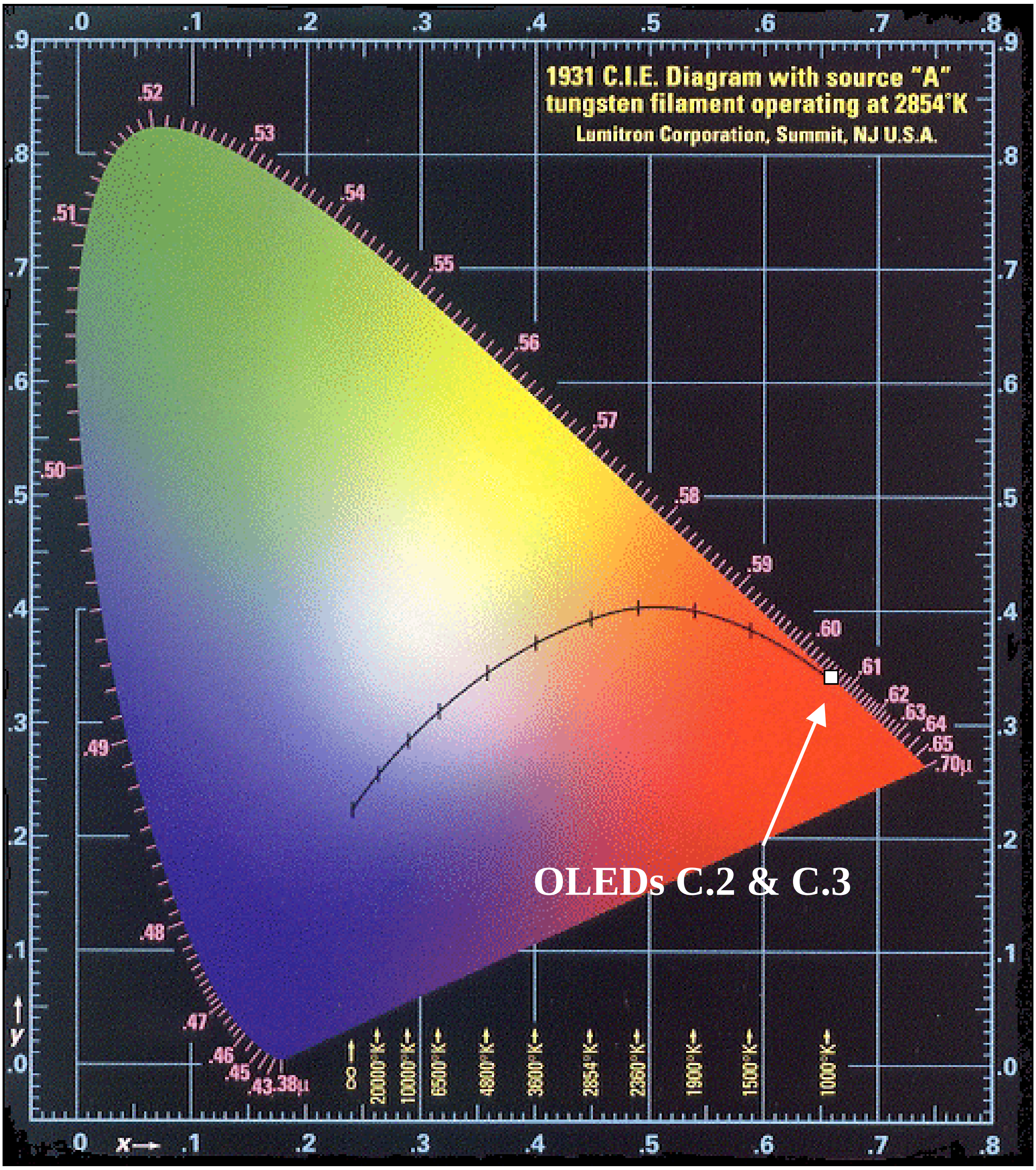

	CIE colour coordinates	
	x	y
CIE 1931 NTSC standard for pure red colour	0.67	0.33
OLEDs **C.2** and **C.3**	0.66	0.34

Figure 86. The CIE chromaticity coordinates of red OLED ***C.2*** *and* ***C.3*** *(open square), where NTSC - National Television System Committee and CIE - Commission Internationale de L'Eclairage or International Commission on Illumination (CIE 1931 chromaticity diagram: www.lumitroncorp.com/rsrcs/CIE.gif).*

9 Summary

The synthesis and characterisation of the new class of compounds, dithienylisothianaphthene phenyldiamines (DTITNPDs) is described. These bifunctional hole transport dyes combine well-known hole-transport property of triaryl amines and thiophenes as well as low band gap nature of isothianaphthene (ITN) moiety. The synthetic strategy is chosen in such a way to obtain low molecular weight and polymeric DTITNPDs. Low molecular weight DTITNPDs **9-11** are synthesised by Pd-catalysed amination of dibromo dithienylisothianaphthene **5** with secondary amines **6-8**. On the other hand, poly(DTITNPD)s **15-17** are obtained via polycondensation of diiodo dithienylisothianaphthene **5** and bis(secondary amine)s **6-8** using a modified Ullmann reaction. The multi-step syntheses of dibromo dithienylisothianaphthene **4** and novel diiodo dithienylisothianaphthene **5** are optimised. The preparation of new bis(secondary amine)s **6-8** are also described. Moreover, the influence of substituents on optical, electro-chemical and thermal properties of DTITNPDs and poly(DTITNPD)s is also investigated.

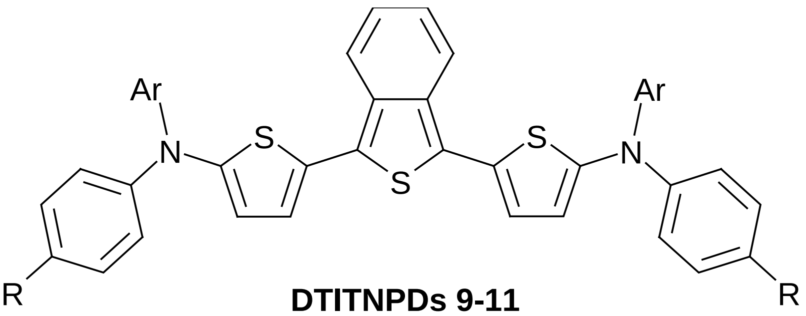

DTITNPDs 9-11

DTITNPDs	**9**	**10**	**11**
Ar	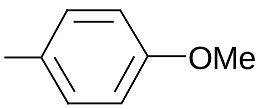	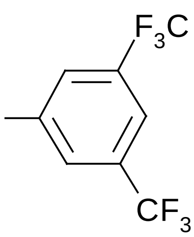	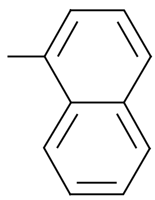
R	—OMe	-	-

*Figure 87. Chemical structures of low molar mass DTITNPDs **9-11**.*

This work also covers the synthesis and characterisation of dithienyl phenyldiamine **12** without ITN moiety and novel dithienylisothianaphthenes (DTITNs) and poly(DTITN)s without triarylamine groups. These compounds are prepared with an aim to compare their properties with DTITNPDs, which carry triarylamine groups. The low molar mass **1-3** (monomers) and polymeric DTITNs **13-14** are obtained. These compounds also possess hole transport property of thiophene and low band gap nature of ITN. Poly(DTITN)s **13-14** are synthesised from monomers, DTITNs **2** and **3** using $FeCl_3$ oxidative polymerisation. The main problem in $FeCl_3$ oxidative polymerisation is the rest Fe content in polymer formed. This problem is successfully overcome here by reducing Fe content up to 0.013 wt. % using improved purification procedure (washing with HCl, H_2O, $NH_{3(aq)}$ and $KSCN_{aq}$). Multi-step syntheses of DTITN monomers are also presented here.

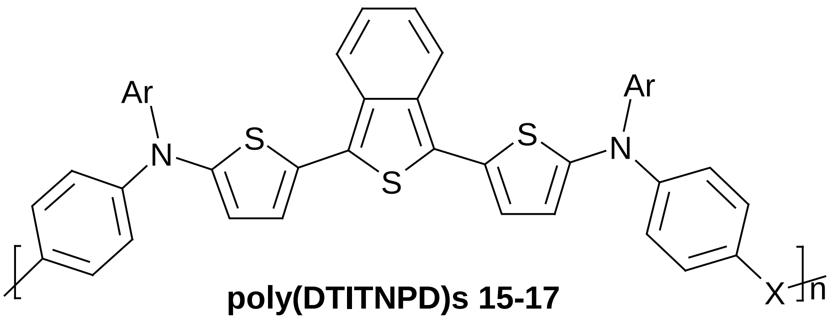

poly(DTITNPD)s 15-17

poly(DTITNPD)s	**15**	**16**	**17**
Ar	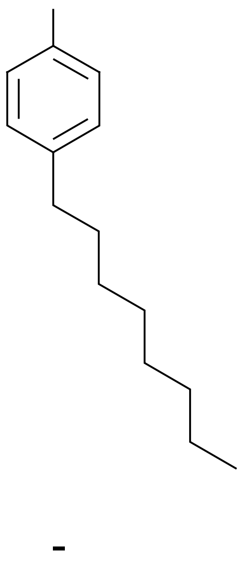	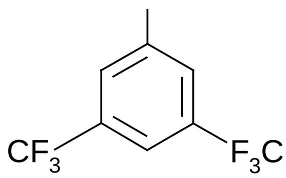	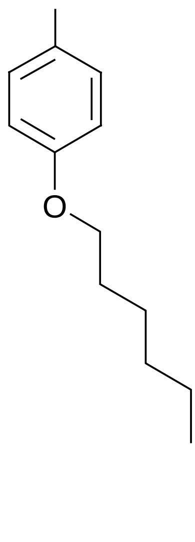
X	-	O	-

*Figure 88. Chemical structures of poly(DTITNPD)s **15-17**.*

The main highlight of this work is the realisation of solution processable and film-forming and air-stable poly(DTITN) and poly(DTITNPD)s in addition to the model compounds DTITNs and DTITNPDs. The synthesised poly(DTITNPD)s possess appreciably high molecular weights. The molecular weight distribution of these polymers is large as obtained from polycondensation.

The model compounds, polymeric DTITNPDs as well as poly(DTITN)s are characterised by means of ^{1}H-NMR-, FT-IR-, MS- and UV-Vis- spectroscopy. Their thermal and electro-chemical behaviour is studied using TGA, DSC and CV measurements. All intermediates, synthesised in this work are also fully characterised by spectroscopic methods discussed above, except UV-Vis spectroscopy. Novel DTITNs and DTITNPDs show good thermal and electro-chemical stability as well as ability to form smooth thin films. DTITNPDs show lower band gap, solubility in common organic solvents and better thermal stability compared to DTITNs. Thus, the strategy of incorporating of ITN and triarylamine groups into one molecule leads to novel new class of materials, DTITNPDs with improved properties. Presence of properties discussed above in these compounds allows using them as hole transport dyes in organic solar cells and as emitter material in organic light-emitting diodes (OLEDs).

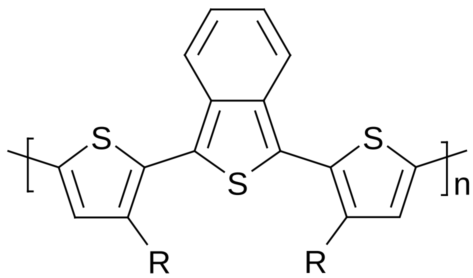

13; R = n-C_6H_{13} **14**; R = -CH_2-$Si(CH_3)_3$

*Figure 89. Chemical structures of poly(DTITN)s **13** and **14**.*

For the application in organic electro-optical devices materials with improved optical and charge transport properties are required. Moreover, these hole transport dyes should match the energy levels (HOMO/LUMO) of the electron transport partner for efficient charge transfer/injection. In this respect, the main attention is placed on variation of energy levels in synthesised molecules by structure modification. The structure modification in DTITN usually changes the LUMO level in the molecule. In contrast to the DTITN, the introduction of different substituents into diphenylamine allows manipulation of HOMO level in DTITNPDs. Thus, the combination of DTITN and triarylamines leads to DTITNPD, where the values of both energy levels can be varied. Novel DTITNPDs exhibit smaller band gap compared to DTITNs. The better delocalised HOMO level in the DTITNPDs compared to DTITNs leads to novel hole transport dyes with E_g < 1.8 eV. In the following, the low molecular weight DTITN **1** is compared to DTITNPD **11** with respect to HOMO/LUMO values. The comparison shows only slight change of LUMO energy value and a decrease of the band gap (E_g) due to HOMO level modification. This fantastic result correlates with theoretical calculations of the energy levels of DTITN and DTITNPD molecules as given in chapter 1 (Motivation and Aim).

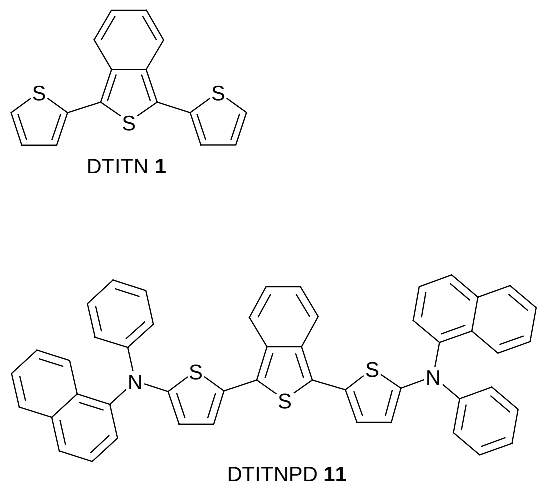

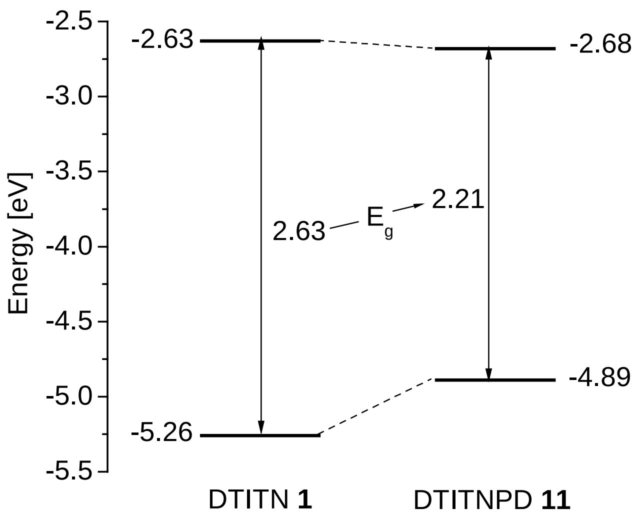

*Figure 90. Energy levels diagram of DTITN **1** and DTITNPD **11**, obtained from CV measurements in carefully dried THF.*

A similar improvement in HOMO/LUMO energy levels is obtained on comparison of poly(DTITN) **13** with poly(DTITNPD) **15** as shown in Figure 91.

The low molar mass DTITNPDs **9** and **10** are tested in plastic solar cells and multi-layer solar cells in combination with electron transport perylene bisimide derivatives and fullerene (C_{60}). The poly(DTITN) **13** is used in plastic solar cell in combination with a soluble fullerene derivative, [6,6]-phenyl-C_{61}-butyric acid methyl ester (PCBM). All of these compounds show good performance in solar cells. The best result is obtained using blend of **13** and PCBM. External quantum efficiency (IPCE spectrum) for this device shows a maximum of ~40 % at 350 nm and a maximum of 15 % at 540 nm, at maximum wavelength of absorption.

A promising result is obtained using **10** as red-emitter in OLEDs. When the **10** doped in Alq_3 at red-emitter **10** concentration of 1 % is used as emitting layer in OLED, the pure red electroluminescence with maximum brightness of 13830 cd/m^2 at operating voltage of 12 V is observed. This device exhibits a high efficiency of 3.8 cd/A at 6 V bias, emitting bright red electroluminescence with CIE coordinates of x = 0.66 and y = 0.34, closely resembling the desired standard red colour (NTSC standard: x = 0.67 and y = 0.34) set for RGB displays.

In near future, the novel poly(DTITNPD)s **15-17** will be tested in plastic solar cells in combination with PCBM. The study of long-term stability of red OLEDs based on DTITNPD **10** is also part of future work, which is necessary for potential industrial application of this material.

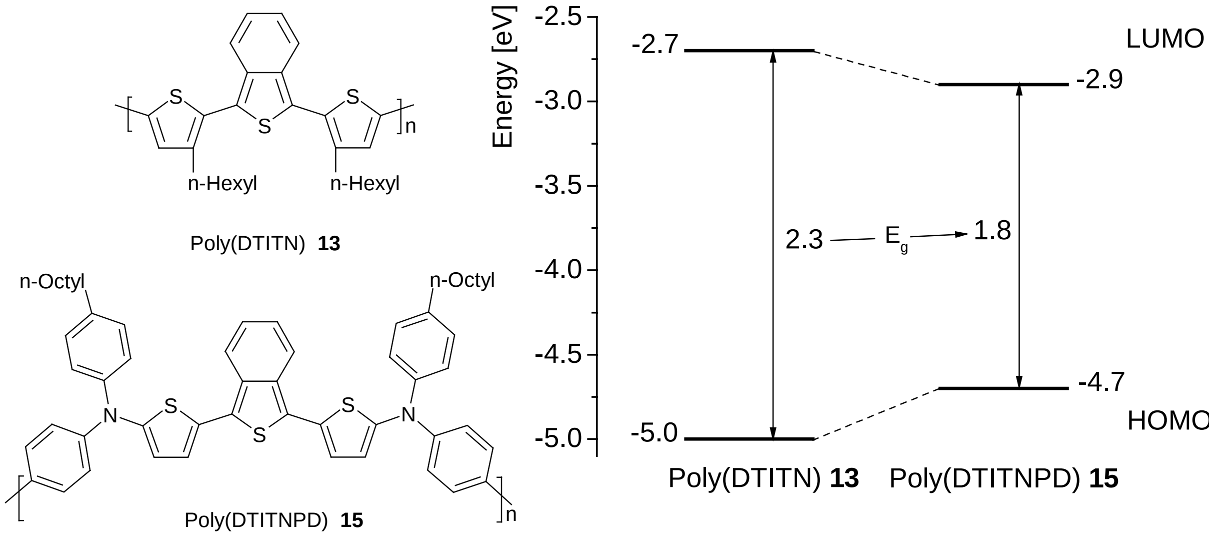

Figure 91. Comparison of HOMO and LUMO energy levels and band gaps, obtained from CV measurements of poly(DTITN) ***13*** *with poly(DTITNPD)* ***15*** *in carefully dried THF.*

Future perspectives and ideas for further improvement of organic solar cells require materials with still lower band gap than DTITNPDs and poly(DTITNPD)s. This is illustrated in Figure 92. There are two possible ways of doing that. The first method is by adapting and replacing the electron transport material (ETM). The second method is by pushing the LUMO of hole transport material (HTM) down to lower values just above that of standard ETL materials such as perylene bisimides or fullerenes.

Here care should be taken to adjust the HOMO value of the low band gap HTM as well to lower values, so that the difference, $HOMO_{HTM}$ - $LUMO_{ETM}$ that corresponds to the maximum theoretically obtainable open-circuit voltage (V_{OC}) in such a cell remains high.

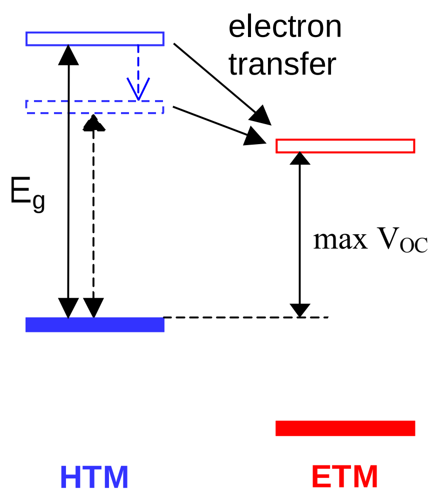

Figure 92. Photoinduced charge transfer from HTM to ETM in which HTM is a low band gap material.

This can be achieved by replacing ITN group in DTITNs and DTITNPDs or their polymeric counterparts with thienothiadazole[134], thienopyrazine[134,135] etc. The chemical structures of these low band gap materials are compared with that of DTITN below. The redox potentials of these compounds measured by cyclic voltammetry (CV) are also given.

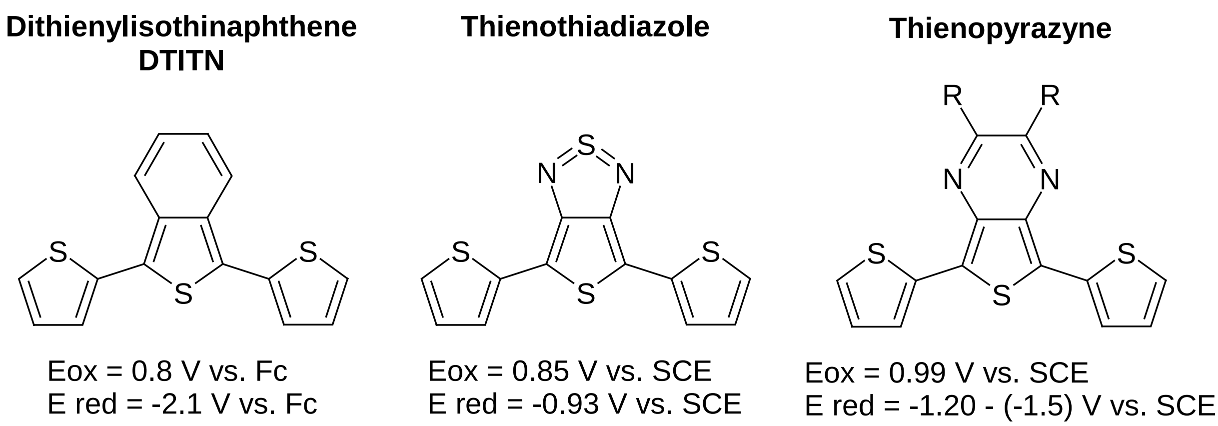

Figure 93. Comparison of redox properties of DTITN to other low band gap materials like thienohiadiazole and thienopyrazine. Where SCE is a KCl saturated calomel electrode, which is one of the commonest reference electrodes.

10 Zusammenfassung

In dieser Arbeit werden erstmalig die Synthese und Charakterisierung der Dithienylisothianaphthenphenyldiamine (DTITNPDs) beschrieben. Diese bifunktionellen Lochtransportfarbstoffe verbinden die bekannten Lochtransporteigenschaften von Triarylaminen und Thiophenen und den niedrigen Bandabstand der Isothianphthene (ITN). Durch die Verbindung dieser Eigenschaften erhält man eine neue Art von Lochtransportfarbstoffen.

Es wurden sowohl niedermolekulare als auch polymere DTITNPD-Derivate synthetisiert. Niedermolekulare DTITNPD **9-11** wurden über eine Pd-katalysierte Aminierung von Dibromodithienylisothianaphthen **4** mit einem sekundären Amin synthetisiert. Mittels Polykondensation von Diiododithienylisothianaphthen **5** und einem bis(sekundären Diamin) **6-8** wurde über eine modifizierte Ullmann Kupplung polymeres DTITNPD dargestellt.

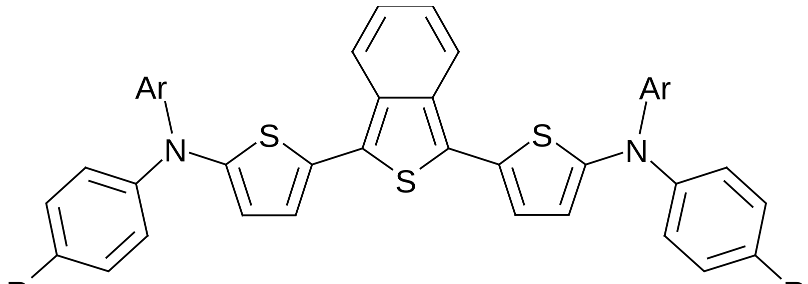

DTITNPDs 9-11

DTITNPDs	**9**	**10**	**11**
Ar	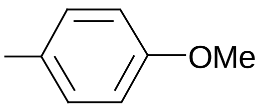	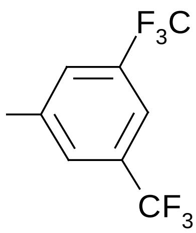	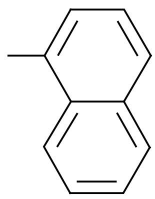
R	–OMe	-	-

*Abbildung 86. Strukturformel der niedermolekularen DTITNPD **9-11**.*

Weiterhin werden die optimierten, mehrstufigen Synthesen von Dibromodithienylisothianaphthen **4** und Diiododithienylisothianaphthen **5** in dieser Arbeit beschrieben, ebenso wie die Darstellung der verwendeten bis(sekundären Amine) **6-8**.
Es wurde der Einfluss verschiedener Substituenten auf die optischen, elektrochemischen und thermischen Eigenschaften von DTITNPDs bzw. Poly(DTITNPD) untersucht.

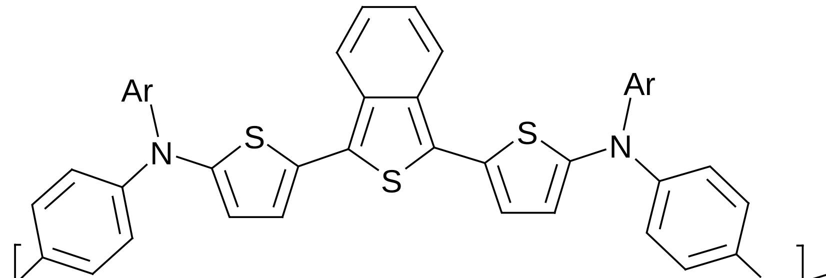

poly(DTITNPD)s 15-17

poly(DTITNPD)s	**15**	**16**	**17**
Ar	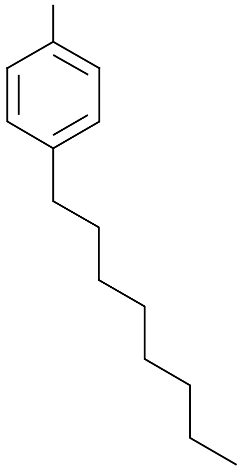	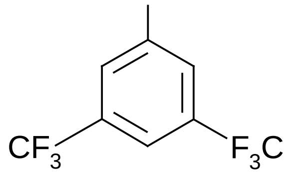	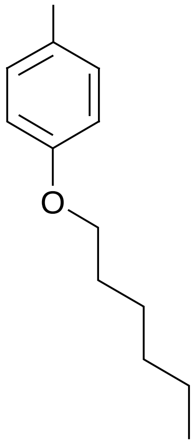
X	-	O	-

Abbildung 87. Strukturformel von Poly(DTITNPD)s ***15-17****.*

Darüber hinaus beschäftigt sich diese Arbeit mit der Synthese und Charakterisierung von Dithienylphenyldiamine **12** ohne den ITN-Bestandteil, von Dithienylisothianaphthenen (DTITNs) und von Poly(DTITN)s ohne die Triarylamingruppen. Diese Substanzen wurden dargestellt, um deren Eigenschaften mit denen von DTITNPDs, welche die Triarylamingruppe beinhalten, zu vergleichen. Es wurden die Monomere **1-3** und polymeres DTITNs synthetisiert. Ebenso wie Thiophen besitzen diese Substanzen gute Lochleitereigenschaften und eine Bandlücke vergleichbar mit ITN. Poly(DTITN)s wurden über eine $FeCl_3$-katalysierte oxidative Polymerisation, aus DTITNs **2** und dem Monomer **3** gewonnen. Das Hauptproblem bei dieser Art der Polymerisation ist die Anreicherung von Eisen im Polymer. Durch eine verbesserte Reinigungsmethode (waschen mit HCl, H_2O, $NH_{3(aq)}$ und $KSCN_{(aq)}$) konnte der Eisenanteil im Polymer auf 0,013 Gew. % reduziert werden.

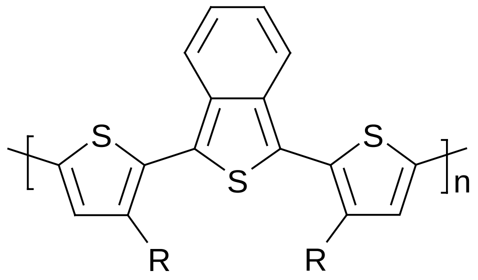

13; R = n-C_6H_{13} **14**; R = -CH_2-$Si(CH_3)_3$

*Abbildung 88. Strukturformel von Poly(DTITN)s **13** and **14**.*

In dieser Arbeit konnten aus Lösung verarbeitbare, filmformende und luftstabile Poly(DTITN) und Poly(DTITNPD)s synthetisiert werden, zusätzlich zu den Modellverbindungen DTITNs und DTITNPDs. Die erhaltenen Poly(DTITNPD)s besitzen ein annehmbar hohes Molekulargewicht. Die Molekulargewichtsverteilung dieses Polymers entspricht der Größenordnung, wie sie bei Polykondensationen üblich sind.

Die Modellverbindungen, Poly(DTITNPD)s und Poly(DTITN)s wurden mittels ^{1}H-NMR, FT-IR, MS und UV-Vis-Spektroskopie charakterisiert. Die thermischen und elektrochemischen Eigenschaften wurden mit Hilfe von TGA, DSC und CV bestimmt. Ebenso wurden alle Zwischenprodukte, die in dieser Arbeit synthetisiert wurden, mit den oben genannten Spektroskopiemethoden, mit Ausnahme der UV-Vis-Spektroskopie, charakterisiert. Sowohl DTITNs als auch DTITNPDs besitzen eine gute thermische und elektrochemische Stabilität und sind gute Filmbildner. Vergleicht man DTITNPD mit DTITN, so weist DTITNPD eine niedrigere Bandlücke, bessere Löslichkeit in gebräuchlichen Lösungsmitteln und bessere thermische Stabilität auf. Daraus wird ersichtlich, dass die Verknüpfung von ITN und Triarylamingruppen zu einer Substanzklasse führt, die verbesserte Eigenschaften aufzeigt. Die oben genannten Eigenschaften erlauben es, diese Substanzen als Lochleiter in organischen Solarzellen und als Emittermaterialien in organischen Leuchtdioden (OLEDs) einzusetzen.

Für die Anwendung in organischen, elektrooptischen Bauelementen, in denen organische Halbleiter hauptsächlich eingesetzt werden, braucht man Materialien mit guten optischen und guten Ladungstransporteigenschaften. Darüber hinaus sollten die Energieniveaus

(HOMO/LUMO) dieser Lochleitermaterialien zu den Energieniveaus der mit ihnen eingesetzten Elektrontransportmaterialien passen, um einen effizienten Ladungstransport bzw. Ladungsinjektion zu gewährleisten. Aufgrund dieser Anforderungen, wurde ein Hauptaugenmerk auf die Variation der Energiestufen bei der Molekülsynthese gelegt. Dies wurde durch Veränderungen in der Molekülstruktur erzielt. Strukturänderungen in DTITN verschieben in der Regel das LUMO des Moleküls. Im Gegensatz dazu kann durch unterschiedliche Substituenten am Diphenylamin das HOMO des DTITNPDs manipuliert werden. Koppelt man diese beiden Komponenten, DTITN und Diphenylamin, zu DTITNPD, erhält man eine Substanz, die eine Variation des HOMOs und des LUMOs erlaubt. Das in dieser Arbeit synthetisierte DTITNPD weist eine niedrigere Bandlücke auf als das DTITN. Das besser delokalsierte HOMO-Niveau im DTITNPD führt zu Lochleitern mit Bandlücken (E_g), die kleiner als 1,8 eV sind.

Im Folgenden werden niedermolekulares DTITN **1** und DTITNPD **11** bezüglich ihrer HOMO/LUMO-Niveaus miteinander verglichen. Dieser Vergleich zeigt, dass sich das LUMO-Energieniveau, von DTITN auf DTITNPD, nur um einen kleinen Betrag ändert. Die Abnahme des Bandabstandes ist hauptsächlich auf eine Verschiebung des HOMO-Niveaus zurückzuführen. Dieses Ergebnis stimmt mit den theoretischen Berechnungen, die für DTITN und DTITNPD in Kapitel 2 durchgeführt wurden, überein.

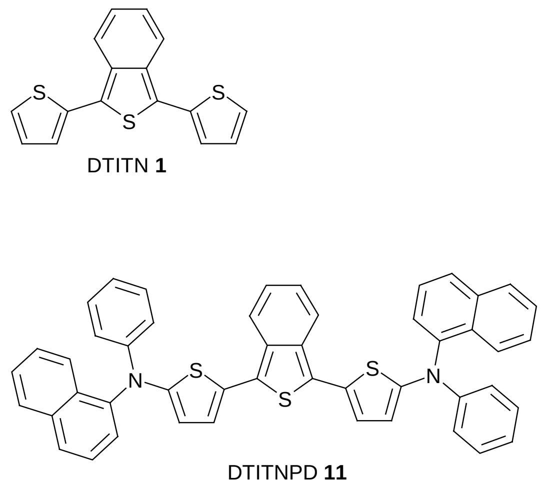

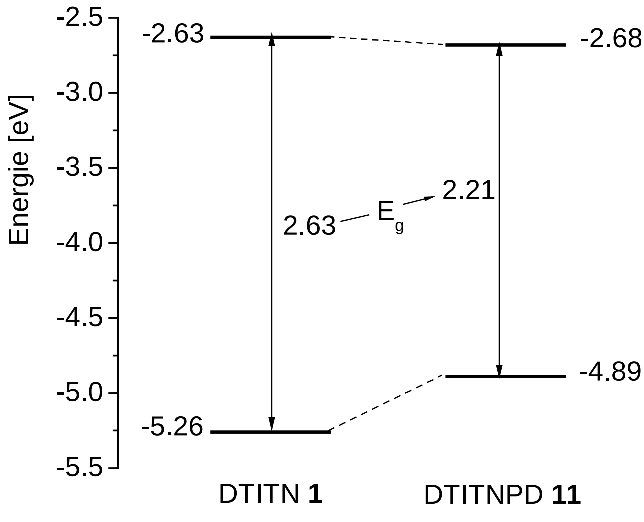

*Abbildung 89. Energiediagramm der Moleküle DTITN **1** und DTITNPD **11**, erhalten aus CV-Messungen, im sorgfältig getrocknetem THF.*

Eine ähnliche Verbesserung bei den HOMO/LUMO-Zuständen wird bei einem Vergleich von Poly(DTITIN) **13** mit Poly(DTITNPD) **15** beobachtet, wie es in Abbildung 90 zu sehen ist.

Die niedermolekularen DTITNPDs **9** und **10** wurden, kombiniert mit Elektronentransportschichten wie Derivaten des Perylenbisimid und Fullerenen (C_{60}), in

Plastik- und Mehrschichtsolarzellen getestet. Das Poly(DTITN) **13** wurde zusammen mit löslichen Fullerenderivaten, [6,6]-Phenyl-C_{61}-buttersäuremethylester (PCBM), in Plastiksolarzellen getestet. Alle Verbindungen zeigten ein gutes Leistungsverhalten in Solarzellen. Das beste Ergebnis wurde mit einer Mischung aus **13** und PCBM erreicht. Die externe Quanteneffizienz (IPCE-Spektrum) für diese Solarzelle hatte ein Maximum von ~40 % bei 350 nm und ein zweites Maximum von ~15 % bei 540 nm, bei der maximalen Absorptionswellenlänge.

Eingesetzt als roter Emitter in organischen Leuchtdioden wurden vielversprechende Ergebnisse mit Substanz **10** erzielt. Bei einer Konzentration von 1 % in Alq_3 erhält man mit **10** eine rein rote Lumineszenz, mit einer Leuchtdichte von mehr als 13830 cd/m^2 bei einer angelegten Spannung von 12 V. Diese Leuchtdiode zeigt eine maximale Effizienz von 3,8 cd/A bei einer Spannung von 6 V. Die CIE-Koordinaten der roten Elektrolumineszenz liegen bei x = 0,66 und y = 0,34. Diese Koordinaten liegen nahe bei dem gewünschten Standardrot für RGB-Schirme (NTSC-Standart: x = 0,67 und y = 0,34).

Es ist geplant, die neu synthetisierten Poly(DTITNPD)s **15-17** zusammen mit PCBM in Plastiksolarzellen zu testen. Des weiteren sind Langzeitstabilitätsuntersuchungen mit DTITNPD **10** als roter Emitter in OLEDs notwendig, um es auf seine kommerzielle Verwendbarkeit zu testen.

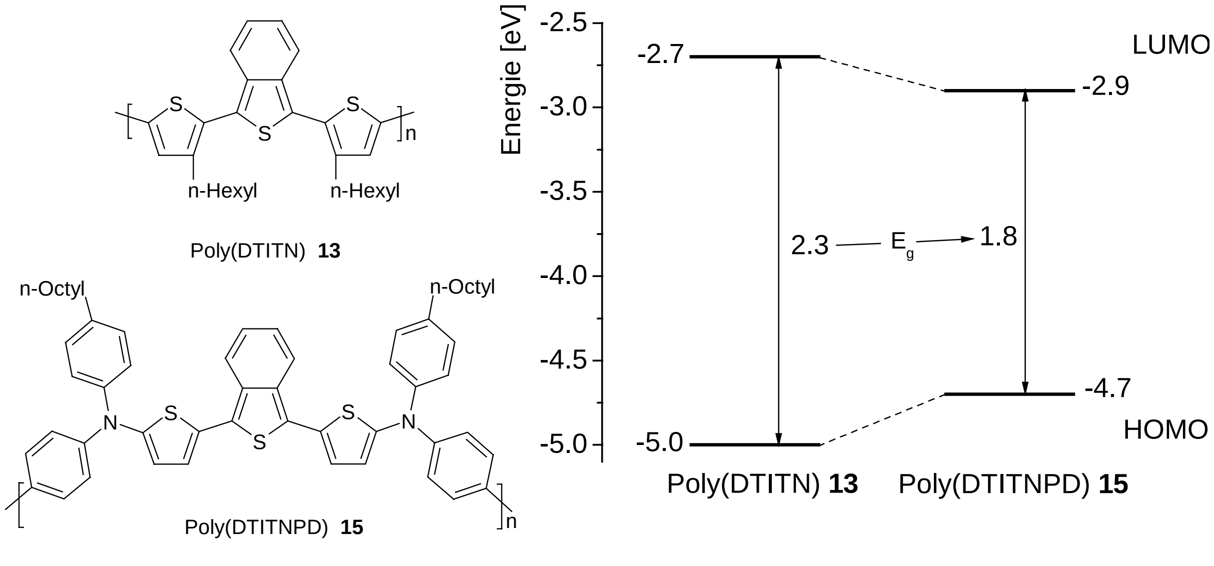

*Abbildung 90. Vergleich der HOMO und LUMO Energieniveaus und der Bandlücken von Poly(DTITN) **13** mit Poly(DTITNPD) **15**, erhalten aus CV-Messungen.*

Um die Effizienz der Solarzellen in Zukunft weiter zu verbessern, benötigt man Materialien, die eine noch niedrigere Bandlücke besitzen als DTITNPDs und Poly(DTITNPD)s, wie es in Abbildung 91 zu sehen ist. Um dies zu erreichen, gibt es zwei Wege. Eine Möglichkeit ist es, das verwendete Elektronentransportmaterial (ETM) anzupassen oder zu ersetzen. Die andere Alternative ist, das LUMO des Lochtransportmaterials (LTM) so zu erniedrigen, dass es knapp über dem LUMO der Standard ETMs, wie Perylenbisimid oder Fulleren, liegt.

Dabei sollte auch das HOMO-Niveau der Lochleiter mit einer engen Bandlücke sorgfältig abgestimmt werden, so dass die Differenz $HOMO_{HTM} - LUMO_{ETM}$, von der das theoretische Maximum der Leerlaufspannung (V_{OC}) abhängig ist, möglichst groß ist.

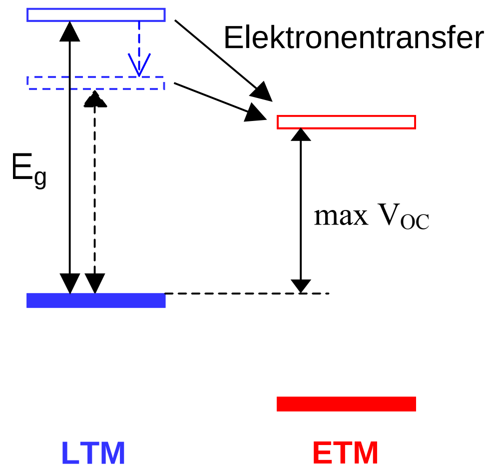

Abbildung 91. Photoinduzierter Ladungstransport zwischen LTM und ETM, wobei das LTM eine enge Bandlücke besitzt.

Dies kann erreicht werden, wenn man den ITN-Teil in DTITN und DTITNPDs oder ihre polymeren Entsprechungen durch Thienothiadazol[133], Thienopyrazin[133, 134] usw. ersetzt. Ein Vergleich zwischen den Strukturformeln dieser Materialien mit einer engen Bandlücke und DTITN ist in folgender Abbildung gezeigt. Die mittels CV gemessenen Redox-Potentiale sind ebenfalls angegeben.

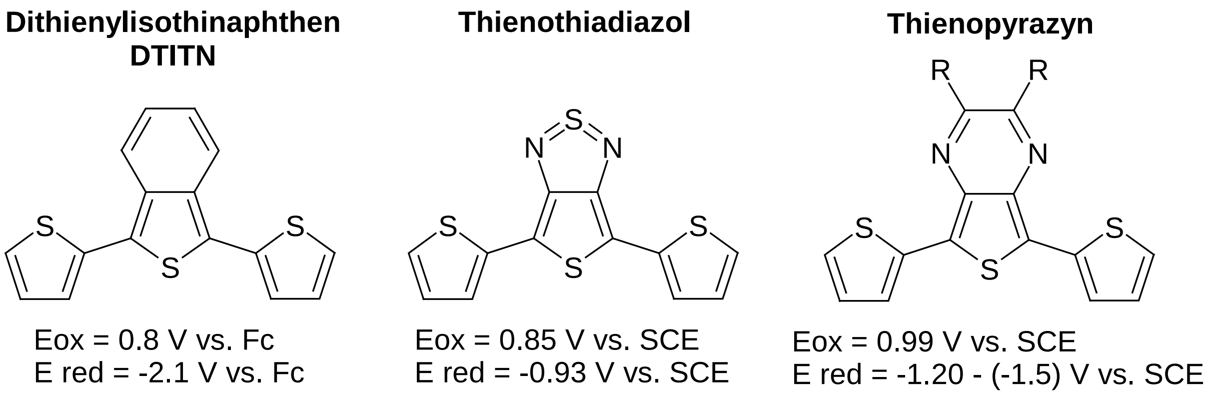

Abbildung 94. Vergleich der Redox-Potentiale von DTITN mit Materialien, die eine niedrige Bandlücke besitzen, wie Thienothiadiazol und Thienopyrazin. SCE ist eine mit KCl gesättigte Calomelelektrode, die zu den am häufigst verwendeten Referenzelektroden zählt.

11 Experimental part

11.1 Solvents and Reagents

The following solvents were used:

Acetic acid was purchased as p.a. grade from Merck.

Acetone was dried over anhydrous $CaSO_4$ and distilled.

Acetonitrile (for CV) was refluxed with 1 % (w/v) P_2O_5 and followed by distillation.

Chloroform ($CHCl_3$) was distilled with 3 % (w/v) P_2O_5 immediately before use.

Chlorobenzene 99% was purchased as p.a. grade from Aldrich.

Cyclohexane was distilled in a glass-packed column.

o-Dichlorobenzene was refluxed and distilled with CaH_2 followed by storage under argon atmosphere.

Dichloromethane (CH_2Cl_2) was distilled with CaH_2.

4,4'-Dimethoxydiphenylamine was purchased from Aldrich and sublimed in high vacuum.

N,N-dimethylacetamide (DMAc) was dried over P_2O_5 followed by vacuum distillation.

N,N-dimethylformamide absolute 99.9% (DMF) was purchased from Aldrich.

Diethyl ether was distilled with 3 % (w/v) P_2O_5.

Dioxane was distilled in a glass-packed column.

Ethanol was distilled in a glass-packed column.

Ethyl acetate was distilled in a glass-packed column.

Isopropanol was distilled in a glass-packed column.

n-Hexane was distilled in a glass-packed column.

Methanol was distilled in a glass-packed column.

Methyl ethyl ketone p.a. (MEK) was purchased from Aldrich.

1-Methyl-2-pyrrolidinone (NMP) was distilled under reduced pressure.

N-(2-naphthyl)aniline was purchased from Aldrich and sublimed in high vacuum.

Petrol ether p.a. (fraction 60-80 °C) was purchased from Merck.

Phthalic acid chloride was purchased from Lancaster and distilled under inert atmosphere.

Tetrahydrofuran (THF; for CV) was purchased from Aldrich in sure seal® bottle.

Tetrahydrofuran (THF; for synthesis) distilled with KOH followed by drying over alox and refluxed with benzophenone from potassium until the blue colour was established. The THF was then distilled and stored under argon atmosphere.

Toluene was distilled with CaH_2 under reduced pressure.

Triethyl amine was dried with CaH_2 followed by distillation in a glass-packed column.

o-Xylene was distilled with CaH_2 under reduced pressure.

The following chemicals were used:

18-crown-6 was purchased from Aldrich was recrystallised from acetonitrile and vacuum dried.

Ammonia aqueous 25 % ($NH_{3\ aq.}$) was purchased from Merck.

Copper powder electrolytic (Cu; mesh 40) was purchased from Aldrich, washed with diluted HNO_3, water, methanol and dried at 60 °C in vacuum.

Diphenyl phosphino ferrocene (DPPF) was purchased from Aldrich and vacuum dried.

1,3-Bis(diphenylphosphino) propane (DPPP) was purchased from Aldrich and vacuum dried.

Hydrochloric acid 31-33 % aqueous (HCl) was purchased from Merck.

Hydrogen peroxide 30 % aqueous (H_2O_2) was purchased from Merck.

8-Hydroxychinolinolato aluminium (III) (Alq_3) was sublimed at a pressure of $< 2.0x10^{-5}$ mbar and a temperature of 280 °C prior to using in physical vapour deposition process.

Lithium fluoride (LiF) was purchased from Aldrich and stored in the glove box.

Palladium acetate ($Pd(OAc)_2$) was purchased from Aldrich and vacuum dried.

Potassium carbonate (K_2CO_3) was purchased from Fluka and stored in the vacuum oven at 60 °C.

Sodium *tert*-butoxide was purchased from Aldrich and vacuum dried.

Sodium hydroxide (NaOH) was purchased from Aldrich.

Sodium sulphate (Na_2SO_4) was purchased from Merck.

Sulphuric acid 96 % (H_2SO_4) was purchased from Merck.

Tri-*tert*.-butyl-phosphine (*tert*.-Bu_3P) was purchased from Aldrich and dissolved in dried toluene (1 g of *tert*.-Bu_3P in 30 ml of toluene).

All other solvents and initial products were purchased from Aldrich, Fluka, Lancaster and were used without any further purification.

11.2 Methods

11.2.1 Cyclic Voltammetry (CV)

Cyclic voltammetry (CV) is one of the most versatile electroanalytical techniques for studying electroactive species. Since it is relatively easy to use and gives a good overview of the redox processes occurring in a certain potential range, it is frequently used within all fields of chemistry. The graph of a cyclic voltammogram reflects the reaction occurring at the electrode surface as the potential is cycled. According to Nernst's equation (equation 1), the ratio of C_{OX}/C_{RED} will change when potential on the working electrode is changed. The value of the formal potential E° for a reversible reaction can be calculated using the anodic and cathodic peak potential (E_{pa} and E_{pc}).

$$E° = (E_{pc} + E_{pa})/2 \qquad \text{(eq. 1)}$$

The obtained reduction and oxidation peak potentials by CV measurements allow the estimation of the LUMO and HOMO levels of the investigated compounds.

A typical three-electrode cell suitable for studies of materials includes a reference electrode, a counter electrode, and a working electrode.

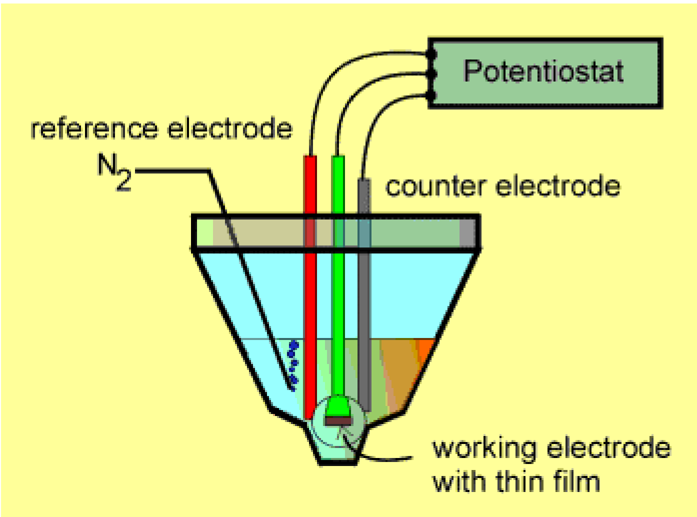

Figure 95. Schematic representation of cyclic voltammetry measurement cell.

CV measurements were carried out using millimolar solutions in highly dried tetrahydrofuran (THF) at room temperature. A glassy carbon disk electrode (0.2 cm^2) coated with a thin polymer film was used as working electrode. A platinum wire was used as a counter electrode and a silver wire in solution of $AgNO_3$ was used as a quasi-reference electrode. Each measurement was calibrated with an internal standard, ferrocene/ferrocenium (Fc) redox system. The HOMO and LUMO values were determined from the value of -4.8 eV for Fc with respect to vacuum level. Scanning rates in the range of 50 to 500 $mV \cdot s^{-1}$ were used.

11.2.2 Differential Scanning Calorimetry (DSC)

Differential scanning calorimetry measurements were carried out using a Diamond DSC from Perkin-Elmer. The heating/cooling rate was 10 $K \cdot min^{-1}$ for all experiments. Sample weights in the range of 15 to 25 mg were used in a 70 µl pellets.

11.2.3 Electroluminescence Emission Spectroscopy

Fluorescence spectra and emission spectra of OLEDs were measured using a Shimadzu RF-5301 PC spectral fluorometer. The excitation beam optical path way was closed. The OLED was placed right in front of the emission beam path way and the device was biased using a Grundig PN 300 power source. Voltage dependent EL spectra were carried out. For a certain bias, the corresponding electroluminescence could be detected and emission spectra were taken.

11.2.4 Elementary Analysis

Elementary analysis of the synthesised polymers was carried out at the *Mikroanalytisches Labor Pascher* (an der Pulvermühle 1, 53424 Remagen, Germany). This Labour provides the possibility to detect the amount of Cu and Fe in solid-state materials.

11.2.5 Flash Column Chromatography

Column chromatography was performed by using silica gel (KIESELGEL 60; Merck) or alumina oxide (Alumina N, Akt. I; ICN Biomedicals GmbH) in 2, 4 or 6 cm thick glass column. First the column was filled up with adsorbent, and then the eluent passed through the column with a force to remove remaining air in adsorbent. Then the substance to be purified was dissolved in a minimum volume of eluent on top of the column followed by elution. During the chromatography the pressure in the column was applied in such a way to get eluent flow in the range of 5 cm of column height pro 60 sec. In a second step purified components was identified by TLC. The solvent was removed using a rotation evaporator.

11.2.6 Fluorescence Spectroscopy

Fluorescence spectra in both solution and film were measured using a Shimadzu RF-5301 PC spectral fluorometer. Excitation wavelength used in excitation beam was equal to corresponding wavelength of maximum absorption from UV-Vis spectroscopy. For measuring fluorescence spectra of solutions the same solutions from UV-Vis spectroscopy were used. On condition that fluorescence in solid state was sufficient, measurements were carried out using thin films on precleaned glass substrates.

11.2.7 Fourier Transformed Infrared Spectroscopy (FT-IR)

Infrared spectra were measured using a BioRad Digilab FTS-40 (FT-IR). Measurements were carried out by using a potassium bromide (KBr) pellet for substances in a solid state and by using sodium chloride pellet for substances in liquid state (16 scans; resolution: 4 cm^{-1}).

11.2.8 Mass Spectrometry

Mass spectra (Finnigan MAT 8500, Varian MAT 112 Spectrometer) were taken at a ionization energy of 70 eV (Electron-Impact).

11.2.9 ^{1}H-NMR-Spectroscopy

Proton Nuclear Magnetic Resonance Spectroscopy was carried out using a AC 250 spectrometer from Bruker (250 MHz) in deuterated chloroform ($CDCl_3$), benzene (C_6D_6), tetrahydrofuran (d_4-THF) or dimethyl sulfoxide (d_6-DMSO). Chemical shifts (δ) were reported in ppm downfield from tetramethylsilane (TMS). All measurements were carried out at room temperature. The following abbreviations were used for signal characterization: d (doublet), t (triplet), m (multiplet, signals without resolution). Signals from spin systems of higher order showing simple line splitting were interpreted like spin systems of 1st order.

11.2.10 Size Exclusion Chromatography (SEC)

Size exclusion chromatography (SEC) measurements were performed on a Waters system with Waters 410 RI and Water 440 UV detectors against polystyrene standards by using THF containing 0.25 wt. % of *tert*-butyl ammonium bromide as eluent at room temperature. The molecular weights and the molecular weight distributions were calculated on the basis of monodispersed polystyrene standards.

11.2.11 Sublimation

Sublimation was performed at a pressure of less than $3.0 \cdot 10^{-5}$ mbar by heating the substance to be purified with an oil bath. High vacuum turbomolecular pump PT151 Kit from Leybold was used. Cooling of the condensing finger of sublimation apparatus was provided by water or water/ice mixture respectively.

11.2.12 Thermo-Gravimetric Analysis (TGA)

Thermo-gravimetric measurements were carried out using a thermoanalysis apparatus TGA/SDTA851^e from Mettler Toledo. Samples for the measurements were prepared by filling alox crucibles. Measurements were performed at a heating rate of 10 K·min^{-1} under a nitrogen flow rate of 75 cm^3·min^{-1} in the temperature range from 30 to 650 K.

11.2.13 Thin-Film Layer Thickness Measurement

Thickness of organic materials spin-coated or vapour deposited onto ITO substrates was in the range of 20-300 nm. Thickness measurements were carried out using a surface profilometer Decktak 3030 ST. The samples for measurement were prepared by scratching thin film using a scalpel. The layer thickness was taken as detected height difference.

11.2.14 Thin Layer Chromatography (TLC)

POLYGRAM SIL G/UV254 and POLYGRAM ALOX N/UV thin layer chromatography cards were purchased from Carl Roth GmbH. Substances were appliquéd on these cards from solution and separated using the given solvent combination respectively.

11.2.15 UV-Vis Spectroscopy

Absorption spectra were measured with a spectrophotometer (Hitachi U-3000). Solution spectra were measured at a concentration varying between 10^{-4} to 10^{-6} M using chlorobenzene, chloroform, cyclohexane, dioxane or THF (all purified according to standard procedures) as solvent. UV-Vis cuvettes with a thickness of 1 cm were used. Extinction coefficient ε is was calculated by equation 2:

$$\varepsilon = \frac{OD}{c \cdot d} \qquad \text{(eq. 2)}$$

where OD is an optical density, c – concentration and d – cuvett thickness.

Thin film solid-state spectra were also carried out. Thin films were prepared either by solution casting or physical vapour deposition on ITO substrates. Film thickness was in the range of 20 to 300 nm. Films were characterised by absorption coefficient α, which was calculated by equation 3:

$$\alpha = 2.303 \cdot \frac{OD}{c \cdot d} \qquad \text{(eq. 3)}$$

11.3 Preparation of Thin Film Devices

11.3.1 ITO Substrates

For the preparation of organic light emitting diodes and organic photovoltaic cells indium tin oxide (ITO) glass substrates were used. The ITO glass pieces (300 mm x 320 mm x 1.10 mm; soda lime float glass, polished with SiO_2 layer; 80 nm ITO, ~ 26 Ω / □) were purchased from Merck. The ITO glass was cut into 76x76 mm squares for use in OLEDs and it was also cut into 24.5x24.5 mm squares for use in solar cells with active layer prepared by spin-coating. The small ITO substrates (24.5x24.5 mm) were etched on one long side 6 mm wide and the 76x76 mm sized substrates were etched on both sides 13 mm wide to avoid shorts between the aluminium cathode and the ITO during contacting. The etching was performed by covering the substrate with an adhesive tape (TESA®). The adhesive tape was pressed carefully onto the substrate in order to result in a sharp etching edge. In a next step the non-covered area was powdered with zinc followed by pouring 15% aqueous HCl onto. After the etching step the substrates were washed with pure water. The described procedure results in complete removal of the ITO. The adhesive tape was removed and the ITO/glass substrates were precleaned with THF by mechanical wiping. Ultrasonic treatment was used next for cleaning the substrates using chloroform and isopropanol each for 15 min respectively. After that the substrates were placed into an oxygen plasma etcher from Anatech Plasma Series (DAIWA DP810 Digital SWR Power Meter) immediately prior to usage. Oxygen plasma treatment was carried out at an oxygen partial pressure of 4.0×10^{-2} bar at 90 W for 600 s.

It should be noted, that the solar cells prepared in Institut für Angewandte Photophysik (IAPP), Technischer Universität Dresden by physical vapour deposition, were fabricated using their own (self-made) ITO glass.

11.3.2 Physical vapour deposition

Physical vapour deposition was used for all organic low molecular weight materials, dielectrics and metals. All physical vapour deposition experiments were performed in high vacuum < 10^{-5} bar. All vapour deposited organic solar cells present in this work were fabricated in cooperation with Dr. Martin Pfeiffer (IAPP, TU Dresden). All vapour deposited OLEDs present in this work were manufactured in cooperation with Marcus Bäte (Macromolecular Chemistry I, University of Bayreuth).

11.3.3 Spin-coating

Spin coater Manueller Belacker B0574 from Hamtech GmbH was used for preparation organic thin films. The pre-cleaned ITO substrates were placed on top of a vacuum chuck. An organic solution was filtered through 0.2 µm PTFE filter onto the substrate using a Pasteur pipette followed by immediately starting rotation (600-3000 rpm for 60 s). By varying the solution's concentration or number of revolution layer thickness can be adjusted.

11.4 OLED measurement

OLEDs fabrication and measurements were performed in cooperation with Markus Bäte (Macromolecular Chemistry I, University of Bayreuth)

11.4.1 Luminance-Current-Voltage characteristics

The set-up provides simultaneous measurement of current [A] and luminance [cd/m^2] in dependence of the applied voltage [V]. The voltage can be applied continuously, stepwise or pulsed. Voltages in the range of –30 V up to +60 V can be applied. Current flow can be measured in the range from 10^{-8} to 0.5 A.

The electroluminescence was measured by positioning the luminance meter LS 100 in front of the light output side (ITO/glass side) of the device. The threshold value for light detection of the LS 100 is 0.001 cd/m^2. All devices were measured in pulsed mode using a voltage range between 0 and 40 V starting at 0 V and increasing the current stepwise by 0.5 V or 1.0 V. The delay time (unbiased) between to voltage steps was set to 2 s. All measurements were performed under ambient conditions if not stated otherwise. Calculation of all other characteristic values like current density, field, photometric efficiency and power efficiency were carried out using the software ORIGIN 6.0 (Microcal).

11.4.2 Color Measurement (CIE)

For measurement of CIE 1931 coordinates a CL-100 from Minolta was used. CIE (Commission International de l'Eclairage or International Commission on Illumination) is an international standards organization founded in 1931. CIE has published a number of colorimetric standards systems called CIE color. These are physical and perceptual based systems where any two colors with the same CIE numbers are perceptually indistinguishable when viewed under standard lighting conditions.

All CIE color models are based on the CIE XYZ color model developed in 1931 and are device independent. X, Y, and Z are abstract color primaries, similar to red, green, and blue (RGB). When the phosphor RGB primaries and the white point temperature are known, the RGB color values can be converted directly into XYZ color values and vice versa. An RGB color is dependent on the device primaries (monitor phosphors) and white point to distinguish what its color looks like. The CIE 1931 spectrum is shown in Figure 96.

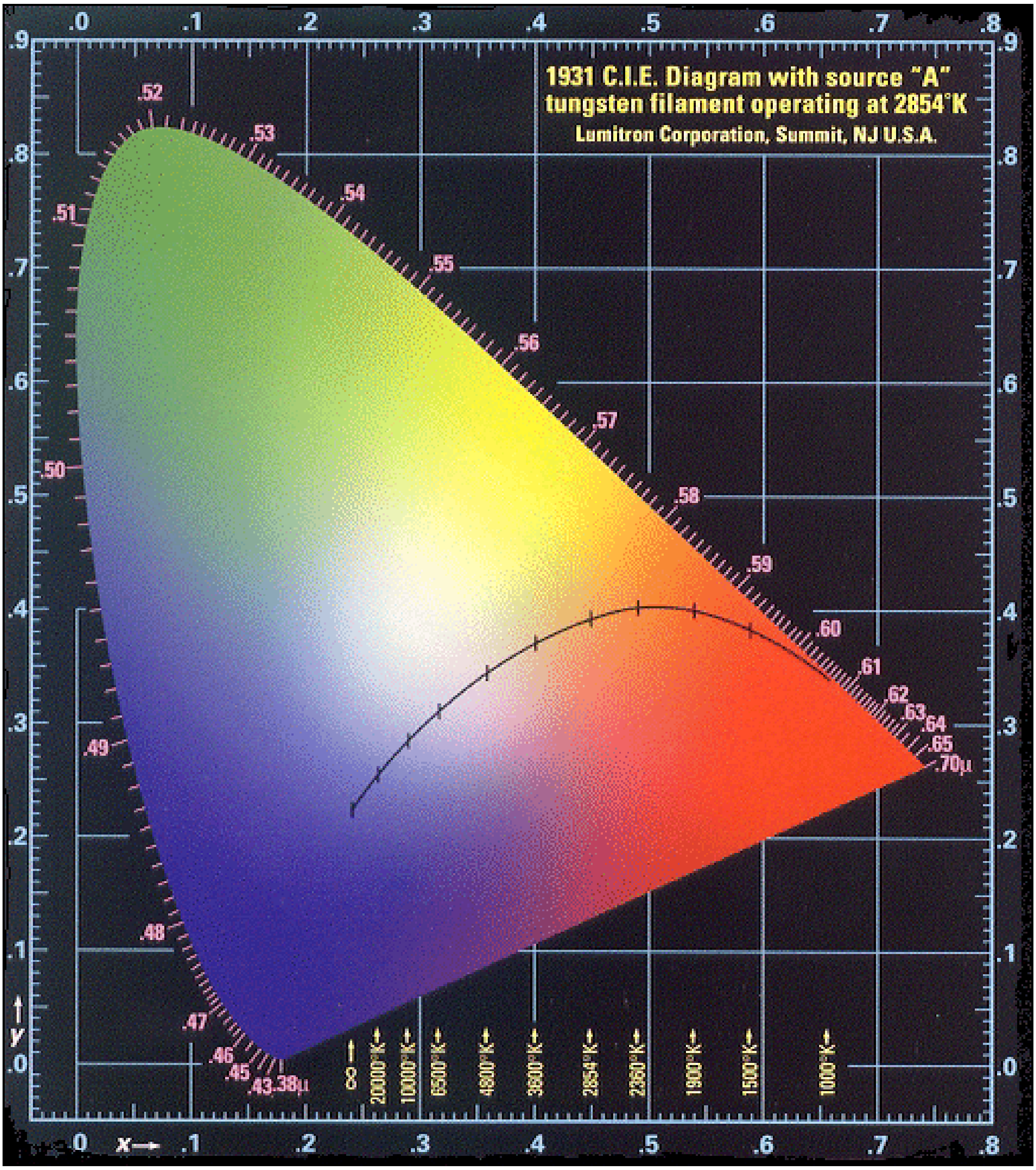

Figure 96. CIE 1931 x & y coordinates along the black body curve. (reference: http://mywebpages.comcast.net/erniew/images/cie.jpg)

11.5 Solar cells measurement

Two techniques commonly used for investigating the photo-electrochemical behaviour of solar cells are *Current-Voltage characteristics* (I-U characteristics) and *Incident Photon to Current conversion Efficiency* (IPCE). These techniques are described below.

11.5.1 Current-Voltage characteristics

The photovoltaic power conversion efficiency (η_c) is defined by equation 4:

$$\eta_c = \frac{V_{OC} \cdot I_{SC} \cdot FF}{P_{In}} \cdot 100 \qquad \text{(eq. 4)}$$

$$FF = \frac{I_{mpp} \cdot V_{mpp}}{I_{SC} \cdot V_{OC}} \cdot 100 \qquad \text{(eq. 5)}$$

where V_{OC} is the open-circuit voltage [V], I_{SC} is the short-circuit photocurrent density [mA/cm^2], *FF* is the fill factor, defined in equation 5 and P_{In} is the incident power of irradiation [mW/cm^2], which is standardised at 1000 W·m^{-2} for solar cell testing with a spectral intensity distribution matching that of the sun on the earth's surface at an incident angle of 45°, which is called the AM 1.5 spectrum.

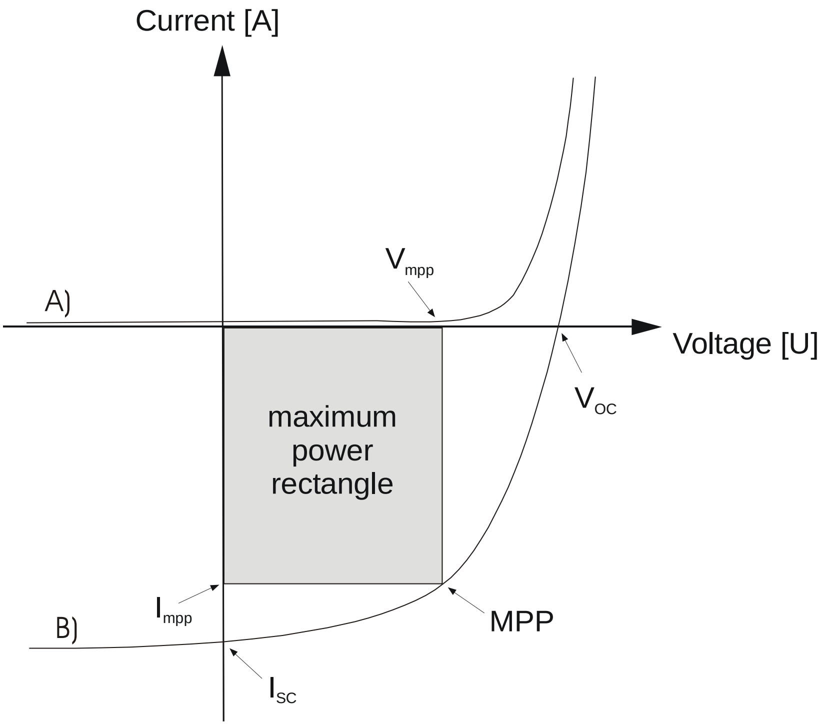

Figure 97. Schematic diagram of I-V characteristics of a photovoltaic cell A) in the dark and B) under illumination; MPP = maximum power point, I_{mpp} = maximum current at MPP, V_{mpp} = maximum Voltage at MPP.

I_{mpp} and V_{mpp} are the current density and voltage at the maximum power point. For testing solar cells in the laboratory, solar simulators are used to imitate AM 1.5 solar irradiation. The picture of the automatic photovoltaic measurement unit with a solar light simulator is given below.

Figure 98. Picture of photovoltaic measurement unit set up.

The thermodynamic limit for the V_{OC} is given by the band gap of the active materials. The band gap limits the splitting of the quasi Fermi level of electron and hole, induced by the light absorption. For organic photovoltaic devices, instead of the band gap the energetic distance between the HOMO of the donor and the LUMO of the acceptor has to be considered as the limitation for the V_{OC}. The I_{SC} is determined by the amount of absorbed light and the internal conversion efficiency. An experimentally accessible value is the external quantum efficiency or *Incident Photon to Current Efficiency*, described in the next section. The FF describes the quality of the diode.

11.5.2 Incident Photon to Current conversion Efficiency (IPCE)

IPCE measurements were carried out in cooperation with Dr. Bin Peng (Macromolecular Chemistry I, University of Bayreuth).

To characterise the spectral response, the monochromatic IPCE [%] of an electrode is recorded as a function of wavelength, the so-called *action spectrum*. The IPCE value is defined as the ratio between the number of generated electrons and the number of incident protons according to equation 6:

$$IPCE = \frac{N_{El}}{N_{Ph}} = \frac{1240 \cdot I_{SC}}{\lambda \cdot P_{In}} \cdot 100 \qquad \text{(eq. 6)}$$

where N_{El} is the number of generated electrons, N_{Ph} is number of incident photons, I_{SC} [mA/cm^2] is the short-circuit photocurrent density for monochromatic irradiation, λ [nm] is the incident photon wavelength and P_{In} [mW/cm^2] is the incident power of monochromatic irradiation. All IPCE action spectrums were recorded under full computer control. The picture of the IPCE measurement set-up is given in Figure 99. Light from a 300 W Xe lamp was focused through a high throughput monochromator onto photovoltaic cell. Short-circuit current was measured using a Keithley model 2400 digital source meter. The curve can be derived from the measured absorption spectrum of the solar cell for comparison. The picture of the IPCE measurement unit is given below.

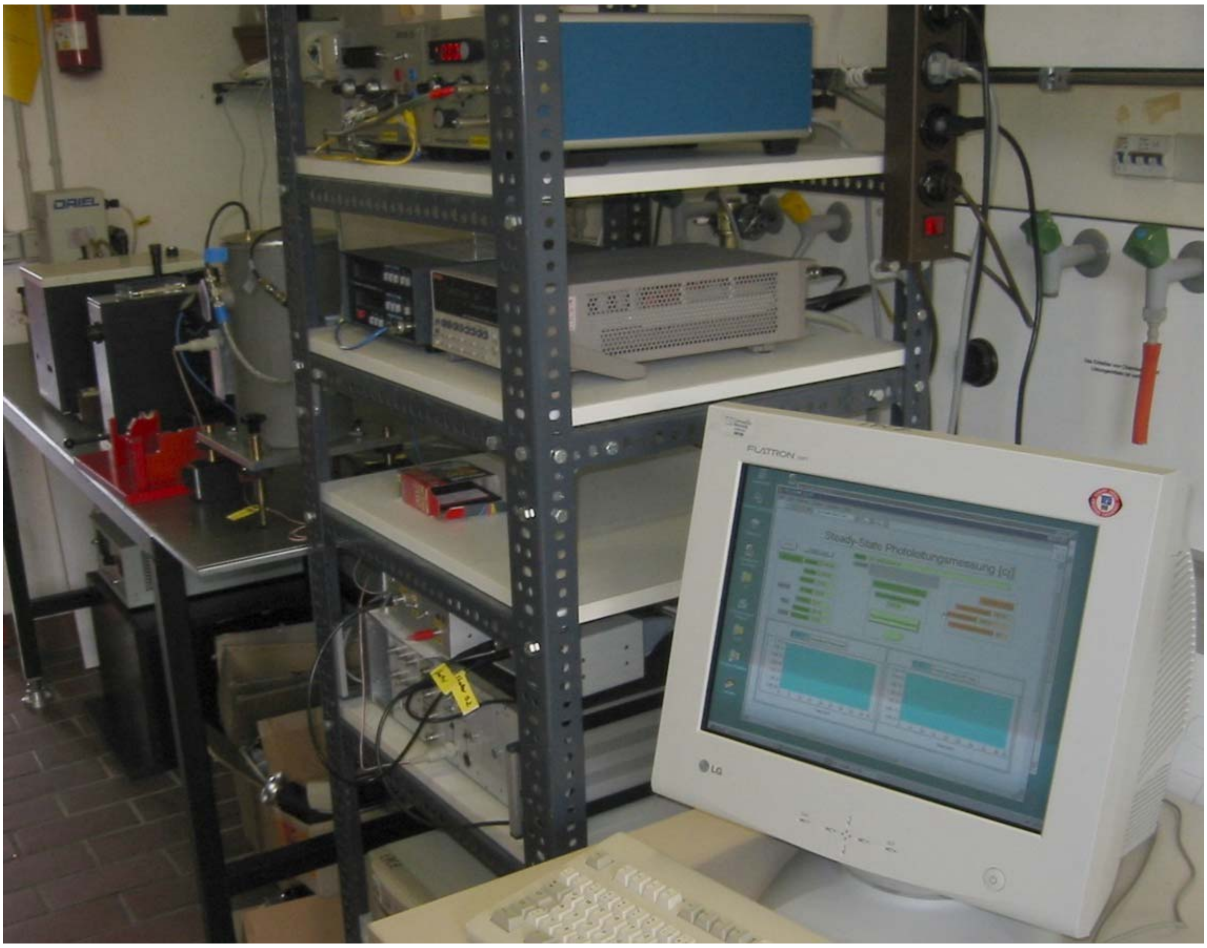

Figure 99. Picture of IPCE measurement unit set-up.

11.6 Synthesis of catalysts

Bis(diphenylphosphino)-1,3-propane-nickel(II)chloride (Ni[dppp]Cl_2) was synthesised according to a procedure known in literature[136].

A hot solution of ligand DPPP (3.011 g; 7.31 mmol) in 40 ml of 2-propanol was added to a solution of $NiCl_2·6H_2O$ (1.995 g; 8.37 mmol) in 35 ml of 2-propanol/methanol mixture with ratio 5:2 accordingly. Immediately brown flaky precipitate was observed, which on heating turned into a fine red microcrystalline powder. This red product was collected and dried in vacuum, giving 3.756 g (95 %)of the catalyst.

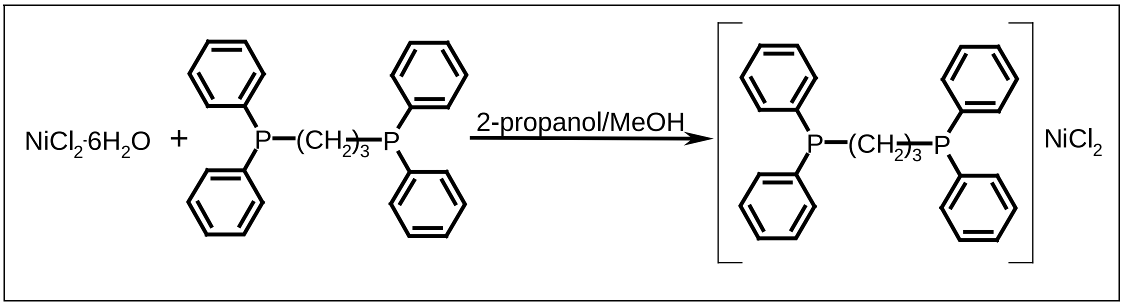

[1,1’-Bis(diphenylphosphino)ferrocene] palladium(II)chloride (Pd(DPPF)Cl_2)

K_2PdCl_4 (0.6528 g; 2 mmol), DPPF (1.1088 g; 2 mmol) and dry CH_2Cl_2 (15 ml) were stirred at 40 °C under Ar for 3 h and over night at room temperature. The product was washed with n-hexane, and dried in vacuum. Yield: 1.42 g (97 %).

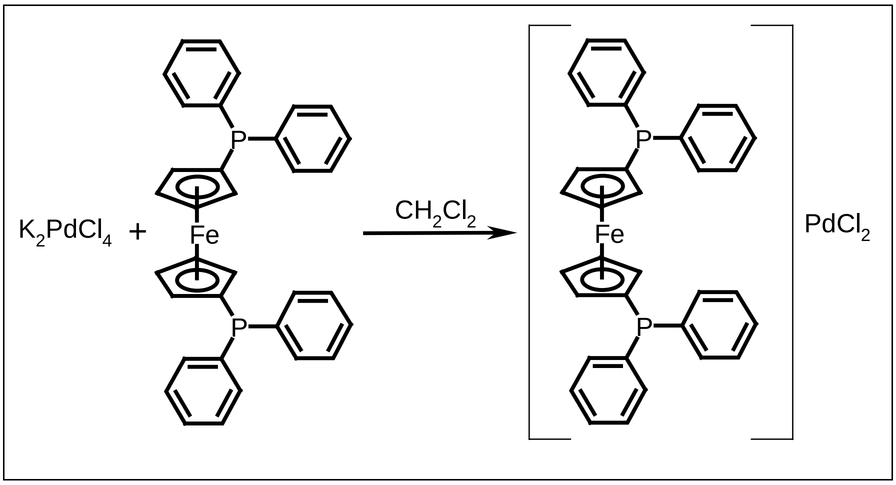

11.7 Synthesis of 1,3-di(2-thienyl)benzo[c]thiophenes **1-3**

11.7.1 1,3-Di(2-thienyl)benzo[c]thiophene **1**

1,3-Di(2-thienyl)benzo[c]thiophene **1** was prepared by a three-step procedure.

Step I. 1,2-Di(S-pyridinyl)benzenedithioate was synthesised according to a procedure as reported by Kiebooms et al.[137] A solution of triethylamine (15 ml), THF (150 ml) and 2-mercaptopyridine (9.35 g; 84 mmol) was stirred for 15 min at 0 °C. A solution of phthalic acid chloride (8.75 g; 42 mmol) in THF (60 ml) was added and reaction was worked up immediately by the addition of 2 % HCl (200 ml; 146 mmol). After extraction with $CHCl_3$ the combined fractions were washed with 10 % NaOH and water until neutral. Finally, drying over Na_2SO_4 and recrystallisation from ethylacetate/ether (10:1) yielded 10.08 g (68 %) of white crystals.

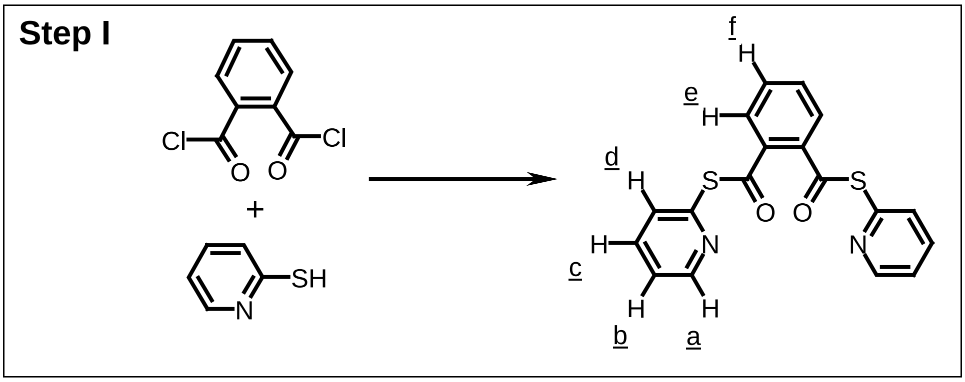

Molecular Weight =352.44
Exact Mass =352
Molecular Formula =C18H12N2O2S2

FT-IR (KBr) ν [cm^{-1}]	3050, 1690, 1664, 1572, 1451, 1420, 1209, 1191, 910, 770, 693
^{1}H-NMR ($CDCl_3$) δ [ppm]	8.62 (d, 2H, d), 7.84 (m, 2H, e), 7.76 (d, m, 4H, a, c), 7.64 (m, 2H, f), 7.28 (m, 2H, b)
MS [m/z]	242 (C_4H_4N–SCO–C_6H_4–CO), 104 (C_6H_4–CO), 78 (C_4H_4N)

Step II. 1,2-Di-2-thienoylbenzene was synthesised according to a procedure known in literature.

General procedure 1.

2-Bromothiophene (8.152 g; 50 mmol) was slowly added to a refluxing mixture of iodine activated magnesium (1.216 g; 50 mmol) in abs. THF (100 ml). After the formation of the Grignard reagent (3h reflux), the cooled reagent was slowly added to a flask containing a solution of 1,2-di(S-pyridinyl)benzenedithioate (8.40 g; 23.8 mmol) in abs. THF (150 ml) at 0 °C. The mixture was stirred for 30 min and 10% HCl (200 ml) was added to hydrolyse the complex formed. The mixture was extracted with ether and the combined organic fractions were washed with 2M NaOH solution, water until neutral and dried over Na_2SO_4. After evaporation of the solvent, a light-brown product was obtained. Finally, purification by column chromatography with cyclohexane/ethylacetate (3:1) yielded 6.79 (95 %) g of yellowish solid.

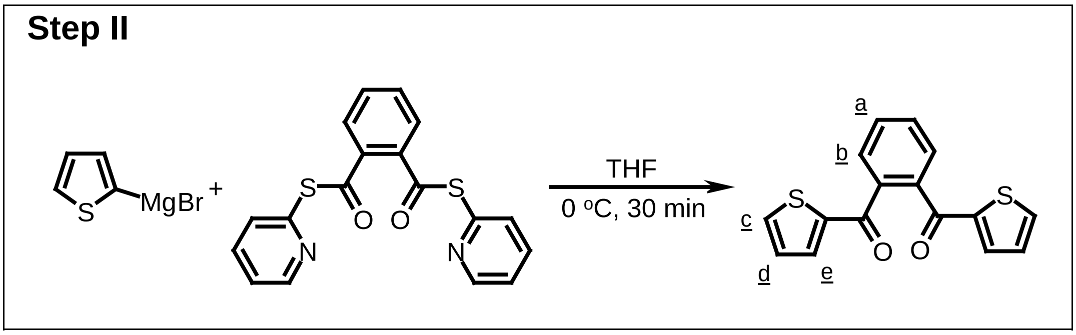

Molecular Weight =298.38
Exact Mass =298
Molecular Formula =C16H10O2S2

FT-IR (KBr) ν [cm^{-1}]	1620, 1585, 1570, 1510, 1410
^{1}H-NMR ($CDCl_3$) δ [ppm]	7.70 (m, 2H, b), 7.60-7.63 (d, m, 4H, a, e), 7.44 (d, 2H, c), 7.05 (t, 2H, d)
MS [m/z]	298 (M^+)

Step III. 1,3-Di(2-thienyl)benzo[c]thiophene 1 was synthesised according to a procedure known in literature.

General procedure 2.

A mixture of 1,2-di-2-thienoylbenzene (1 g; 50 mmol), 2,4-bis-(4-methoxyphenyl)-1,3-dithia-2,4-diphosphetane-2,4-disulfide, known as Lawesson reagent, (20 g; 50 mmol) and CH_2Cl_2 (1 L) was refluxed for 30 min. After evaporation of CH_2Cl_2, ethanol (1 L) was added and the mixture was refluxed for additional 30 min. Finally 2 L of water was added, and the product was extracted with ether. The combined ether fractions were washed with copious amount 10 % NaOH and water and dried. The ether was evaporated, and the remaining solid was taken up in a minimum quantity of $CHCl_3$ and precipitated in n-hexane. The solid was filtered and product was purified by a column chromatography on silica gel column using n-hexane as eluent. Yield is 9.98 g (66 %) of orange solid.

Step III

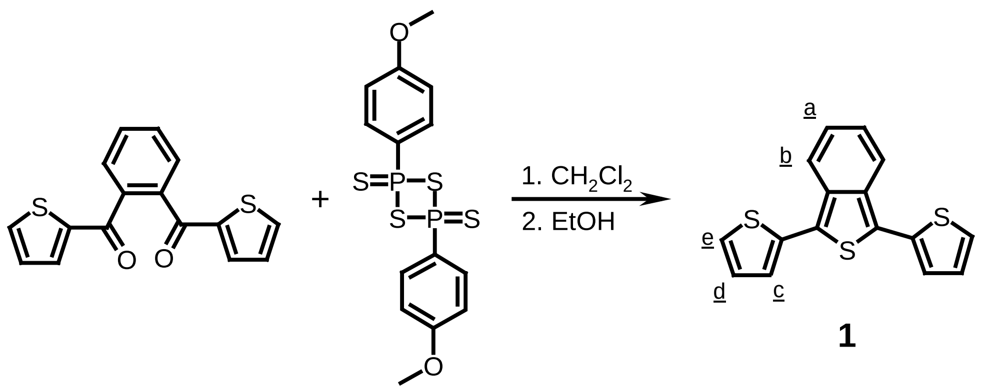

Molecular Weight =298.45
Exact Mass =298
Molecular Formula =C16H10S3

FT-IR (KBr) ν [cm^{-1}]	1530, 1216, 1182, 841, 738
^{1}H-NMR (CDCl3) δ [ppm]	7.95 (m, 2H, a), 7.33-7.35 (m, d, 4H, b, c), 7.14-7.15 (m, d, 4H, d, e)
MS [m/z]	298 (M^+)
UV-Vis λ_{max}^{abs} [nm]	436 ($CHCl_3$)
Fluorescence λ_{max}^{fl} [nm]	517 ($CHCl_3$)
Band gap (UV-Vis) [eV]	2.40 ($CHCl_3$)
CV HOMO [eV]	-5.26
LUMO [eV]	-2.63

11.7.2 1,3-Bis(3-hexyl-2-thienyl)benzo[c]thiophene **2**

Preparation of **2** was done similar to the above general procedures, but by using 2-magnesiumbromo-3-hexylthiophene instead of 2-(magnesiumbromo)thiophenes in the final step. The synthesis of 2-bromo-3-hexylthiophene by two steps is described here first.

Step I. 3-Hexylthiophene was synthesised via modified procedure as reported by Pham et al.[138]

In a flask fitted with a condenser and an argon inlet, iodine activated magnesium (0.729 g; 30 mmol) was introduced together with anhydrous ether (8 ml). A solution of 1-bromohexane (5.117 g; 31 mmol) in anhydrous ether (8 ml) was then added slowly using a syringe. After starting the reaction a gentle reflux was maintained by moderate cooling. The resulting adduct was stirred for 2 hours and then taken using a syringe and was added dropwise to a second flask containing 3-bromothiophene (4.841 g; 30 mmol) and bis(diphenylphosphino)-1,3-propane-nickel(II)chloride ($NidpppCl_2$) (0.2 g) in anhydrous ether (10 ml) in ice bath under stirring. The resulting adduct was allowed to warm up to ambient temperature before being stirred for 24 hours. The reaction mixture was worked up by adding aqueous 1 % HCl (60 ml; ~16 mmol). The organic layer was washed with water, dried and concentrated. The crude product was distilled under 0.13 mbar at 58 °C. 2.56 g (51%) of a colourless liquid was obtained.

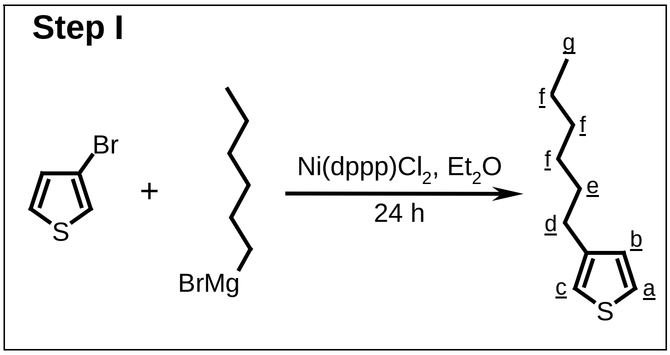

Molecular Weight =168.30
Exact Mass =168
Molecular Formula =C10H16S

FT-IR (NaCl) ν [cm^{-1}]	3105, 2956, 2926, 2856, 1465, 771
^{1}H-NMR ($CDCl_3$) δ [ppm]	7.21 (m, 1H, c), 6.93-6.91 (d, d 2H, a, c), 2.61 (t, 2H, d), 1.60 (m, 2H, e), 1.29 (m, 6H, f), 0.87 (t, 3H, g)
MS [m/z]	168 (M^+), 98 (CH_2^+–C_4H_3S)

Step II. 2-Bromo-3-hexylthiophene was synthesised according to a procedure as reported by Hoffmann et al.[139]

General procedure 3.

To a solution of 3-hexylthiophene in (3.1 g; 18.4 mmol) in $CHCl_3$ (15ml) and acetic acid (15 ml) portions of bromosuccinimide (3.27 g; 18.4 mmol) were added over 30 min at 0 °C. After being stirred for additional 30 min at 0 °C, the mixture was diluted with water and extracted with $CHCl_3$. The extracts were washed first with 2M KOH and with water, and then dried over Na_2SO_4. The residue obtained after removal of solvent was purified by a column chromatography on silica gel with cyclohexane/ethylacetate (20:1) as eluent to give 2-bromo-3-hexylthiophene (3.06 g; 67 %).

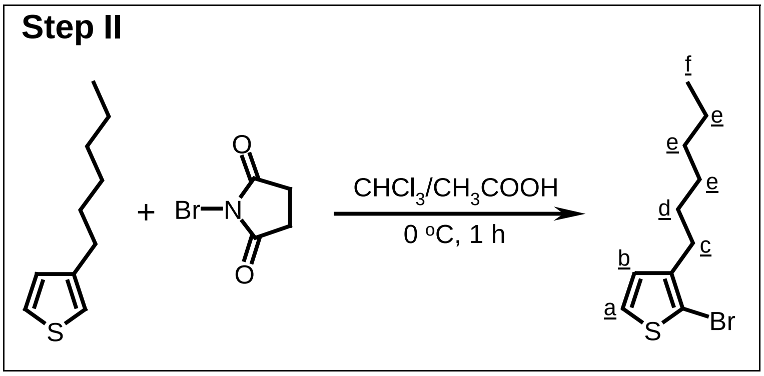

Molecular Weight =247.20
Exact Mass =247
Molecular Formula =C10H15BrS

FT-IR (NaCl) ν [cm^{-1}]	3107, 2956, 2926, 2856, 1467, 1409, 992, 830, 713, 635
^{1}H-NMR ($CDCl_3$) δ [ppm]	7.15 (d, 1H, a), 6.78 (d, 1H, b), 2.54 (t, 2H, c), 1.55 (m, 2H, d), 1.28 (m, 6H, e), 0.87 (t, 3H, f)
MS [m/z]	246 (doublet), 97 ($(CH_2–C_4H_3S)^+$)

1,2-Bis(3-hexyl-2-thienoyl)benzene was prepared via General procedure 1 using 2-bromo-3-hexylthiophene (5 g; 20.2 mmol), magnesium (0.48 g; 20.2 mmol), 1,2-di(S-pyridinyl)benzenedithioate (3.40 g; 9.6 mmol) and THF (total amount - 70ml). Yield: 3.54 g (74 %).

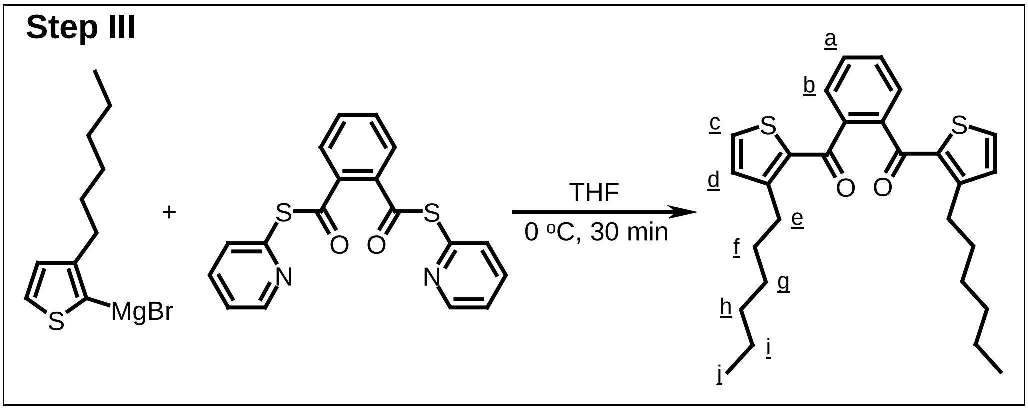

Molecular Weight =466.71
Exact Mass =466
Molecular Formula =C28H34O2S2

FT-IR (NaCl) ν [cm^{-1}]	3101, 3067, 3018, 2956, 2928, 2856, 1638, 1519, 1465, 1408, 1294, 1278, 1250, 912
^{1}H-NMR ($CDCl_3$) δ [ppm]	7.62 (m, 2H, b), 7.55 (m, 2H, a), 7.40 (d, 2H, c), 6.96 (d, 2H, d), 2.78 (t, 4H, e), 1.52 (m, 4H, f), 1.22 (m, 12H, g-i), 0.83 (t, 6H, j)
MS [m/z]	466 (M^+)

1,3-Bis(3-hexyl-2-thienyl)benzo[c]thiophene 2 was prepared via General procedure 2 using 1,2-bis(3-hexyl-2-thienoyl)benzene (2.2 g; 4.7 mmol), Lawesson reagent (1.9 g; 4.7 mmol) in 150 ml of CH_2Cl_2. 1.78 g of yellow oil was collected. Purification by column chromatography using $CHCl_3$/n-hexane (1:2) mixture as eluent yielded 1.78 g (81 %) of yellowish thick liquid.

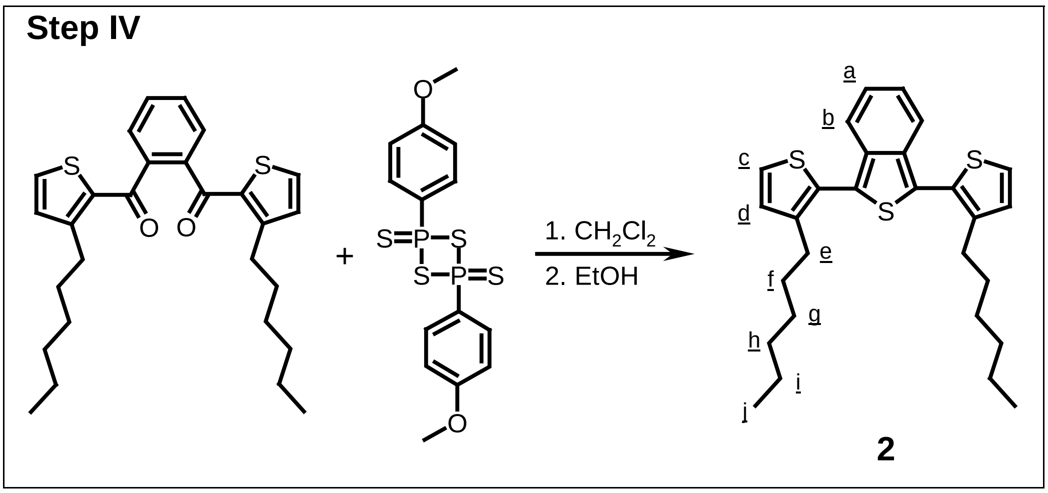

Molecular Weight =466.78
Exact Mass =466
Molecular Formula =C28H34S3

FT-IR (NaCl) ν [cm^{-1}]	3065, 2956, 2926, 2856, 1457, 747
^{1}H-NMR ($CDCl_3$) δ [ppm]	7.56 (m, 2H, b), 7.36 (d, 2H, c), 7.08 (m, 2H, a), 7.04 (d, 2H, d), 2.64 (t, 4H, e), 1.57 (m, 4H, f), 1.19-1.24 (m, 12H, g-i), 0.78 (t, 6H, j)
MS [m/z]	466 (M^+)
UV-Vis λ_{max}^{abs} [nm]	392 (cyclohexane)
Fluorescence λ_{max}^{fl} [nm]	517 (cyclohexane)
Band gap (UV-Vis) [eV]	2.74 (cyclohexane)
CV HOMO [eV]	-5.34
LUMO [eV]	-2.32

11.7.3 1,3-Bis[3-((trimethylsilyl)methyl)-2-thienyl]benzo[c]thiophene **3**

1,3-Bis[3-((trimethylsilyl)methyl)-2-thienyl]benzo[c]thiophene **3** was prepared by a four-step procedure.

Step I. 3-((Trimethylsilyl)methyl)thiophene was synthesised according to a modified procedure as reported by Tamao et al.[140] by using THF/ether mixture as a solvent and more concentrated reaction media.

To a mixture of 3-bromothiophene (8.17 g; 50.1 mmol), Ni(dppp)Cl_2 (0.15 g; 0.3 mmol) in abs. THF (15 ml) was added a solution of ((trimethylsilyl)methyl) magnesium chloride (70 mmol; 1M solution) in dry ether at 0 °C. The mixture was refluxed for 6 h. Reaction was worked up by adding aqueous solution of 1 % HCl. 8.06 g (94 %) of pure product was obtained after standard work up (washing with 1M NaOH, water and drying over Na_2SO_4).

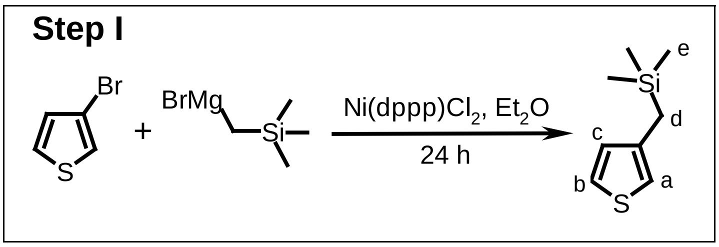

Molecular Weight =170.35
Exact Mass =170
Molecular Formula =C8H14SSi

FT-IR (NaCl) ν [cm^{-1}]	3102, 2955, 2893, 1531, 1411, 1381, 1248, 1169, 953, 844, 782
^{1}H-NMR ($CDCl_3$) δ [ppm]	7.17 (m, 1H, a), 6.77 (d, 1H, b), 6.66 (d, 1H, c), 2.08 (m, 2H, d), -0.02 (s, 9H, e)
MS [m/z]	97 $(CH–C_4H_3S)^+$, 73 $((CH_3)_3Si)^+$

Step II. 2-Bromo-3-((trimethylsilyl)methyl)thiophene was prepared by General procedure 3 using 3-((trimethylsilyl)methyl)thiophene at -40 °C for 3.5 h. The residue obtained after removal of the solvent was purified by column chromatography on silica gel with $CHCl_3$/n-hexane (20:1) as eluent giving the monobromide 10.3 g (80 %) as colourless oil.

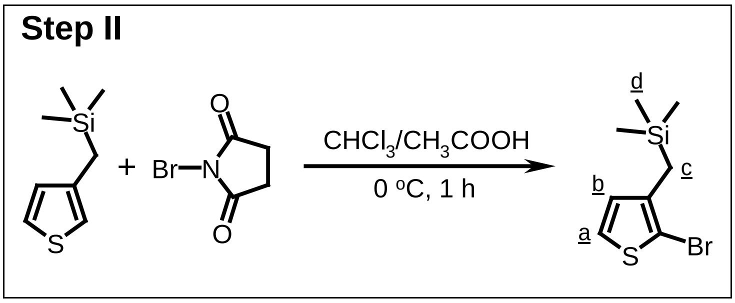

Molecular Weight =249.25
Exact Mass =249
Molecular Formula =C8H13BrSSi

FT-IR (NaCl); ν [cm^{-1}]	2955, 2894, 1537, 1411, 1249, 848
^{1}H-NMR ($CDCl_3$); δ [ppm]	7.14 (d, 1H, a), 6.64 (d, 1H, b), 2.06 (s, 2H, c), 0.02 (s, 9H, d)
MS [m/z]	250 and 248 (doublet), 169, 73

Step III. 1,3-Bis(3-((trimethylsilyl)methyl)thienoyl)benzene was prepared by *General procedure 1* using 2-bromo-3-((trimethylsilyl)methyl)thiophenes (2.1 g; 8.4 mmol), magnesium (0.2 g; 8.4 mmol), 1,2-di(S-pyridinyl)benzenedithioate (1.27 g; 3.6 mmol) in THF (total amount – 45 ml). 1.15 g (68 %) of yellowish thick oil was collected.

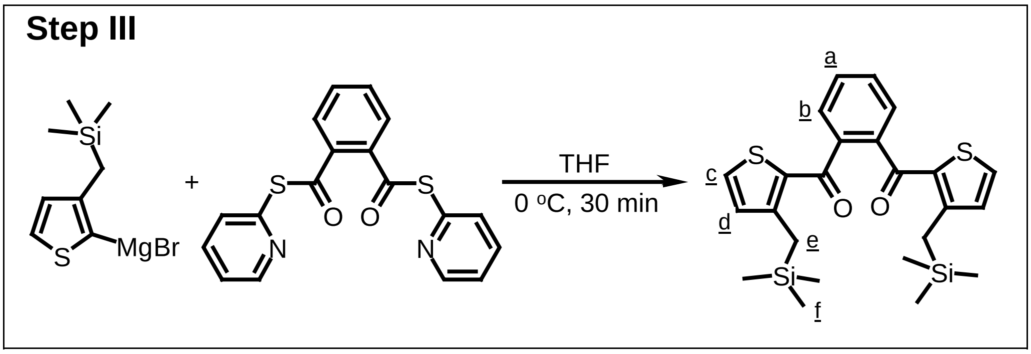

Molecular Weight =470.81
Exact Mass =470
Molecular Formula =C24H30O2S2Si2

FT-IR (KBr); ν [cm^{-1}]	3099, 2953, 2897, 1619, 1507, 1402, 1271, 853
^{1}H-NMR ($CDCl_3$); δ [ppm]	7.62 (m, 2H, b), 7.52 (m, 2H, a), 7.35 (d, 2H, c), 6.77 (d, 2H, d), 2.67 (s, 4H, e), -0.06 (s, 18H, f)
MS [m/z]	470 (M^+)
m.p. [°C]	119.6

Step IV. 1,3-Bis(3-((trimethylsilyl)methyl)-2-thienyl)benzo[c]thiophene 3 was synthesised by General procedure 2 from 1,2-bis[3-((trimethylsilyl)methyl)-2-thienoyl]benzene (1.60 g; 3.4 mmol) and Lawesson reagent (1.37g; 3.4 mmol) in CH_2Cl_2 (150 ml). Purification by column chromatography using CH_2Cl_2/n-hexane (9:1) mixture as eluent yielded 1.40 g (88 %) of yellow oil.

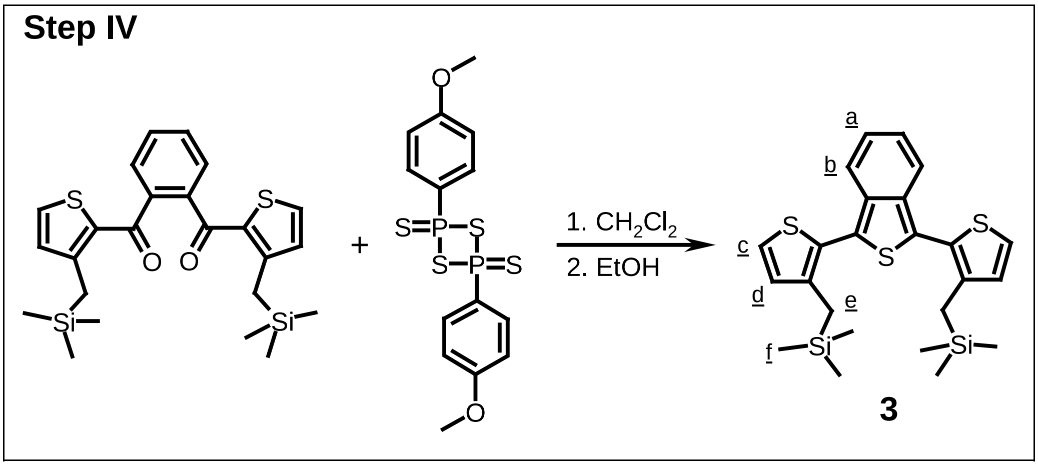

Molecular Weight =470.87
Exact Mass =470
Molecular Formula =C24H30S3Si2

FT-IR (NaCl) ν [cm^{-1}]	3102, 3057, 2955, 2893, 1529, 1380, 1249, 844, 742
^{1}H-NMR ($CDCl_3$) δ [ppm]	7.55 (m, 2H, b), 7.33 (d, 2H, c), 7.07 (m, 2H, a), 6.89 (d, 2H, d), 2.23(s, 4H, e), -0.13 (s, 18H, f)
MS [m/z]	470 (M^+)
UV-Vis λ_{max}^{abs} [nm]	398 (cyclohexane)
Fluorescence λ_{max}^{fl} [nm]	516 (cyclohexane)
Band gap (UV-Vis); [eV]	2.70 (cyclohexane)
CV HOMO [eV]	-5.40
LUMO [eV]	-2.42

11.8 Synthesis of 1,3-bis(5-halogeno-2-thienyl)benzo[c]thiophenes **4**, **5**

11.8.1 1,3-Bis(5-bromo-2-thienyl)benzo[c]thiophene **4**

1,3-Bis(5-bromo-2-thienyl)benzo[c]thiophene was synthesised according to a modified procedure as that in literature using a mixture of chloroform and acetic acid as solvent.

Under exclusion of light portions of NBS (1.193 g; 6.7 mmol) was slowly added to a mixture of 1,3-di-2-thienylbenzo[c]thiophene (1 g; 3.35 mmol) in glacial AcOH and $CHCl_3$ (250 and 50 ml each) at –40 °C. After stirring at -45 °C for 2.5 h reaction mixture was worked up. The reaction mixture was washed with 1M NaOH, water and dried over Na_2SO_4. The product was purified by column chromatography on silica gel using n-hexane as eluent and, finally, crystallised. 1.06 g of red crystals was collected (yield: 70 %).

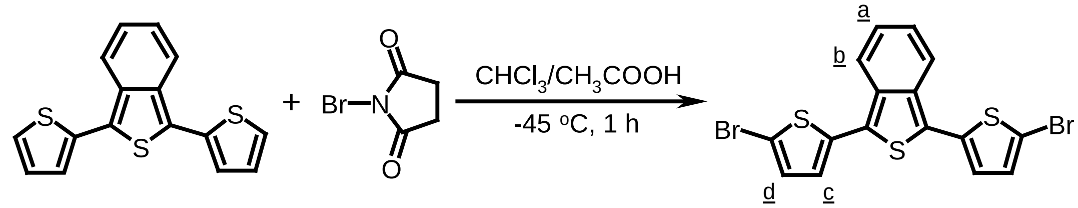

4

Molecular Weight =456.24
Exact Mass =456
Molecular Formula =C16H8Br2S3

FT-IR (KBr) ν [cm^{-1}]	3061, 1528, 1488, 1431, 1190, 968, 877, 778, 734
^{1}H-NMR ($CDCl_3$) δ [ppm]	7.63 (m, 2H, b), 7.16 (m, 2H, a), 7.05-7.07 (d, d 4H, c, d)
MS [m/z]	456 (M^+, triplet)

11.8.2 1,3-Bis(5-iodo-2-thienyl)benzo[c]thiophene **5**

Four different methods were used for synthesis of this compound as written below. And the target product was obtained only after using the *Method D*.

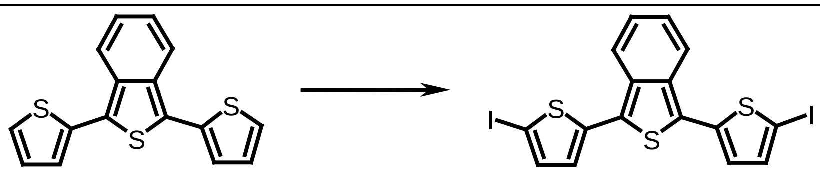

5

Method A: Iodination with KI, KIO_3 in acetic acid/water 15:1 for 2 h at 80 ºC resulted no products due to bad solubility of the reagent in reaction mixture. No products were observed.

Method B: Iodination with iodine, 1,1-bis(trifluoroacetoxy)iodobenzene in chloroform for 15 min at RT resulted only black residue due to forming of oligomers as shows SEC analysis.

Method C: Iodination with N-iodosuccinimide in tetrahydrofuran at –78 ºC resulted no products.

Method D: Under exclusion of light, a solution of N-iodosuccinimide (6.80 g; 30.22 mmol) in DMF (abs., 200 ml) was added dropwise to a solution of 1,3-di-2-thienylbenzo[c]thiophene (4.4 g; 14.74 mmol) in DMF (abs., 130 ml) at -55 °C. The resulting mixture was kept for 4h at -55 °C and then was allowed to warm up to the room temperature overnight. Black precipitate was collected on a glass filter, washed with water and dried in vacuum. The rest from reaction mixture was diluted with water, extracted with CH_2Cl_2, washed with water and dried over Na_2SO_4. The black precipitate and the extract were combined. Final purification by a column chromatography on a silica gel with n-hexane/THF (20:1) yielded 4.28 g (52 %) of the red solid. After that the product was recrystallised in n-hexane/$CHCl_3$ (10:1) mixture, giving bright fluorescent, dark red needles.

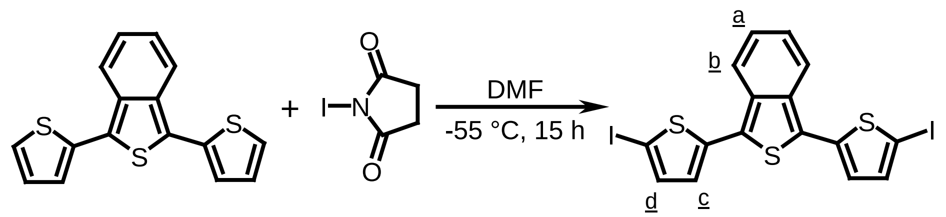

5

Molecular Weight =550.24
Exact Mass =550
Molecular Formula =C16H8I2S3

FT-IR (KBr) ν [cm^{-1}]	1529, 1189, 875, 777, 582
^{1}H-NMR ($CDCl_3$) δ [ppm]	7.82 (m, 2H, b), 7.26 (d, 2H, d), 7.15 (m, 2H, a), 6.99 (d, 2H, c)
MS [m/z]	550 (M^+)

11.9 Synthesis of 4,4'-diarylamino biphenyls **6**, **8** and 4,4'-diarylamino biphenylether **7**

11.9.1 N,N'-di(4-octylphenyl)-4,4'-diaminobiphenyl **6**

General procedure 4.

Pd(DPPF)Cl_2 (0.285 g; 0.3 mmol), DPPF (0.554 g; 1 mmol), sodium *tert*-butoxide (2.16 g; 22.5 mmol), 4,4'-diiodobiphenyl (2.03 g; 5 mmol) and p-octylaniline (3.08 g; 15 mmol) in dried toluene (25 ml) were mixed at room temperature and refluxed under Ar for 16h. Toluene was removed under reduced pressure. Reaction mixture was dissolved in THF and filtered through alox on a glass filter to remove polar impurities. And the product was precipitated in methanol from concentrated THF solution (THF/methanol 20:200 ml). The precipitate was dissolved in CH_2Cl_2, washed with aqueous 32% HCl to remove aniline, washed again with water and dried over Na_2SO_4. After evaporation of CH_2Cl_2, the product was dissolved in THF and precipitated in methanol twice. 1.28 g (46 %) of white solid was collected. On UV-light product shows nice deep-blue fluorescence.

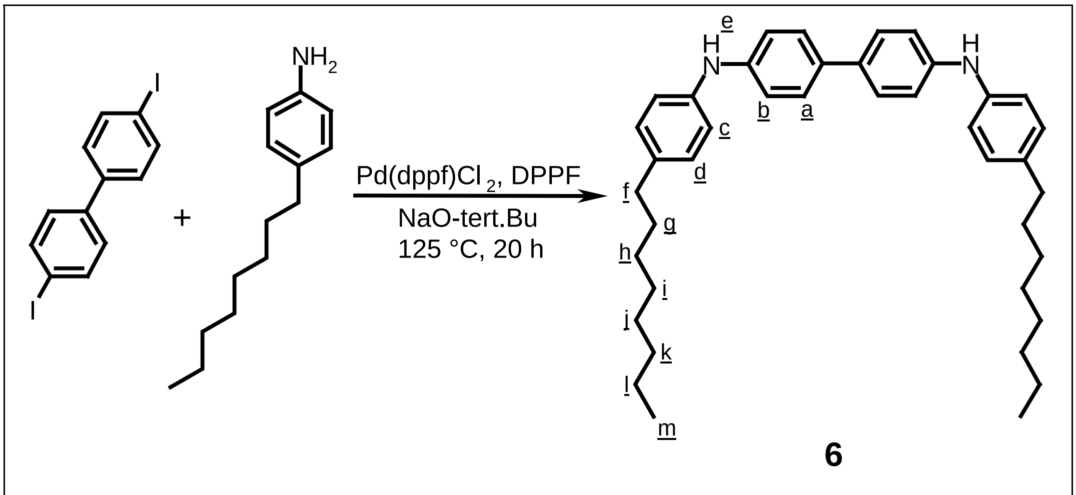

Molecular Weight =560.87
Exact Mass =560
Molecular Formula =C40H52N2

FT-IR (KBr) ν [cm^{-1}]	3415, 3028, 2956, 2916, 2848, 1612, 1519, 1314, 816
^{1}H-NMR (C_6D_6) δ [ppm]	7.46 (d, 4H, d), 7.05 (d, 4H, c), 6.97 (d, 8H, a, b), 5.07 (s, 2H, e), 2.55 (t, 4H, f), 1.62 (m, 4H, g), 1.27 (m, 20H, h, i, j, k, l), 0.91 (t, 6H, m)
MS [m/z]	560 (M^+)

11.9.2 4,4'-Oxybis[N-(2,4-di(trifluoromethyl)phenyl)]benzeneamine **7**

4,4'-Oxybis[N-(2,4-di(trifluoromethyl)phenyl)]benzeneamine **7** was prepared *General procedure 4* using 4,4'-(bisiodobiphenyl)ether (1.59 g; 3.76 mmol), 3,5-(bistrifluoromethyl)aniline (2.59 g; 11.3 mmol), Pd(DPPF)Cl_2 (0.212 g; 0.26 mmol), DPPF (0.416 g; 0.75 mmol) and sodium *tert*-butoxide (1.27 g; 13.2 mmol) in dried toluene (15 ml). Precipitation from THF into methanol, n-hexane or petrolether (b.p. 60-80 °C) did not work. The residue was purified by column chromatography with cyclohexane/ethylacetate (5:1) as eluent. 1.40 g (60 %) of white solid was collected.

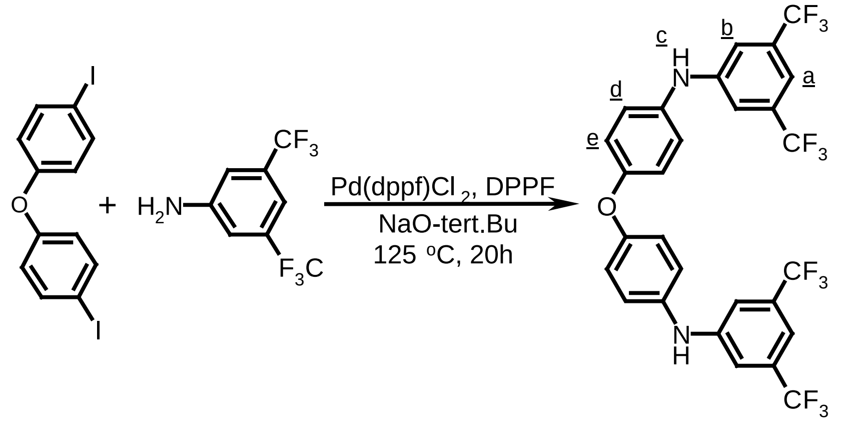

7

Molecular Weight =624.43
Exact Mass =624
Molecular Formula =C28H16F12N2O

FT-IR (KBr) ν [cm^{-1}]	3405, 1618, 1497, 1378, 1274, 1168, 1139, 870
^{1}H-NMR ($CDCl_3$) δ [ppm]	7.26 (s, 12H, a, b), 7.12 (d, 4H, e), 7.06 (d, 4H, d), 5.88 (s, 2H, c)
MS [m/z]	624 (M^+)

11.9.3 N,N'-di(4-hexyloxyphenyl)-4,4'-diaminobiphenyl **8**

N,N'-di(4-hexyloxyphenyl)-4,4'-diaminobiphenyl **8** was prepared via *general procedure 4* using p-hexyloxyaniline (2.89 g; 15 mmol), 4,4'-diiodobiphenyl (2.03 g; 5 mmol), Pd(DPPF)Cl_2 (0.285 g; 0.3 mmol), DPPF (0.554 g; 1 mmol) and sodium *tert*-butoxide (2.16 g; 22.5 mmol) in dried toluene (22 ml). 1.36 g (79 %) of white solid was collected.

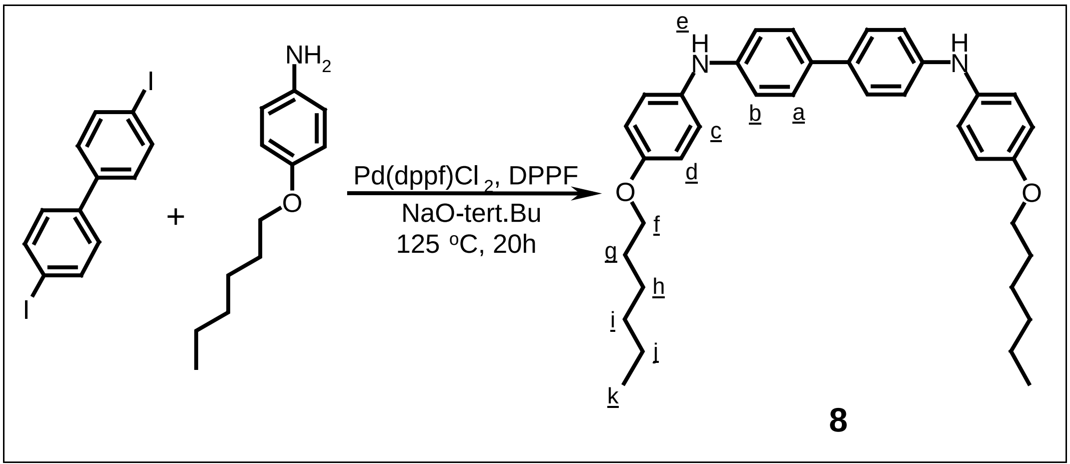

Molecular Weight =536.76
Exact Mass =536
Molecular Formula =C36H44N2O2

FT-IR (KBr) ν [cm^{-1}]	3420, 3029, 2954, 2934, 2871, 1611, 1517, 1250, 817
^{1}**H-NMR** ($CDCl_3$) δ [ppm]	7.37 (d, 4H, d), 7.04 (d, 4H, c), 6.95 (d, 4H, a), 6.86 (d, 4H, b), 5.50 (s, 2H, e), 3.92 (t, 4H, f), 1.76 (m, 4H, g), 1.45 (m, 4H, h), 1.32 (m, 4H, i, j), 0.89 (t, 6H, k)
MS [m/z]	536 (M^+)

11.10 Synthesis of 1,3-bis(5’-diarylaminothiophene-2-yl)benzo[c]thiophenes **9-11**

11.10.1 (1,2'-Bisthienylbenzo[c]thiophene)-5,5'-diamine,-N,N,N',N'-tetra-p-metoxy-phenyl **9**

General procedure 5.

Pd(DPPF)Cl_2 (0.09 g; 0.11 mmol), DPPF (0.183g; 0.33 mmol), sodium *tert*-butoxide (0.77 g; 8 mmol), 4,4’-dimethoxydiphenylamine (2 g; 8.7 mmol), 1,3-bis(5-bromo-2-thienyl)benzo[c]thiophene (1.6 g; 3.5 mmol) and o-xylene (100 ml) were refluxed under Ar for 18 h. After completion of the reaction, the mixture was filtered through silica gel column to remove the salts, o-xylene was removed in vacuum. The residue was purified by column chromatography with n-hexane/ether 1:1 as eluent. 1.53 g (58 %) of a deep violet-red solid was collected.

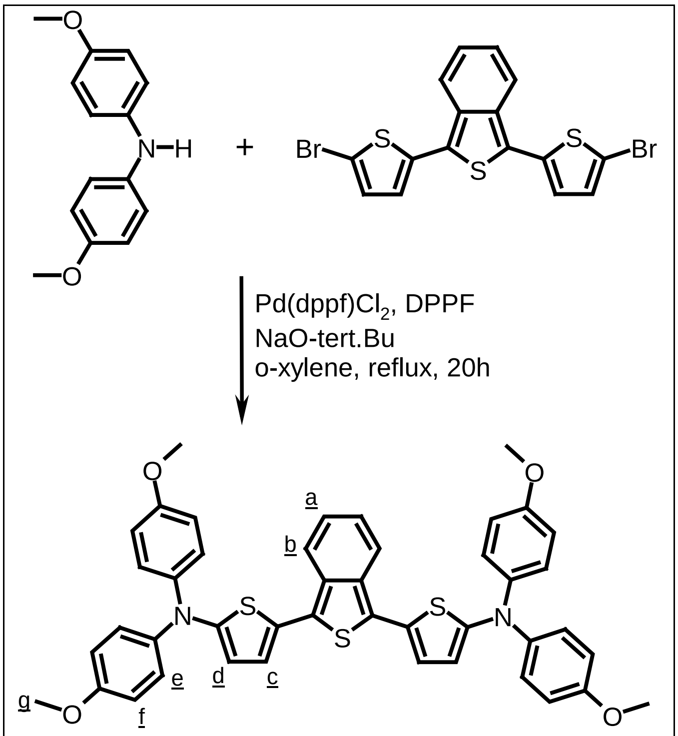

9

Molecular Weight =752.98
Exact Mass =752
Molecular Formula =C44H36N2O4S3

FT-IR (KBr) ν [cm^{-1}]	2929, 2831, 1503, 1462, 1242, 1038, 829, 749
^{1}H-NMR (C_6D_6) δ [ppm]	7.94 (m, 2H, b), 7.19 (d, 8H, f), 6.98 (d, 2H, c), 6.78 (m, 2H, a), 6.73 (d, 8H, e), 6.48 (d, 2H, d), 3.28 (s, 12H, g)
MS [m/z]	752 (M^+)
UV-Vis λ_{max}^{abs} [nm]	518 (dioxane), 540 (film)
Fluorescence λ_{max}^{fl} [nm]	625 (dioxane), 647 (film)
Band gap (UV-Vis) [eV]	1.91 (dioxane), 1.65 (film)
CV HOMO [eV]	-4.61
LUMO [eV]	-2.60
T_d (5 % weight loss) [°C]	320
T_g [°C]	54
Melting point [°C]	229

11.10.2 [1,2'-Bisthienylbenzo[c]thiophene]-5,5'-diamine,-N,N'-di-(di-2,4-trifluoromethyl)phenyl-N,N'-diphenyl **10**

10 was prepared by two-step synthesis.

Step I. 1-Anilino(di-2,4-trifluoromethyl)phenyl. $Pd(OAc)_2$ (0.2 g; 0.9 mmol), DPPF (1.5 g; 2.7 mmol), sodium *tert*-butoxide (4.8 g; 50 mmol), 1-iodo-3,5-bis(trifluoromethyl)benzene (11.2 g; 32.94 mmol), aniline (3.23 g; 34.6 mmol) and toluene (150 ml) were refluxed under Ar for 10h. Toluene was removed under reduced pressure. Reaction mixture was diluted with CH_2Cl_2 and filtered through a glass filter to remove the insoluble part. Then a solution of the product in CH_2Cl_2 was passed through very small silica gel column to remove polar impurities. After evaporation of solvent 9.94 g of yellowish-brown crystals were obtained. Further purification by crystallisation from n-hexane yielded white needles 8.15 g (81 %).

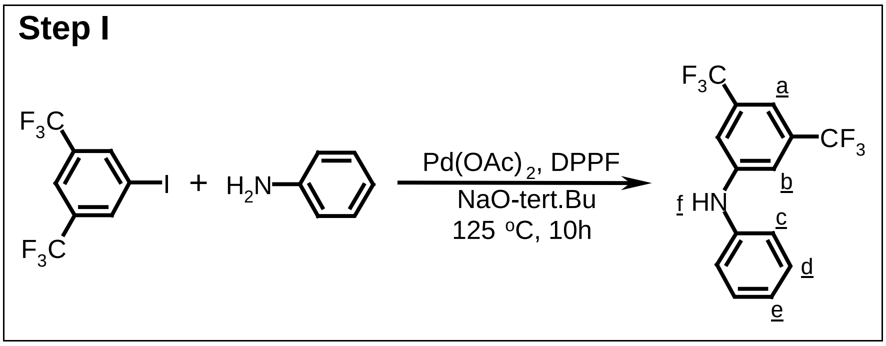

Molecular Weight =305.22
Exact Mass =305
Molecular Formula =C14H9F6N

FT-IR (KBr) ν [cm^{-1}]	3441, 3102, 3044, 1597, 1521, 1384, 1282, 1119, 958, 874
^{1}H-NMR ($CDCl_3$) δ [ppm]	7.29-7.39 (m, 5H, c-e), 7.10-7.14 (m, 3H, a, b), 5.96 (s, 1H, f)
MS [m/z]	305 (M^+)

Step II. [1,2'-Bisthienylbenzo[c]thiophene]-5,5'-diamine,-N,N'-di-(di-2,4-trifluoromethyl)phenyl-N,N'-diphenyl 10.

10 was prepared by General procedure 5 using $Pd(OAc)_2$ as a catalyst (0.03 g; 0.1 mmol), DPPF as a ligand (0.17g; 0.3 mmol), sodium *tert*-butoxide as a base (1 g; 9.9 mmol), 1,3-bis(5-bromo-2-thienyl)benzo[c]thiophene (1.5 g; 3.3 mmol) and 1-anilino(di-2,4-trifluoromethyl)phenyl (3 g; 9.9 mmol), and toluene as a solvent . The residue was purified by column chromatography with n-hexane/CH_2Cl_2 (5:1) as eluent. 2.3 g (77 %) of bright fluorescent red powder was collected. 1 g of the product was further purified by train sublimation to give nice dark red crystals with extremely high purity.

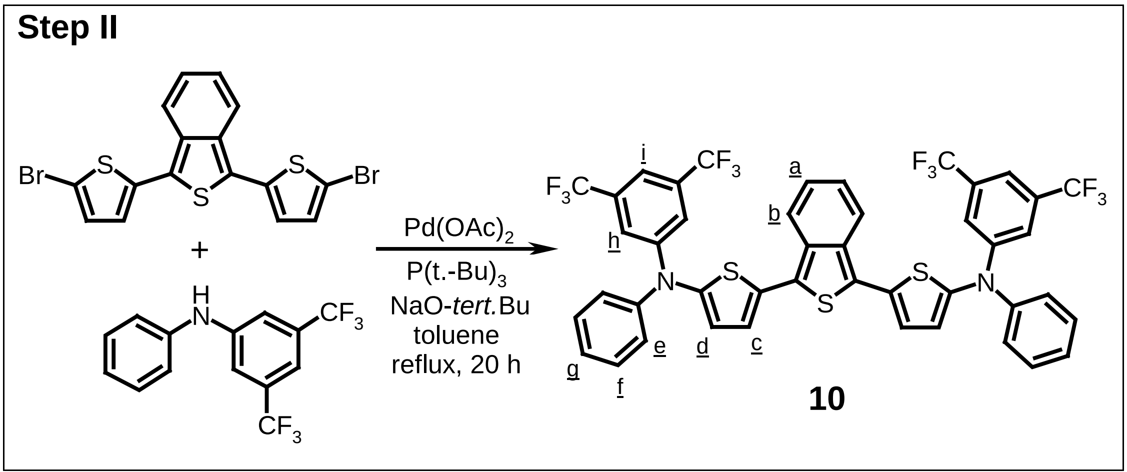

10

Molecular Weight =904.87
Exact Mass =904
Molecular Formula =C44H24F12N2S3

FT-IR (KBr) ν [cm^{-1}]	3064, 2932, 1615, 1545, 1498, 1468, 1377, 1278, 1133, 878, 743
^{1}H-NMR ($CDCl_3$) δ [ppm]	7.85 (m, 2H, b), 7.37-7.46 (m, 10H, e-g), 7.28 (m, 6H, h, i), 7.15 (d, 2H, c), 7.10 (m, 2H, a), 6.81 (d, 2H, d)
MS [m/z]	904 (M^+)
UV-Vis λ_{max}^{abs} [nm]	470 (cyclohexane), 483 (film)
Fluorescence λ_{max}^{fl} [nm]	539 (cyclohexane), 613 (film)
Band gap (UV-Vis) [eV]	2.14 (cyclohexane), 2.07 (film)
CV HOMO [eV]	-4.84
LUMO [eV]	-2.75
T_d (5 % weight loss) [°C]	333
T_g [°C]	48
Melting point [°C]	182.9

11.10.3 (1,2'-Bisthienylbenzo[c]thiophene)-5,5'-diamine,-N,N'-di-1-naphthalenyl-N,N'-diphenyl **11**

11 was prepared by General procedure 5 using Pd(DPPF)Cl_2 as a catalyst (0.033 g; 0.04 mmol), DPPF as a ligand (0.066g; 0.12 mmol), sodium *tert*-butoxide as a base (0.125 g; 1.3 mmol), 1,3-bis(5-bromo-2-thienyl)benzo[c]thiophene (0.28 g; 0.61 mmol) and N-(2-naphthyl)aniline (0.3 g; 1.4 mmol), and o-xylene as a solvent . The residue was purified by column chromatography with n-hexane/toluene 1:1 as eluent. 0.12 g (28 %) of a deep red solid was collected.

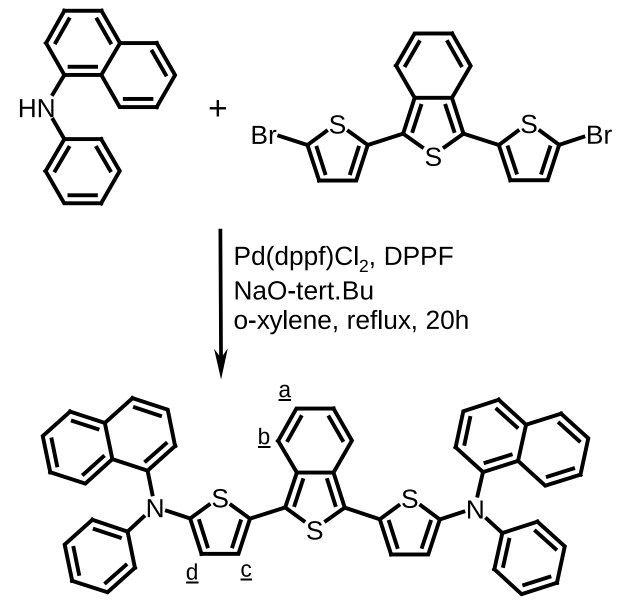

11

Molecular Weight =733.00
Exact Mass =732
Molecular Formula =C48H32N2S3

FT-IR (KBr) ν [cm^{-1}]	3058, 2923, 1593, 1492, 1288, 743
^{1}H-NMR (C_6D_6) δ [ppm]	7.92 (m, 2H, b), 7.70 (d, 2H, Ar-H), 7.53 (m, 4H, Ar-H), 7.41 (m, 4H, Ar-H), 7.26 (m, 8H, Ar-H), 7.12 (t, 4H, Ar-H), 7.00 (d, 2H, c), 6.93 (t, 2H, Ar-H), 6.86 (m, 2H, a), 6.60 (d, 2H, d)
MS [m/z]	732 (M^+)
UV-Vis λ_{max}^{abs} [nm]	497 (cyclohexane), 522 (film)
Fluorescence λ_{max}^{fl} [nm]	611 (cyclohexane), not observed (film)
Band gap (UV-Vis) [eV]	2.07 (cyclohexane), 1.88 (film)

CV HOMO [eV]	-4.71
LUMO [eV]	-2.68
$\mathbf{T_d}$ (5 % weight loss) [°C]	337
$\mathbf{T_g}$ [°C]	71
Melting point [°C]	185.6

11.11 Synthesis of N,N'-di-1-naphthalenyl-N,N'-diphenyl-[2,2'-bithiophene]-5,5'-diamine **12**

12 was prepared by General procedure 5, which is similar to method used for synthesis of **12** by Wong et al.[141] Pd(DPPF)Cl_2 (0.25 g; 0.3 mmol), DPPF (0. 5 g; 0.9 mmol), sodium *tert*-butoxide (2.1 g; 22 mmol), N-(2-naphthyl)aniline (5.04 g; 23 mmol), 5,5-dibromo-2,2'-bithienyl (3 g; 9.3 mmol) and o-xylene (100 ml) were refluxed under Ar for 18 h. After competition of the reaction, the mixture was filtered through silica gel column to remove the salts, o-xylene was removed in vacuum, and final purification was done by column chromatography on silica gel with n-hexane/ether 9:1 as eluent. Yield is 2.8 g (50 %) of an yellow solid.

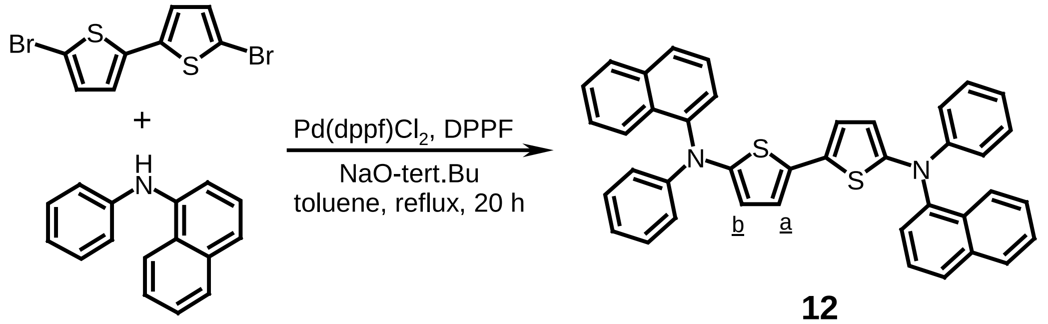

12

Molecular Weight =600.81
Exact Mass =600
Molecular Formula =C40H28N2S2

FT-IR (KBr) ν [cm^{-1}]	3055, 1627, 1592, 1524, 1491, 1465, 1282, 1231, 748, 694
^{1}H-NMR (C_6D_6) δ [ppm]	7.61 (d, 2H, Ar-H), 7.47-7.53 (m, 4H, Ar-H), 7.31-7.34 (m, 4H, Ar-H), 7.18-7.22 (m, 8H, Ar-H), 7.07 (t, 4H, Ar-H), 6.87 (t, 2H, Ar-H), 6.68 (d, 2H, a), 6.41 (d, 2H, b)

MS [m/z]	600 (M^+)
UV-Vis λ_{max}^{abs} [nm]	397 (cyclohexane)
Fluorescence λ_{max}^{fl} [nm]	464 (cyclohexane)
Band gap (UV-Vis) [eV]	2.73 (cyclohexane)
CV HOMO [eV]	-4.85
LUMO [eV]	not observed
$\mathbf{T_d}$ (5 % weight loss) [°C]	335
$\mathbf{T_g}$ [°C]	57
Melting point [°C]	208

11.12 Synthesis of poly(1,3-di-2-thienylbenzo[c]thiophene)s **13, 14**

11.12.1 Poly(1,3-bis(3-hexyl-2-thienyl)benzo[c]thiophene) **13**

General procedure 6

To a solution of 1,3-bis(3-hexyl-2-thienyl)benzo[c]thiophene (7.5 g; 16.2 mmol) in dried $CHCl_3$ (300 ml), powder of anhydrous $FeCl_3$ (10.54 g; 65 mmol) was added slowly during 6 h under Ar at room temperature. After stirring for additional 18 h the reaction mixture was poured into n-hexane, and bluish-black powder (17.3 g) was precipitated. Soxhlet extraction with methanol to remove Fe salts and unreacted monomer yielded 7.2 g (96 %) of brown solid. Further Soxhlet extraction with THF yielded 5.18 g (79 %) of THF extract and 1.95 g (26 %) of a black residue insoluble in THF (0.38 % Fe content), which is also insoluble in common organic solvents such as $CHCl_3$, chlorobenzene, NMP, DMF and DMAc. The THF extract was dissolved in small amount of THF and precipitated into n-hexane. 1.7 g (23 %) of precipitated solid and, after evaporation of solvents from mother liquor, 3.46 g (46 %) of residue were collected. 1.7 g of precipitated solid and 3.46 g of collected residue were examined by SEC as polymer and oligomeric fraction respectively.

Resulted 1.7 g of THF soluble polymer had a large Fe content (0.43 % of Fe), which makes the product unsuitable for application in solar cells.

Fe content in the soluble polymer fraction (1.7 g) was reduced from 0.43 wt. %% to 0.013 wt. % by *the improved purification procedure* given below:

1. diluting reaction mixture with $CHCl_3$
2. washing with 15 wt.% HCl to remove possible Fe containing compounds such a $FeCl_3$, $FeCl_2$, Fe_2O_3, $Fe(OH)_2$, $Fe(OH)_3$
3. washing with water until neutral
4. dedoping of the organic material by refluxing the $CHCl_3$ solution with aqueous 25 % NH_3 for 30 min 3 times (colour of the material has changed from deep blue to reddish-brown)
5. washing with water until neutral
6. washing with aqueous KSCN solution to remove the rest of Fe
7. washing with water
8. evaporation of the $CHCl_3$ and drying the remaining brown solid in vacuum
9. Soxhlet extraction with THF to isolate insoluble in THF fraction
10. precipitation of the target polymer from THF solution into n-hexane

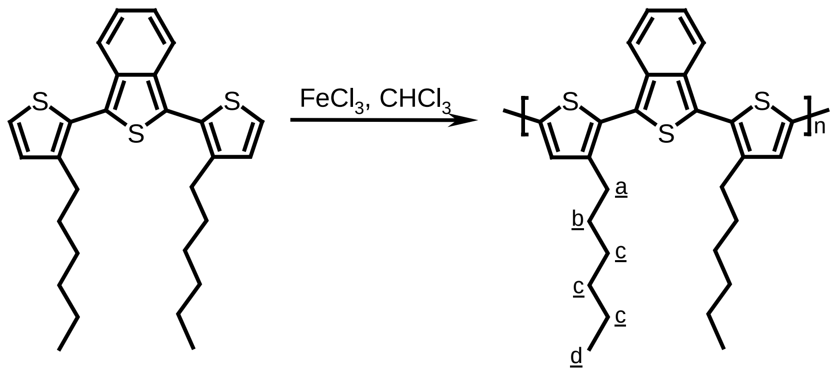

13

FT-IR (KBr) ν [cm^{-1}]	3060, 2952, 2924, 2854, 1641, 1453, 830, 746
^{1}H-NMR (THF); δ [ppm]	7.71, 7.55, 7.33, 7.11 (8H), 2.70 (4H), 1.65 (4H), 1.23 (12H), 0.81 (6H)
UV-Vis λ_{max}^{abs} [nm]	447 (chlorobenzene), 447 (film)
Fluorescence λ_{max}^{fl} [nm]	597 nm ($CHCl_3$)
Band gap (UV-Vis) [eV]	2.21 (chlorobenzene), 2.03 (film)
CV HOMO [eV]	-4.96
LUMO [eV]	-2.68

SEC	**M_n** [g/mol]	6.991
	M_w [g/mol]	26.818
	M_p [g/mol]	10.997
T_d (5 % weight loss) [°C]		315
T_g [°C]		90

11.12.2 Poly(1,3-bis(3-((trimethylsilyl)methyl)-2-thienyl)benzo[c]thiophene) **14**

Polymer 2 was prepared by general procedure 6 using 1,3-bis(3-((trimethylsilyl)methyl)-2-thienyl)benzo[c]thiophenes (1.15 g; 2.44 mmol) and powder of anhydrous $FeCl_3$ (1.62 g; 10 mmol) in dried $CHCl_3$ (50 ml). After reaction was worked up, a 2.63 g of bluish-black powder was precipitated. Further purification by washing the product with hot methanol (Soxhlet extraction) yielded 1.03 g (89 %) of dedoped brown compound. Following extraction with THF yielded 0.68 g (59 %) of insoluble in THF fraction (0.091 wt. % Fe content) and 0.31 g (27 %) of THF extract. THF extract was examined by SEC as oligomeric mixture and analysed by UV-Vis spectroscopy. THF insoluble fraction, which is also insoluble in common organic solvents such as $CHCl_3$, chlorobenzene, NMP, DMF and DMAc, was characterised by FT-IR spectroscopy, TGA and DSC.

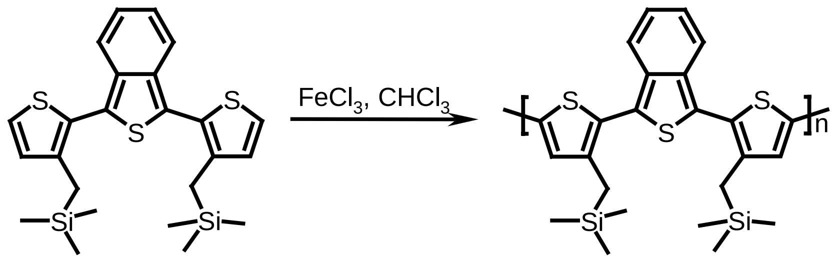

14

FT-IR (KBr) ν [cm^{-1}]		3050, 2917, 2858, 2819, 1636, 1444, 828, 745
UV-Vis λ_{max}^{abs} [nm]*		446 (THF), 456 (film)
SEC	**M_n** [g/mol]*	580
	M_w [g/mol]*	2000
T_d (5 % weight loss) [°C]		352
T_g [°C]		111

* - measured from THF soluble fraction fraction

11.13 Synthesis of poly[1,3-bis(5'-diarylaminothiophene-2-yl)benzo[c]thiophene]s **15-17**

11.13.1 Poly[1,3-bis(5'-diarylaminothiophene-2-yl)benzo[c]thiophene] **15**

General procedure 7

1,3-Bis(5-iodo-2-thienyl)benzo[c]thiophene (0.5141 g; 0.934 mmol), N,N'-di(4-octylphenyl)-4,4'-diaminobiphenyl (0.5241 g; 0.934 mmol), copper [0] (0.2375 g; 3.7 mmol), 18-crown-6 as a phase-transfer catalyst (49.37 mg; 0.187 mmol) and potassium carbonate (1.033 g; 7.47 mmol) in anhydrous o-dichlorobenzene (7 ml) were mixed at room temperature and refluxed under nitrogen atmosphere for 5 days. Reaction mixture was diluted with THF, filtered off. After removing the solvent the polymer was dissolved in $CHCl_3$, dedoped by refluxing $CHCl_3$ solution with 25 % aqueous ammonia for 30 min, washed with water, methanol and dried in vacuum.

Further purification was done by precipitation the polymer from $CHCl_3$ into n-hexane 3 times and then by reprecipitation the polymer from $CHCl_3$ into cyclohexane. After drying in high vacuum 0.51 g of polymer was collected, yield: 63 %.

11.13.1.1 Poly[1,3-bis(5'-diarylaminothiophene-2-yl)benzo[c]thiophene] ***15a***

Polymer **15a** was synthesised and purified using the same conditions as used for the preparation of polymer **15**, but in 40 % more diluted reaction media. Yield: 0.3 g (48 %).

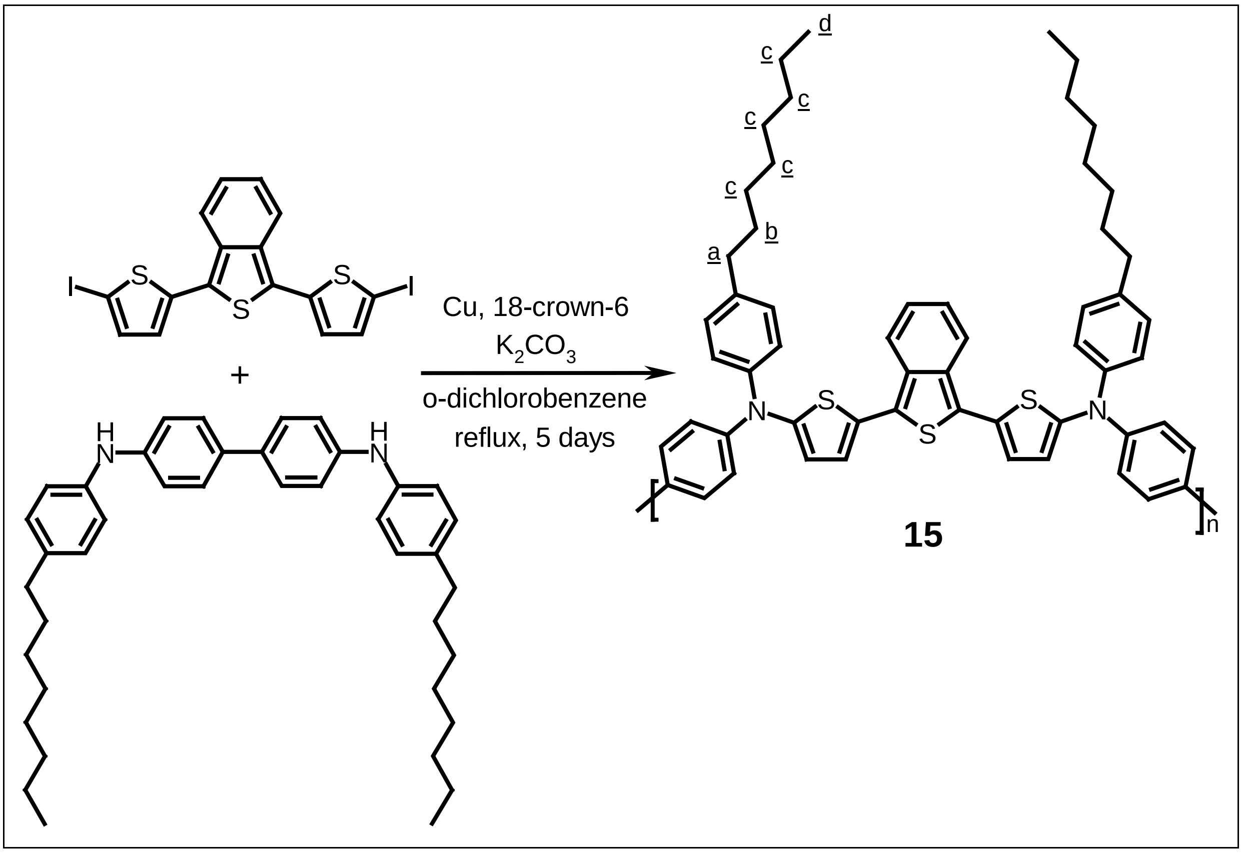

FT-IR (KBr) ν [cm^{-1}]	3029, 2924, 2852, 1603, 1494, 1284, 1061, 815	
^{1}H-NMR ($CDCl_3$) δ [ppm]	7.89, 7.34, 7.14, 6.80 (m, phenyl and thienyl protons), 2.53 (m, a), 1.55 (m, b), 1.24 (m, c), 0.84 (m, d)	
UV-Vis λ_{max}^{abs} [nm]	497 ($CHCl_3$), 520 (film)	
Fluorescence λ_{max}^{fl} [nm]	585 ($CHCl_3$)	
Band gap (UV-Vis) [eV]	1.92 ($CHCl_3$), 1.74 (film)	
CV HOMO [eV]	-4.34	
LUMO [eV]	-2.36	
SEC $\mathbf{M_w}$ [g/mol]	10.484	* [7.730]
$\mathbf{M_n}$ [g/mol]	127.520	*[23.182]
$\mathbf{M_p}$ [g/mol]	146.580	*[12.465]
$\mathbf{T_d}$ (5 % weight loss) [°C]	381	
$\mathbf{T_g}$ [°C]	132	

* - for the polymer **15a**

11.13.2 Poly[1,3-bis(5'-diarylaminothiophene-2-yl)benzo[c]thiophene] **16**

Poly(dithienylisothianaphthene diamine) **16** was synthesised via general procedure 7 using 1,3-bis(5-iodo-2-thienyl)benzo[c]thiophene (0.67 g; 1.2176 mmol), 4,4'-oxybis[N-(2,4-di(trifluoromethyl)phenyl)]benzeneamine (0.7603 g; 1.2176 mmol), copper[0] (0.39 g; 6.09 mmol), 18-crown-6 as a phase-transfer catalyst (64.4 mg; 0.2435 mmol) and potassium carbonate (1.35 g; 9.74 mmol) in anhydrous o-dichlorobenzene (7 ml).

Further purification was done by precipitation the polymer from $CHCl_3$ into cold n-hexane 3 times and then by Soxhlet extraction with methanol. After drying in high vacuum 0.47 g of polymer was collected, yield: 43 %.

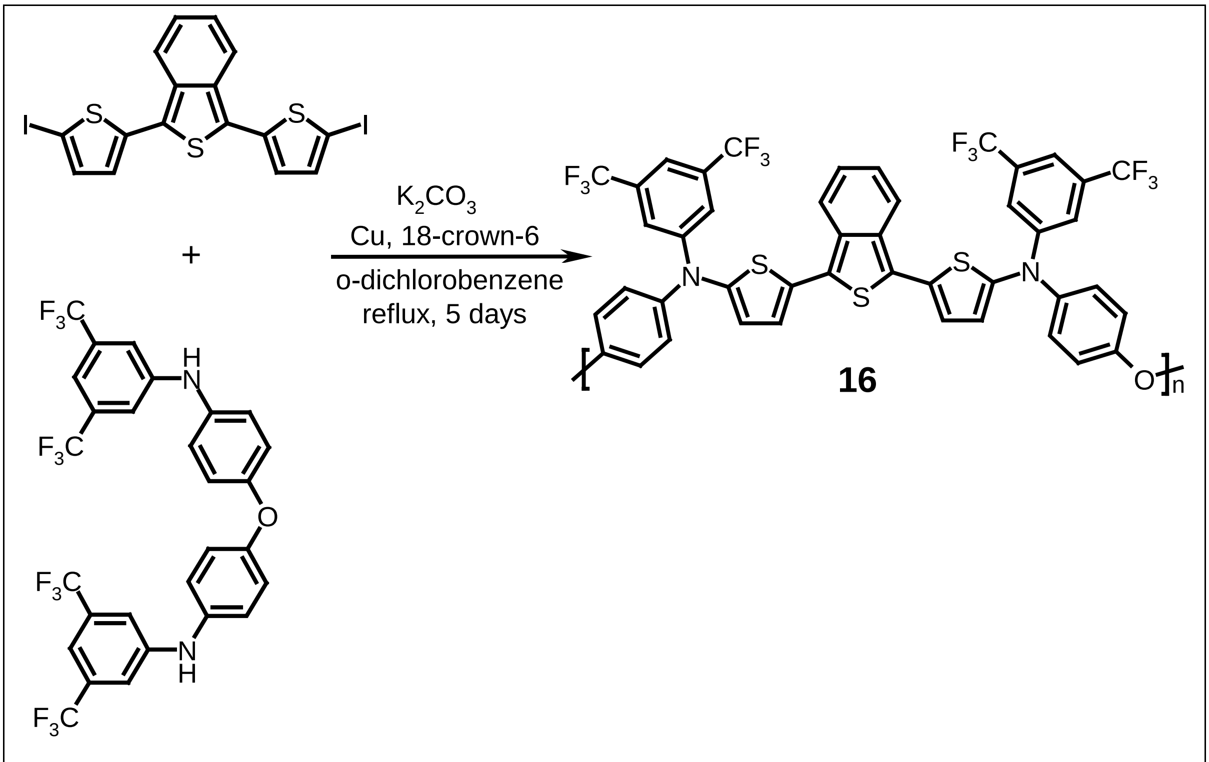

FT-IR (KBr) ν [cm^{-1}]	3064, 2926, 2851, 1617, 1495, 1378, 1277, 1229, 1176, 1133, 875, 682
^{1}H-NMR ($CDCl_3$) δ [ppm]	7.97, 7.43, 7.28, 7.13, 6.82 (m, phenyl and thienyl protons)
UV-Vis λ_{max}^{abs} [nm]	526 ($CHCl_3$), 538 (film)
Fluorescence λ_{max}^{fl} [nm]	584 nm ($CHCl_3$)
Band gap (UV-Vis) [eV]	1.86 ($CHCl_3$), 1.68 (film)
CV HOMO [eV]	-4.41
LUMO [eV]	-2.61

SEC	$\mathbf{M_w}$ [g/mol]	5.977
	$\mathbf{M_n}$ [g/mol]	47.535
	$\mathbf{M_p}$ [g/mol]	45.275
$\mathbf{T_d}$ (5 % weight loss) [°C]		393
$\mathbf{T_g}$ [°C]		108

11.13.3 Poly[1,3-bis(5'-diarylaminothiophene-2-yl)benzo[c]thiophene] **17**

Polymer **17** was prepared via general procedure 7 using 1,3-bis(5-iodo-2-thienyl)benzo[c]thiophene (0.65 g; 1.1813 mmol), N,N'-di(4-hexyloxyphenyl)-4,4'-diaminobiphenyl (0.63407 g; 1.1813 mmol), copper[0] (0.375 g; 5.91 mmol), 18-crown-6 as a phase-transfer catalyst (62.4 mg; 0.2362 mmol) and potassium carbonate (1.31 g; 9.45 mmol) in anhydrous o-dichlorobenzene (8 ml).

Further purification was done by precipitation the polymer from $CHCl_3$ into n-hexane 3 times and then by reprecipitation the polymer from $CHCl_3$ into petrol ether (fraction with a b.p. 60-80 °C). After drying in high vacuum 0.77 g of polymer was obtained, yield: 78 %.

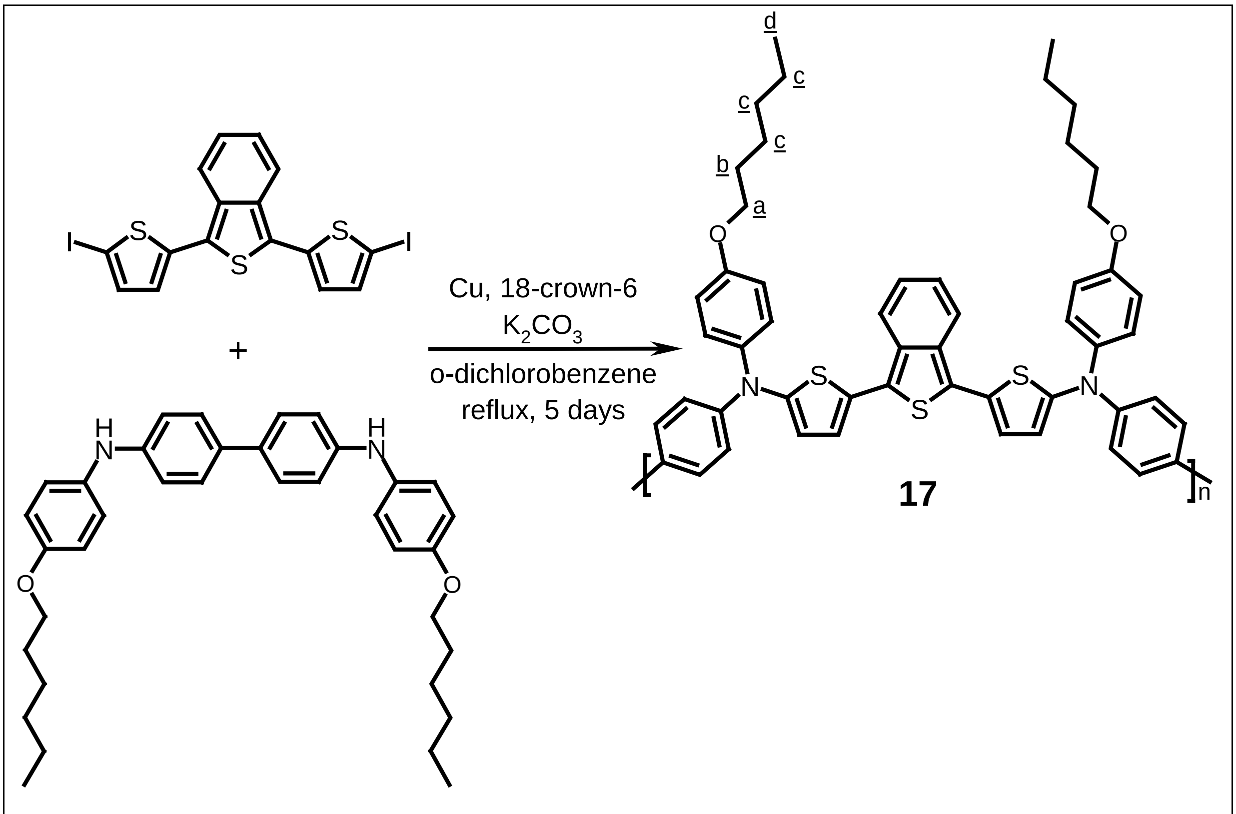

FT-IR (KBr) ν [cm^{-1}]	3033, 2928, 2858, 1606, 1492, 1240, 820
^{1}H-NMR ($CDCl_3$) δ [ppm]	7.97, 7.34, 7.14, 6.82 (m, phenyl and thienyl protons), 3.88 (m, <u>a</u>), 1.71 (m, <u>b</u>), 1.31 (m, <u>c</u>), 0.87 (m, <u>d</u>)
UV-Vis λ_{max}^{abs} [nm]	430-520 ($CHCl_3$), 440-540 (film)
Fluorescence λ_{max}^{fl} [nm]	581 nm ($CHCl_3$)
Band gap (UV-Vis) [eV]	1.87 ($CHCl_3$), 1.75 (film)
CV HOMO [eV]	-4.40
LUMO [eV]	-2.55
SEC $\mathbf{M_w}$ [g/mol]	7.241
$\mathbf{M_n}$ [g/mol]	28.989
$\mathbf{M_p}$ [g/mol]	18.822
$\mathbf{T_d}$ (5 % weight loss) [°C]	385
$\mathbf{T_g}$ [°C]	130

12 Formula index

1,3-Di-2-dithienylbenzo[c]thiophenes

DTITNs

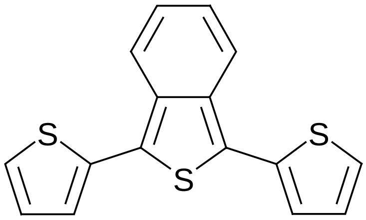

1

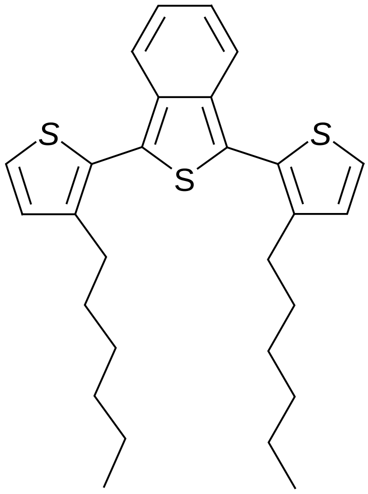

2

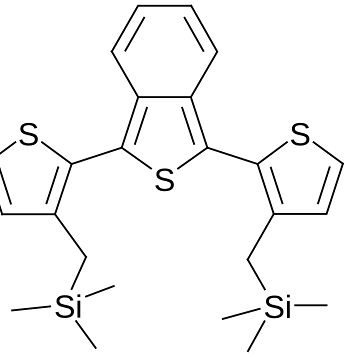

3

1,3-Bis(5-halogeno-2-thienyl)benzo[c]thiophenes

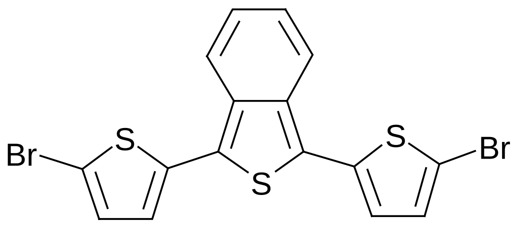

4

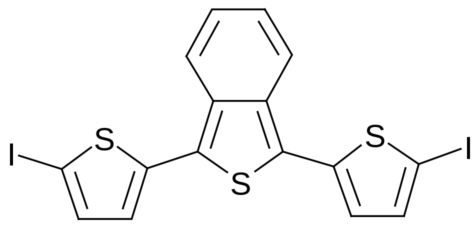

5

4,4'-Diarylamino biphenyls

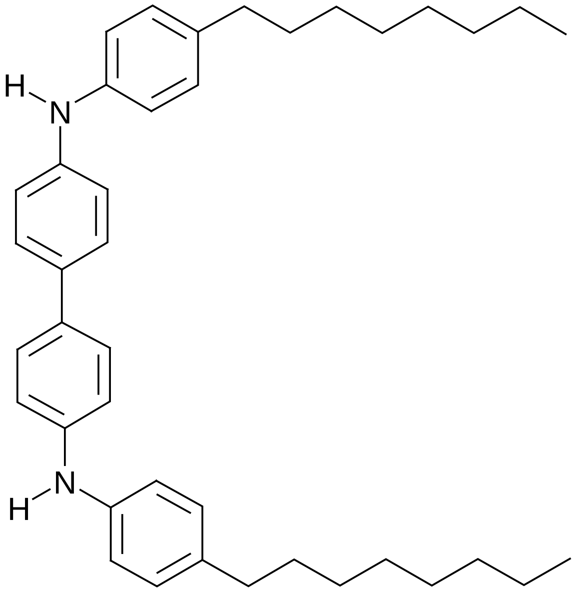

6

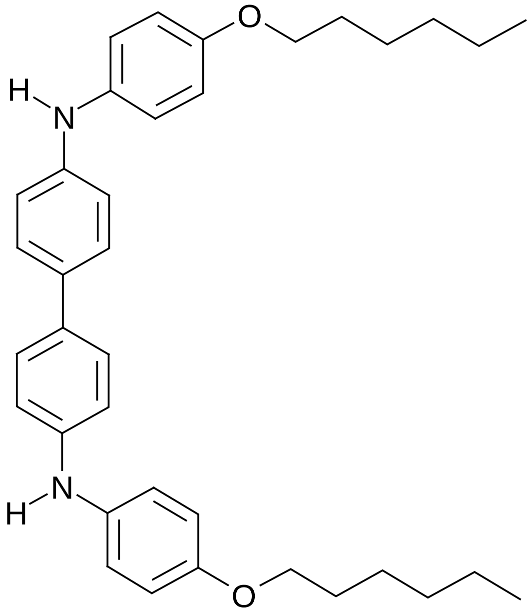

8

4,4'-Diarylamino biphenylether

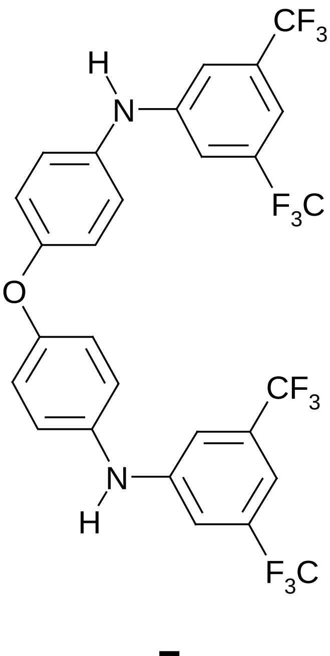

7

1,3-Bis(5'-diarylaminothiophene-2-yl)benzo[c]thiophenes

DTITNPDs

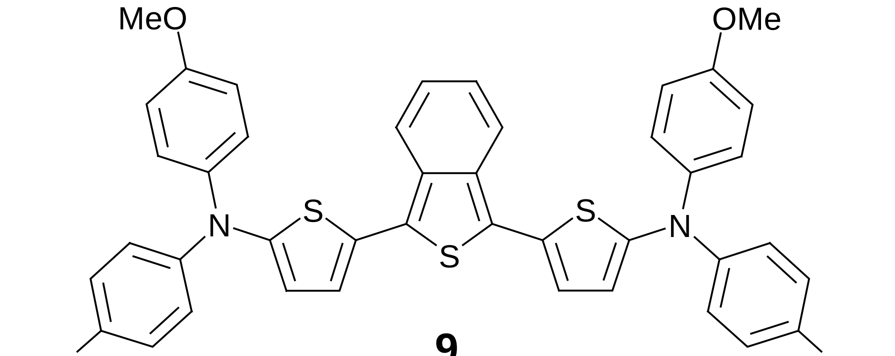

9

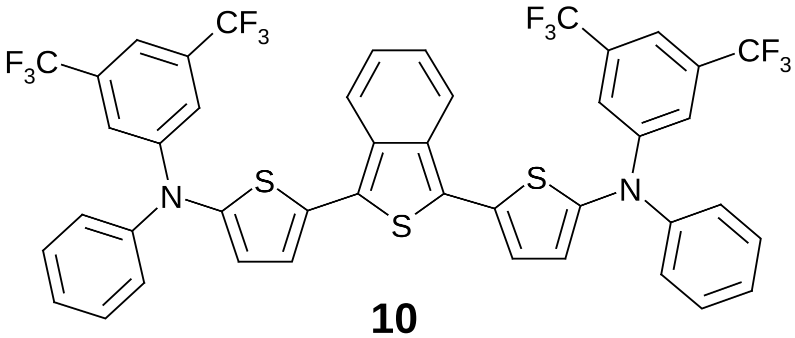

10

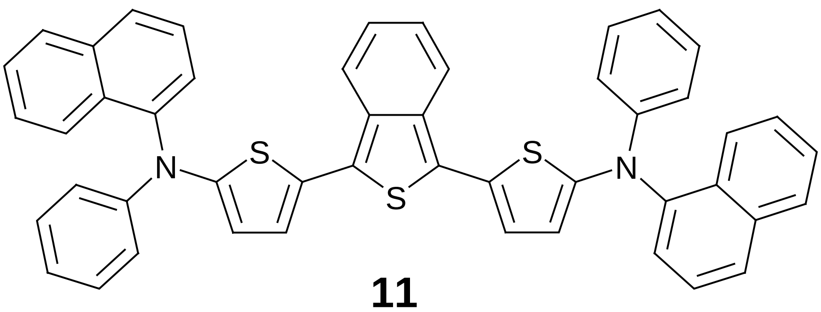

11

2,2'-Bithiophene-5,5'-diarylamine

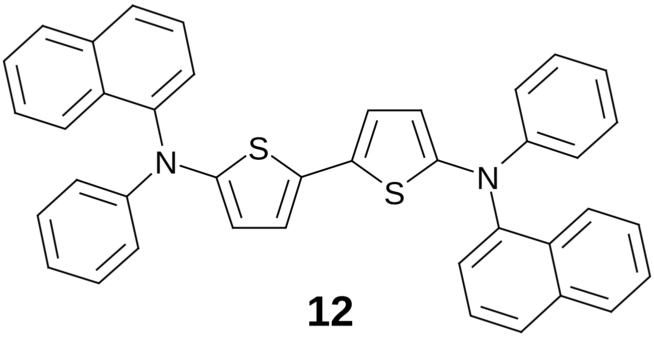

12

Poly(1,3-di-2-dithienylbenzo[c]thiophene)s

poly(DTITN)s

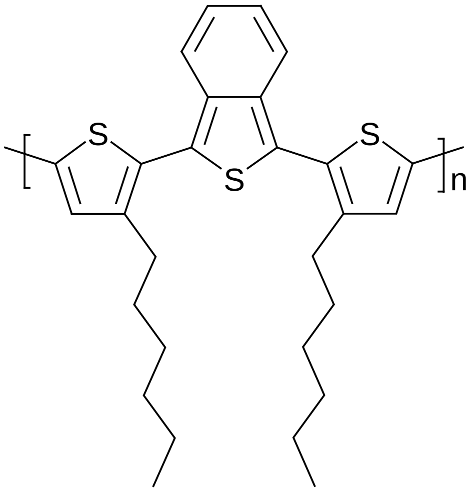

13

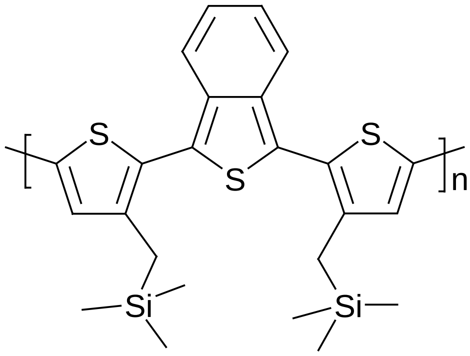

14

Poly[1,3-bis(5’-diarylaminothiophene-2-yl)benzo[c]thiophene]s poly(DTITNPD)s

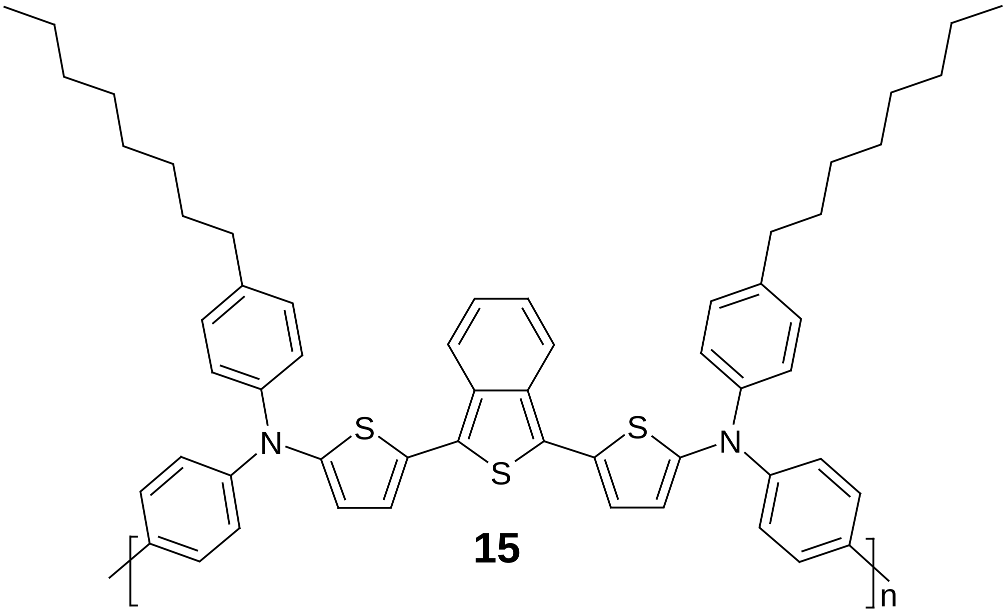

15

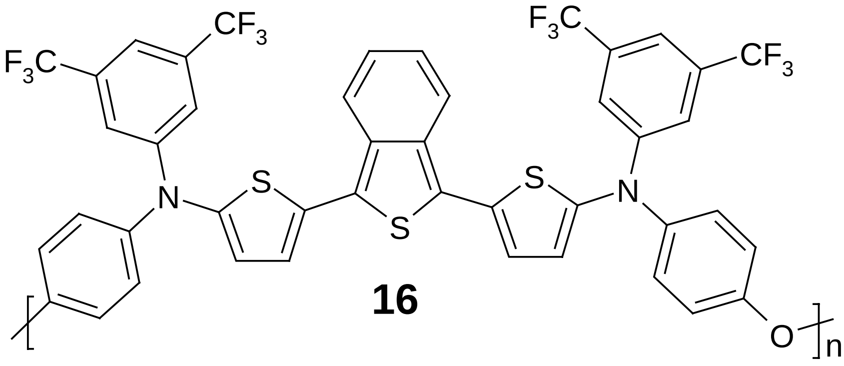

16

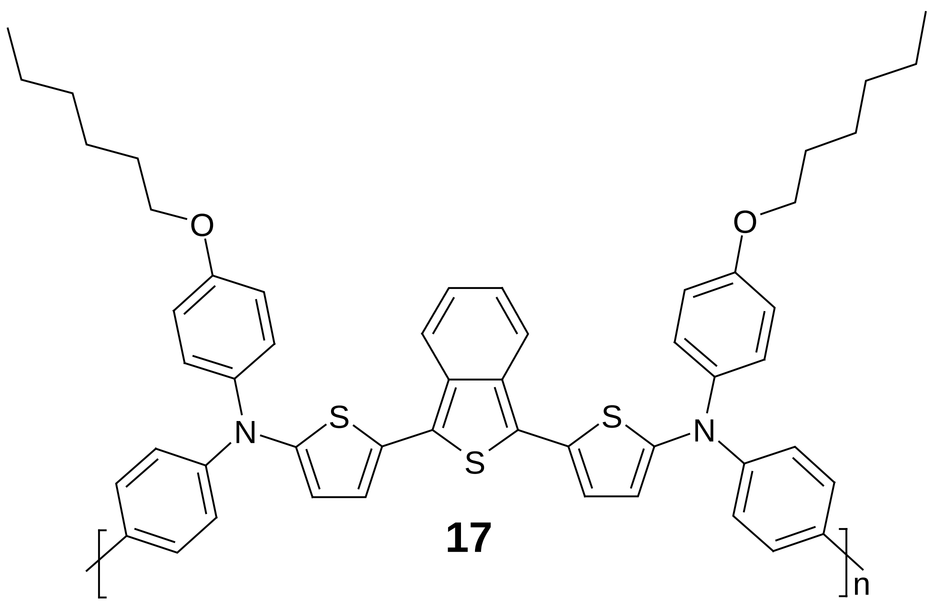

17

13 List of publications

A - Publication in scientific journals:

A1. "Synthesis and characterisation of poly(triarylamine)s containing isothianaphthene Moieties" Kisselev, Roman; Thelakkat, Mukundan submitted to *Macromolecules* in **March 2004**.

A2. "Optical and electronic contributions in double-heterojunction organic thin film solar cells" Hänsel, Helmut; Zettl, Heiko; Krausch, Georg; Kisselev, Roman; Thelakkat, Mukundan; Schmidt, Hans-Werner *Adv. Mater.* **2003**, *15(24)*, 2056-2060.

A3. "Combinatorial study of the long-term stability of organic thin-film solar cells" Hänsel, Helmut; Zettl, Heiko; Krausch, Georg; Schmitz, Christoph; Kisselev, Roman; Thelakkat, Mukundan; Schmidt, Hans-Werner *Appl. Phys. Lett.* **2002**, *81(11)*, 2106-2108.

A4. "Synthesis of novel 1,3-bis(5-diarylaminothiophen-2-yl)isothianaphthenes" Kisselev, Roman; Thelakkat, Mukundan *Chem. Commun.* **2002**, 1530–1531.

B - Oral presentations:

B1. "Low band gap materials with dithienylisothianaphthene diamines" Kisselev, Roman; Thelakkat, Mukundan *International workshop, KOPO-03, Blaubeuren,* **4th November 2003**.

B2. "Bifunctional materials for solar cell applications" Peter, Katja; Kisselev, Roman; Thelakkat, Mukundan *Organic Photovoltaics Symposium, SPIE, San Diego, USA,* **7th August 2003**.

B3. "Organic functional materials for OLEDs and photovoltaics" Kisselev, Roman; Peter, Katja; Thelakkat, Mukundan *IAPP, Technische Universität, Dresden,* **2nd Juni 2003**.

C - Poster presentations:

C1. "Synthesis and characterisation of new, bifunctional block copolymers" Peter, Katja; Kisselev, Roman; Lindner, Stefan; Thelakkat, Mukundan *Science Bazaar 2003- Organic and dye sensitized solar cells*, *Linz*, **September 2003**.

C2. "Novel low band gap materials based on isothianaphthene diamines for organic solar cells" Kisselev, Roman; Thelakkat, Mukundan, *International meeting SCELL 2004, Badajoz, Spain*, **13d-15th May 2004**.

14 References

1 Tang, C. W.; Vanslyke, S. A. *Appl. Phys. Lett.* **1987**, *51*, 913.

2 Burroughes, J. H.; Bradley, D. D. C.; Brown, A. R.; Marks, R. N.; Mackay, K.; Friend, R. H.; Burns, P. L.; Holmes, A. B. *Nature* **1990**, *347*, 539.

3 Tang, C. W. *Appl. Phys. Lett.* **1986**, *48*, 183.

4 Yu, G.; Gao, J.; Hummelen, J. C.; Wudl, F.; Heeger, A. J. *Science* **1995**, *270*, 1789.

5 Halls, J. J. M.; Walsh, C. A.; Greenham, M. C.; Marseglia, E. A.; Friend, R. H.; Moratti, S. C.; Holmes, A. B. *Nature* **1995**, *376*, 498.

6 Drury, C. J.; Mutsaers, C. M. J.; Hart, C. M.; Matters, M.; de Leeuw, D. M. *Appl. Phys. Lett.* **1998**, *73(1)*, 108.

7 (a) Garnier, F.; Horowitz, G.; Peng, X.; Fichou, D. *Solid State Commun.* **1989**, *72*, 4. (b) Garnier, F.; Hajlaoui, R.; El Kassmi, M. *Appl. Phys. Lett.* **1998**, *73*, 1721.

8 (a) Sirringhaus, H.; Tessler, N.; Friend, R. H. *Science* **1998**, *280*, 1741. (b) Li, X. C.; Sirringhaus, H.; Garnier, F.; Holmes, A. B.; Moratti, S. C.; Feeder, N.; Clegg, W.; Teat, S. J.; Friend, R. H. *J. Am. Chem. Soc.* **1998**, *120*, 2206.

9 (a) Bao, Z.; Lovinger, A. J.; Brown, J. *J. Amer. Chem. Soc.* **1998**, *120*, 207. (b) Bao, Z.; Dodabalapur, A.; Lovinger, A. J. *Appl. Phys. Lett.* **1996**, *69*, 4108. (c) Bao, Z.; Lovinger, A. J. *Chem. Mater*. **1999**, *11*, 2607.

10 (a) Ducharme, S.; Scott, J. C.; Twieg, R. J.; Moerner, W. E. *Phys. Rev. Lett.* **1991**, *66*, 1846. (b) Moerner, W. E.; Silence, S. M. *Chem. Rev.* **1994**, *94*, 127. (c) Moerner, W. E.; Silence, S. M.; Hache, F.; Bjorklund, G. C. *J. Opt. Soc. Am. B*. **1994**, *11*, 320.

11 (a) Hofmann, U.; Schloter, S.; Schreiber, A.; Hoechstetter, K.; Bauml, G.; Zilker, S. J.; Haarer, D.; Thelakkat, M.; Schmidt, H.-W., Ewert, K.; Eisenbach, C.-D. *Proc. SPIE-Int. Soc. Opt. Eng.* **1998**, *3417*, 124. (b) Zilker, S. J. *ChemPhysChem* **2000**, *1*, 72.

12 (a) Meerholz, K.; Volodin, B. L.; Sandalphon; Kippelen, B.; Peyghambarian, N. *Nature*, **1994**, *371*, 497. (b) Volodin, B. L.; Kippelen, B.; Meerholz, K.; Javidi, B.; Peyghambarian, N. *Nature*, **1996**, *383*, 58.

13 Kaliski, Ofra *Business Communications Company, Inc*. GB-253 (Organics for electro-optical applications)

14 (a) Brabec, C. J.; Sariciftci, N. S.; Hummelen, J. C. *Adv. Funct. Mater.* **2001**, *11(1)*, 15. (b) Shaheen, S. E.; Brabec, C. J.; Sariciftci, N. S. *Appl. Phys. Lett.* **2001**, *78(6)*, 841.

15 (a) Fuchigami, H.; Tsumura, A.; Koezuka, H. *Appl. Phys. Lett.* **1993**, *63*, 1372. (b) Gundlach, D. J.; Lin, Y. Y.; Jackson, T. N.; Nelson, S. F.; Schlom, D. G. *IEEE Electron Device Lett.* **1997**, *18*, 87.

16 http://www.eliatech.com

17 Pope, M.; Kallmann, H. P.; Magnante, P. *J. Chem. Phys.* **1963**, *38*, 2042.

18 (a) Cao, Y.; Parker, I. D.; Yu, G.; Zhang, C.; Heeger, A. J. *Nature* **1999**, *397*, 414. (b) Wilson, J. S.; Dhoot, A. S.; Seeley, A. J. A. B.; Khan, M. S.; Kohler, A.; Friend, R. H. *Nature* **2001**, *413*, 828. (c) Wohlgenannt, W.; Jiang, X. M.; Vardeny, Z. V.; Janssen, R. A. J. *Phys. Rev. Lett*. **2002**, *88*, 197401.

19 Greenham, N. C.; Friend, R. H. *Solid State Phys.* **1995**, *49*, 1.

20 Ishii, H.; Sugiyama, K.; Ito, E.; Seki, K. *Adv. Mater.* **1999**, *11(8)*, 605.

21 (a) Baldo, M. A.; O'Brien, D.F.; You, Y.; Schoustikov, A.; Sibley, S.; Thompson, M. E.; Forrest, S. R. *Nature* **1998**, *395*, 151. (b) Baldo, M. A.; Lamansky, S.; Burrows, P. E.; Thompson, M. E.; Forrest, S. R. *Appl. Phys. Lett.* **1999**, *75*, 4.

22 (a) Baldo, M. A.; Thompson, M. E.; Forrest, S. R. *Nature* **2000**, 40*3*, 750. (b) Lamansky, S.; Kwong, R. C.; Nugent, M.; Djurovic, P. I.; Thompson, M. E. *Org. Electron*. **2001**, *2*, 53.

23 Gong, X.; Robonson, M. R.; Ostrowski, J. C.; Moses, D.; Bazan, G. C.; Heeger, A. J. *Adv. Mater*. **2002**, *14*, 581.

24 Tang, C. W.; Van Slyke, S. A.; Chen, C. H. *J. Appl. Phys.* **1989**, *65*, 3610.

25 McGehee, M. D.; Bergstedt, T.; Zhang, C.; Saab, A. P.; O'Regan, M. B.; Bazan, G. C.; Srdanov, V. I.; Heeger, A. J. *Adv. Mater*. **1999**, *11(16)*, 1349.

26 Liang, C. J.; Zhao, D.; Hong, Z. R.; Zhao, D. X.; Liu, X. Y.; Li, W. L.; Peng, J. B.; Yu, J. Q.; Lee, C. S.; Lee, S. T. *Appl. Phys. Lett*. **2000**, *76(1)*, 67.

27 Chen, C. H.; Shi, J.; Tang, C. W. *Macromol. Symp*. **1997**, *125*, 1.

28 Friend, R. H.; Gymer, R. W.; Holmes, A. B.; Burroughes, J. H.; Marks, R. N.; Taliani, C.; Bradley, D. D. C.; Dos Santos, D. A.; Bredas, J. L.; Loegdlund, M.; Salaneck, W. R. *Nature* **1999**, *397*, 121.

29 Mitschke, U.; Bäuerle, P. *J. Mater. Chem*. **2000**, *10*, 1471.

30 Greiner, A. *Polym. Adv. Technol*. **1998**, *9*, 371.

31 Andersson, M. R.; Berggren, M.; Inganaes, O.; Gustafsson, G.; Gustafsson-Carlberg, J. C.; Selse, D.; Hjertberg, T.; Wennerstroem, O. *Macromolecules*, **1995**, *28*, 7525.

32 (a) Goetzberger, A.; Luther, J.; Willeke, G. *Solar Energy Materials & Solar Cells* **2002**, *74*, 1. (b) Nelson, J. *Current Opinion in Solid State & Materials Science* **2002**, *6*, 87. (c) Nunzi, J.-M. *C. R. Physique* **2002**, *3*, 523.

33 O'Regan, B.; Graetzel, M. *Nature* **1991**, *353*, 737.

34 (a) Greenham, N. C.; Peng, X.; Alivisatos, A. P. *Phys. Rev. B* **1996**, *54*, 17628. (b) Huynh, W. U.; Dittmer, J. J.; Alivisatos, A. P. *Science* **2002** *295*, 2425.

35 Peumans, P.; Forrest, S. R. *Appl. Phys. Lett*. **2001**, *79*, 128.

36 Padinger, F.; Rittberger, R. S.; Sariciftci, N. S. *Adv. Funct. Mater*. **2003**, *13(1)*, 85.

37 Krueger, J.; Plass, R.; Graetzel, M.; Matthieu, H. J. *Appl. Phys. Lett*. **2002**, *81*, 367.

38 Gregg, B. A.; Hanna, M. C. *J. Appl. Phys*. **2003**, *93*, 3605.

39 Sariciftci, N. S.; Smilowitz, L.; Heeger, A. J.; Wudl, F. *Science* **1992**, *258,* 1474.

40 Goetzberger, A.; Luther, J.; Willeke, G. *Solar Energy Materials & Solar Cells* **2002,** *74*, 1.

41 HAmerican Society for Testing and Materials (ASTM)H (Hhttp://www.astm.org/H)

42 Emin, D. in; Skotheim, T. A. (Ed.) *Handbook of Conducting Polymers* **1996**, *Vol. 2, Chapter 26*.

43 Maruyama, Y.; Iwasaki, N. *Chem. Phys. Lett.* **1974**, *24*, 26.

44 (a) Plazek, D. J.; Magill, J. H. *J. Chem. Phys.* **1966**, *45*, 3038. (b) Greet, R. J.; Turnbull, D. *J. Chem. Phys.* **1966**, *46*, 1243.

45 Shirota, Y. *J. Mater. Chem*. **2000**, *10*, 1.

46 Katz, H. E. *J. Mater. Chem.* **1997**, *7*, 369.

47 Diaz, A. F. *Chem. Scr.* **1981**, *17*, 142.

48 Tourillon, G.; Garnier, F. *J. Electroanal. Chem.* **1982**, *135*, 173.

49 Bargon, J.; Mohamand, S.; Waltman, R. J. *IBM J. Res. Develop.* **1983**, *27*, 330.

50 Delamer, M.; Lacaze, P. C.; Dumousseau, J. Y.; Dubois, J. E. *Electrochim. Acta* **1982**, *27*, 61.

51 (a) Diaz, A. F.; Logan, J. A. *Electroanal. Chem.* **1980,** *111*, 111. (b) McDiarmid, A. G.; Chiang, J. C.; Halpern, M.; Huang, H. S.; Su, S. L.; Somasiri, N. L. D.; Wu, W.; Yaniger, S. I. *Mol. Cryst. Liq. Cryst.* **1985**, *121*, 173. (c) Genies, E. M.; Tsintavis, C.; Syed, A. A. *Mol. Cryst. Liq. Cryst.* **1985**, *121*, 181.

52 (a) Sato, M.; Tanaka, S.; Kaeriyama, K. *J. Chem. Soc., Chem. Commun*. **1986**, 873. (b) Jen, K. Y.; Miller, G. G.; Elsenbaumer, R. L. *J. Chem. Soc., Chem. Commun*. **1986**, 1346.

53 (a) Leclerc, M.; Guay, J.; Dao, L. H. *Macromolecules* **1982**, *22*, 649. (b) Wei, Y.; Focke, W. W.; Wnek, G. E.; Ray, A.; MacDiarmid, A. G. *J. Phys. Chem.* **1989**, *93*, 495.

54 Halls, J. J.; Pichler, K.; Friend, R. H.; Moratti, S. C.; Holmes, A. B. *Appl. Phys. Lett.* **1996**, *68*, 3120.

55 Ajayaghosh, Ayyappanpillai *Chem. Soc. Rev*. **2003**, *32*, 181.

56 Thelakkat, M. *Macromol. Mater. Eng*. **2002**, *287(7)*, 442.

57 Borsenberger, P. M.; Weiss, D. S. “Organic Photoreceptors for Imaging Systems” Marcel Dekker, New York **1993**.

58 Heun, S.; Borsenberger, P. M. *Chem. Phys*. **1995**, *200*, 245.

59 Borsenberger, P. M.; Pautmeier, L.; Richert, R.; Baessler, H. *J. Chem. Phys*. **1991**, *94*, 8276.

60 Borsenberger, P. M.; Gruenbaum, W. T.; Sorriero, L. J.; Zumbuliadis, N. *Jpn. J. Appl. Phys*. **1995**, *34*, 1597.

61 Thelakkat, M.; Bacher, A.; Fink, R.; Haubner, F.; Schmidt, H.-W. *Macromol. Symp* **1997**, *125*, 157.

62 Gauthier, S.; Frechet, J. M. J. *Synthesis (Communications)* **1987**, 383.

63 Ostrauskaite, J.; Karikal, H.R.; Leopold, A.; Haarer D.; Thelakkat, M. *J. Mater. Chem.* **2002**, *12*, 58.

64 Tanaka, S.; Iso, T.; Doke, Y. *Chem. Commun*. **1997**, 2063.

65 (a) Schmitz, C.; Thelakkat, M.; Schmidt, H.-W. *Adv. Mater*. **1999**, *11*, 821. (b) Schmidt, H.-W.; Schmitz, C.; Poersch, P.; Thelakkat, M. *Proc. SPIE-Int. Soc. Opt. Eng.* **1999**, *3797*, 58.

66 Schmitz, C.; Poersch, P.; Thelakkat, M.; Schmidt, H.-W.; Montali, A.; Feldman, K.; Smith, P.; Weder, C. *Adv. Funct. Mater*. **2001**, *11*, 41.

67 (a) Goodson, F.E.; Hartwig, J.F. *Macromolecules* **1998**, *31*, 1700. (b) Goodson, F.E.; Hauck, S.I.; Hartwig, J. F. *J. Amer. Chem. Soc.* **1999**, *121*, 7527.

68 Yu, W.-L.; Pei, J.; Huang, W.; Heeger, A. J. *Chem. Commun*. **2000**, 681.

69 (a) Haridas, K. R.; Ostrauskaite, J.; Thelakkat, M.; Heim, M.; Bilke, R.; Haarer, D. *Synth. Met*. **2001**, *121*, 1573. (b) Jaeger, C.; Bilke, R.; Heim, M.; Haarer, D.; Karickal, H.; Thelakkat, M. *Synth. Met*. **2001**, *121*, 1543.

70 (a) Jaeger, C.; Bilke, R.; Heim, M.; Haarer, D.; Karickal, H.; Thelakkat, M. *Proc. SPIE-Int. Soc. Opt. Eng.* **2001**, *4108*, 104. (b) Moerner, W. E.; Silence, S. M.; Hache, F.; Bjorklund, G. C. *J. Opt. Soc. Am. B*. **1994**, *11*, 320.

71 (a) Kim, D. U.; Tsutsui, T.; Saito, S. *Chem. Lett*. **1995**, 587. (b) Kim, D. U.; Tsutsui, T.; Saito, S. *Polymer* **1995**, *36*, 2481. (c) Kim, D. U.; Tsutsui, T. *J. Appl. Phys*. **1996**, *80*, 4785.

72 (a) Rost, H.; Teuschel, A.; Pfeiffer, S.; Hoerhold, H.-H. *Synth. Met*. **1997**, *84*, 269. (b) Pfeiffer, S.; Rost, H.; Hoerhold, H.-H. *Macromol. Chem. Phys*. **1999**, *200*, 2471. (c) Hertel, D.; Baessler, H.; Scherf, U.; Hoerhold, H.-H. *J. Chem. Phys*. **1999**, *110*, 9214. (d) Zheng, M.; Bai, F.; Li, Y.; Yu, G.; Zhu, D. *J. Polym. Sci., Part A: Polym. Chem.* **1999**, *37*, 2587. (e) Zheng, M.; Bai, F.; Zhu, D. *J. Appl. Polym. Sci.* **1999**, *74*, 3351. (f) Liu, Y.; Liu, M. S.; Li, X.-C.; Jen, A. K.-Y. *Chem. Mater.* **1998**, *10*, 3301. (g) Liu, Y.; Liu, M. S.; Jen, A. K.-Y. *Acta Polym.* **1999**, *50*, 105. (h) Li, X.-C.; Liu, Y.; Liu, M. S.; Jen, A. K.-Y. *Chem. Mater*. **1999**, *11*, 1568.

73 (a) Kawai, T.; Kuwabara, T.; Wang, S.; Yoshino, K. *Jpn. J. Appl. Phys.* **1990**, *29*, 602. (b) Bobacka, J.; Ivaska, A.; Grzeszczuk, M. *Synth. Met.* **1991**, *44*, 9.

74 (a) Kim, S. R.; Choi, S. A.; Kim, J. D.; Kim, K. J.; Lee, C.; Rhee, S. B. *Synth. Met.* **1995**, *71*, 2027. (b) Chan, H. S. O.; Ng, S. C.; Seow, S. H. *Synth. Met.* **1994**, *66*, 177. (c) Chan, H. S. O.; Toh, C. S.; Gan, L. M. *J. Mater. Chem.* **1995**, *5*, 631.

75 Dekker, Marcel *Handbook of Conducting Polymers* New York **1998**, *2nd ed.* and New York **1986**, *1st ed.*

76 Chen, L.; Godovski, D.; Inganaes, O.; Hummelen, J. C.; Janssens, R. A. J.; Svensson, M.; Andersson, M. R. *Adv. Mater.* **2000**, *12(18)*, 1367.

77 McCullough, R. D. *Adv. Mater.* **1998**, *10(2)*, 93.

78 Katz, H. E.; Bao, Z.; Gilat, S. L. *Acc. Chem. Res.* **2001**, *34*, 359.

79 Sato, M.; Morii, H. *Macromolecules* **1991**, *24*, 1196.

80 Mao, H.; Xu, B.; Holdcroft, S. *Macromolecules* **1993**, *26*, 1163.

81 Sugimoto, R.; Takeda, S.; Gu, H. B.; Yoshino, K. *Chem. Express* **1986**, *1(11)*, 635.

82 (a) Andersson, M. R.; Selse, D.; Berggren, M.; Jaervinen, H.; Hjertberg, T.; Inganaes, O.; Wennerstroem, O.; Oesterholm, J.-E. *Macromolecules* **1994**, *27*, 6503. (b) Andersson, M. R.; Mammo, W.; Olinga, T.; Svensson, M.; Theander, M.; Inganaes, O. *Synth. Met.* **1999**, *101*, 11. (c) Levesque, I.; Leclerc, M. *J. Chem. Soc.*, *Chem. Commun*. **1995**, 2293.

83 Loewe, R. S.; Khersonsky, S. M.; McCullough, R. D. *Adv. Mater.* **1999**, *11*, 250.

84 Chen, T.-A.; Rieke, R. D. *J. Am. Chem. Soc*. **1995**, *117*, 233.

85 Guillerez, S.; Bidan, G. *Synth. Met*. **1998**, *93***,** 123.

86 (a) McCullough, R. D.; Ewbank. P. C.; Loewe, R. S. *J. Am. Chem. Soc.* **1997**, *119*, 633. (b) Iraqi, A.; Barker, G. W. *J. Mater. Chem.* **1998**, *8*, 25.

87 Roncali, J. *Chem. Rev*. **1997**, *97*, 173.

88 Pomerantz, *M. Handbook of Conducting Polymers*.

89 Wudl, F.; Kobayashi, M.; Heeger, A. J. *J. Org. Chem*. **1984**, *49*, 3382.

90 Svensson, M.; Zhang, F.; Veenstra, S. C.; Verhees, W. J. H.; Hummelen, J. C.; Kroon, J. M.; Inganaes, O.; Andersson, M. R. *Adv. Mater*. **2003**, *15(12)*, 988.

91 Vangeneugden, D. L.; Vanderzande, D. J. M.; Salbeck, J.; van Hal, P. A.; Janssen, R. A. J.; Hummelen, J. C.; Brabec, C. J.; Shaheen, S. E.; Sariciftci, N. S. *J. Phys. Chem. B* **2001**, *105*, 11106.

92 Yu, G.; Nishino, H.; Heeger, A. J.; Chen, T.-A.; Rieke, R. D. *Synth. Met.* **1995**, *72*, 249.

93 Mohanakrishnan, A. K.; Lakshmikantham, M. V.; McDougal, C.; Cava, M. P.; Baldwin, J. W.; Metzger, R. M. *J. Org. Chem*. **1998**, *63*, 3105.

94 Gritzner, G.; Kuta, J. *Pure Appl. Chem*. **1984**, *56*, 462.

95 Pommerehne, J.; Vestweber, H.; Gusws, W.; Mahrt, R.F.; Bässler, H.; Porsch M.; Daub, J. *Adv. Mater.* **1995**, *7*, 55.

96 Mitschke, U.; Bäuerle, P. *J. Chem. Soc., Perkin Trans. 1* **2001**, 740.

97 Yang, B. H.; Buchwald, S. L. *Journal of Organometallic Chemistry* **1999**, *576*, 125.

98 (a) Driver M. S.; Hartwig, J. F. *J. Amer. Chem. Soc.* **1996**, *118*, 7217.

99 Kisselev, R.; Thelakkat, M. *Chem. Commun*. **2002**, 1530.

100 Wong, K.; Hung, T.; Kao, S.; Chou, C.; Su, Y. *Chem. Commun.* **2001**, *(17)*, 1628.

101 Cornil, J.; Beljonne, D.; Heller, C. M.; Campbell, I. H.; Laurich, B. K.; Smith, D. L.; Bradley, D. D. C.; Muellen, K.; Bredas, J. L. *Chemical Physics Letters* **1997**, *278*, 139.

102 Kasha, M.; Rawls, H. R.; El-Bayoumi, M. A. *Pure Appl. Chem*. **1965**, *11*, 371.

103 Hochstrasser, R. M.; Kasha, M. *Photochemistry and Photobiology* **1964**, *3*, 317.

104 Bilke, R.; Leicht, A.; Jaeger, C.; Thelakkat, M.; Schmitz, C.; Karikal, H.; Haarer, D. *Synthetic Metals* **2001**, *124*, 91.

105 Kiebooms, R.; Hoogmartens, I.; Adriaensens, P.; Vanderzande, D.; Gelan, J. *Macromolecules* **1995**, *28*, 4961.

106 Paulussen, H.; Vanderzande, D.; Gelan, J. *Synth. Met.* **1997**, *84*, 415.

107 (a) Okuda, Y.; Lakshmikantham, M. V.; Cava, M. P. *J. Org. Chem.* **1991**, *56*, 6024. (b) Lorcy, D.; Cava, M. P. *Adv. Mater.* **1992**, *4*, 562.

108 (a) Friedrichsen, W. *Adv. Het. Chem.* **1980**, *26*, 135. (b) Volz, W.; Voss, J. *Phosphorus, Sulfur and Silicon* **1990**, *53*, 429.

109 (a) McCullough, R. D.; Lowe, R. D.; Jayaraman, M.; Anderson, D. L. *J. Org. Chem.* **1993**, *58*, 904. (b) Jiang, X.; Harima, Y.; Yamashita, K.; Tada, Y.; Ohshita, J.; Kunai, A. *Synthetic Metals* **2003**, *135-136*, 351.

110 Sugimoto, R.; Takeda, S.; Gu, H. B.; Yoshino, K. *Chem. Express* **1986**, *1(11)*, 635.

111 Andersson, M. R.; Pei, Q.; Hjertberg, T.; Inganaes, O.; Wennerstroem, O.; Oesterholm, J.-E. *Synth. Met.* **1993**, *55*, 1227.

112 Niemi, V. M.; Knuuttila, P.; Oesterholm, J.-E.; Korvola, J. *Polymer* **1992**, *33*, 1559.

113 (a) Baeuerle, P.; Goetz, G.; Emerle, P.; Port, H. *Adv. Mater*. **1992**, *4*, 564. (b) Hoogmartens, I.; Adriaensens, P.; Carleer, R.; Vanderzande, D.; Martens, H.; Gelan, J. *Synth. Met.* **1992**, *51*, 219. (c) Musinanni, S.; Ferraris, J. P. *J. Chem. Soc., Chem. Commum.* **1993**, 172.

114 Kiebooms, R.; Adriaensens, P.; Vanderzande, D.; Gelan, J. *J. Org. Chem.* **1997**, *62*, 1473.

115 (a) Vangeneugden, D. L.; Kiebooms, R. H. L.; Andriaensens, P.; Vandrzande, D. J. M.; Gelan, J. M. J. V.; Desmet, J.; Huyberechts, G. *Acta Polym.* **1998**, *49*, 687. (b) Vangeneugden, D. L.; Kiebooms, R. H. L.; Vandrzande, D. J. M.; Gelan, J. M. J. V. *Synthetic Metals* **1999**, *101*, 120.

116 Taka, T.; Nyholm, P.; Laakso, J.; Loponen, M. T.; Oesterholm, J. E. *Synthetic Metals*, **1991**, *41*, 903.

117 Yue, S.; Berry, G. C.; McCullough, R.D. *Macromolecules* **1996**, *29*, 933.

118 Drechsel, J.; Mannig, B.; Kozlowski, F.; Gebeyehu, D.; Werner, A.; Koch, M.; Leo, K.; M. Pfeiffer *Thin Solid Films* **2004**, *451-452*, 515.

119 Pfeiffer, M.; Beyer, A.; Plönnings, B.; Nollau, A.; Fritz, T.;Leo, K.; Schlettwein, D.; Hiller, S.; Wöhrle, D. *Solar Energy Materials & Solar Cells* **2000**, *63*, 83.

120 Jungmann, Gert *Dissertation* **2000**, University of Bayreuth, Germany.

121 (a) Wakimoto, T.; Murayama, R.; Nagayama, K.; Okuda, Y.; Nakada, H.; Tohma, T. *SID96 Dig*. **1996**, 849. (b) Nakamura, H.: Hosokawa, C.; Kusumoto, T. *Inorganic and Organic Electroluminescence/EL96,* Berlin (Eds: Mauch, R. H.; Gumlich, H. E.) Wissenschaft und Technik, Berlin **1996**, p. 65.

122 Bulovic, V.; Shoustikov, A.; Baldo, M. A.; Bose, E.; Kozlov, V. G.; Thompson, M. E.; Forrest, S. R. *Chem. Phys. Lett.* **1998**, *287*, 455.

123 Chen, C. H.; Tang, C. W.; Shi, J.; Klubek, K. P. *Macromol. Symp.* **1998**, *125*, 49.

124 (a) Burrows, P. E.; Forrest, S. R.; Sibley, S. P.; Thompson, M. E. *Appl. Phys. Lett.* **1996**, *69*, 2959. (b) Shoustikov, A.; You, Y. J.; Burrows, P. E.; Thompson, M. E.; Forrest, S. R. *Synth. Met.* **1997**, *91*, 217.

125 (a) Kido, J.; Nagai, K.; Ohashi, Y. *Chem. Lett*. **1990**, 657. (b) Kido, J.; Nagai, K.; Okuyama, Y.; Skothiem, T. *Chem. Lett*. **1991**, 1267. (c) Kido, J.; Hayase, H.; Hongawa, K.; Nagai, K.; Okuyama, K. *Appl. Phys. Lett.* **1994**, *65*, 2124.

126 Picciolo, L. C.; Murata, H.; Kafafi, Z. H. *Appl. Phys. Lett*. **2001**, *78*, 2378.

127 Zhang, X. H.; Chen, B. J.; Lin, X. Q.; Wong, Q. Y.; Lee, C. S.; Kwong, H. L.; Lee, S. T.; Wu, S. K. *Chem. Mater.* **2001**, *13*, 1565.

128 Thelakkat, M.; Schmitz, C.; Neuber, C.; Schmidt, H.-W. *Macromol. Rapid. Commun*. **2004**, *25*, 204.

129 Borsenberger, P. M.; Mey, W.; Chowdry, A. *J. Appl. Phys*. **1978**, *49*, 273.

130 Philips, J. P. *Chem. Rev*. **1956**, *56*, 272.

131 Steger, H. F.; Corsini, A. *J. Inorg. Nucl. Chem*. **1973**, *35*, 1621.

132 Yeh, H.-C.; Chan, L.-H.; Wu, W.-C.; Chen, C.-T. *J. Mater. Chem*. **2004**, *14*, 1293.

133 Shi, J.; Tang, C. W. *Appl. Phys. Lett*. **1997**, *70(13)*, 31.

134 Kitamura, C.; Tanaka, S.; Yamashita, Y. *Chem. Mater*. **1996**, *8*, 570.

135 Tanaka, S.; Yamashita, Y. *Synthetic Metals* **1995**, *69*, 599.

136 Van Hecke, G. R.; Horrocks, W. D. *J. Inorg. Chem.* **1966,** *5(11)*, 1968.

137 Kiebooms, R.; Adriaensens, P.; Vanderzande, D.; Gelan, J. *J. Org. Chem*. **1997**, *62*, 1473.

138 Pham, C. V.; Mark, H. B.; Zimmer, H. *Synthetic Communications* **1986**, *16(6)*, 689.

139 Hoffmann, K. J.; Carlsen, P. H. J. *Synthetic Communications* **1999**, *29(9)*, 1607.

140 Tamao, K.; Kodama, S.; Nakajima, I.; Kumada, M.; Minato, A.; Suzuki, K. *Tetrahedron* **1982**, *38(22)*, 3347.

141 Wong, K. T.; Hung, T. H.; Chou, C. H.; Su, Y. O.; Kao, S. C. *Chem. Commun*. **2001**, *17*, 1628.